

A DENSITY FUNCTIONAL THEORY STUDY OF CATALYTIC EPOXIDATION OF
ETHYLENE AND PROPYLENE

A THESIS SUBMITTED TO
THE GRADUATE SCHOOL OF NATURAL AND APPLIED SCIENCES
OF
MIDDLE EAST TECHNICAL UNIVERSITY

BY

MEHMET FERDİ FELLAH

IN PARTIAL FULFILLMENT OF THE REQUIREMENTS
FOR
THE DEGREE OF DOCTOR OF PHILOSOPHY
IN
CHEMICAL ENGINEERING

OCTOBER 2009

Approval of the thesis:

**A DENSITY FUNCTIONAL THEORY STUDY OF CATALYTIC
EPOXIDATION OF ETHYLENE AND PROPYLENE**

submitted by **MEHMET FERDİ FELLAH** in partial fulfillment of the requirements for the degree of **Doctor of Philosophy in Chemical Engineering Department, Middle East Technical University** by,

Prof. Dr. Canan Özgen
Dean, Graduate School of **Natural and Applied Sciences**

Prof. Dr. Gürkan Karakaş
Head of Department, **Chemical Engineering**

Prof. Dr. Işık Önal
Supervisor, **Chemical Engineering Dept., METU**

Examining Committee Members:

Prof. Dr. Hayrettin Yücel
Chemical Engineering Dept., METU

Prof. Dr. Işık Önal
Chemical Engineering Dept., METU

Prof. Dr. İnci Eroğlu
Chemical Engineering Dept., METU

Prof. Dr. Şakir Erkoç
Physics Dept., METU

Assoc. Prof. Dr. Nahit Aktaş
Chemical Engineering Dept., Yüzüncü Yıl University

Date: October 26, 2009

I hereby declare that all information in this document has been obtained and presented in accordance with academic rules and ethical conduct. I also declare that, as required by these rules and conduct, I have fully cited and referenced all material and results that are not original to this work.

Name, Last name: **MEHMET FERDİ FELLAH**

Signature:

ABSTRACT

A DENSITY FUNCTIONAL THEORY STUDY OF CATALYTIC EPOXIDATION OF ETHYLENE AND PROPYLENE

Fellah, Mehmet Ferdi

Ph.D., Department of Chemical Engineering

Supervisor: Prof. Dr. Işık Önal

October 2009, 211 pages

The reactions which give the products ethylene oxide, vinyl alcohol, vinyl aldehyde and vinyl radical for ethylene oxidation and the reactions which give propylene oxide, propanal, acetone and pi-allyl radical for propylene oxidation were investigated by using Density Functional Theory (DFT) method with B3LYP/LanL2DZ and 6-31g(d,p) basis sets in Gaussian'03 software. Silver and silver oxide were used as catalyst surface cluster models. Surface comparison was made for silver (111), (110) and (100) surfaces. Ethylene oxidation reaction was studied on these silver surfaces. Oxygen effect on ethylene oxide formation reaction was also investigated on silver (111) surface. Ethylene and propylene oxidation reactions were completed on both $Ag_{13}(111)$ and $Ag_{14}O_9(001)$ surface clusters. VASP software which utilizes periodic plane wave basis sets was also used to compare trends of reactions for ethylene and propylene oxidations obtained by using Gaussian'03 software.

According to results, silver (110) surface is more active for ethylene oxide formation than (111) and (100) surfaces. Hill site of (110) surface is much more active than hollow site of (110) surface since oxygen atom weakly adsorbed on hill site. Ethyl aldehyde and vinyl alcohol can not be formed on Ag(111) surface because of those higher activation barriers while ethylene oxide can be formed on cluster. Activation barrier for ethylene oxide formation decreases with increasing oxygen coverage on Ag(111) surface. Ethylene oxametallocycle intermediate molecule was not formed on Ag₂O(001) surface while it is formed on surface oxide structure on Ag(111). Ethyl aldehyde and vinyl alcohol are not formed on silver oxide (001) surface.

For propylene oxidation, Π -allyl formation path has the lowest activation barrier explaining why silver is not a good catalyst for the propylene oxide formation while it is a good catalyst for the ethylene oxide formation. This situation is valid for silver oxide. Propylene oxide selectivity increased in the gas phase oxidation. The qualitative relative energy trend obtained by VASP software is the similar with that of calculations obtained by using GAUSSIAN'03 software.

Keywords: DFT, Silver, Silver oxide, Catalyst, Epoxidation, Ethylene, Ethylene oxide, Propylene, Propylene oxide, Reaction mechanism,

ÖZ

ETİLEN VE PROPİLENİN KATALİTİK EPOKSİDASYONUNUN YOĞUNLUK FONKSİYON TEORİSİ (DFT) ÇALIŞMASI

Fellah, Mehmet Ferdi

Doktora, Kimya Mühendisliği Bölümü

Tez Yöneticisi: Prof. Dr. Işık Önal

Ekim 2009, 211 sayfa

Etilen oksidasyonu için etilen oksit, vinil alkol, vinil aldehit ve vinil radikalini veren tepkimeler ve propilen oksidasyonu için propilen oksit, propanal, aseton ve pi-alil radikalini veren tepkimeler Yoğunluk Fonksiyon Teorisi (DFT) metodu ve B3LYP/LanL2DZ ve 6-31g(d,p) fonksiyon setleri Gaussian'03 yazılımı kullanılarak incelenmiştir. Katalizör yüzey modelleri olarak gümüş ve gümüş oksit yüzeyleri kullanılmıştır. Gümüş (111), (110) ve (100) yüzeyleri için yüzey karşılaştırması yapılmıştır. Etilen oksit tepkimesi bu yüzeyler üzerinde çalışılmıştır. Gümüş (111) yüzeyi üzerinde etilen oksit üretimi üzerine oksijen miktarının etkisi incelenmiştir. Etilen ve propilen oksidasyon tepkimeleri hem $Ag_{13}(111)$ yüzeyi ve hem de $Ag_{14}O_9(001)$ yüzeyi üzerinde tamamlanmıştır. Etilen ve propilen oksidasyonları için tepkimelerin eğilimlerini karşılaştırmak için devamlı sonsuz bir yapı kullanan VASP yazılımı da kullanılmıştır.

Sonuçlara göre, (111) yüzeyi gümüş katalizörü için en dengeli yüzeydir. (110) yüzeyi etilen oksit üretimi için (111) ve (100) yüzeylerinden daha aktiftir. (110) yüzeyinin tepe kısmı çukur kısmından daha aktiftir. Etilen oksit yapı üzerinde oluşabilirken, etil aldehit ve vinil alkol yüksek aktivasyon bariyerleri nedeniyle Ag(111) yüzeyi üzerinde oluşmamaktadırlar. Etilen oksit oluşumunun aktivasyon bariyeri artan oksijen miktarı ile azalmaktadır. Etilen oksametalköprüsü ara ürünü Ag(111) yüzeyi üzerinde oluşurken Ag₂O(001) yüzeyi üzerinde oluşmamaktadır. Etil aldehit ve vinil alkol yüksek aktivasyon bariyerleri nedeniyle Ag₂O(001) yüzeyi üzerinde de oluşmamaktadırlar.

Propilen oksidasyonu için, pi-alil üretimi tepkimesinin en düşük aktivasyon bariyerine sahip olması gümüşün neden etilen oksit üretimi için iyi bir katalizör olup propilen oksit üretimi için iyi bir katalizör olmadığını açıklar. Bu durum gümüş oksit içinde geçerlidir. Propilen oksit seçiciliği gaz faz oksidasyonu ile artmaktadır. VASP yazılımı kullanılarak elde edilen tepkimelerin nitelik bakımından görelî enerji eğilimleri Gaussian'03 yazılımı kullanılarak elde edilen ile benzerdir.

Anahtar Kelimeler: DFT, Gümüş, Gümüş oksit, Katalizör, Etilen, Etilen oksit, Propilen, Propilen oksit, Tepkime mekanizması

To My Family

ACKNOWLEDGMENTS

First of all, I would like to express my sincere appreciation to my supervisor Prof. Dr. Işık ÖNAL for his guidance, advice, criticism, encouragements and insight throughout the research.

I would like to thank to members of my PhD progress committee, Prof. Dr. Hayrettin YÜCEL and Assoc. Prof. Dr. Nahit AKTAŞ, for their criticism during my progress presentations.

I would like to thank to members of *the DFT Research Group*, especially M. Oluş ÖZBEK for his guidance for VASP software. I would like to thank to Derya DÜZENLİ for friendship and sharing of some results of her PhD study.

This thesis was completed as a part of Faculty Development Program (ÖYP). This research was supported in part by TÜBİTAK through TR-Grid e-Infrastructure Project hosted by TÜBİTAK ULAKBİM and METU.

I wish to thank to my father who I remember with respect and longing and to my mother for their encouragement and great support.

Finally, I would like send my best gratitude to my wife Emine and my daughter Zeynep Nisa for adding meaning to my life.

TABLE OF CONTENTS

ABSTRACT.....	iv
ÖZ.....	vi
ACKNOWLEDGMENTS.....	ix
TABLE OF CONTENTS.....	x
CHAPTERS	
1. INTRODUCTION.....	1
1.1. Importance of Catalysis.....	1
1.2. Light Alkenes Epoxidation.....	2
1.3. Computational Chemistry.....	5
1.3.1. Molecular Mechanics (MM) Methods.....	8
1.3.2. Semi- Empirical and Empirical Methods.....	10
1.3.3. ab-initio Methods.....	12
1.3.3.1. Hartree-Fock (HF) Methods.....	12
1.3.3.2. Møller-Plesset Perturbation Theory (MP) Methods.....	13
1.3.3.3. Density Functional Theory (DFT) Methods.....	14
1.4. Theoretical and Simulation Methods for Catalysis.....	19
1.5. The Objective of This Study.....	24

2. LITERATURE SURVEY.....	25
3. SURFACE MODELS AND CALCULATION METHODS.....	41
3.1. Computational Procedure for GAUSSIAN Software.....	41
3.1.1. Silver Surface Model.....	41
3.1.2. Silver Oxide Surface Model.....	46
3.1.3. Calculation Approach.....	50
3.2. Computational Procedure for VASP Software.....	52
4. RESULTS AND DISCUSSION.....	54
4.1. Comparison of Silver Surfaces.....	54
4.2. Ethylene Epoxidation.....	56
4.2.1. Ethylene Epoxidation on Small Silver (111), (110) and (100) Surface Clusters.....	56
4.2.1.1. Ethylene Epoxidation on Ag ₅ (111) Surface Cluster.....	56
4.2.1.2. Ethylene Epoxidation on Ag ₅ (110) Surface Cluster.....	59
4.2.1.3. Ethylene Epoxidation on Ag ₅ (100) Surface Cluster.....	65
4.2.2. Ethylene Epoxidation on Silver Surface.....	69
4.2.2.1. Ethylene Epoxidation on Ag ₁₃ (111) Cluster.....	70
4.2.2.1.1. Vinyl Radical Formation Path.....	71
4.2.2.1.2. Ethylene Oxide Formation Path.....	72
4.2.2.1.3. Vinyl Alcohol Formation Path.....	74
4.2.2.1.4. Vinyl Aldehyde Formation Path.....	75
4.2.2.2. Ethylene Epoxidation on Ag ₁₃ (111)(4O) Cluster (Oxygen coverage effect).....	79
4.2.2.3. Ethylene Epoxidation on Slab Surface	84
4.2.3. Ethylene Epoxidation on Silver Oxide Ag ₁₄ O ₉ (001) Surface	88
4.2.3.1. Vinyl Radical Formation Path.....	89

4.2.3.2. Ethylene Oxide Formation Path.....	90
4.2.3.3. Vinyl Aldehyde Formation Path.....	92
4.2.3.4. Vinyl Alcohol Formation Path.....	93
4.3. Propylene Epoxidation.....	98
4.3.1. Propylene Epoxidation on Silver Surface.....	98
4.3.1.1. Propylene Epoxidation on Ag ₁₃ (111) Cluster.....	100
4.3.1.1.1. π -Allyl Formation Path.....	100
4.3.1.1.2. Propylene Oxide Formation Path.....	101
4.3.1.1.3. Propanal Formation Path.....	106
4.3.1.1.4. Acetone Formation Path.....	107
4.3.1.2. Propylene Epoxidation on Slab Surface	111
4.3.2. Propylene Epoxidation on Silver Oxide Ag ₁₄ O ₉ (001) Surface	115
4.3.2.1. π -Allyl Formation Path.....	116
4.3.2.2. Propylene Oxide Formation Path.....	117
4.3.2.3. Propanal Formation Path.....	123
4.3.2.4. Acetone Formation Path.....	124
4.3.3. Propylene Epoxidation in Gas Phase.....	127
5. CONCLUSIONS.....	134
REFERENCES.....	137
APPENDICES	
A. DENSITY FUNCTIONAL THEORY.....	146
A.1. Overview of Method.....	146
A.2. Derivation and Formalism.....	147

A.3. Approximations (Exchange-correlation functionals).....	151
A.4. Applications.....	152
B. BASIS SETS.....	154
B.1. Notation.....	155
B.2. Treating Core Electrons.....	158
B.3. Common Basis Sets.....	160
C. OPTIMIZED GEOMETRIES AND PARAMETERS OF REACTANTS AND PRODUCTS.....	162
D. SAMPLE INPUT AND OUTPUT FILES.....	167
VITA.....	208

LIST OF TABLES

TABLES

Table 3.1 Wyckoff parameters of Silver.....	42
Table 3.2 Calculated values of the fractional atomic coordinates and the atomic positions of unit cell of Silver.....	42
Table 3.3 Cell parameters of Silver Oxide.....	46
Table 3.4 Calculated values of the fractional atomic coordinates and the atomic positions of unit cell of Silver Oxide.....	47
Table 4.1 Comparison of activation barriers for ethylene oxide formation on (111), (110) and (100) silver surfaces	68
Table 4.2 Comparison of activation barriers for ethylene oxide formation on silver (111) surface.....	78
Table 4.3 A comparison for ethylene oxide formation with different oxygen coverage values on (111) silver surface.....	83
Table 4.4 The comparison of the activation energy barriers of ethylene epoxidation reactions on [Ag ₁₄ O ₉] cluster representing (001) silver oxide.....	97
Table 4.5 Comparison of activation barriers for propylene epoxidation reactions on silver.....	109
Table D.1 Input file of the calculation for optimization of ethylene molecule in Gaussian 03 software.....	167
Table D.2 Output file of the calculation for optimization of ethylene molecule in Gaussian 03 software.....	168

Table D.3 Input file of the calculation for optimization of Ag ₁₃ O cluster in Gaussian 03 software.....	184
Table D.4 Input files of the calculation for optimization of ethylene molecule in VASP software.....	191
Table D.5 Output file of the calculation for optimization of ethylene molecule in VASP software.....	192
Table D.6 Input file of the calculation for optimization of Ag(3x3) slab in VASP software.....	206

LIST OF FIGURES

FIGURES

Figure 1.1 Ethylene epoxidation reaction (Geometries were optimized by using Gaussian 03 software)	3
Figure 1.2 Propylene epoxidation reaction (Geometries were optimized by using Gaussian 03 software)	5
Figure 1.3 Number of publications of DFT (Wolfram, 2001) (Numbers for years between 2000 and 2008 were obtained by using ISI Web of Knowledge)	17
Figure 1.4 A comparison of calculation methods.....	18
Figure 1.5 SPE Computational CPU time requirements of methods a) for propylene molecule and b) for C60 molecule.....	18
Figure 1.6 A comparison of calculated and experimental chemisorption energies for different adsorbates on different metal surfaces (van Santen, 2006).	21
Figure 1.7 Characteristic models for modeling. Silver (111) surface a) cluster approach, b) embedding scheme (QM region is represented by ball-bond view and MM region is represented by wire frame view), c) periodic slab model.....	23
Figure 2.1 Calculated IR vibrational spectra of oxametallacycles on an Ag ₃ cluster. (a) OMME structure; (b) OME structure; (c) HREEL spectrum of the surface intermediate (Linic, 2001).....	27
Figure 2.2 Schematic of the reaction coordinate for	

oxametallacycle ringclosure to yield EO (Linic,2001).....	28
Figure 2.3 Relative energy diagram for the conversion of gas-phase C ₂ H ₄ to epoxide, on the high coverage Ag _{1.8} O (Ag ₁₁ O ₆) layer on Ag(111) (Bocquet, 2003).....	31
Figure 2.4 Reaction profiles for epoxide and aldehyde formation by rearrangement of OMMP (Torres, 2007).....	39
Figure 3.1 Unit cell of Silver.....	43
Figure 3.2 Five times enlarged silver unit cell in X,Y and Z directions.....	43
Figure 3.3 Silver surfaces a) Top view of (111) surface, b) Side view of (111) surface, c) Top view of (110) surface, d) Side view of (110) surface, e) Top view of (100) surface, f) Side view of (100) surface.....	44
Figure 3.4 Ag ₁₃ (111) surface cluster used in this study a) Top view, b) Side view.....	45
Figure 3.5 Unit cell of Silver Oxide.....	47
Figure 3.6 Five times enlarged silver oxide unit cell in X,Y and Z directions.....	48
Figure 3.7 Ag ₁₄ O ₉ (001) surface cluster used in this study a) Top view, b) Side view.....	49
Figure 3.8 a) 4 Layers-(3x3) silver (111) slab, b) 2 times enlarged slab in X and Y direction.....	53
Figure 4.1 Silver surface clusters a) Ag ₅ (111) surface cluster, b) Ag ₅ (110) surface cluster, c) Ag ₅ (100) surface cluster.....	55
Figure 4.2 Equilibrium geometry for atomic oxygen adsorption on Ag ₅ (111)	56
Figure 4.3 Relative energy profile along reaction coordinate (C1-O) for ethylene oxide formation on oxygen atom adsorbed on 5 atoms (111) silver surface cluster.	57

Figure 4.4 Relative energy profile along reaction coordinate (C2-O) for ethylene oxide formation on oxygen atom adsorbed on 5 atoms (111) silver surface cluster.	58
Figure 4.5 Large Ag(110) surface. a: Hill site, b: Hollow site.....	59
Figure 4.6 Equilibrium geometry for atomic oxygen adsorption on Ag5(110). a) Top view b) Side view.	60
Figure 4.7 Equilibrium geometry for atomic oxygen adsorption on Ag8(110). a) Top view b) Side view.	60
Figure 4.8 Relative energy profile along reaction coordinate (C1-O) for ethylene oxide formation on oxygen atom adsorbed on 5 atoms (110) silver surface cluster.	62
Figure 4.9 Relative energy profile along reaction coordinate (C2-O) for ethylene oxide formation on oxygen atom adsorbed on 5 atoms (110) silver surface cluster.	62
Figure 4.10 Relative energy profile along reaction coordinate (C1-O) for ethylene oxide formation on oxygen atom adsorbed on 8 atoms (110) silver surface cluster.	63
Figure 4.11 Relative energy profile along reaction coordinate (C2-O) for ethylene oxide formation on oxygen atom adsorbed on 8 atoms (110) silver surface cluster.	64
Figure 4.12 Equilibrium geometry for atomic oxygen adsorption on Ag5(100). a) Top view b) Side view.	65
Figure 4.13 Relative energy profile along reaction coordinate (C1-O) for ethylene oxide formation on oxygen atom adsorbed on 5 atoms (100) silver surface cluster.....	66
Figure 4.14 Relative energy profile along reaction coordinate (C2-O) for ethylene oxide formation on oxygen atom adsorbed on 5 atoms (100) silver surface cluster.....	67

Figure 4.15 A reaction mechanism for ethylene epoxidation.....	69
Figure 4.16 Equilibrium geometry for atomic oxygen adsorption on Ag ₁₃ (111) a) Top view b) Side view.....	71
Figure 4.17 Relative energy profile along reaction coordinates (H-O) for C-H activation of ethylene on oxygen atom adsorbed on 13 atoms (111) silver surface cluster.	72
Figure 4.18 Relative energy profile along reaction coordinate (C1-O) for ethylene oxide formation on oxygen atom adsorbed on 13 atoms (111) silver surface cluster.	73
Figure 4.19 Relative energy profile along reaction coordinate (C2-O) for ethylene oxide formation on oxygen atom adsorbed on 13 atoms (111) silver surface cluster.	74
Figure 4.20 Relative energy profile along reaction coordinate (H-O) for vinyl alcohol formation on oxygen atom adsorbed on (001) silver surface cluster.	75
Figure 4.21 Relative energy profile along reaction coordinate (H-C2) for ethyl aldehyde formation on oxygen atom adsorbed on (001) silver surface cluster.	76
Figure 4.22 A summary energy diagram showing a comparison of the entire paths for ethylene epoxidation on (111) silver cluster.....	77
Figure 4.23 Equilibrium geometry for atomic oxygen adsorption on Ag ₁₃ (111) a) Top view b) Side view.	79
Figure 4.24 Relative energy profile along reaction coordinate (C1-O1) for ethylene oxide formation on oxygen atoms (4O) adsorbed on 13 atoms (111) silver surface cluster.....	80
Figure 4.25 Relative energy profile along reaction coordinate (C2-O1) for ethylene oxide formation on oxygen atoms (4O) adsorbed on 13 atoms (111) silver surface cluster.....	81

Figure 4.26 A summary energy diagram showing a comparison for ethylene oxide formation on (111) surface with different coverage values.	82
Figure 4.27 Optimized geometry of atomic O adsorption on slab a) Top view, b) Side view.	84
Figure 4.28 Optimized geometry of OMME on slab a) Top view, b) Side view.	85
Figure 4.29 Optimized geometry of ethylene oxide ethyl aldehyde on slab a) Top view, b) Side view.	85
Figure 4.30 Optimized geometry of ethyl aldehyde on slab a) Top view, b) Side view.	86
Figure 4.31 Optimized geometry of vinyl alcohol on slab a) Top view, b) Side view.	86
Figure 4.32 A summary energy diagram for ethylene epoxidation on 4-layer-(3x3) slab.	87
Figure 4.33 Relative energy profile along reaction coordinates (H-O) for C-H activation of ethylene on oxygen atom adsorbed on (001) silver oxide surface cluster.	89
Figure 4.34 Relative energy profile along reaction coordinate (C1-O) for ethylene oxide formation on oxygen atom adsorbed on (001) silver oxide surface cluster.	90
Figure 4.35 Relative energy profile along reaction coordinate (C2-Ag4) for oxametallacycle molecule formation on oxygen atom adsorbed on (001) silver oxide surface cluster.	91
Figure 4.36 Relative energy profile along reaction coordinate (C2-O) for ethylene oxide formation on oxygen atom adsorbed on (001) silver oxide surface cluster.	92
Figure 4.37 Relative energy profile along reaction coordinate (H-C2)	

for ethyl aldehyde formation on oxygen atom adsorbed on (001) silver oxide surface cluster.	93
Figure 4.38 Relative energy profile along reaction coordinate (H-O1) for vinyl alcohol formation on oxygen atom adsorbed on (001) silver oxide surface cluster.	94
Figure 4.39 A summary energy diagram showing a comparison of the entire paths for ethylene epoxidation on (001) silver oxide cluster.....	96
Figure 4.40 A reaction mechanism for propylene epoxidation.....	98
Figure 4.41 7 Relative energy profile along reaction coordinates (H-O) for C-H activation of propylene on oxygen atom adsorbed on 13 atoms (111) silver surface cluster.	100
Figure 4.42 Relative energy profile along reaction coordinate (C1-O) for ethylene oxide formation on oxygen atom adsorbed on (111) silver surface cluster.	101
Figure 4.43 Relative energy profile along reaction coordinate (C2-Ag4) for oxametallacycle molecule formation on oxygen atom adsorbed on (111) silver surface cluster.	102
Figure 4.44 Relative energy profile along reaction coordinate (C2-O) for ethylene oxide formation on oxygen atom adsorbed on (111) silver surface cluster.	103
Figure 4.45 Relative energy profile along reaction coordinate (C2-O) for ethylene oxide formation on oxygen atom adsorbed on (111) silver surface cluster.	104
Figure 4.46 Relative energy profile along reaction coordinate (C1-Ag4) for oxametallacycle molecule formation on oxygen atom adsorbed on (111) silver surface cluster.	105
Figure 4.47 Relative energy profile along reaction coordinate (C1-O) for ethylene oxide formation on oxygen atom adsorbed on (111)	

silver surface cluster.	106
Figure 4.48 Relative energy profile along reaction coordinate (H-C2) for propanal formation on oxygen atom adsorbed on (111) silver surface cluster.	107
Figure 4.49 Relative energy profile along reaction coordinate (H-C1) for acetone formation on oxygen atom adsorbed on (111) silver surface cluster.	108
Figure 4.50 A summary energy diagram showing a comparison of the entire paths for propylene epoxidation on (111) silver cluster.....	110
Figure 4.51 OMMP1 on slab (a) Top view, (b) Side view.....	111
Figure 4.52 OMMP2 on slab (a) Top view, (b) Side view.....	112
Figure 4.53 Propylene oxide on slab (a) Top view, (b) Side view.....	112
Figure 4.54 Propanal on slab (a) Top view, (b) Side view.....	113
Figure 4.55 Acetone on slab (a) Top view, (b) Side view.....	113
Figure 4.56 A summary energy diagram for ethylene epoxidation on 4-layer-(3x3) slab.	114
Figure 4.57 Relative energy profile along reaction coordinate (H-O1) for C-H activation of propylene on (001) silver oxide surface cluster.....	117
Figure 4.58 Relative energy profile along reaction coordinate (C1-O1) for propylene oxide formation on (001) silver oxide surface cluster.....	118
Figure 4.59 Relative energy profile along reaction coordinate (C2-Ag2) for oxametallacycle molecule formation on (001) silver oxide surface cluster.	119
Figure 4.60 Relative energy profile along reaction coordinate (C2-O1) for propylene oxide formation on (001) silver oxide surface cluster.	120
Figure 4.61 Relative energy profile along reaction coordinate (C2-O1) for propylene oxide formation on (001) silver	

oxide surface cluster.	121
Figure 4.62 Relative energy profile along reaction coordinate (C1-Ag2) for oxametallacycle molecule formation on (001) silver oxide surface cluster.	122
Figure 4.63 Relative energy profile along reaction coordinate (C1-O1) for propylene oxide formation on (001) silver oxide surface cluster.	123
Figure 4.64 Relative energy profile along reaction coordinate (H-C2) for propanal formation on (001) silver oxide surface cluster.....	124
Figure 4.65 Relative energy profile along reaction coordinate (H-C1) for acetone formation on (001) silver oxide surface cluster.....	125
Figure 4.66 A summary energy diagram showing a comparison of the entire paths for propylene epoxidation on (111) silver oxide surface cluster.	126
Figure 4.67 Equilibrium final geometry for Reaction-40.....	128
Figure 4.68 a) Transition state geometry, b) Equilibrium final geometry for Reaction-41	129
Figure 4.69 a) Transition state geometry, b) Equilibrium final geometry for Reaction-42	130
Figure 4.70 a) Transition state geometry, b) Equilibrium final geometry for Reaction-43	131
Figure 4.71 A summary energy diagram showing a comparison of steps (1-4) for gas phase propylene epoxidation reactions.....	133
Figure C.1 Optimized geometry of Ethylene a) in Gaussian 03 software b) in VASP software.	162
Figure C.2 Optimized geometry of Ethylene Oxide a) in Gaussian 03 software b) in VASP software.	163
Figure C.3 Optimized geometry of Vinylalcohol a) in Gaussian 03	

software b) in VASP software.	163
Figure C.4 Optimized geometry of Vinylaldehyde a) in Gaussian 03 software b) in VASP software.	164
Figure C.5 Optimized geometry of Propylene a) in Gaussian 03 software b) in VASP software.	164
Figure C.6 Optimized geometry of Propyleneoxide a) in Gaussian 03 software b) in VASP software.	165
Figure C.7 Optimized geometry of Acetone a) in Gaussian 03 software b) in VASP software.	165
Figure C.8 Optimized geometry of Propanal a) in Gaussian 03 software b) in VASP software.	166

CHAPTER 1

INTRODUCTION

1.1. Importance of Catalysis

A catalyst, by definition, is a material that is used to convert reactants to products without itself being consumed. The goal then is to tailor atomically the structure of an active catalyst so as to convert reactants directly to products without the production of by-products along the way which typically go on to become waste. Catalysts then by nature would help eliminate the production of side products, thus eliminating most waste (van Santen and Neurock, 2006).

In terms of chemical conversions, catalysts are responsible for the production of over 60% of all chemicals that are made and are used in over 90% of all chemical processes worldwide. This accounts for 20% of the Gross Domestic Products in the USA. Catalyst manufacturing alone accounts for over \$10 billion in sales worldwide and is spread out across four major sectors: refining, chemicals, polymerization, and exhaust emission catalysts (Thomas and Thomas 1997, Gates et al. 1979). Refining is the largest sector with the production of catalysts for alkylation, cracking, hydrodesulphurization, fluid catalytic cracking, hydrocracking, isomerization, and reforming chemistry. The value derived from catalyst sales, however, is really only a very small fraction of the total value derived from catalysis overall, which includes the value of the products that are produced, i.e. chemical intermediates,

polymers, pesticides, pharmaceuticals, and fuels. The overall impact of catalysis is estimated to be \$10 trillion per year. The intermediates made by catalysis are used in the production of materials, chemicals, and control devices that cross many different manufacturing industries including petroleum, chemicals, pharmaceuticals, automotives, electronic materials, food and energy (van Santen and Neurock, 2006).

It is clear that catalysis plays an important role in society today and will be a critical technology for advancing our future.

1.2. Light Alkenes Epoxidation

The heterogeneous epoxidation of alkenes, especially ethene (ethylene) and propene (propylene), is a topic of enduring interest—both from the point of view of fundamental chemistry, and with respect to the importance, or potential importance, of these processes in modern chemical technology. The reactions involved are mechanistically interesting and both epoxides are commercially valuable intermediates (Lambert et al., 2005).

Ethylene (ethene), C_2H_4 , is the largest volume building block for many petrochemicals. This olefin is used to produce many end products such as plastics, resins, fibers, etc (Kirk-Othmer Encyclopedia of Chemical Technology).

The primary use for ethylene oxide, C_2H_4O , is in the manufacture of derivatives such as ethylene glycol, surfactants, and ethanolamines. Although early manufacture of ethylene oxide was accomplished by the chlorohydrin process the direct oxidation process has been used almost exclusively since 1940. In 1931, Lefort achieved direct oxidation of ethylene to ethylene oxide using a silver catalyst. Compared to the chlorohydrin process, direct

oxidation eliminates the need for large volumes of chlorine. Also, there are no chlorinated hydrocarbon by-products to be sold, processing facilities can be made simpler, and operating costs are lower (Kirk-Othmer Encyclopedia of Chemical Technology).

Ethylene oxide is produced by oxidizing ethylene (See Figure 1.1). The reaction is carried out over a supported metallic silver catalyst at 250–300°C and 1–2 MPa (10–20 bar). A few parts per million (ppm) of 1,2-dichloroethane are added to the ethylene to inhibit further oxidation to carbon dioxide and water. This results in chlorine generation, which deactivates the surface of the catalyst (Kirk-Othmer Encyclopedia of Chemical Technology).

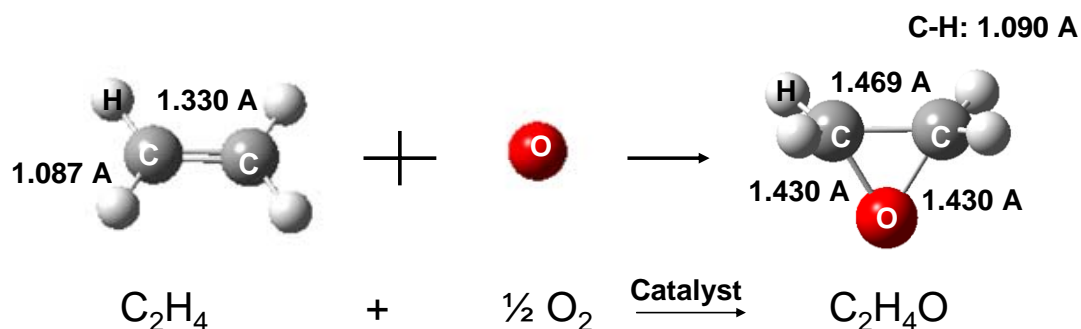


Figure 1.1 Ethylene epoxidation reaction (Geometries were optimized by using Gaussian 03 software)

Propylene (propene), CH_3CHCH_2 , is perhaps the oldest petrochemical feedstock and is one of the principal light olefins. It is used widely as an alkylation or polymer-gasoline feedstock for octane improvement. In addition, large quantities of propylene are used in plastics as polypropylene, and in chemicals, e.g., acrylonitrile, propylene oxide, 2-propanol, and cumene (Kirk-Othmer Encyclopedia of Chemical Technology).

Propene oxide ($\text{CH}_3\text{CHCH}_2\text{O}$), which is also known as propylene oxide, methyloxirane, or 1,2-epoxypropane, is one of the most important starting materials in the chemical industry. The production of propene oxide consumes over 10% of all propene produced (Nijhuis et al., 2006).

Propene epoxide is an even more valuable product than ethene epoxide: it is a strategically important and versatile chemical intermediate whose manufacture accounts for $\sim 10\%$ of total European usage of propene. Two thirds of this is consumed in the manufacture of polyether polyols, the rest being converted to propene glycols, glycol ethers and other materials that have a wide range of applications. However, heterogeneous epoxidation of propene is a much tougher problem to solve: Ag catalysts deliver only very low selectivity over a wide range of conditions and catalyst formulations. As a result, propylene epoxide is currently produced by either (i) the old chlorohydrin process, environmentally unfriendly because it involves the use of chlorine or (ii) a newer homogenous route that involves co-production of propene epoxide and styrene. It has been proposed, and seems to be generally agreed, that the difficulty with propene epoxidation resides in the ease with which an allylic hydrogen atom may be stripped from the molecule, a process that presumably shuts off the epoxidation channel and results in combustion (Lambert et al., 2005).

Because these co-products are produced in a volume that is ~ 3 times larger than that of propene oxide, the economy of the process is primarily dominated by the market of the co-product. A major research effort has been made in the development of alternative direct epoxidation processes seen in Figure 1.2 for the production of propene oxide (Nijhuis et al., 2006).

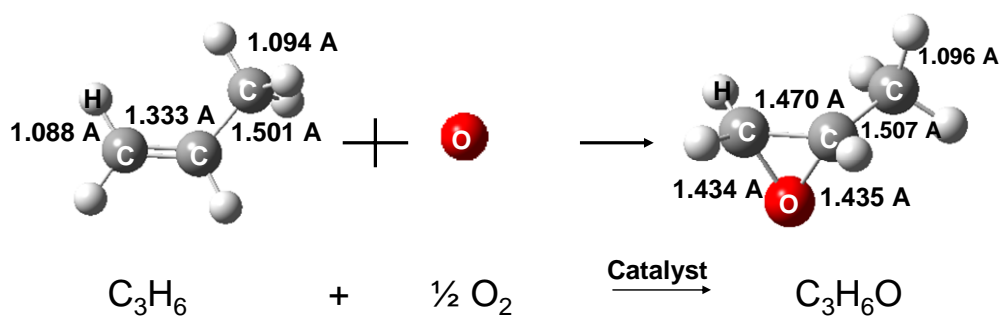


Figure 1.2 Propylene epoxidation reaction (Geometries were optimized by using Gaussian 03 software)

1.3. Computational Chemistry

Computational chemistry is a branch of chemistry that uses the results of theoretical chemistry incorporated into efficient computer programs to calculate the structures and properties of molecules and solids, applying these programs to real chemical problems. Examples of such properties are structure, energy and interaction energy, charges, dipoles and higher multipole moments, vibrational frequencies, reactivity or other spectroscopic quantities, and cross sections for collision with other particles. The term computational chemistry is also sometimes used to cover any of the areas of science that overlap between computer science and chemistry. Electronic configuration theory is the largest subdiscipline of computational chemistry.

The term theoretical chemistry may be defined as a mathematical description of chemistry, whereas computational chemistry is usually used when a mathematical method is sufficiently well developed that it can be automated for implementation on a computer. Note that the words exact and perfect do not appear here, as very few aspects of chemistry can be computed exactly. Almost every aspect of chemistry, however, can be described in a qualitative or approximate quantitative computational scheme.

Molecules consist of nuclei and electrons, so the methods of quantum mechanics apply. Computational chemists often attempt to solve the non-relativistic Schrödinger equation, with relativistic corrections added, although some progress has been made in solving the fully relativistic Schrödinger equation. It is, in principle, possible to solve the Schrödinger equation, in either its time-dependent form or time-independent form as appropriate for the problem in hand, but this in practice is not possible except for very small systems. Therefore, a great number of approximate methods strive to achieve the best trade-off between accuracy and computational cost. Present computational chemistry can routinely and very accurately calculate the properties of molecules that contain no more than 10-40 electrons. The treatment of larger molecules that contain a few dozen electrons is computationally tractable by approximate methods such as density functional theory (DFT). There is some dispute within the field whether the latter methods are sufficient to describe complex chemical reactions, such as those in biochemistry. Large molecules can be studied by semi-empirical approximate methods. Even larger molecules are treated with molecular mechanics methods which belong to classical mechanics in general.

In theoretical chemistry, chemists and physicists together develop algorithms and computer programs to predict atomic and molecular properties and reaction paths for chemical reactions. Computational chemists, in contrast, may simply apply existing computer programs and methodologies to specific chemical questions. There are two different aspects to computational chemistry:

- Computational studies can be carried out in order to find a starting point for a laboratory synthesis, or to assist in understanding experimental data, such as the position and source of spectroscopic peaks.

- Computational studies can be used to predict the possibility of so far entirely unknown molecules or to explore reaction mechanisms that are not readily studied by experimental means.

Thus computational chemistry can assist the experimental chemist or it can challenge the experimental chemist to find entirely new chemical objects.

Several major areas may be distinguished within computational chemistry:

- The prediction of the molecular structure of molecules by the use of the simulation of forces to find stationary points on the energy hyper surface as the positions of the nuclei are varied.
- Storing and searching for data on chemical entities (see chemical databases).
- Identifying correlations between chemical structures and properties (see QSPR and QSAR).
- Computational approaches to help in the efficient synthesis of compounds.
- Computational approaches to design molecules that interact in specific ways with other molecules (e.g. drug design).
- Computational approaches to identify the catalytic surface reaction mechanisms.

1.3.1. Molecular Mechanics (MM) Methods

In many cases, large molecular systems can be modeled successfully while avoiding quantum mechanical calculations entirely. Molecular mechanics simulations, for example, use a single classical expression for the energy of a compound, for instance the harmonic oscillator. All constants appearing in the equations must be obtained beforehand from experimental data or ab-initio calculations.

The database of compounds used for parameterization - (the resulting set of parameters and functions is called the force field) - is crucial to the success of molecular mechanics calculations. A force field parameterized against a specific class of molecules, for instance proteins, would be expected to only have any relevance when describing other molecules of the same class.

The term molecular mechanics refers to the use of Newtonian mechanics to model molecular systems. Molecular mechanics approaches are widely applied in molecular structure refinement, molecular dynamics simulations, Monte Carlo simulations and ligand docking simulations. Molecular mechanics is used to study small chemical systems with a few atoms, or large biological systems or material assemblies with many thousands to millions of atoms. These systems can be investigated either in vacuum or in presence of solvent such as water. The simulations in vacuum are referred to as gas-phase simulations while the presence of solvent molecules is referred to as explicit solvent simulations. In another type of simulation, the effect of solvent is estimated by use of empirical mathematical expression, known as implicit solvation simulation.

Molecular mechanics methods are based on the following principles:

- Nuclei and electrons are considered as a single atom-like particle,

- Atom-like particles are spherical (radii is obtained from measurements or theoretical considerations) and is assigned a net charge (obtained from theoretical considerations),
- Interactions are based on springs (representing bonds) and classical potentials,
- Interactions must be preassigned to specific sets of atoms,
- Interactions determine the spatial distribution of atom-like particles and their energies.

This function, referred to as potential function, computes the molecular potential energy as a sum of energy terms that describe the deviation of bond lengths, bond angles and torsion angles away from equilibrium values, plus terms for non-bonded pairs of atoms describing Van der Waals and electrostatic interactions. The set of parameters consisting of equilibrium bond lengths, bond angles, partial charge values, force constants and Van der Waals parameters are collectively known as force field. Different implementations of molecular mechanics use slightly different mathematical expressions, and therefore, different constants for potential function. The common force-fields in use today have been developed by using high level quantum calculations and fitting to experimental data. The technique, known as energy minimization, is used to minimize the potential function. Lower energy states are more stable and are commonly investigated due to their role in chemical and biological processes. A molecular dynamics simulation, on the other hand, computes the behavior of system as a function of time. It involves solving Newton's equation of motion, $F = ma$. Integration of Newton's equation of motion, using different integration algorithms, leads to atomic trajectories in space and time. The forces on atoms are defined as the negative gradient of the potential energy function. The energy

minimization technique is useful for obtaining a static picture for comparison between states or similar systems, while molecular dynamics provides information about the dynamic processes with the inclusion of temperature effects.

1.3.2. Semi- Empirical and Empirical Methods

Semi-empirical quantum chemistry methods are based on the Hartree-Fock formalism, but make many approximations and obtain some parameters from empirical data. They are very important in computational chemistry for treating large molecules where the full Hartree-Fock method without the approximations is too expensive. The use of empirical parameters appears to allow some inclusion of correlation effects into the methods.

Semi-empirical methods follow what are often called empirical methods where the two-electron part of the Hamiltonian is not explicitly included. For n -electron systems, this was the Hückel method proposed by Erich Hückel, and for all valence electron systems, the Extended Hückel method proposed by Roald Hoffmann.

Within the framework of Hartree-Fock calculations, some pieces of information (such as two-electron integrals) are sometimes approximated or completely omitted. In order to correct for this loss, semi-empirical methods are parametrized, that is their results are fitted by a set of parameters, normally in such a way as to produce results that best agree with experimental data, but sometimes also adjusted in accordance with ab-initio results (Wolfram and Holthausen, 2001).

Semi-empirical calculations are much faster than their ab-initio counterparts. Their results, however, can be very wrong if the molecule being computed is

not similar enough to the molecules in the database used to parameterize the method.

Semi-empirical calculations have been most successful in description of organic chemistry, where only a few elements are used extensively and molecules are of moderate size.

As with empirical methods, we can distinguish methods that are restricted to pi-electrons. These methods exist for the calculation of electronically excited states of polyenes, both cyclic and linear. These methods, such as the Pariser-Parr-Pople method (PPP), can provide good estimates of the pi-electronic excited states, when parameterized well. Indeed, for many years, the PPP method outperformed ab-initio excited state calculations. In contrast to their Hartree-Fock-based Semiempirical methods counterparts (i.e. MOPAC), the pi-electron theories have a very strong ab-initio basis. The PPP formulation is actually an approximate pi-electron effective operator, and the empirical parameters, in fact, include effective electron correlation effects. A rigorous, ab-initio theory of the PPP method is provided by diagrammatic, multi-reference, high order perturbation theory (Freed, Brandow, etc).

Methods such as CNDO/2, INDO and NDDO were introduced by John Pople. These methods are now rarely used but the methodology often forms the basis of later methods.

Methods that are in the MOPAC and/or AMPAC computer programs which are originally from the group of Michael Dewar are MINDO, MNDO, AM1, PM3 and SAM1. Here the objective is to use parameters to fit experimental heats of formation. Methods whose primary aim is to calculate excited states and hence predict electronic spectra include ZINDO and SINDO (Wolfram and Holthausen, 2001).

1.3.3. ab-initio Methods

The programs used in computational chemistry are based on many different quantum-chemical methods that solve the molecular Schrödinger equation associated with the molecular Hamiltonian. Methods that do not include any empirical or semi-empirical parameters in their equations - being derived directly from first principles, with no inclusion of experimental data - are called ab-initio methods. This does not imply that the solution is an exact one. They are all approximate quantum mechanical calculations. It means that a particular approximation is carefully defined and then solved as exactly as possible. If numerical iterative methods have to be employed, the aim is to iterate until full machine accuracy is obtained (the best that is possible with a finite word length on the computer). There are three ab-initio methods. These are Hartree-Fock (HF) method, Density Functional Theory (DFT) method and Møller-Plesset Perturbation Theory (MP) method.

1.3.3.1. Hartree-Fock (HF) Methods

The simplest type of ab-initio electronic structure calculation for molecules is the Hartree-Fock Roothaan (HFR) scheme. Only its average effect is included in the calculation. As the basis set size is increased the energy and wave function tend to a limit called the Hartree-Fock limit. Many types of calculations, known as post-Hartree-Fock methods, begin with a Hartree-Fock calculation and subsequently correct for electron-electron repulsion, referred to also as electronic correlation. As these methods are pushed to the limit, they approach the exact solution of the non-relativistic Schrödinger equation. In order to obtain exact agreement with experiment, it is necessary to include relativistic and spin orbit terms, both of which are only really important for heavy atoms. In all of these approaches, in addition to the choice of method, it is necessary to choose a basis set. This is set of

functions, usually centered on the different atoms in the molecule, which are used to expand the molecular orbital with the LCAO ansatz. Ab-initio methods need to define a level of theory (the method) and a basis set.

The Hartree-Fock wave function is a single configuration or determinant. In some cases, particularly for bond breaking processes, this is quite inadequate and several configurations need to be used. Here the coefficients of the configurations and the coefficients of the basis functions are optimized together. The total molecular energy can be evaluated as a function of the molecular geometry, in other words the potential energy surface (Wolfram and Holthausen, 2001).

One of the limitations of HF calculations is that they do not include electron correlation. This means that HF takes into account the average affect of electron repulsion, but not the explicit electron-electron interaction. Within HF theory the probability of finding an electron at some location around an atom is determined by the distance from the nucleus but not the distance to the other electrons. This is not physically true, but it is the consequence of the central field approximation, which defines the HF method.

1.3.3.2. Møller-Plesset Perturbation Theory (MP) Methods

Correlation can be added as a perturbation from the Hartree-Fock wave function. This is called Møller-Plesset perturbation theory. In mapping the HF wave function onto a perturbation theory formulation, HF becomes a first-order perturbation. Thus, a minimal amount of correlation is added by using the second order MP2 method. Third-order (MP3) and fourth-order (MP4) calculations are also common. The accuracy of an MP4 calculation is roughly equivalent to the accuracy of a CISD calculation. MP5 and higher calculations

are seldom done due to the high computational cost (N^{10} time complexity or worse).

Møller-Plesset calculations are not variational. In fact, it is not uncommon to find MP2 calculations that give total energies below the exact total energy. Depending on the nature of the chemical system, there seem to be two patterns in using successively higher orders of perturbation theory. For some systems, the energies become successively lower and closer to the total energy in going from MP2 to MP3, to MP4, and so on, as shown in Figure 3.2. For other systems, MP2 will have energy lower than the exact energy, MP3 will be higher, MP4 will be lower, and so on, with each having an error that is lower in magnitude but opposite in sign. If the assumption of a small perturbation is not valid, the MPn energies may diverge. This might happen if the single determinant reference is a poor qualitative description of the system. One advantage of Møller-Plesset is that it is size extensive (Wolfram and Holthausen, 2001).

1.3.3.3. Density Functional Theory (DFT) Methods

Density functional theory (DFT) methods are often considered to be ab-initio methods for determining the molecular electronic structure, even though many of the most common functional use parameters are derived from empirical data, or from more complex calculations. This means that they could also be called semi-empirical methods. It is best to treat them as a class on their own. In DFT, the total energy is expressed in terms of the total electron density rather than the wave function. In this type of calculation, there is an approximate Hamiltonian and an approximate expression for the total electron density. DFT methods can be very accurate for little computational cost. The drawback is, that unlike ab-initio methods, there is

no systematic way to improve the methods by improving the form of the functional (Wolfram and Holthausen, 2001).

Description of the theory

Traditional methods in electronic structure theory, in particular Hartree-Fock theory and its descendants, are based on the complicated many-electron wavefunction. The main objective of density functional theory is to replace the many-body electronic wavefunction with the electronic density as the basic quantity. Whereas the many-body wavefunction is dependent on $3N$ variables, three spatial variables for each of the N electrons, the density is only a function of three variables and is a simpler quantity to deal with both conceptually and practically (Wolfram and Holthausen, 2001).

Although density functional theory has its conceptual roots in the Thomas-Fermi model, DFT was not put on a firm theoretical footing until the Hohenberg-Kohn (HK) theorems. The first of these demonstrates the existence of a one-to-one mapping between the ground state electron density and the ground state wavefunction of a many-particle system. Further, the second HK theorem proves that the ground state density minimizes the total electronic energy of the system. The original HK theorems held only for the ground state in the absence of magnetic field, although they have since been generalized. The first Hohenberg-Kohn theorem is only an existence theorem, stating that the mapping exists, but does not provide any such exact mapping. It is in these mappings that approximations are made. (The theorems can be extended to the time-dependent domain (TDDFT), which can be also used to determine excited states)

The most common implementation of density functional theory is through the Kohn-Sham method. Within the framework of Kohn-Sham DFT, the

intractable many-body problem of interacting electrons in a static external potential is reduced to a tractable problem of non-interacting electrons moving in an effective potential. The effective potential includes the external potential and the effects of the Coulomb interactions between the electrons, e.g. the exchange and correlation interactions. Modeling the latter two interactions becomes the difficulty within KS DFT. The simplest approximation is the local-density approximation (LDA), which is based upon exact exchange energy for a uniform electron gas, which can be obtained from the Thomas-Fermi model, and from fits to the correlation energy for a uniform electron gas (Wolfram and Holthausen, 2001).

DFT has been very popular for calculations in solid state physics since the 1970s. In many cases DFT with the local-density approximation gives quite satisfactory results, for solid-state calculations, in comparison to experimental data at relatively low computational costs when compared to other ways of solving the quantum mechanical many-body problem. However, it was not considered accurate enough for calculations in quantum chemistry until the 1990s, when the approximations used in the theory were greatly refined to better model the exchange and correlation interactions. DFT is now a leading method for electronic structure calculations in both fields. Despite the improvements in DFT, there are still difficulties in using density functional theory to properly describe intermolecular interactions, especially van der Waals forces (dispersion), or in calculations of the band gap in semiconductors. Its poor treatment of dispersion renders DFT unsuitable (at least when used alone) for the treatment of systems which are dominated by dispersion (e.g. interacting noble gas atoms) or where dispersion competes significantly with other effects (e.g. in biomolecules). The development of new DFT methods designed to overcome this problem, by alterations to the functional or by the inclusion of additive terms, is a current research topic. Figure 1.3 shows the number of publications where

the phrases 'DFT' or 'density functional theory' appear in the title or abstract or topic from a search covering the years from 1990 to 2007.

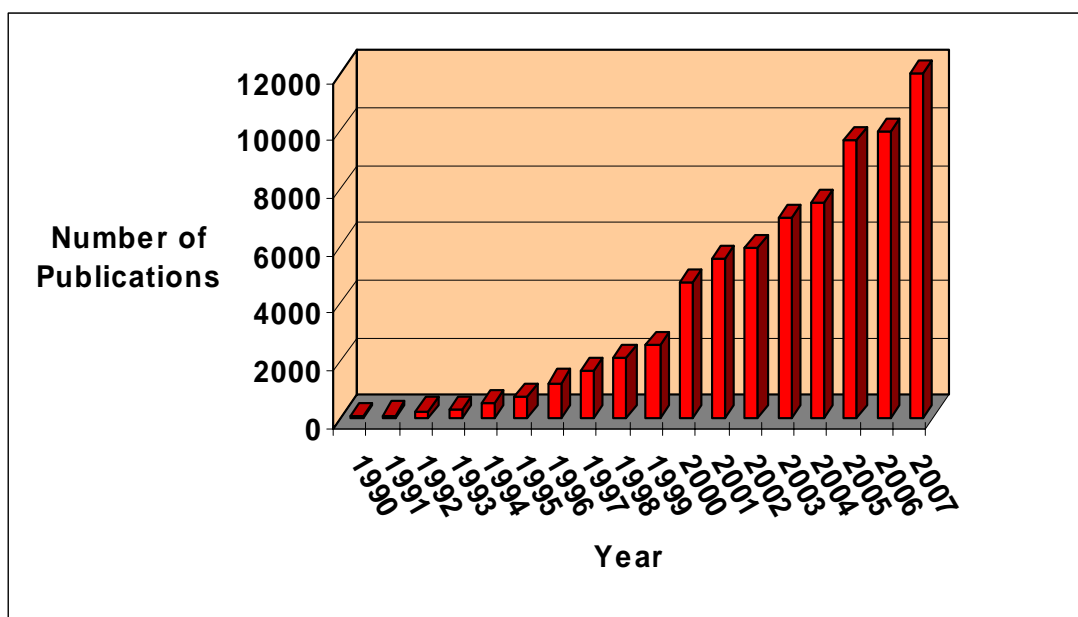


Figure 1.3 Number of publications of DFT (Wolfram and Holthausen, 2001) (Numbers for years between 2000 and 2007 were obtained by using ISI Web of Knowledge)

Figure 1.4 shows a comparison of calculation types according to the accuracy and computational effort. While going to MP2 method, accuracy and computational effort increases. Figure 1.5 also shows computational SPE CPU time requirements of calculation methods for propylene molecule and C60 molecule. SPE calculations for these molecules were done on PC with 8 cores and 15 GB Ram in Gaussian'03 software. B3LYP/6-31g** method and MP2/6-31g** method were used for DFT and MP2 calculations, respectively. As seen from the parts a and b of Figure 1.5, CPU time changes with numbers of atoms in system and it exponentially increases with increasing atom numbers.

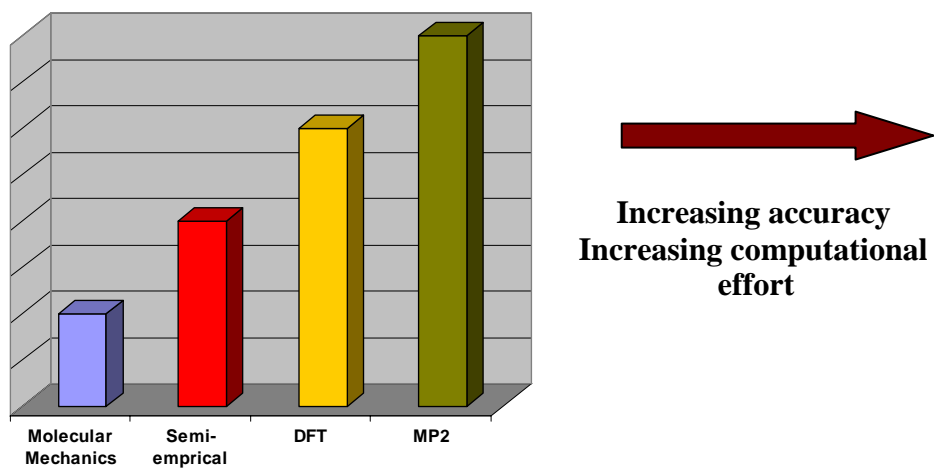


Figure 1.4 A comparison of calculation methods

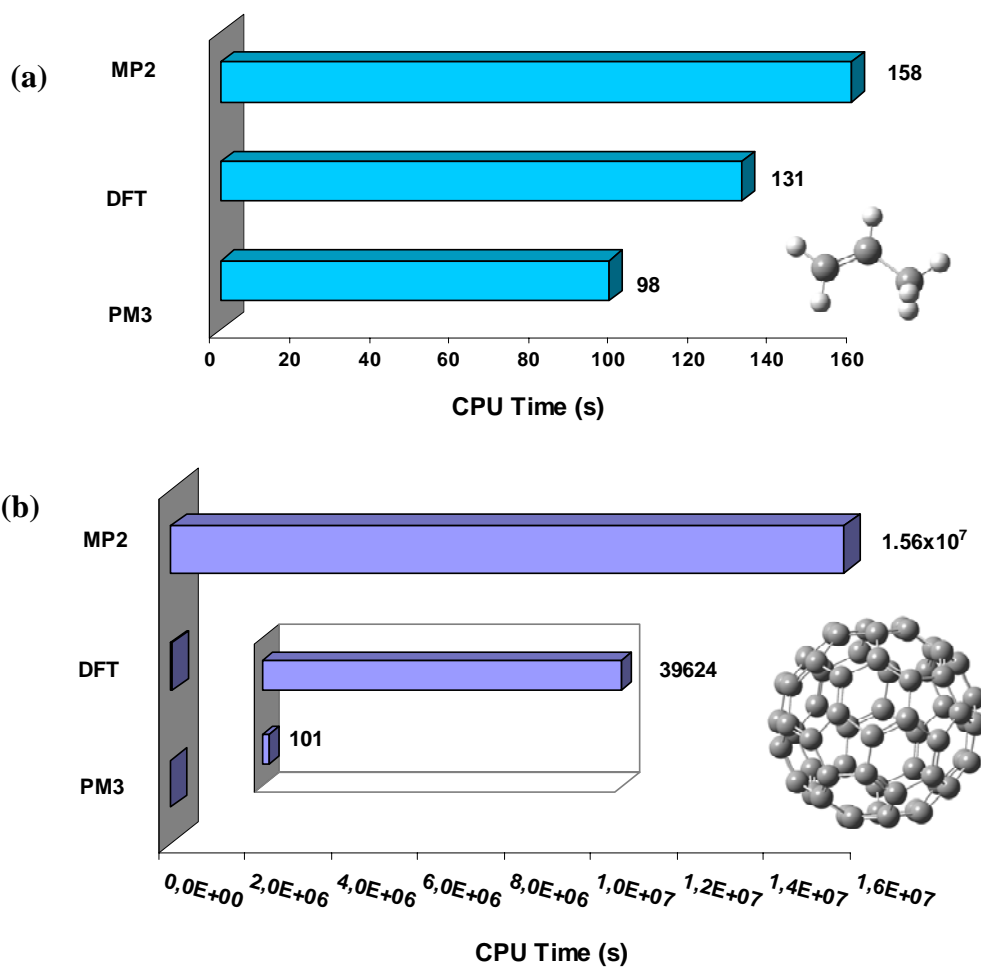


Figure 1.5 SPE Computational CPU time requirements of methods a) for propylene molecule and b) for C60 molecule

1.4. Theoretical and Simulation Methods for Catalysis

One of the ultimate goals in modeling heterogeneous catalytic reaction systems would be the development of a multiscale approach that could simulate the numerous of atomic scale transformations which occur on the catalyst surface as they unfold as a function of time, processing conditions and catalyst structure and composition. The simulation would establish all of the elementary physicochemical paths available at a specific instant in time, determine the most likely reaction paths by which to proceed and then accurately calculate the elementary kinetics for each process along with the influence of the local reaction environment internal on the simulation. Additionally, the simulation would predict how changes in the particle size, morphology, chemical composition, shape and atomic configurations would influence the catalytic performance, including activity, selectivity and lifetime (van Santen and Neurock, 2006).

The detailed prediction on the state of adsorbed species can be validated by comparison with experimental studies on well-defined model surfaces and model catalytic systems under controlled reaction conditions for which adequate theoretical modeling techniques are available. This includes the prediction of adsorbate surface structure, their properties and their reactivity. This can be determined by comparing the surface structure of adsorbed intermediates under idealized conditions measured through scanning tunneling microscopy (STM), and low energy electron diffraction (LEED), vibrational frequencies from high resolution electron energy loss spectroscopy (HREELS) or reflection adsorption infrared spectroscopy (RAIRS), and their adsorption and reactivity measured from temperature programmed desorption (TPD) and temperature programmed reaction (TPR) spectroscopy, or microcalorimetry. This provides quantitative information on the elementary adsorption and reaction steps that occur on these model surfaces (van Santen and Neurock, 2006).

Most of the calculations on heterogeneous catalytic systems today use ab-initio density functional theoretical methods. DFT (density functional theory) is fairly robust and allows a first-principle-based treatment of complex metal and metal oxide systems whereby electron correlation is included at significantly reduced CPU cost. DFT can be used to calculate structural properties and typically reports accuracies to within 0.05 Å and 1-2°, overall adsorption and reaction energies that are typically within 20-35 kJ/mol and spectroscopic shifts that are within a few percent of experimental data (van Santen and Neurock, 2006).

A comparison between experimental adsorption energies for different adsorbates on different metal surfaces estimated from UHV temperature-programmed desorption studies and those calculated using density functional theory is shown in Figure 1.6. Although this is a very useful first step, the differences are certainly not within the 5 kJ/mol engineering accuracy that one would like.

The success in modeling catalytic systems depends not only on the accuracy of the methods employed, but also on the reality of the model chosen to mimic the actual reaction system studied. A single metal atom, for example, would be a poor choice for modeling a transition-metal surface regardless of the accuracy of the method used. The model can not capture the metal band structure. This leads to errors that are at least as large as those from the accuracy of the method (van Santen and Neurock, 2006).

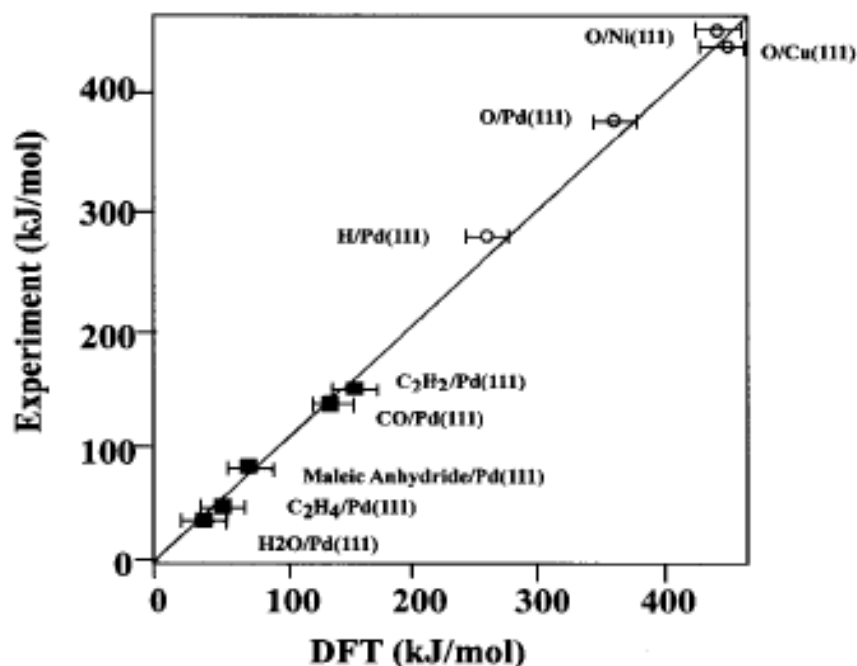


Figure 1.6 A comparison of calculated and experimental chemisorption energies for different adsorbates on different metal surfaces where empty circles are used for atomic adsorption and dark squares are used for adsorption of molecules (van Santen and Neorock 2006).

There are three different techniques that are currently used to model the structure at the active site, known as cluster, embedded cluster, and periodic methods. Each method has its own set of advantages and disadvantages. Characteristic models for each of these systems are presented in Figure 1.7.

In the cluster approach, a discrete number of atoms are used to represent only the very local region about the active site. The basic premise is that chemisorption and reactivity are local phenomena, primarily affected only by the nearby surface structure.

In the embedded cluster approach, a rigorous QM (Quantum Mechanics) method is used to model the local region about the active site. This primary cluster is then embedded into a much larger model which simulates the

external structural and electronic environment. The outer model employs a much simpler quantum-mechanical treatment or an empirical force field to simulate the external environment but still tends to treat the atomic structure explicitly. This minimizes cluster-size artifacts. The outer model can subsequently be embedded in yet a third model, which is made of point charges in order to treat longer range electrostatic interactions and the Madelung potential.

The last approach is the periodic slab method. In this approach one defines a unit cell which comprises a large enough surface ensemble. Periodic boundary conditions are then used to expand the cell in the x, y, and/or z directions, thus providing the electronic structure for linear, slab (surface), and bulk materials, respectively (van Santen and Neurock, 2006).

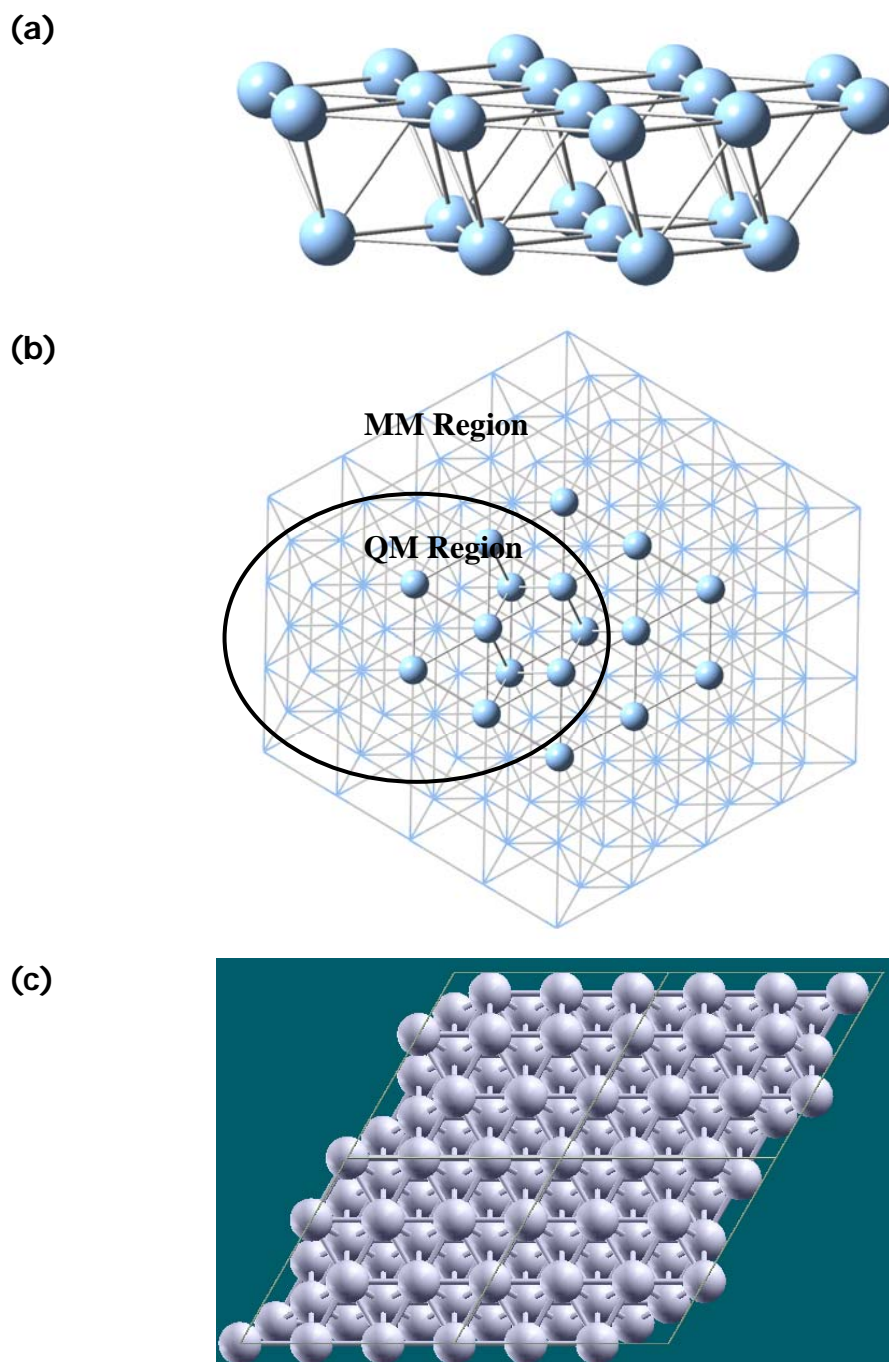


Figure 1.7 Characteristic models for modeling. Silver (111) surface a) cluster approach, b) embedding scheme (QM region is represented by ball-bond view and MM region is represented by wire frame view), c) periodic slab model

1.5. The Objective of This Study

The aim of this study is to investigate and compare ethylene and propylene epoxidation reactions and to identify the mechanistic steps via which these reactions occur on both Silver and Silver Oxide surfaces by use of DFT calculations. These calculations were studied in Gaussian'03 and VASP softwares. Besides investigating reactions which give main products such as ethylene oxide and propylene oxide, the reactions which result in ethylene aldehyde, vinyl alcohol and vinyl radical for ethylene epoxidation and propanal, acetone and pi-allyl radical for epoxidation of propylene on silver and silver oxide surfaces were studied. All coordinate driving calculations which give the relative energy profile for a reaction were made by using Gaussian 03 software which uses a cluster surface model.

CHAPTER 2

LITERATURE SURVEY

The heterogeneous epoxidation of alkenes, especially ethylene and propene, is a topic of enduring interest—both from the point of view of fundamental chemistry, and with respect to the importance, or potential importance, of these processes in modern chemical technology. The reactions involved are mechanistically interesting and both epoxides are commercially valuable intermediates.

Ethylene is the largest volume building block for many petrochemicals. This olefin is used to produce many end products such as plastics, resins, fibers and ethylene oxide, etc. Although early manufacture of ethylene oxide was accomplished by the chlorohydrin process, the direct oxidation process has been used almost exclusively since 1940. Compared to the chlorohydrin process, direct oxidation eliminates the need for large volumes of chlorine. Also, there are no chlorinated hydrocarbon by-products to be sold, processing facilities can be made simpler, and operating costs are lower. In direct ethylene oxidation reaction, Ag is used as catalyst (Kirk-Othmer Encyclopedia of Chemical Technology).

Propylene oxide is a significant organic chemical used primarily as a reaction intermediate for production of polyether polyols, propylene glycol, alkanolamines, glycol ethers, and many other useful products. Propene epoxide is an even more valuable product than ethylene epoxide: it is a

strategically important and versatile chemical intermediate. However, heterogeneous epoxidation of propene is a much tougher problem to solve: Ag catalysts deliver only very low selectivities over a wide range of conditions and catalyst formulations. As a result, propylene epoxide is currently produced by either (i) the old chlorohydrin process, environmentally unfriendly because it involves the use of chlorine or (ii) a newer homogenous route that involves co-production of propene epoxide and styrene. It has been proposed that the difficulty with propene epoxidation resides in the ease with which an allylic hydrogen atom may be stripped from the molecule, a process that presumably shuts off the epoxidation channel and results in combustion (Lambert et al., 2005).

There is a long history of experimental research for ethylene oxide formation due to its industrial importance. Ethylene epoxidation on silver was experimentally studied by several research groups (Campbell, 1984, 1985, 1986; Carter and Goddard, 1988; Sachtler et al., 1981; Verykios et al., 1980; Larrabee and Kuczkowski, 1978; Barteau, 1981; Akimoto et al., 1982; Kanoh et al., 1979; Linic and Barteau, 2001, 2004; Geenen et al., 1982). Considerable effort has been devoted to understanding the mechanism of silver-catalyzed ethylene epoxidation as outlined in reviews by several studies (Verykios et al., 1980; Sachtler et al., 1981; van Santen and Kuipers, 1987). The issues most often addressed have been the roles of oxygen and the promoters in the reaction. Grant and Lambert (Lambert et al., 1985) carried out fundamental studies using primarily Ag 111 and Ag 110 single crystals which provided evidence for the key role of atomic rather than molecular oxygen in both the epoxidation and combustion reactions. Attempts to use the analogy of ethylene epoxidation in propylene epoxidation with molecular O₂ over Ag/Al₂O₃ catalyst, however, failed due to the presence of allylic H atoms in propylene, which upon facile abstraction result in rapid combustion of propylene to CO₂ and water (Cant and Hall, 1978; Imachi et al., 1981; Akimoto et al., 1982).

As part of a continuing effort to understand the mechanism of olefin epoxidation, Barteau and co-workers (Mavrikakis et al., 1998; Jones et al., 1998; Medlin and Barteau, 1999) used density functional theory (DFT) calculations to demonstrate that surface oxametallacycles are moderately stable with respect to the corresponding gas-phase monoolefin epoxides. Linic and Barteau (Linic, 2002) used temperature programmed desorption, high-resolution electron energy loss spectroscopy (HREELS), and density functional theory (DFT) to investigate the adsorption and reaction of ethylene oxide (EO) on the Ag(111) surface and observed that when the ring-opening of EO is activated, a stable surface intermediate is formed. HREELS and DFT studies suggested that this stable intermediate is a surface oxametallacycle. Figure 2.1 shows computed IR spectra Ag_3 clusters for the OME (Oxygen-Metal-Ethylene) and OMME (Oxygen-Metal-Metal-Ethylene) structures and experimental HREEL spectrum of the surface intermediate.

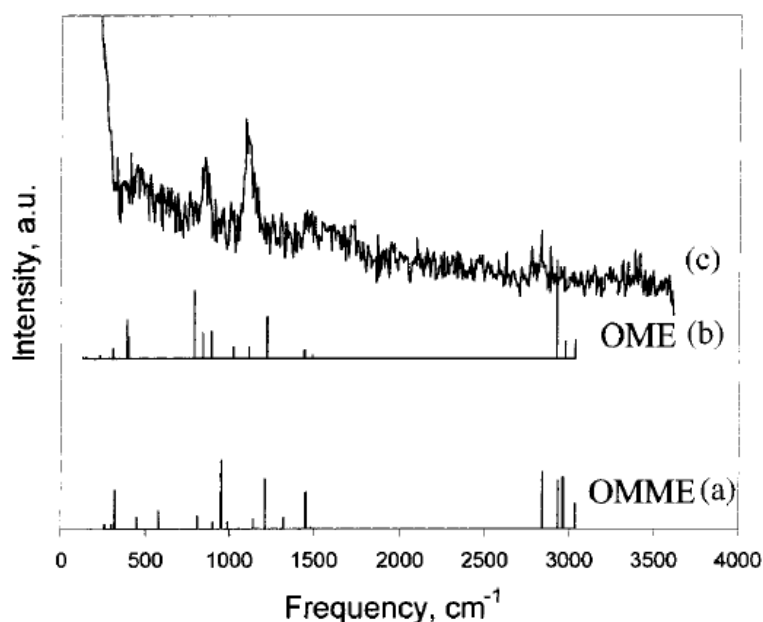


Figure 2.1 Calculated and experimental IR vibrational spectra of oxametallacycles on an Ag_3 cluster. (a) OMME structure; (b) OME structure; (c) HREEL spectrum of the surface intermediate (Linic and Barteau, 2001).

By comparing the calculated spectra to the HREEL spectrum obtained after EO was adsorbed onto Ag(111) at 250 K, shown in Figure 2.1, it was reported that oxametallacycle structure is the best geometry for the surface intermediate (Linic and Barteau, 2001).

Moreover, the activation energies observed for the reaction of the oxametallacycle to form EO were in an excellent agreement with the values reported for the steady-state ethylene epoxidation process. Linic and Barteau (Linic and Barteau, 2003a; 2003b) further used DFT calculations to investigate a possible reaction coordinate for the epoxidation of ethylene on silver and concluded that reactions of surface oxametallacycles control the selectivity of ethylene epoxidation on silver catalysts at moderate conversions. They obtained various surface intermediates and transition states along the reaction coordinate with structures, binding energies, and vibrational frequencies that were in good agreement with experimental results.

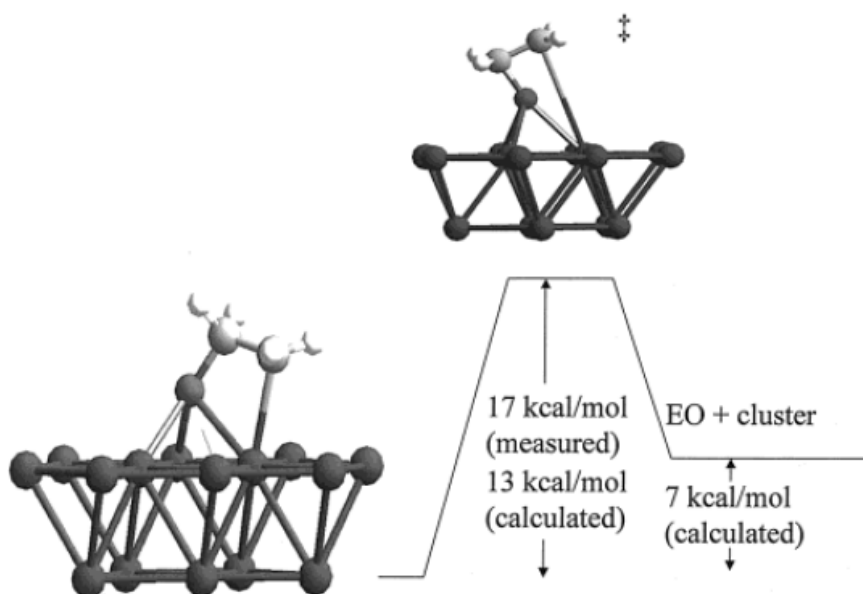


Figure 2.2 Schematic of the reaction coordinate for oxametallacycle ringclosure to yield EO (Linic and Barteau, 2001).

DFT calculations indicated that ethylene reacts with adsorbed oxygen to form a surface intermediate, identified as a surface oxametallacycle. This intermediate reacts through a transition state to form gas-phase ethylene oxide. Schematic of the reaction coordinate for oxametallacycle ring closure to yield EO is shown in Figure 2.2. Activation barrier for ethylene oxide formation was experimentally reported as 17 kcal/mol on Ag(111) surface and 16 kcal/mol as theoretical (on Ag₁₅(111) surface cluster) in their study (Linic and Barteau, 2003b).

In another theoretical DFT study (Torres et al., 2005), a comparison between Ag(111) and Cu(111) surfaces for ethylene oxide formation was made. It was reported that activation barrier for this reaction is 18.5 kcal/mol for Ag(111) surface and 16.8 kcal/mol for Cu(111) surface. A semiempirical method (AM1-d) was used for ethylene oxide formation on both Ag(111) and Ag(110) surfaces by Jomoto and co-workers (Jomoto et al., 2002). They reported that activation barrier is 19.2 kcal/mol for (111) surface and 13.6 kcal/mol for (110) surface (hill site).

Ethylene oxide formation from the ethylene oxametallacycle was studied experimentally and theoretically on Ag(110) surface by several studies (Medlin and Barteau, 2001; Lukaski and Barteau, 2009). The activation barrier for ethylene oxide formation on Ag₁₂(110) was calculated to be 9.6 kcal/mol. A comparison for the selectivity of epoxidation of ethylene was experimentally made for both Ag(111) and Ag(110) surfaces (Campbell, 1985). In this study, it was reported that the (111) plane is thought to predominate on the surface of real catalysts, due to its thermodynamic stability. (110) surface is more active than (111) and (100) surfaces. It was also experimentally reported that the activity of (111) surface is a factor of 2 less than that of the (110) surface.

Nano clusters have been also investigated for ethylene oxide formation reaction. Ag₇ silver nano clusters (as neutral and ionic) were used by Yu (Yu, 2006). They reported barrier heights are between 0.7 and 6.5 kcal/mol.

There is no theoretical study of ethylene epoxidation on silver oxide in literature except for surface oxide structures such as Ag₁₁O₆ (Bocquet et al., 2003; 2003; 2005) and Ag₁₂O₆ (Gao et al., 2007) on silver (111) surface and Ag₂O⁺ cation (Roithova and Schröder, 2007). Recent experimental and theoretical STM studies indicate stoichiometries such as Ag_{1.83}O (Bocquet et al., 2005; 2003) and Ag_{1.33}O (Michaelides et al., 2005; Schmid et al., 2006). Bocquet and co-workers (Carlisle et al., 2000; Michaelides et al., 2003) have characterized two stable O phases which are low coverage (0.05 ± 0.02 ML) O adatom phase and an Ag_{1.8}O oxide overlayer on Ag(111) by the scanning tunneling microscope (STM) and DFT. They reported that a DFT-derived phase diagram predicted that the Ag_{1.8}O oxide overlayer would be stable under typical industrial conditions for epoxidation (Michaelides et al., 2003). It was reported that a stoichiometry of Ag_(x=2 ± 0.2)O and an ionic component in the Ag_{3d} spectrum at 367.7 eV allow to conclude the formation of a surface silver (I) oxide that is confirmed by the similarity of its spectral characteristics with those of bulk Ag₂O (Bukhtiyarov et al., 2003).

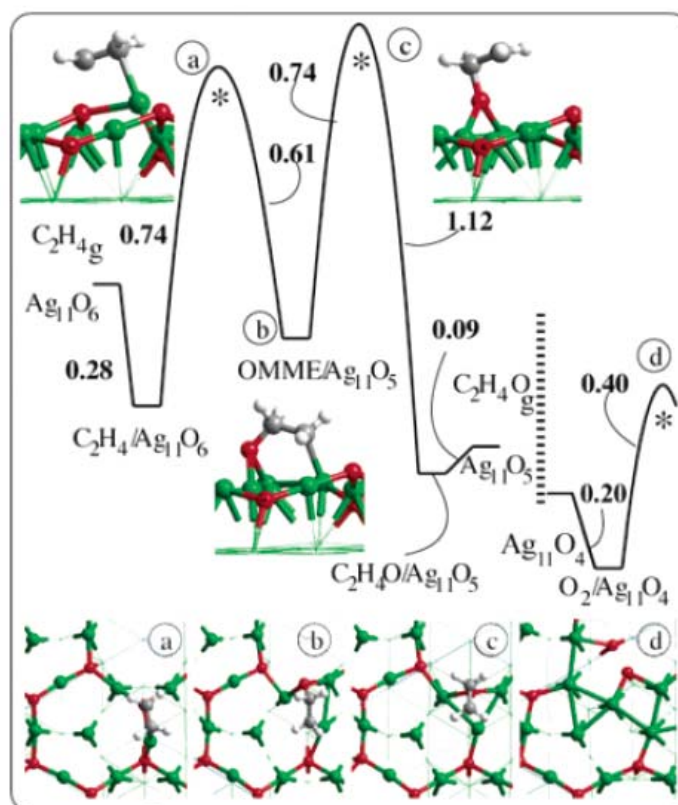


Figure 2.3 Relative energy diagram for the conversion of gas-phase C_2H_4 to epoxide, on the high coverage $Ag_{1.8}O$ ($Ag_{11}O_6$) layer on $Ag(111)$ (Energies are in unit of eV) (Bocquet et al., 2003)

Kobayashi et al. have investigated the reaction mechanisms for propylene and ethylene oxide formation on Ag and Au catalysts using 5 and 7 atom cluster models by means of DFT method. They reported that the reaction with an O_2 molecule will leave an active O atom on the surface, and furthermore in the reaction with an O atom, it has to be bound on the surface at the beginning. Experimentally, the adsorption and dissociation of O_2 molecule is very fast, and the adsorption of O species is much stronger than that of ethylene. A characteristic difference between Au and Ag is a high energy for Au_5-O intermediate, which means that dissociated O atom is unstable on Au_5 cluster. Compared to the reaction on Ag_5 cluster, Au_5 cluster does not effectively stabilize and catalyze ethylene oxidation. They finally reported that Au metal was not a good catalyst for ethylene oxide formation

since adsorption of the dissociated O atom is not stable on Au₅ cluster. The energetics of propylene and oxygen species on Ag₅ cluster reveals that the H atom abstraction leading to p-allyl occurs more easily than the O atom insertion leading to propylene oxide with either O₂ or O species as oxidizing agent. The same reactions were reexamined with a larger Ag₇ cluster modeling the step site. The p-allyl formation was favored with O₂ molecule, and both of the reactions proceed without selectivity with O atom (Kobayashi et al., 2006).

Joshi and coworkers studied partial oxidation of propylene to propylene oxide using H₂ and O₂ on a neutral Au₃ cluster by using DFT. The O₂ adsorbed on Au₃ facilitates the dissociative adsorption of H₂ to form a OOH intermediate, which remains adsorbed on the Au₃. The activation barrier for this step is only 2.2 kcal/mol. The activation barrier for propylene epoxidation step is 19.6 kcal/mol. Product propylene oxide (PO), which interacts with the Au₃, requires about 11.5 kcal/mol to desorb. This activation barrier is comparable to the barriers reported (15-20 kcal/mol) in several other olefin epoxidation mechanisms on Ti sites in the absence of Au. Therefore, we advance the possibility of the Au playing a larger role than the mere production of the oxidizing agent from the H₂ and O₂ by offering a competitive epoxidation channel to that occurring on Ti (Joshi et al., 2006).

Chretien and coworkers have studied interaction between gold and silver clusters and propene by using DFT method. The behavior of the system for partial oxidation is strongly dependent on the size of the gold and silver clusters. They reported that for a given cluster size, the electron affinities of the Ag clusters are smaller than the ones of the Au clusters. Since electron affinity is a measure of the tendency of the cluster to accept an electron. They predict that propene will bind more weakly to Ag_n than Au_n. The electron affinities of the mixed Au/Ag clusters are in between the ones of the pure Au and Ag clusters. Therefore, the desorption energy of propene from

the mixed Au/Ag clusters should be larger than from the Ag clusters and less than that of the Au clusters. Moreover, propene should bind more strongly to a Ag atom in the mixed cluster than in the pure Ag cluster and more weakly to the Au cluster in the mixed cluster than on the same Au atom in a pure Au cluster. The electronegativity of Au is larger than that of silver, so the silver atoms in the mixed cluster are more positive than in the pure Ag clusters and the Au clusters in the mixed clusters are more negative than those in the pure Au (Chretien et al., 2004a; 2004b; 2004c).

The properties of supported Au at different coverages with TiO₂ have been described by Lopez and Nørskov (Lopez and Nørskov, 2002). They say that the catalytic properties of gold depend on the support, the preparation method and the size of the metallic clusters. They reported that at low coverages, the most stable site is the adsorption on the protruding O atoms while at medium coverages the fivefold coordinated Ti is preferred and at higher coverages several sites at the rutile surface are simultaneously occupied.

Most recent experimental publications on the direct gas phase oxidation of propylene to propylene oxide by molecular oxygen reported that the yield and selectivity of reaction is very low. Although the direct oxidation of ethylene by molecular oxygen to ethylene oxide has been commercialized with silver catalysts, it is known that the analogous direct oxidation of propylene exhibits a low selectivity of less than 15%. Some patent suggest that the use of metal promoted silver catalysts for propylene oxide (PO) synthesis. These promoted catalysts also exhibit low selectivity to PO. Multi-component systems such as copper-phosphate-potassium, uranium dioxide, or thallium-cobalt mixed oxides have been reported for the gas-phase oxidation of propylene, all of which suffer from low PO selectivity. In fact, the production of PO by the direct, i.e. non-catalytic, gas-phase interaction of

propylene and oxygen was higher than in the presence of catalysts considered (Mills and Nicole, 2004).

Gold exhibited high selectivity when finely dispersed on titania catalysts in the presence of hydrogen. Haruta and co-workers have reported of more than 90 % PO (propylene oxide) selectivity with 1-2 % conversion at temperature 303 and 393 K at a space velocity of about 1000 h⁻¹. In subsequent papers the researchers also reported PO and/or propanol (PaL) formation from propylene and the promotional effect by cesium which had significant influence on H₂ and O₂ consumption over Au/Ti-MCM-41 catalysts (Hayashi et al., 1998).

While Nijhuis et al. confirmed the reproducibility of the results over Au/TS-1 and Au/TiO₂, they have also suggested that high yields of propylene oxide (PO) may be limited by the oligomerization of PO. Some recent patents also claim high selectivity to PO by passing propylene, H₂ and O₂ over novel supported precious metal catalysts (mainly Au-based) however, the yields were generally under 1% (Nijhuis et al., 1999).

Silica supported, sodium promoted ion oxide catalysts were found to catalyze the gas-phase oxidation of propylene with nitrous oxide. PO (propylene oxide) selectivity of 40-60% at 6-12% propylene conversion was achieved. However, the use of nitrous oxide as a reactant renders this process uneconomical (Duma and Hönicke, 1999).

In a report (Laufer and Hoelderich, 2001), the direct oxidation with an O₂-H₂ gas mixture in the presence of precious metal containing Ti-catalysts shows an alternative route to oxidize propylene to propylene oxide (PO). They showed that milder reduction condition at 50 °C decreased the side reaction of hydrogenation but only very low PO yields were obtained. The pre-impregnation of the catalyst with salt and the use of alcohols or ketones

as solvent for the impregnation of the catalyst with precious metal improved the PO selectivity.

Propylene epoxidation over a Pd–Pt/TS-1 catalyst with in situ formed hydrogen peroxide carried out in a fixed bed reactor under high pressure conditions was reported by Jenzer et al. They observed that the initial propylene oxide selectivity was very high, 99% at 3.5% conversion, but the catalyst deactivated rapidly with time-on-stream and successively the formation of methyl formate became the prevalent reaction. Using carbon dioxide, instead of nitrogen, had a beneficial effect on the formation of propylene oxide, and even higher yields were obtained when increasing the pressure from 50 to 120 bar (supercritical fluid phase) (Jenzer et al., 2001).

Ti and Al containing MCM-41 (Al-c-MCM-41 and Al-Ti-c-MCM-41) have been synthesized and tested for direct oxidation of propylene with molecular oxygen by Murata et al. Al-Ti-c-MCM-41 is more effective than Al-c-MCM-41, while no product was formed for MCM-41 alone. It is also found that MCM-22 with Si/Al₂ ratio of 30 and Na/SiO₂ ratio of 0.18 is active for the reaction and a highest PO yield of 11.3% was obtained at 573 K and 3% when Si/Al₂ of 150 and Si/Ti ratios 100 were used at 523 °C. And they showed that the catalyst system consisting of Pd, Ti-modified MCM-22, and methanol was found to catalyze the epoxidation of propylene with molecular oxygen without hydrogen and PO was formed with a PO yield above 19.5% and 458 turnovers based on palladium. In their next study they indicated that the catalytic system containing Pd(Oac)₂ and peroxo-heteropoly compound [(C₆H₁₃)₄N]₃{PO₄[W(O)(O₂)₂]₄} (denoted by THA-PW4) in methanol showed 81.6% selectivity for propylene oxide at a propylene conversion of 42.7 % using molecular oxygen as an oxidant in an autoclave reactor at 373 K for 6 h, whereas, Pd(Oac)₂ or THA-PW4 alone showed low conversions (Murata et al., 2003; 2003; 2004).

Direct oxidation of propylene was studied through the application of the techniques of combinatorial catalysts by Miyazaki et al. (Miyazaki et al., 2003). They prepared catalytic materials containing different metal loading levels and showed that the most PO active metal calcinations were Rh, Mn and Mo. In the second step of search, catalytic materials containing binary combinations of metals were prepared and tested. However, the binary catalytic materials that exhibited the highest PO production levels always contained Rh, the combination of Rh-Ag, Rh-Zn and Rh-Cr were significant leads with regard to high PO and low CO₂ production.

Nijhuis et al. have reported a review of the existing processes used for the production of propylene oxide. The existing processes used for the production of propene oxides, the chlorohydrin and hydroperoxide processes, and their advantages and disadvantages and the new processes and catalysts under development for the propene oxide production are discussed, as well as the challenges that are still limiting the applications of some of those prospects are discussed. The most important new developments for the production of propene oxide reported in this paper are the hydrogen peroxide combination process, the ethene oxide like silver catalysts, the molten salt systems, and the gold-titania catalyst systems (Nijhuis et al., 2006).

MoO₃-modified supported silver catalyst on direct gas-phase epoxidation of propylene to propylene oxide (PO) by molecular oxygen was investigated by Jin et al. The effect of promoter and support on the performance of the Ag–MoO₃ catalyst and their role were investigated by XPS, XRD, SEM, BET surface area, NH₃-TPD, CO₂-TPD techniques and so on. Over the 20 % Ag–4% MoO₃/ZrO₂ catalyst at 400 °C, 0.1 Mpa and space velocity of 7500 h⁻¹, the selectivity to PO of 60.3 % was achieved with the O₂ conversion of 4.8 %; under the space velocity of 12 000 h⁻¹, the selectivity to PO was 71.5 % with 2.5 % O₂ conversion and they showed that suitably larger particles of

Ag and highly dispersed MoO_3 on the $\text{Ag-MoO}_3/\text{ZrO}_2$ catalyst are beneficial to improve the selectivity to propylene oxide (Jin et al., 2004; 2005).

Ananieva and Reitzmann studies at vapour phase epoxidation of propene with nitrous oxide over alkaline containing silica supported iron oxide catalysts. A reaction network is deduced from the trends of product selectivities as function of propene conversion using different catalysts. Rates of the reactions were affected by catalyst composition, which influenced acid-base properties, number of silanol groups and surface area. A PO selectivity of 75% and PO space-time yields of 0.02–0.03 gPO g⁻¹cat h⁻¹ were obtained with a catalyst containing ironoxo-species and caesium ions /-oxides (Ananieva and Reitzmann, 2004).

Amano et al. studied the photo-oxidation of propylene with molecular oxygen over silica-supported vanadium oxide catalysts (VS) at 323 K. The addition of Rb ions to VS resulted in the great improvement of the formation rate of propylene oxide in the photo-oxidation of propylene (175 $\mu\text{mol g}^{-1} \text{h}^{-1}$ for Rb-ion-modified VS, V_2O_5 loading 0.5 wt %, Rb/V = 1.5). The photocatalytic activity was significantly enhanced when the Rb/V ratio was greater than 1.0 (Amano and Tanaka, 2005).

Direct epoxidation of propylene by oxygen was investigated over Ag-based catalysts containing an added 3d transition-metal species (Mn, Fe, Co, or Ni) were investigated by Takahashi et al. They reported that the yield of propylene oxide (PO) depended strongly on the type of metal: the addition of Ni afforded the highest yield of PO at similar values for the conversion of propylene (4–6%). The highest PO selectivity four times that obtained with the Ag single catalyst was obtained at 33 mol% Ni. X-ray diffraction analysis and transmission electron microscopy results showed that the dispersion of Ag particles in the Ag–Ni catalysts increased with increasing Ni content,

which suggests that Ni atoms controlled the Ag particle size by suppressing the sintering of Ag particles (Takahashi et al., 2005).

Lu et al. have investigated propylene epoxidation by air on NaCl-modified silver (NaCl/Ag) catalysts. They characterized the catalysts using X-ray diffraction (XRD) and X-ray photoelectron spectroscopy (XPS). They found that the addition of NaCl to silver significantly increases the propylene oxide (PO) selectivity. The PO yield has a maximum when the NaCl loading is about 10 wt%. Also 12.4% conversion of propylene and 31.6% selectivity to PO are obtained on the NaCl/Ag (10 wt%) catalyst at 350 °C, space velocity $1.8 \times 10^4 \text{ h}^{-1}$ and $\text{C}_3\text{H}_6:\text{O}_2 = 1:2$. XPS and XRD characterizations show that AgCl formed on the silver catalyst was favorable to propylene epoxidation (Lu et al., 2002).

Propylene epoxidation with molecular oxygen as the oxidant using a series of supported Ag catalysts was studied by same group (Lu et al.). They reported that the silver catalysts supported on high surface area supports such as MgO gave low TOF values for PO formation, while the silver catalysts supported on medium surface area supports such as $\alpha\text{-Al}_2\text{O}_3$ and low surface area supports such as CaCO_3 gave high TOF values for PO formation. That is that $\alpha\text{-Al}_2\text{O}_3$ and CaCO_3 were suitable supports for propylene epoxidation and that on the latter Ag particles between 400 and 700 nm gave the highest selectivity to propylene oxide (PO) (Lu et al., 2006).

Wang and coworkers investigated the effects of calcinations atmosphere of the Ag/TS-1 catalyst and other Ti-containing supports on propylene epoxidation using oxygen as the oxidant in a fixed-bed quartz reactor. They reported that 2 wt.% Ag/TS-1 calcined in air is optimum; the Ag/Ti-containing catalysts have catalytic activities in the reaction. The framework titanium species plays an important role, while the extra framework titanium species (280–290 nm) also has weak epoxidation activity in the gas-phase

epoxidation of propylene; excessive extra framework titanium species (280–290 nm) can decrease PO selectivity. The oxidized silver ions are the main active sites for the gas-phase epoxidation of propylene (Wang et al., 2004).

Lu et al. have studied the effect of particle size on ethylene and propylene epoxidation on a series of silver catalysts supported on CaCO_3 with loading levels of 0.5–56 wt%. They showed that large particles favor ethylene epoxidation by 3–5-fold at 473–493 K, whereas particle size does not have a large effect on propylene epoxidation. X-Ray diffraction measurements indicate that the bulk of the particles consist of silver in a metallic state, but in situ ultraviolet–visible (UV–vis) spectroscopy distinctly shows that in addition to a metallic component, small particles have silver in Ag^+ state. The small particles are probably covered by a layer of Ag_2O , which results in lower selectivity for epoxidation for both propylene and ethylene oxidation in the small size regime (Lu et al., 2005).

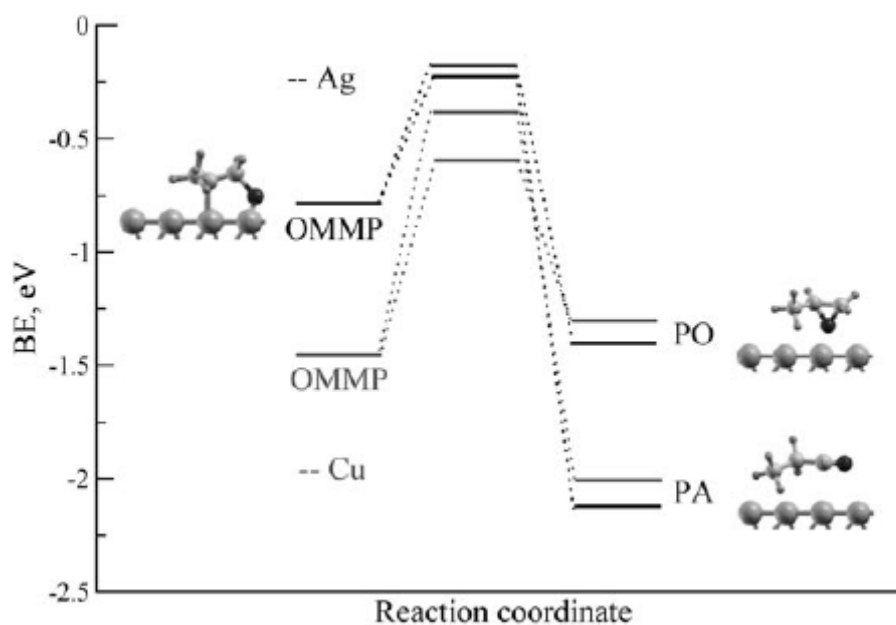


Figure 2.4 Reaction profiles for epoxide and aldehyde formation by rearrangement of OMMP (Torres et al., 2007).

Propylene oxidation on silver and copper (111) surfaces was investigated in a theoretical study (Torres et al., 2007). They used VASP software and periodic method and reported that pi-allyl formation route is more favor than propylene oxide formation route on silver surface. It was also studied aldehyde (propanal) formation route on both surfaces. Figure 2.4 represents reaction profiles of propylene oxide and propanal formation paths on silver and copper surfaces.

CHAPTER 3

SURFACE MODELS AND CALCULATION METHODS

3.1. Computational Procedure for GAUSSIAN Software

All calculations for this case are based on **DFT** (Kohn and Sham, 1965) as implemented in **Gaussian 2003** suit of program (Frisch et al., 2004). Becke's (Becke, 1988,1989) three-parameter hybrid method involving the Lee, Yang, and Parr (Lee et al., 1988) correlation functional (**B3LYP**) formalism by use of Los Alamos **LANL2DZ** (Hay and Wadt, 1985) effective core pseudo-potentials (**ECP**) for silver atoms and **6-31G(d,p)** (Blaudeau et al., 1997) basis set is utilized for carbon, oxygen and hydrogen atoms. It was reported that the hybrid B3LYP method presents excellent descriptions of various reaction profiles, geometries, reaction energies, reaction barriers, and vibrational analyses (Schneider et al., 1997). Energy profile and equilibrium geometry (EG) calculations were in general performed for determination of activation barriers and relative energies.

3.1.1. Silver Surface Model

Silver unit cell has a face centered cubic (fcc) lattice structure with lattice parameter $a = 4.08 \text{ \AA}$ and space group number 225 (Wyckoff, 1963). Wyckoff parameters of silver summarized in Table 3.1 are used to obtain unit cell. By using these parameters, the fractional atomic coordinates were

obtained. Then, these values were multiplied by the lattice parameter in order to obtain the atomic positions of a unit cell of silver in XYZ coordinates in units of Angstrom. Calculated values of the fractional atomic coordinates and the atomic positions of the unit cell of silver are given in Table 3.2. The unit cell geometry of silver is shown in Figure 3.1.

Table 3.1 Wyckoff parameters of Silver

Atom Positions	000
	$\frac{1}{2}0\frac{1}{2}$
	$\frac{1}{2}\frac{1}{2}0$
	$0\frac{1}{2}\frac{1}{2}$
Lattice Parameter	4.08 Å

Table 3.2 Calculated values of the fractional atomic coordinates and the atomic positions of unit cell of Silver

Atom	Fractional Atomic Coordinates			Atomic Positions		
	X	Y	Z	x=X.a	y=Y.a	z=Z.a
Ag	0	0	0	0	0	0
Ag	0.5	0	0.5	2.039	0	2.039
Ag	0.5	0.5	0	2.039	2.039	0
Ag	0	0.5	0.5	0	2.039	2.039

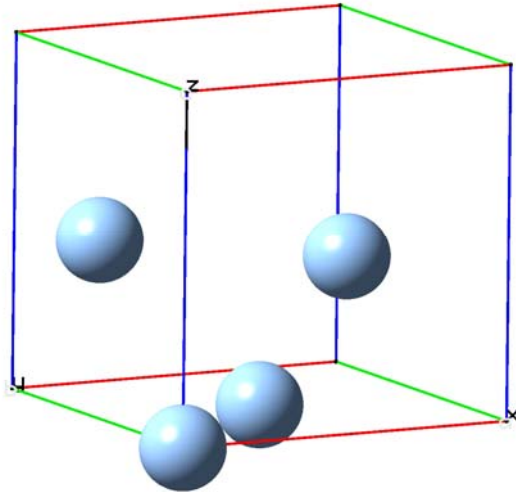


Figure 3.1 Unit cell of Silver

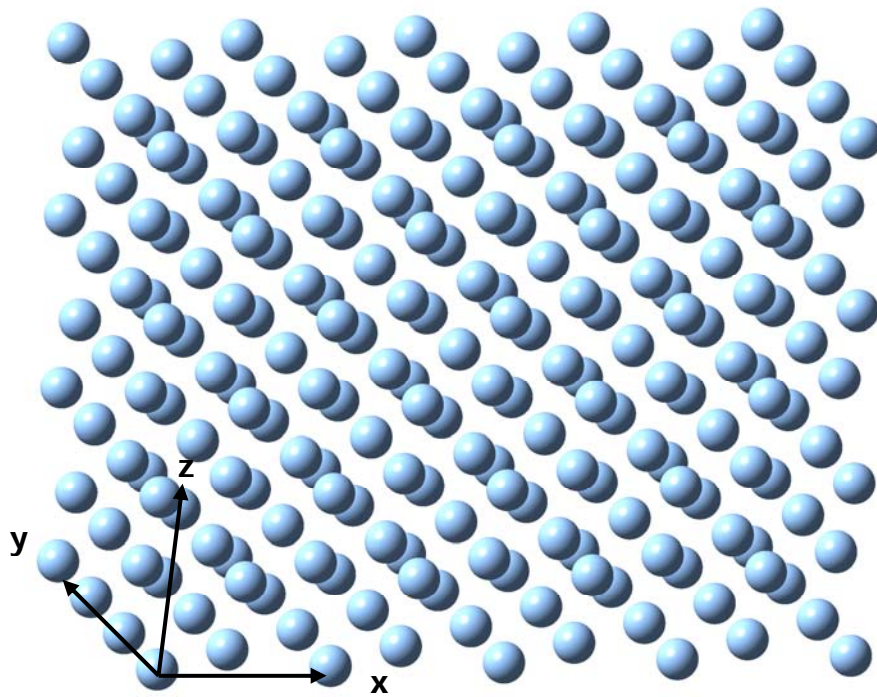


Figure 3.2 Five times enlarged silver unit cell in X,Y and Z directions

In order to obtain a silver cluster, unit cell is enlarged in X, Y and Z directions by several times. Figure 3.2 shows enlargement of silver 5 times in X, Y and Z directions. Silver (111), (110) and (100) surfaces represented in Figure 3.3 are obtained by reduction from the enlarged unit cell.

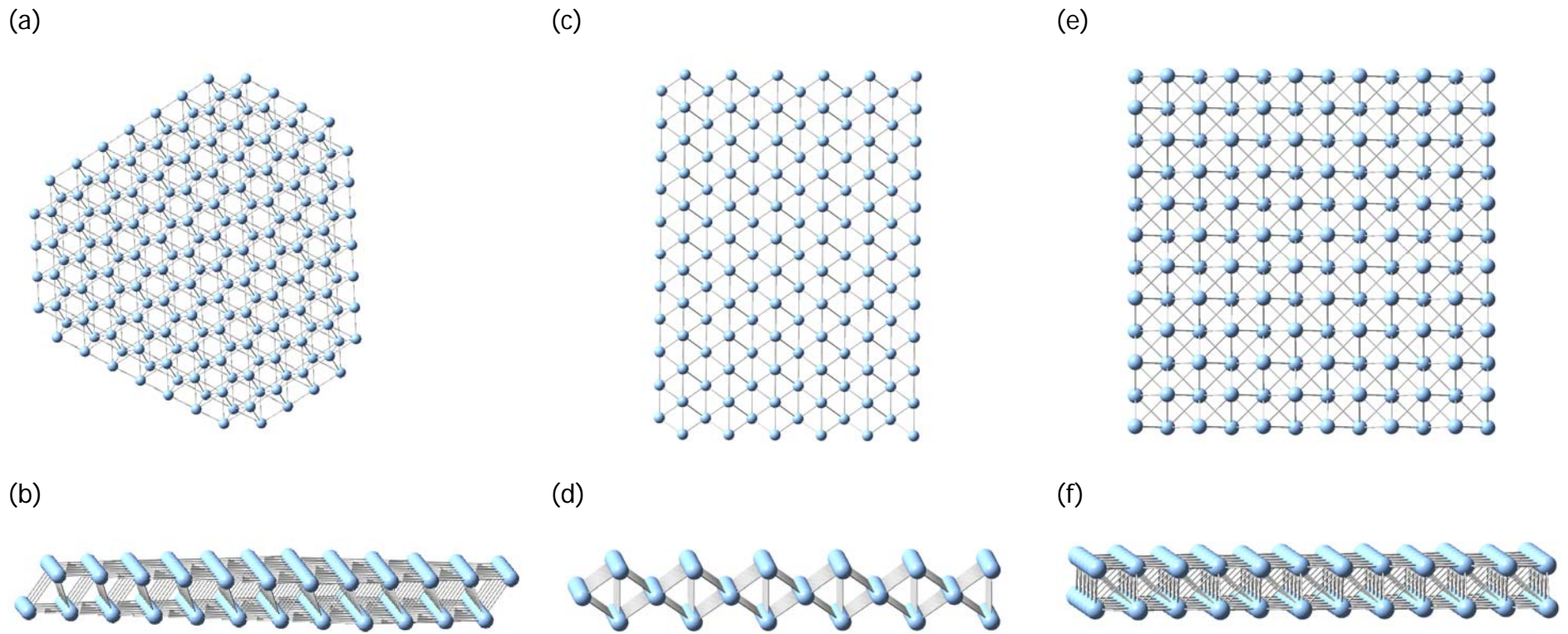
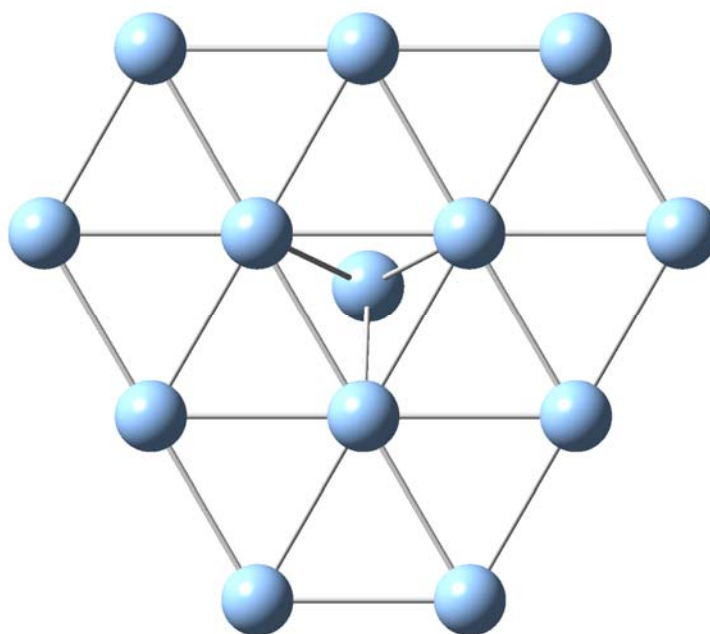


Figure 3.3 Silver surfaces a) Top view of (111) surface, b) Side view of (111) surface, c) Top view of (110) surface, d) Side view of (110) surface, e) Top view of (100) surface, f) Side view of (100) surface

Since chemisorptions and reactivity are local phenomena, primarily affected only by the nearby surface structure (van Santen and Neurock, 2006), a cluster containing 13 silver atoms shown in Figure 3.4 were used for ethylene and propylene oxidation reactions on Gaussian 03 software. The dangling bonds of the silver atoms of the surface cluster are terminated with H atoms which are not shown in Figure 3.4 to obtain a neutral cluster. All of the cluster atoms except the reactant and product molecules were kept fixed.

(a)



(b)

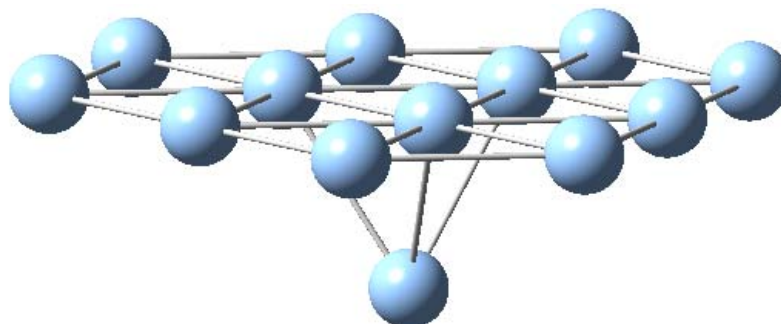


Figure 3.4 $\text{Ag}_{13}(111)$ surface cluster used in this study a) Top view, b) Side view

3.1.2. Silver Oxide Surface Model

Silver oxide unit cell has a face centered cubic lattice structure with lattice parameter $a = 4.723 \text{ \AA}$ and space group number 224 (Karakaya and Thompson, 1992). Cell parameters of silver oxide summarized in Table 3.3 are used to obtain unit cell. The fractional coordinates were obtained by using these parameters. Then, these values were multiplied by the lattice parameter in order to obtain the atomic positions of unit cell of silver oxide in XYZ coordinates in unit of Angstrom. Calculated values of the fractional atomic coordinates and the atomic positions of unit cell of silver oxide are given in Table 3.4. The geometry of unit cell of silver oxide is given Figure 3.5.

Table 3.3 Cell parameters of Silver Oxide

Atom Positions	Ag	000 $\frac{1}{2}0\frac{1}{2}$ $\frac{1}{2}\frac{1}{2}0$ $0\frac{1}{2}\frac{1}{2}$
	O	$\frac{1}{4}\frac{1}{4}\frac{1}{4}$ $\frac{3}{4}\frac{3}{4}\frac{3}{4}$
Lattice Parameter	4.723 \AA	

In order to obtain a silver oxide cluster, unit cell is enlarged in X, Y and Z directions by several times. Figure 3.6 shows enlargement of silver oxide 5 times in X, Y and Z directions.

Table 3.4 Calculated values of the fractional atomic coordinates and the atomic positions of unit cell of Silver Oxide

Atom	Fractional Atomic Coordinates			Atomic Positions		
	X	Y	Z	$x=X.a$	$y=Y.a$	$z=Z.a$
Ag	0	0	0	0	0	0
Ag	0	0.5	0.5	0	2.3615	2.3615
Ag	0.5	0	0.5	2.3615	0	2.3615
Ag	0.5	0.5	0	2.3615	2.3615	0
O	0.25	0.25	0.25	1.18075	1.18075	1.18075
O	0.75	0.75	0.75	3.54225	3.54225	3.54225

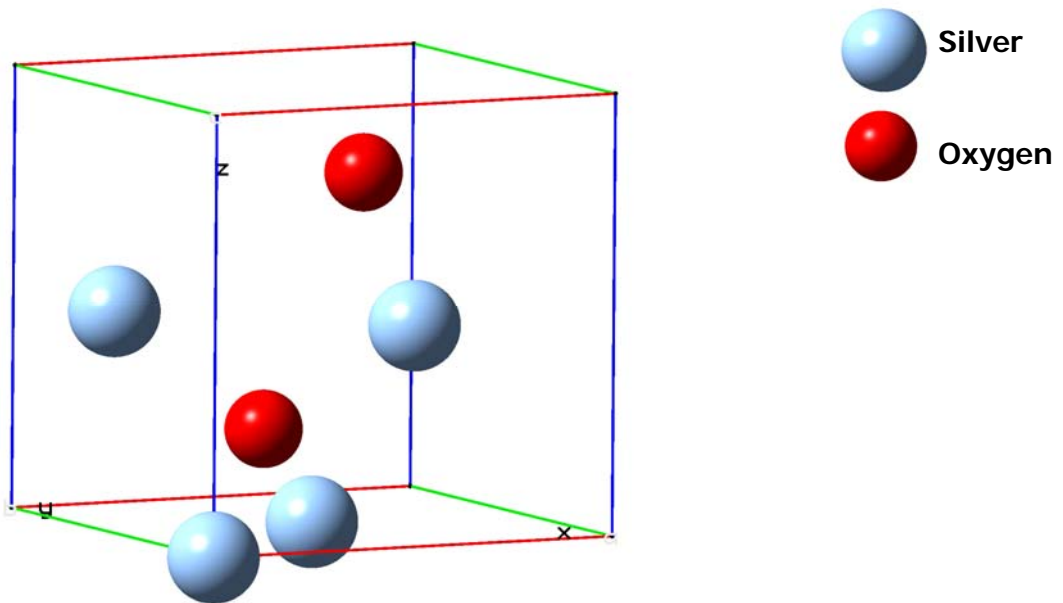


Figure 3.5 Unit cell of Silver Oxide

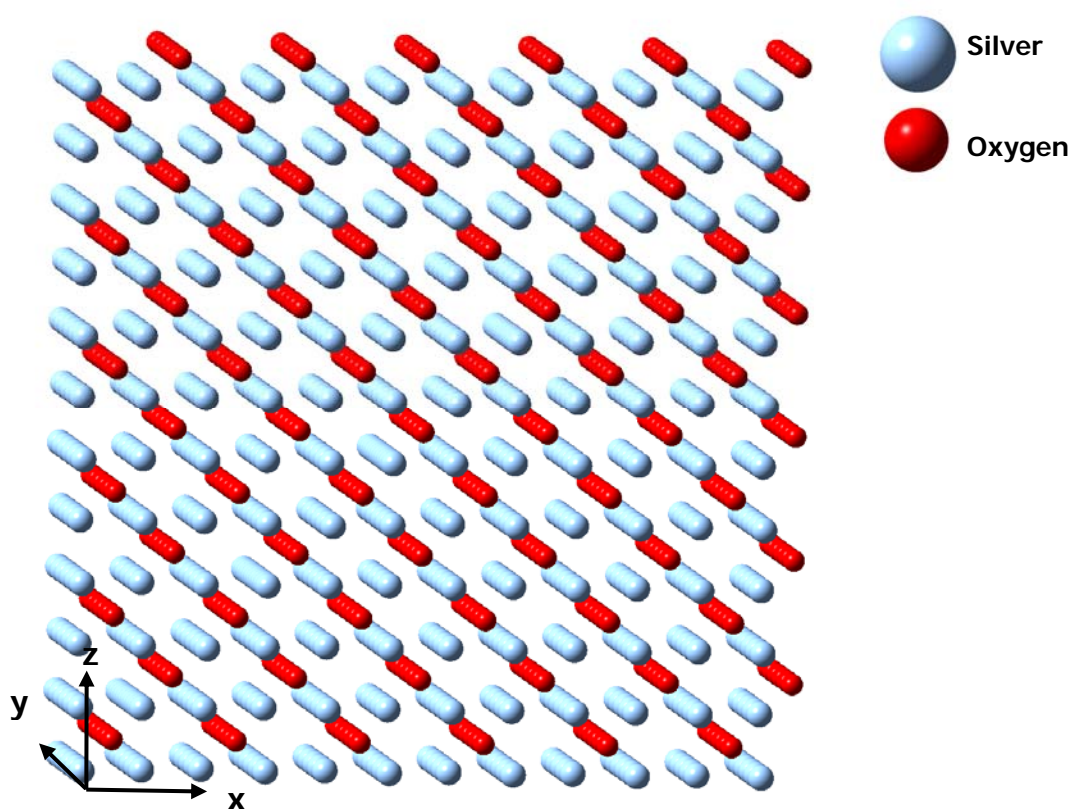


Figure 3.6 Five times enlarged silver oxide unit cell in X,Y and Z directions

Silver oxide modeled as $\text{Ag}_{14}\text{O}_9(001)$ and shown in Figure 3.7 was used for ethylene and propylene epoxidation reactions on Gaussian 03 software. The dangling bonds of the silver atoms and oxygen atoms of the surface cluster are terminated with H atoms which are not shown in Figure 3.7 to obtain a neutral cluster. All of the cluster atoms except the active oxygen atom (O1) of the cluster were kept fixed; and all of the atoms of the reactant and product molecules were relaxed together with the active oxygen atom (O1).

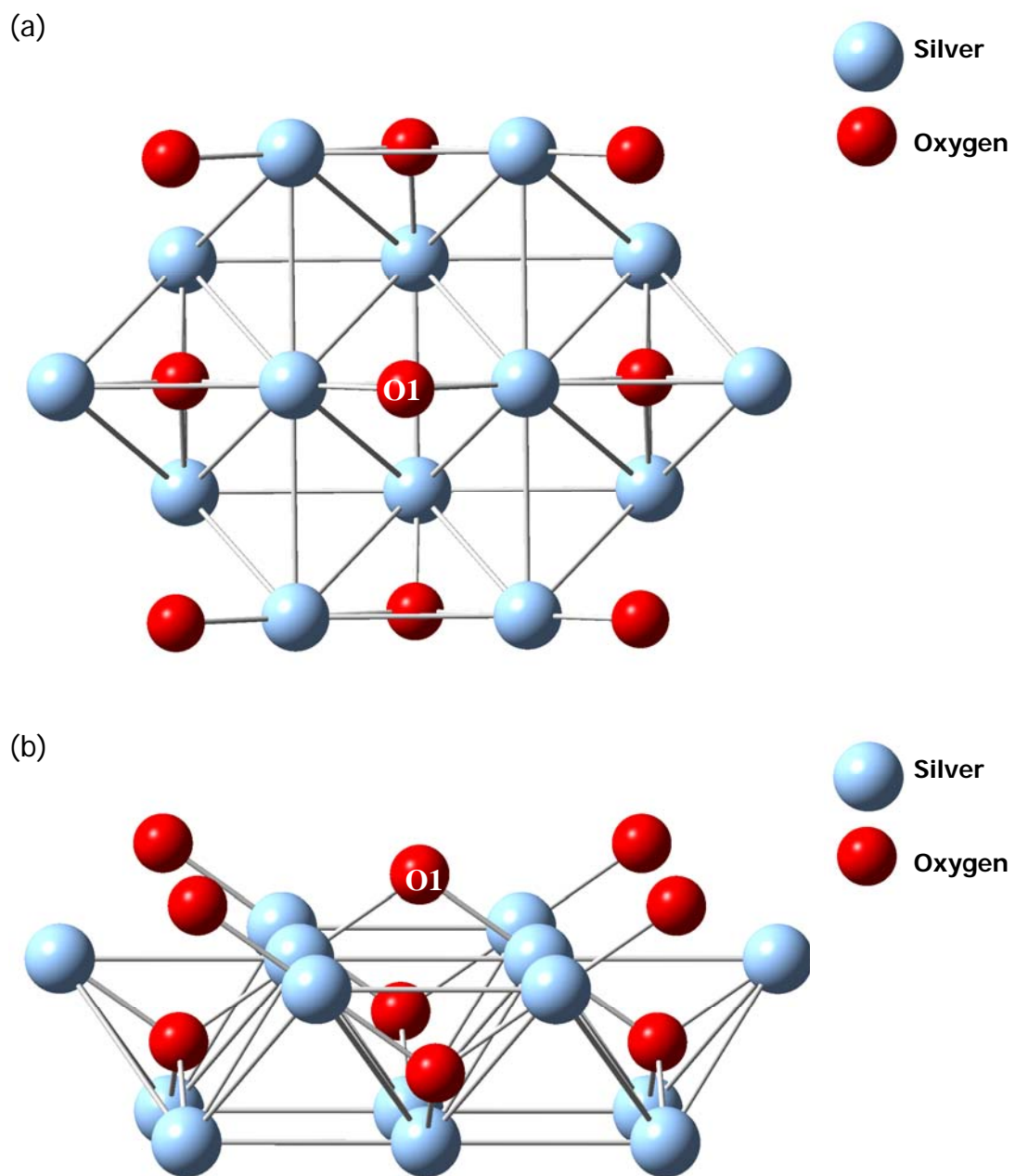


Figure 3.7 $\text{Ag}_{14}\text{O}_9(001)$ surface cluster used in this study a) Top view, b) Side view

3.1.3. Calculation Approach

The computational strategy employed in this case is as follows:

Initially, the correct spin multiplicity of the cluster and adsorbing molecule is determined by Single Point Energy (SPE) calculations. SPE's are calculated with different spin multiplicity numbers for each cluster system and the spin multiplicity number which corresponds to the lowest SPE is accepted as the correct spin multiplicity (SM).

$$SM = 2S + 1 \quad (3.1)$$

where S is the total spin for the molecule. The cluster and the adsorbing molecules are then fully optimized geometrically by means of EG calculations by using SM found for molecules.

The adsorbing molecule is first located over the active site of the cluster at a selected distance and a coordinate driving calculation is performed by selecting a reaction coordinate in order to obtain the variation of the relative energy with a decreasing reaction coordinate to get an energy profile as a function of the selected reaction coordinate distance. In the coordinate driving calculation all points on the reaction coordinate profile are obtained by using EG calculation. This means that all points on the reaction coordinate profile are optimized geometries. These energy profiles help also us to find transition state geometry and final equilibrium. Single point equilibrium geometry calculations were also performed where necessary by locating the adsorbing molecule in the vicinity of the catalytic cluster. Coordinate driving calculations result in an energy profile. The resulting relative energies for the cluster and reactant molecule complex are plotted against the reaction coordinate. The relative energy known as binding energy is defined as the following formula:

$$\Delta E = E_{System} - E_{FirstPointoftheSystem} \quad (3.2)$$

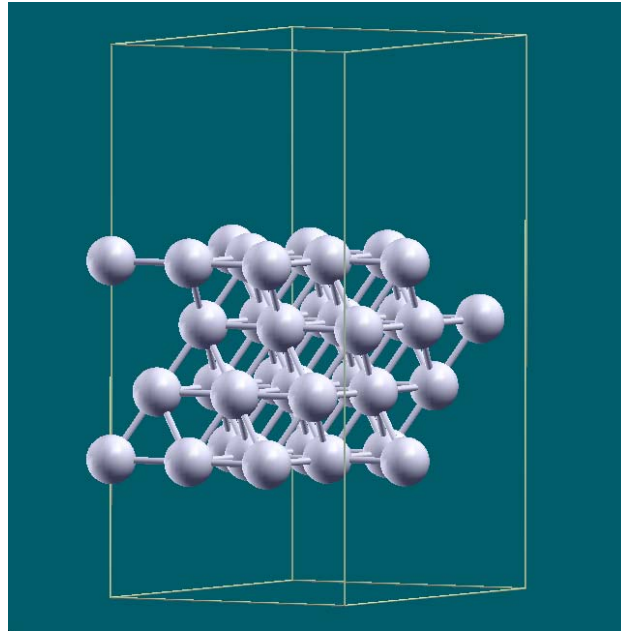
where E_{System} is the calculated energy of the given geometry containing the cluster and the adsorbing molecule at any distance, $E_{FirstPointoftheSystem}$ is the energy of the first point of the relative energy profile. After obtaining the energy profile for the reaction step, the geometry with the minimum energy on the energy profile is re-optimized by means of EG calculations to obtain the final geometry for the particular reaction step. In this re-optimization calculation, the reaction coordinate is not fixed. Transition states (TS) have been calculated using the synchronous quasi-Newtonian method of optimization, QST3 (Peng and Schlegel, 1993). Peak points on the relative energy profile are accepted as approximate transition state (ATS) if TS geometry is not found.

All energies and energy differences are reported for 0 K without zero point energy (ZPE) corrections. The ZPE corrections would likely be similar for each of these cluster systems and thus would not influence conclusions based on the relative energies. Computed $\langle S^2 \rangle$ values confirmed that the spin contamination was very small (within 2% after annihilation). Spin contamination is negligible if the values of $\langle S^2 \rangle$ are smaller than 10% (Young, 2001). Vibrational analysis was performed for transition states to confirm that they have only one imaginary mode of vibration. Convergence criteria which are gradients of maximum force, RMS force, and maximum displacement and RMS displacement in Gaussian'03 software are 0.000450, 0.000300, 0.001800 and 0.001200, respectively.

3.2. Computational Procedure for VASP Software

The calculations for this case were carried out using **VASP** code (Kresse et al., 1996), which uses periodic plane wave basis sets. The many-body systems are described with **PAW** (Kresse et al., 1996; Blöchl, 1994), and **GGA** (Perdew et al., 1992) for the exchange and the correlation energy proposed by Perdew and Wang (**PW91**) (Wang and Perdew, 1991). Except for the molecules and atoms in the gas phase, dipole corrections are included for the asymmetric slab calculations. The cut-off energies and k-points (Monkhorst Pack) used are; 341 eV and (4x4x1) for 4 layer p(3x3) slabs. Vacuum region was determined as 20 Å. Slab (4 layers (3x3) cell) used in this section contains 36 silver atoms. Silver atoms of the bottom layer were only kept fixed during all VASP calculations. This slab is represented in Figure 3.8.

(a)



(b)

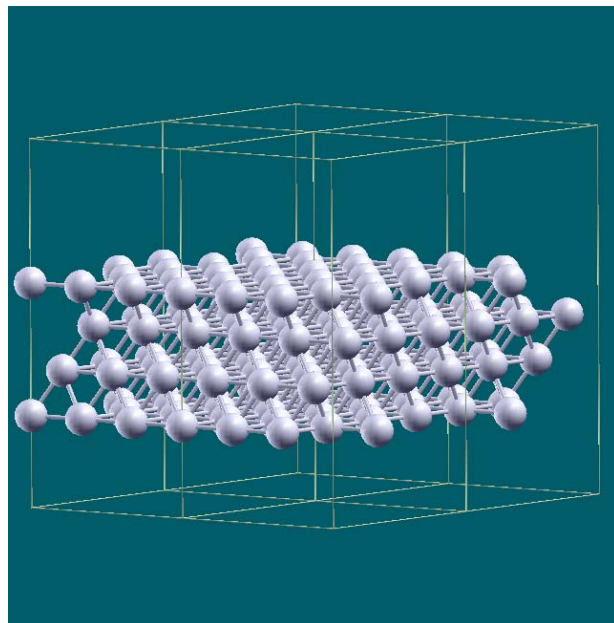


Figure 3.8 a) 4 Layers-(3x3) silver (111) slab, b) 2 times enlarged slab in X and Y direction

CHAPTER 4

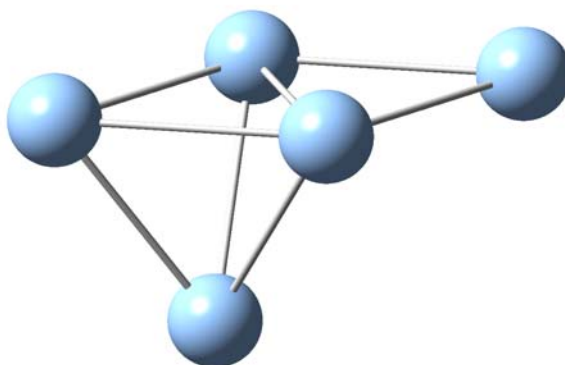
RESULTS AND DISCUSSION

4.1. Comparison of Silver Surfaces

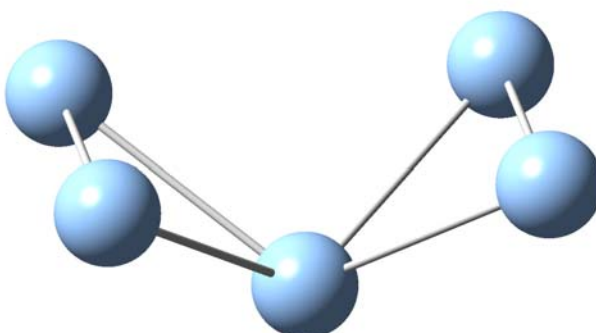
It was experimentally reported that the (111) plane is thought to predominate on the surface of real catalysts, due to its thermodynamic stability (Campbell, 1985). Thus, silver (111) surface cluster was used for ethylene and propylene partial oxidation reactions.

Three small surface clusters containing 5 silver atoms shown in parts a, b and c of Figure 4.1 respectively were also used for ethylene oxidation reaction to see effect of silver surface on that reaction. These small clusters were obtained by using silver (111), (110) and (100) surfaces.

(a)



(b)



(c)

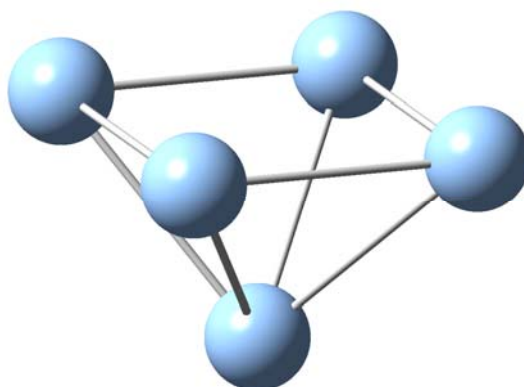


Figure 4.1 Silver surface clusters a) $\text{Ag}_5(111)$ surface cluster, b) $\text{Ag}_5(110)$ surface cluster, c) $\text{Ag}_5(100)$ surface cluster

4.2. Ethylene Epoxidation

4.2.1. Ethylene Epoxidation on Small Silver (111), (110) and (100) Surface Clusters

4.2.1.1. Ethylene Epoxidation on Ag₅(111) Surface Cluster

a) Adsorption of Atomic Oxygen

Oxygen was atomically adsorbed onto the 5 Ag atoms cluster and the equilibrium geometry as well as the relative energy of adsorption were calculated. Figure 4.2 shows the optimized equilibrium geometry of atomic oxygen adsorption on the Ag cluster simulating Ag₅(111) surface. In calculating the optimized geometry Ag atoms are kept fixed in accordance with Ag (111) surface crystallography dimensions and O atom position is optimized. The relative energy of adsorption value of atomic oxygen obtained in this study is found to be -64.66 kcal/mol.

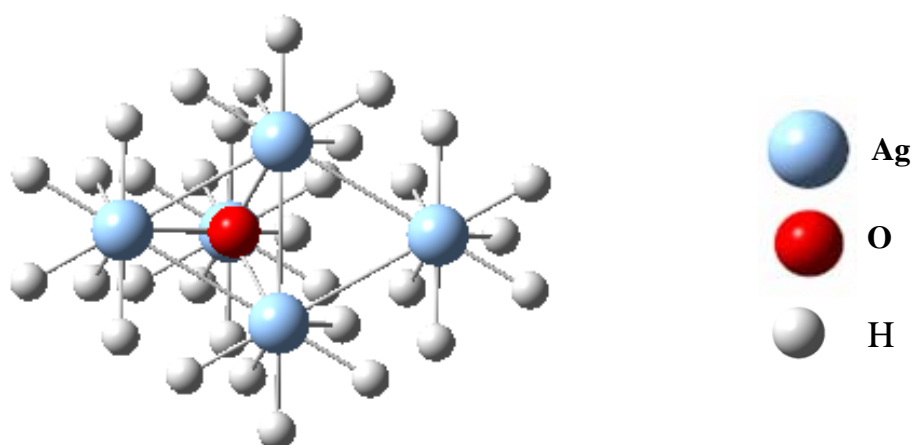


Figure 4.2 Equilibrium geometry for atomic oxygen adsorption on Ag₅(111)

b) O Adatom Insertion into the C-C Bond of Ethylene to Form Ethylene Oxide

One possible step along the reaction coordinate is the adsorption of ethylene (reaction 1) onto the oxygen atom-adsorbed Ag cluster to form ethylene oxide. Figure 4.3 shows the relative energy profile obtained when a reaction coordinate between the adsorbed O atom and one carbon atom of ethylene molecule (C1-O) is chosen. The initial C1-O distance for the initial geometry is taken as 3.00 Å. There is an energy barrier of 10.91 kcal/mol. The final geometry which is similar to an oxametallacycle molecule is found at a relative energy value of -11.07 kcal/mole.

Ethylene adsorption

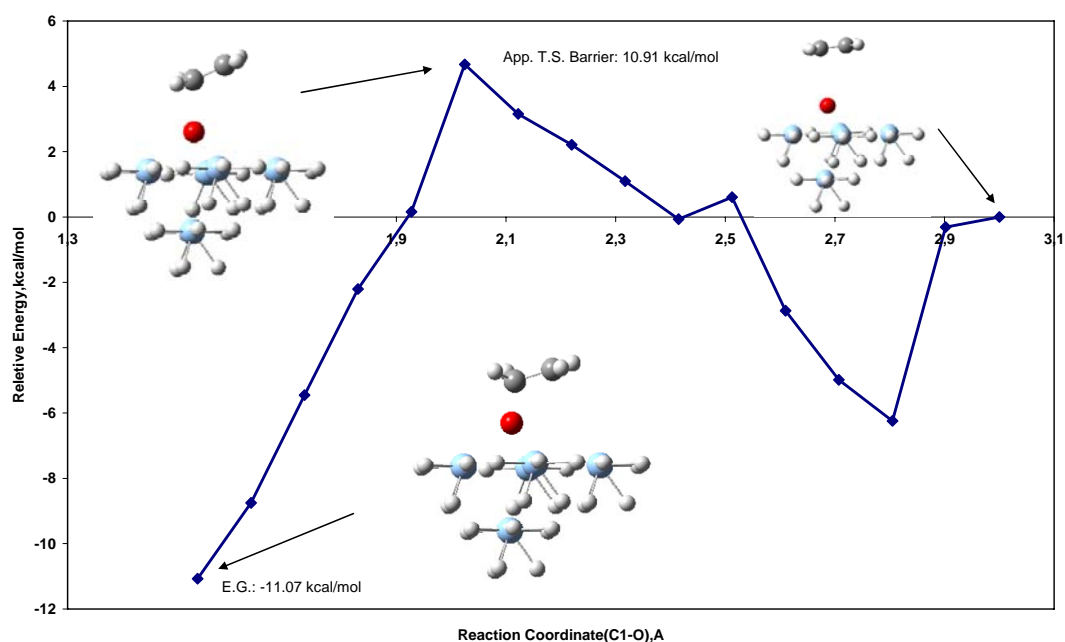


Figure 4.3 Relative energy profile along reaction coordinate (C1-O) for ethylene oxide formation on oxygen atom adsorbed on 5 atoms (111) silver surface cluster.

The next step (reaction 2) is taken to be a reaction coordinate between the O atom and other carbon atom of ethylene molecule (C2-O). Figure 4.4 shows the relative energy profile obtained. The initial geometry is oxametallacycle geometry where the initial C2-O distance is found as 2.498 Å. This geometry and the final geometry of the first step which has a reaction coordinate between C1 and O is the same. A relative energy barrier of an approximate transition state for the second step is 17.23 kcal/mol. The final geometry of ethylene oxide on the cluster is found at a relative energy value of 11.14 kcal/mol. The approximate activation barrier of ethylene oxide formation reaction which has a reaction coordinate between the adsorbed O atom and the second carbon atom of ethylene molecule (C2-O) is accepted the activation barrier on Ag₅(111) cluster.

Ethylene oxide formation

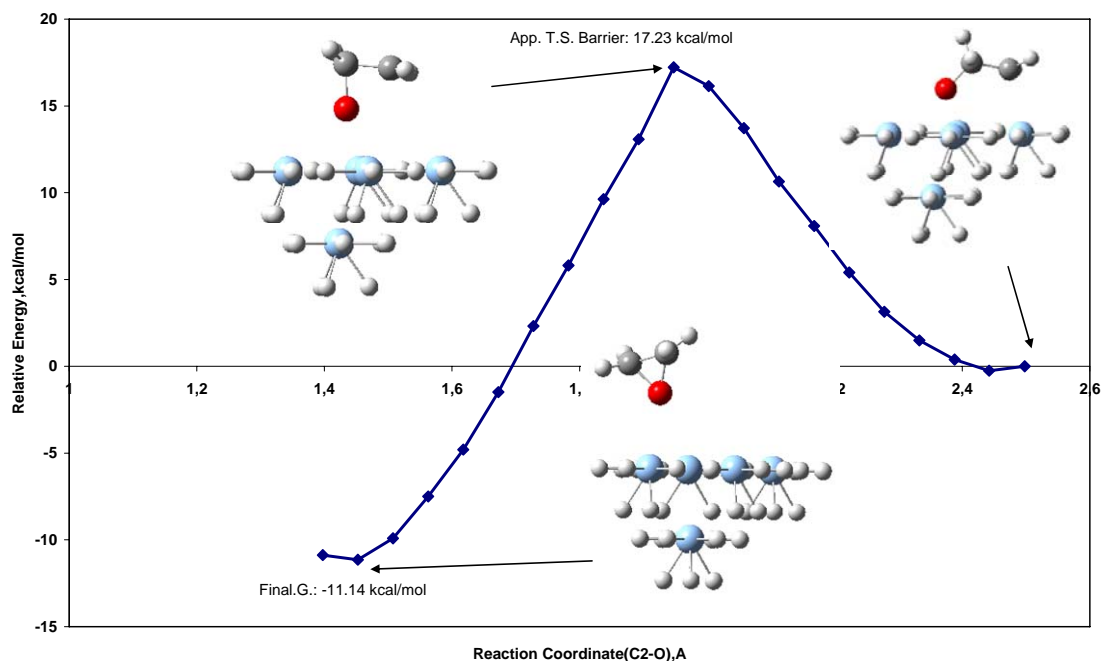
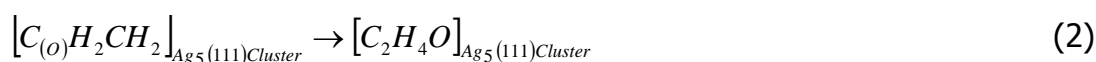


Figure 4.4 Relative energy profile along reaction coordinate (C2-O) for ethylene oxide formation on oxygen atom adsorbed on 5 atoms (111) silver surface cluster.

4.2.1.2. Ethylene Epoxidation on Ag₅(110) Surface Cluster

The (110) surface of the silver is different from other surfaces such as (111) and (100). It is not a flat surface as (111) or (100); it has a zigzag form shown in Figure 4.5. 5 and 8 Ag atoms clusters are used for (110) surface since each site may have different activity. Ag₅ cluster has a Hill site and Ag₈ cluster has a Hollow site.

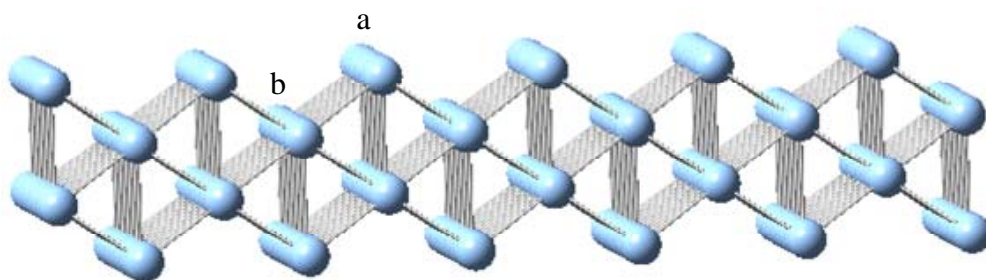


Figure 4.5 Large Ag(110) surface. a: Hill site, b: Hollow site

a) Adsorption of Atomic Oxygen on Active Sites

Figure 4.6 depicts the optimized equilibrium geometry of atomic oxygen adsorption on the Ag cluster simulating Ag₅(110) surface. The relative energy of adsorption value of atomic oxygen obtained in this cluster is found to be -90.25 kcal/mol. The relative energy of adsorption value of atomic oxygen obtained in Ag₈(110) surface cluster shown in Figure 4.7 is found to be -57.86 kcal/mol.

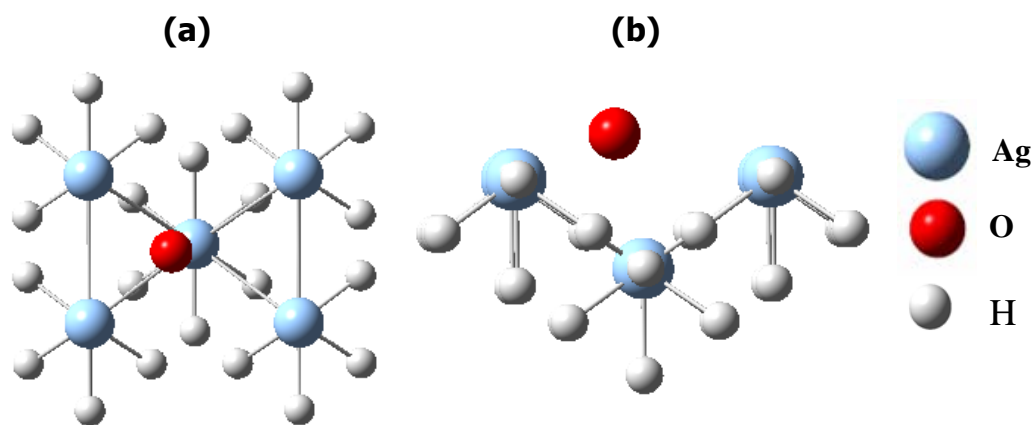


Figure 4.6 Equilibrium geometry for atomic oxygen adsorption on $\text{Ag}_5(110)$.
a) Top view b) Side view.

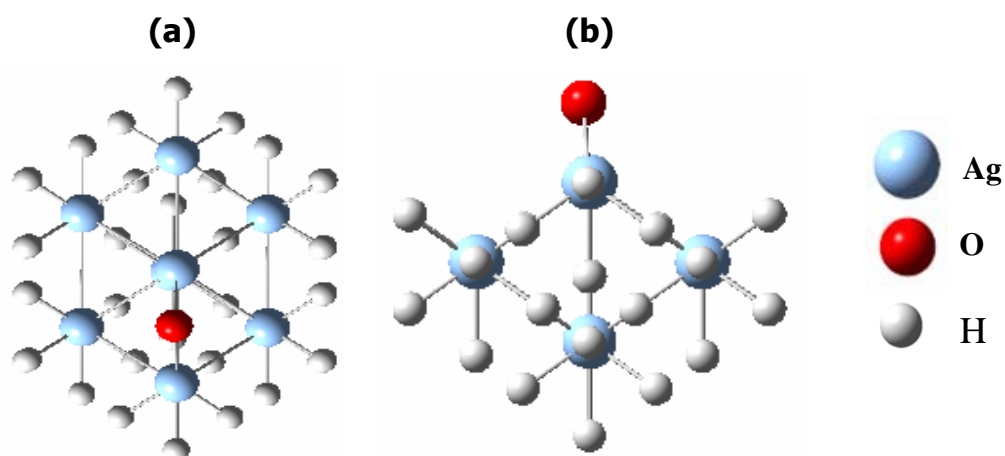


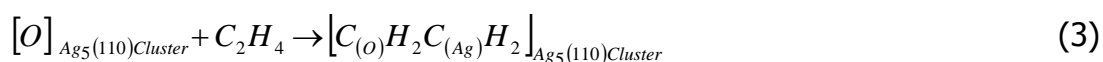
Figure 4.7 Equilibrium geometry for atomic oxygen adsorption on $\text{Ag}_8(110)$.
a) Top view b) Side view.

b) O Adatom Insertion into the C-C Bond of Ethylene to Form Ethylene Oxide

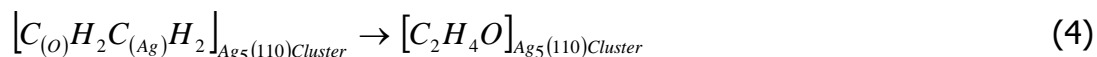
Figure 4.8 represents the relative energy profile for reaction 3 obtained when a reaction coordinate between the adsorbed O atom and one carbon atom of ethylene molecule (C1-O) is chosen for $\text{Ag}_5(110)$ surface cluster. The initial C1-O distance for the initial geometry is taken as 3.50 Å. There is a small energy barrier of 4.54 kcal/mol. The final geometry which is similar to an

oxametallacycle molecule is found at a relative energy value of -14.13 kcal/mole. The next step (reaction 4) is taken to be a reaction coordinate between the O atom and other carbon atom of ethylene molecule (C2-O). Figure 4.9 shows the relative energy profile obtained. The initial geometry is oxametallacycle geometry where the initial C2-O distance is found as 2.448 Å. This geometry and the final geometry of the first step which has a reaction coordinate between C1 and O is the same. A relative energy barrier of an approximate transition state for the second step is 58.15 kcal/mol. The final geometry of ethylene oxide on the cluster is found at a relative energy value of 57.44 kcal/mol. The approximate activation barrier of ethylene epoxidation which has a reaction coordinate between the adsorbed O atom and the second carbon atom of ethylene molecule (C2-O) is accepted the activation barrier for ethylene oxide formation reaction on Ag₅(110) cluster.

Ethylene adsorption



Ethylene oxide formation



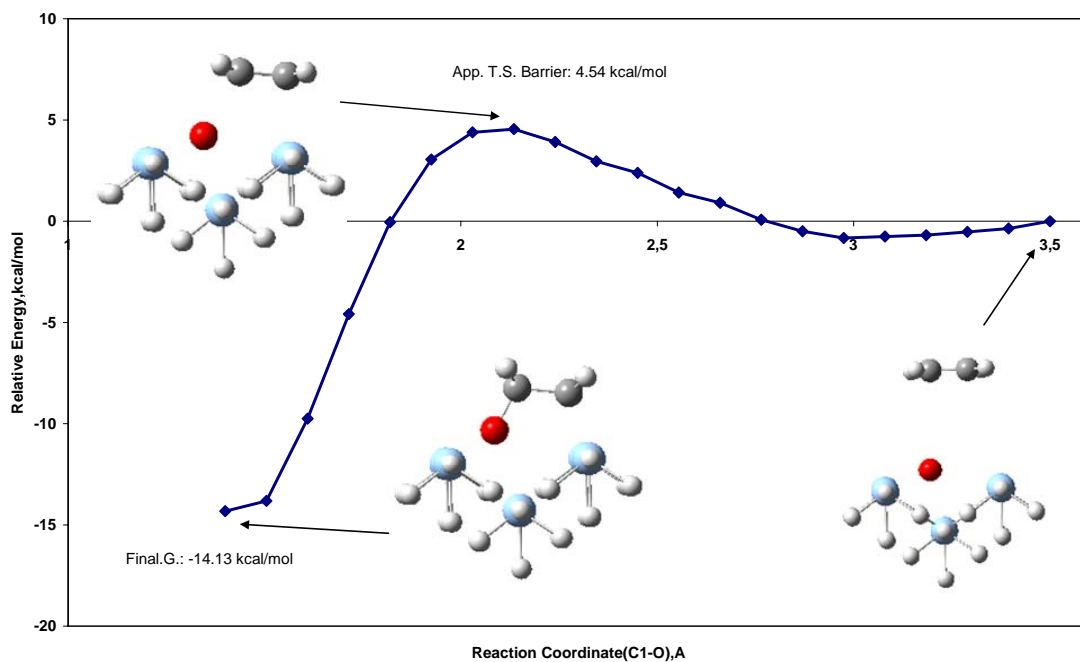


Figure 4.8 Relative energy profile along reaction coordinate (C1-O) for ethylene oxide formation on oxygen atom adsorbed on 5 atoms (110) silver surface cluster.

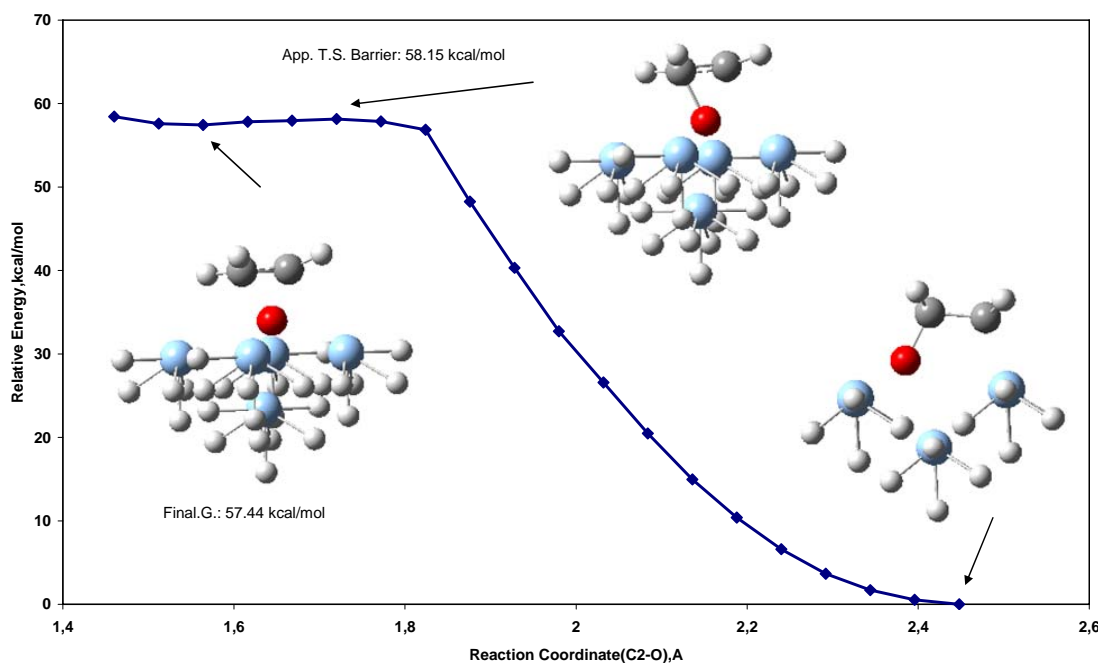


Figure 4.9 Relative energy profile along reaction coordinate (C2-O) for ethylene oxide formation on oxygen atom adsorbed on 5 atoms (110) silver surface cluster.

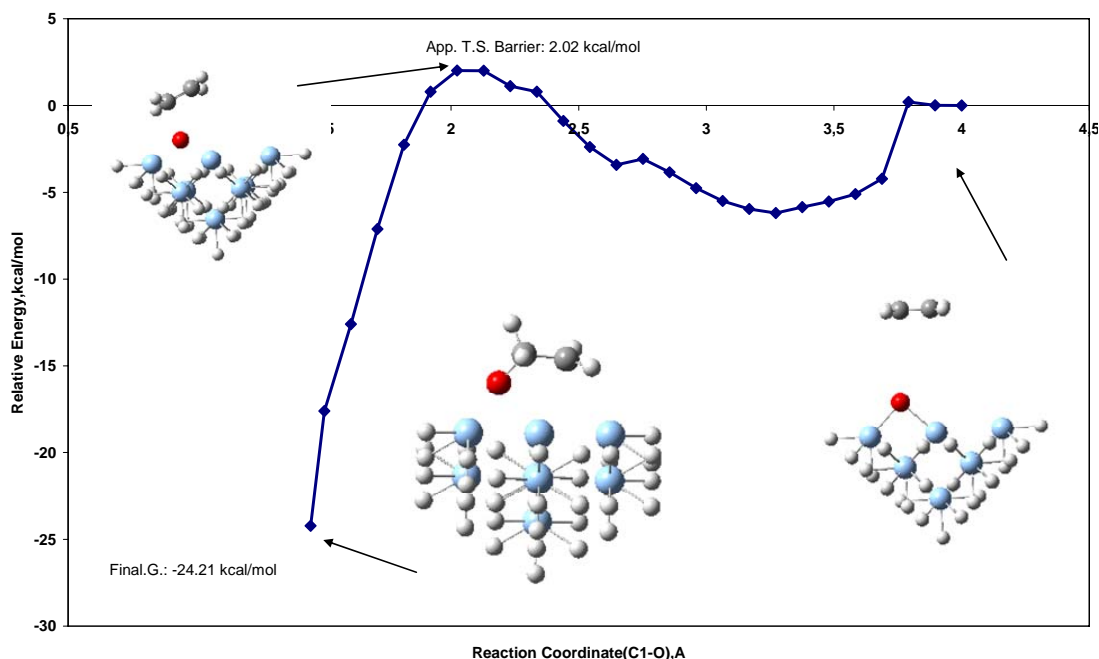
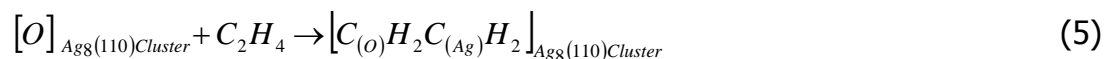


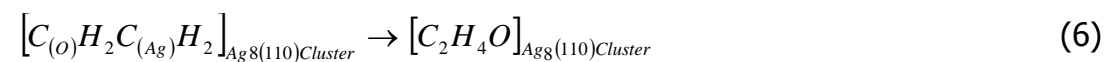
Figure 4.10 Relative energy profile along reaction coordinate (C1-O) for ethylene oxide formation on oxygen atom adsorbed on 8 atoms (110) silver surface cluster.

Figure 4.10 illustrates the relative energy profile for reaction 5 obtained when a reaction coordinate between the adsorbed O atom and one carbon atom of ethylene molecule (C1-O) is chosen for $\text{Ag}_8(110)$ surface cluster. The initial C1-O distance for the initial geometry is taken as 4.00 Å. There is a small energy barrier of 2.02 kcal/mol. The final geometry which is similar to an oxametallacycle molecule is found at a relative energy value of -24.21 kcal/mole. The next step (reaction 6) is taken to be a reaction coordinate between the O atom and other carbon atom of ethylene molecule (C2-O).

Ethylene adsorption



Ethylene oxide formation



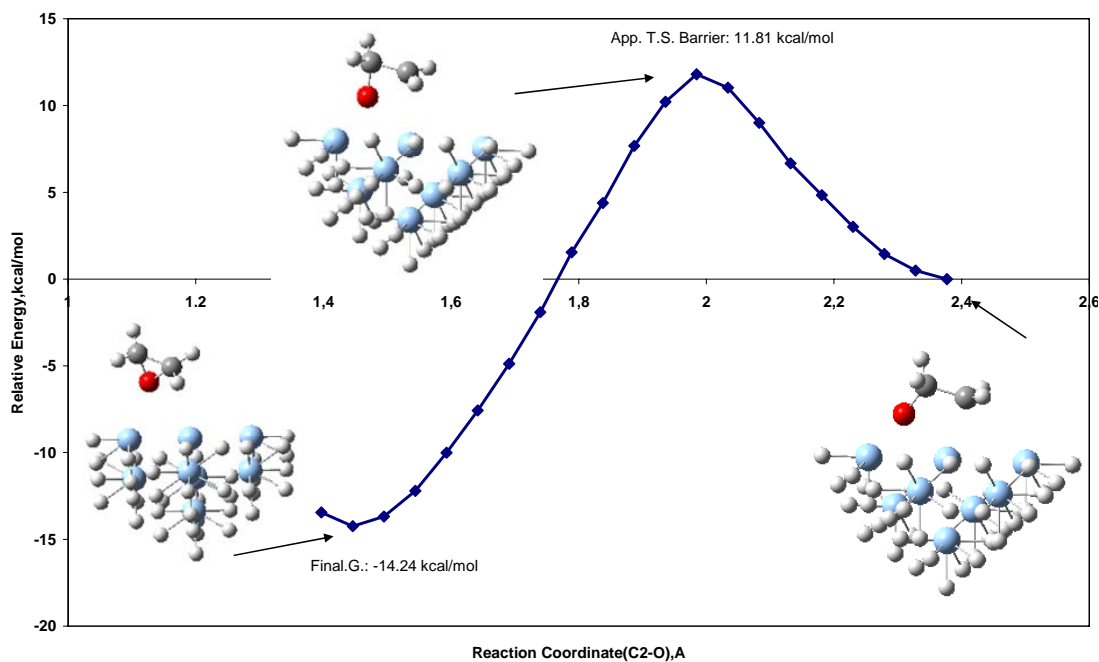


Figure 4.11 Relative energy profile along reaction coordinate (C2-O) for ethylene oxide formation on oxygen atom adsorbed on 8 atoms (110) silver surface cluster.

The relative energy profile obtained is represented in Figure 4.11. The initial geometry is oxametallacycle geometry where the initial C2-O distance is found as 2.377 Å. This geometry and the final geometry of the first step which has a reaction coordinate between C1 and O is the same. A relative energy barrier of an approximate transition state for the second step is 11.81 kcal/mol. The final geometry of ethylene oxide on the cluster is found at a relative energy value of -14.24 kcal/mol. The approximate activation barrier of ethylene epoxidation which has a reaction coordinate between the adsorbed O atom and the second carbon atom of ethylene molecule (C2-O) is accepted the activation barrier for ethylene oxide formation reaction on $\text{Ag}_8(110)$ cluster.

4.2.1.3. Ethylene Epoxidation on Ag₅(100) Surface Cluster

a) Adsorption of Atomic Oxygen

Figure 4.12 shows the optimized equilibrium geometry of atomic oxygen adsorption on the Ag cluster simulating Ag₅(100) surface. The relative energy of adsorption value of atomic oxygen obtained in this cluster is found to be -73.36 kcal/mol.

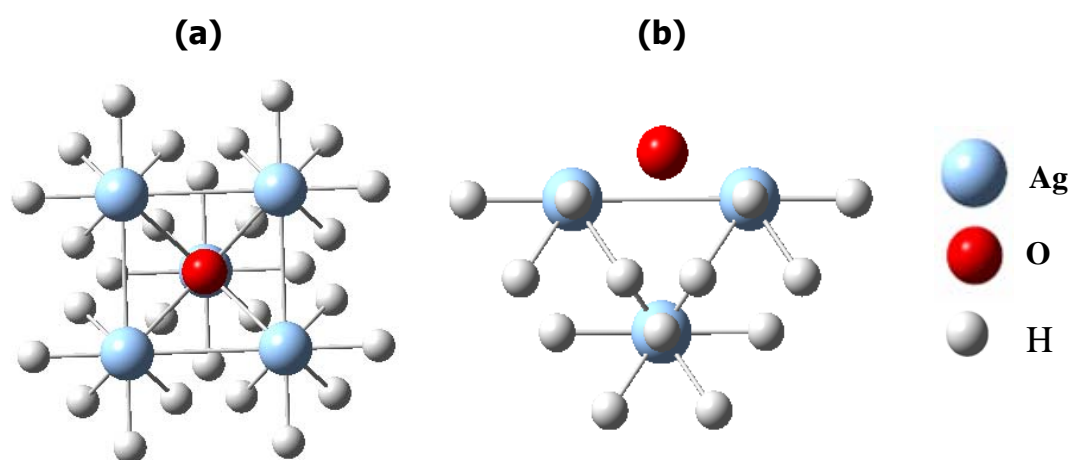


Figure 4.12 Equilibrium geometry for atomic oxygen adsorption on Ag₅(100). a) Top view b) Side view.

b) O Adatom Insertion into the C-C Bond of Ethylene to Form Ethylene Oxide

Figure 4.13 depicts the relative energy profile for reaction 7 obtained when a reaction coordinate between the adsorbed O atom and one carbon atom of ethylene molecule (C1-O) is chosen for Ag₅(100) surface cluster. The initial C1-O distance for the initial geometry is taken as 3.50 Å. There is an energy barrier of 9.9 kcal/mol. The final geometry which is similar to an oxametallacycle molecule is found at a relative energy value of 0.89

kcal/mole. The next step (reaction 8) is taken to be a reaction coordinate between the O atom and other carbon atom of ethylene molecule (C2-O).

Ethylene adsorption

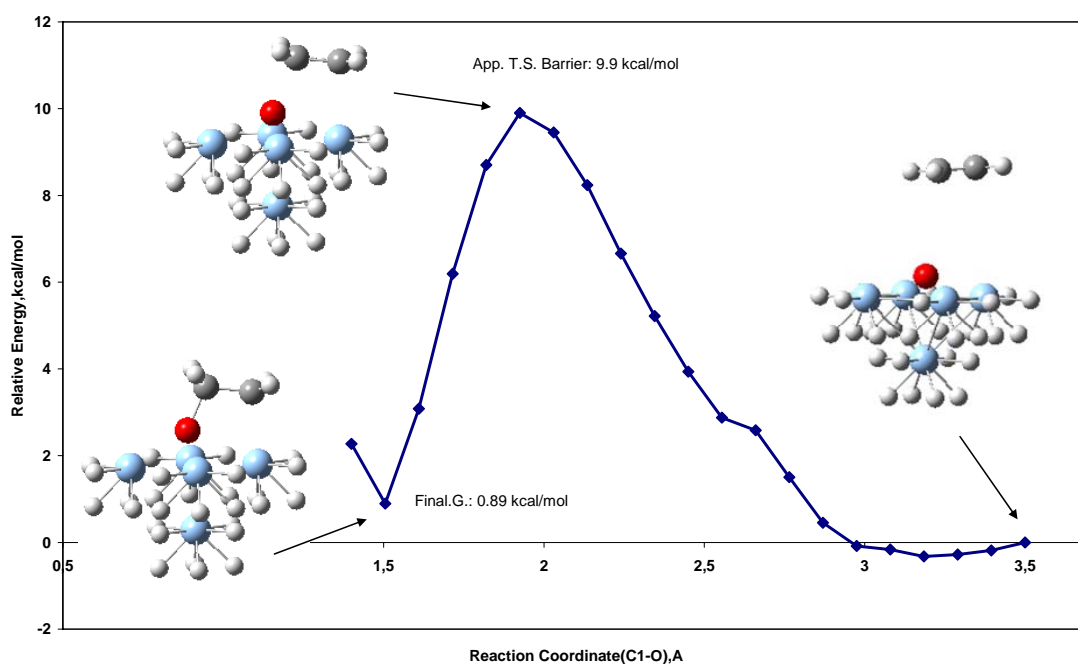
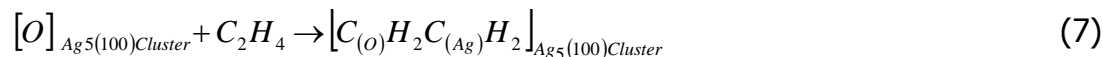
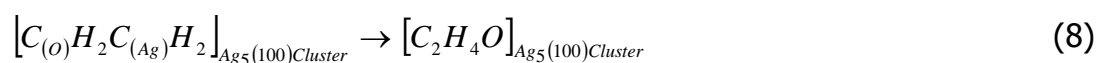


Figure 4.13 Relative energy profile along reaction coordinate (C1-O) for ethylene oxide formation on oxygen atom adsorbed on 5 atoms (100) silver surface cluster

Ethylene oxide formation



The relative energy profile obtained is shown in Figure 4.14. The initial geometry is oxametallacycle geometry where the initial C2-O distance is found as 2.386 Å. This geometry and the final geometry of the first step which has a reaction coordinate between C1 and O is the same. A relative

energy barrier of an approximate transition state for the second step is 17.89 kcal/mol. The final geometry of ethylene oxide on the cluster is found at a relative energy value of -11.44 kcal/mol. The approximate activation barrier of ethylene epoxidation which has a reaction coordinate between the adsorbed O atom and the second carbon atom of ethylene molecule (C2-O) is accepted the activation barrier for ethylene oxide formation reaction on $\text{Ag}_5(100)$ cluster.

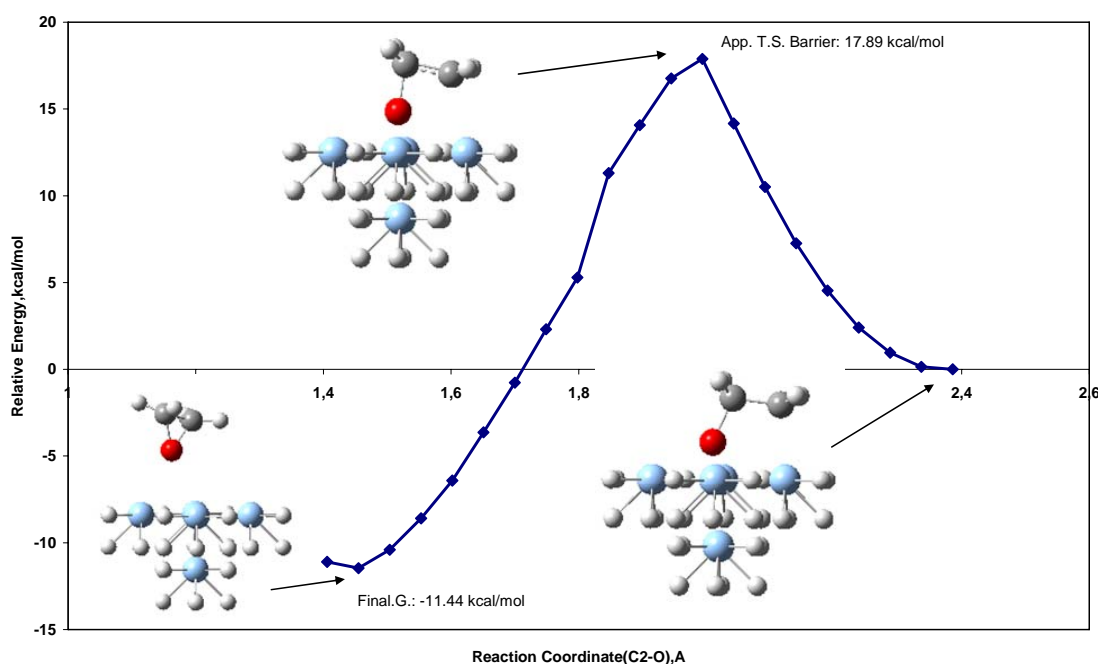


Figure 4.14 Relative energy profile along reaction coordinate (C2-O) for ethylene oxide formation on oxygen atom adsorbed on 5 atoms (100) silver surface cluster

Table 4.1 gives a comparison of activation barriers computed in this study with experimental and theoretical studies. As seen, silver (110) surface is more active for ethylene oxide formation than (111) and (100) surfaces. But, activation barrier of the (111) plane is very close to experimental value, since it is a predominate surface of the real silver catalyst, due to its thermodynamic stability. (110) surface is more active than (111) and (100)

surfaces. It was also experimentally reported that the activity of (111) surface is a factor of 2 below the (110) surface (Campbell, 1985). Hill site of (110) surface is more active than Hollow site of (110) surface since oxygen atom weakly adsorbed on Hill site.

Table 4.1 Comparison of activation barriers for ethylene oxide formation on (111), (110) and (100) silver surfaces

Activation Barrier, kcal/mol				
Theoretical				Experimental (on Ag/ α - Al_2O_3 catalyst)
Surfaces				
111	110		100	
	Hollow site	Hill site		
17.2 ^a 13 ^b 16 ^d	58.15 ^a	11.8 ^a 9.6 ^c 15 ^c	17.9 ^a	17 ^b , 22 ^e , 14 ^f , 17 ^g

^a This Study

^b Linic et al.(2002)

^c Medlin et al. (2001)

^d Linic et al.(2003)

^e Larrabe et.al.(1978)

^f Akimoto et. al. (1982)

^g Kanoh et. al. (1979)

4.2.2. Ethylene Epoxidation on Silver Surface

Several products such as ethylene oxide, vinyl alcohol, vinyl aldehyde and vinyl radical can be formed during the epoxidation of ethylene with atomic oxygen. These products are formed via different reactions which are parts of a mechanism of ethylene epoxidation. This reaction mechanism is shown in Figure 4.15.

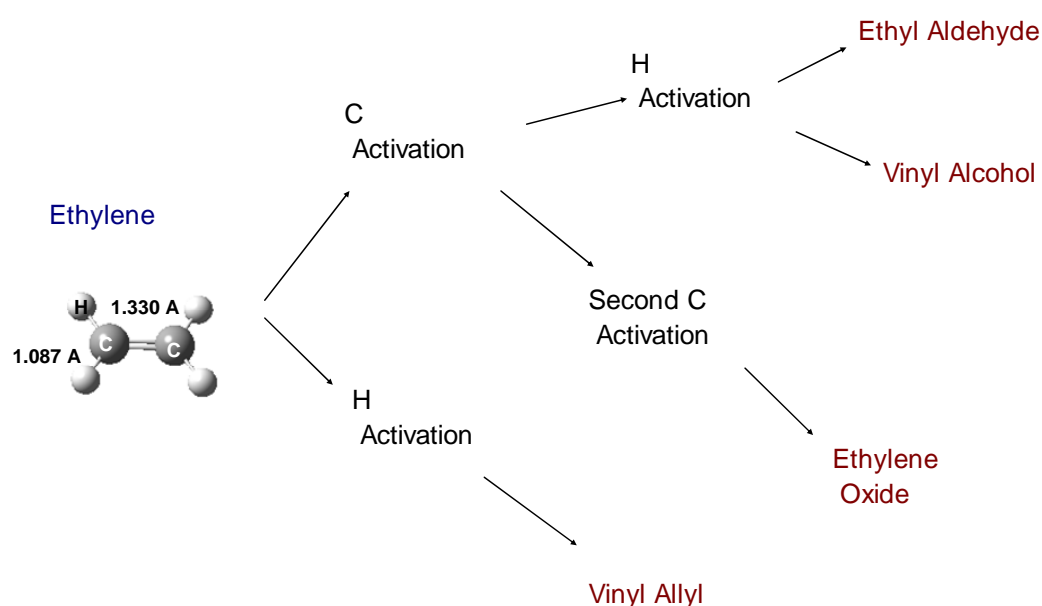
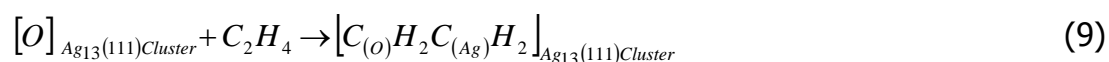


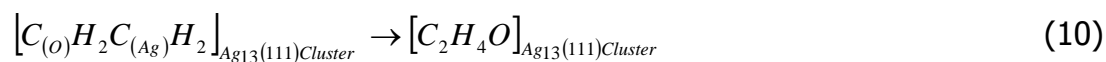
Figure 4.15 A reaction mechanism for ethylene epoxidation

The proposed reaction steps for the oxidation of ethylene on the cluster are:

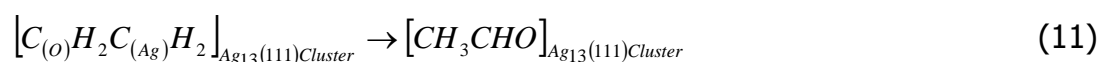
Step 1, ethylene adsorption



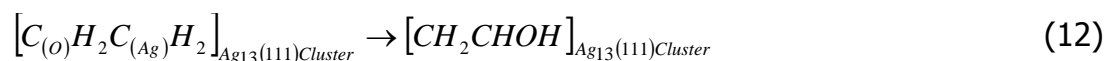
Step 2, ethylene oxide formation



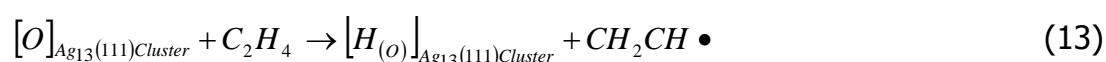
Step 3, ethyl aldehyde formation



Step 4, vinyl alcohol formation



Step 5, vinyl radical formation

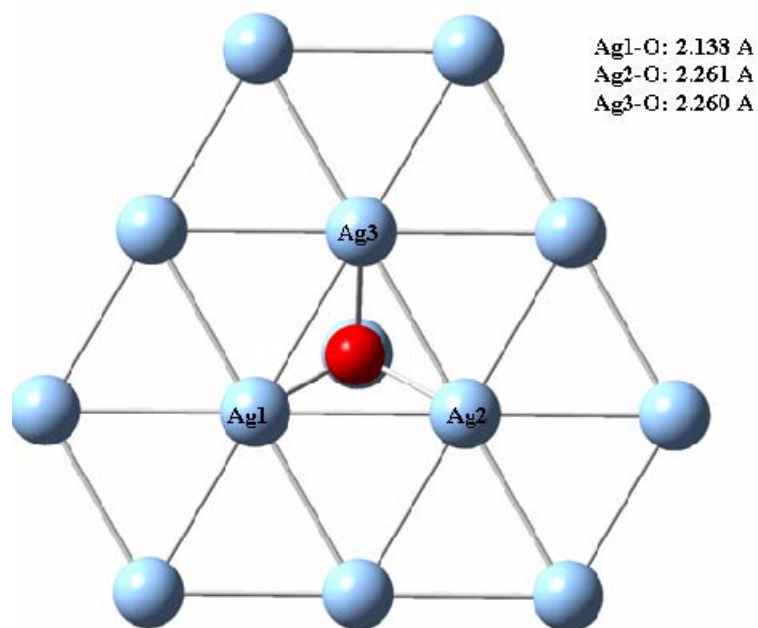


4.2.2.1. Ethylene Epoxidation on Ag₁₃(111) Cluster

Adsorption of Atomic Oxygen

Oxygen was atomically adsorbed onto the 13 Ag atoms cluster and the equilibrium geometry as well as the relative energy of adsorption were calculated. Figure 4.16 demonstrates the optimized equilibrium geometry of atomic oxygen adsorption on the Ag cluster simulating Ag₁₃(111) surface. In calculating the optimized geometry Ag atoms are kept fixed in accordance with Ag₁₃(111) surface crystallography dimensions and O atom position is optimized. The relative energy of adsorption value of atomic oxygen obtained in this study is found to be -37.05 kcal/mol.

(a)



(b)

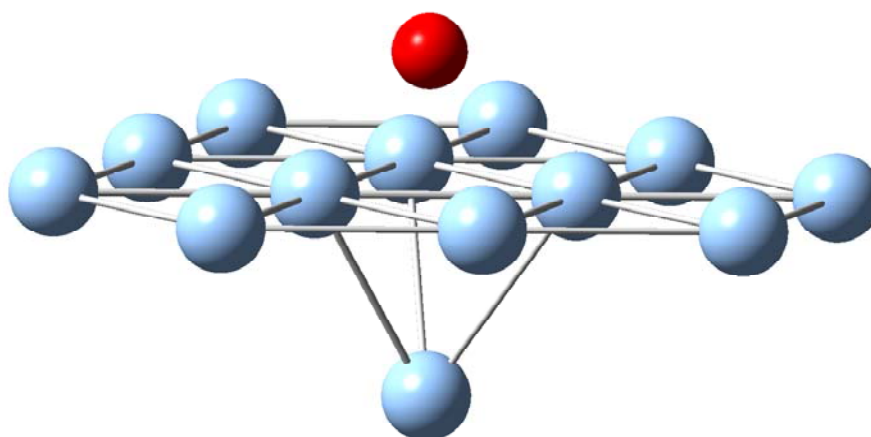


Figure 4.16 Equilibrium geometry for atomic oxygen adsorption on Ag₁₃(111) a) Top view b) Side view

4.2.2.1.1. Vinyl Radical Formation Path

Figure 4.17 represents the relative energy profile for step 5 (Reaction 13) obtained when a reaction coordinate between the adsorbed O atom and one hydrogen atom of ethylene molecule (H-O) is chosen. The initial O-H

distance is taken as 3.00 Å. A relative energy barrier of an approximate transition state is 16.37 kcal/mol. The final geometry is found at an endothermic relative energy value of 13.18 kcal/mole.

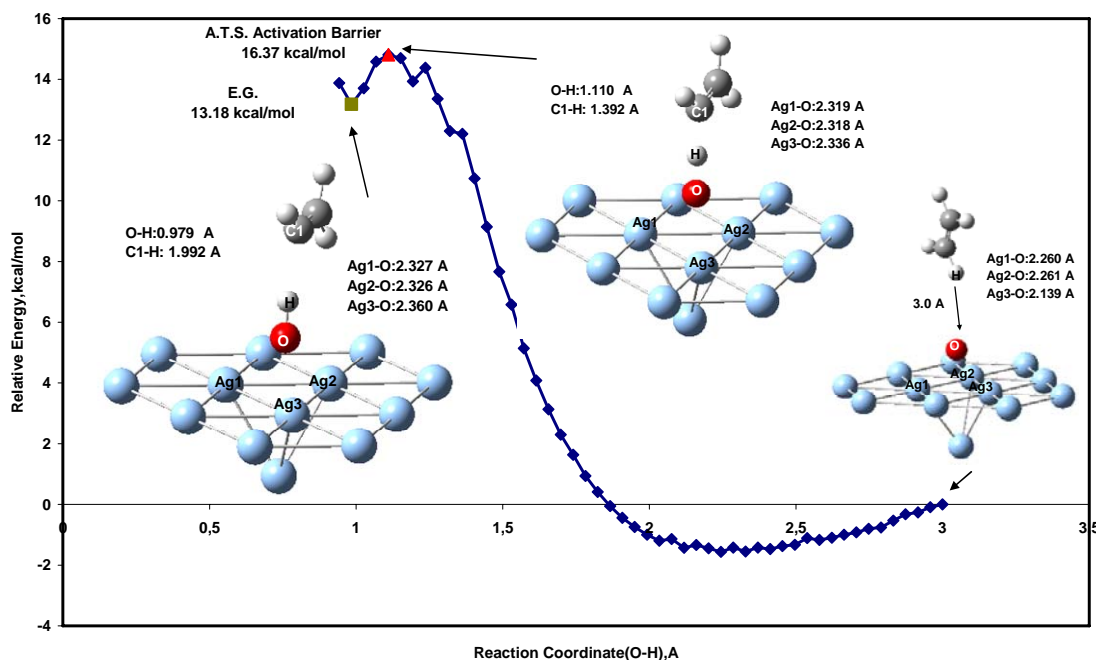


Figure 4.17 Relative energy profile along reaction coordinates (H-O) for C-H activation of ethylene on oxygen atom adsorbed on 13 atoms (111) silver surface cluster.

4.2.2.1.2 Ethylene Oxide Formation Path

Another possible step along the reaction coordinate is the adsorption of ethylene (Step 1, reaction 9) onto the oxygen atom-adsorbed Ag cluster to form ethylene oxide. Figure 4.18 shows the relative energy profile obtained when a reaction coordinate between the adsorbed O atom and one carbon atom of ethylene molecule (C1-O) is chosen. The initial C1-O distance for the initial geometry is taken as 3.00 Å. There is an energy barrier of 9.25 kcal/mol. The final geometry which is similar to an oxametallacycle molecule is found at a relative energy value of -27.44 kcal/mole.

The next step (reaction 10, step 2) is taken to be a reaction coordinate between the O atom and other carbon atom of ethylene molecule (C2-O). The relative energy profile obtained is shown in Figure 4.19. The initial geometry is oxametallacycle geometry where the initial C2-O distance is found as 2.47 Å. This geometry and the final geometry of the first step which has a reaction coordinate between C1 and O is the same. A relative energy barrier of an approximate transition state for the second step is 24.03 kcal/mol. The final geometry of ethylene oxide on the cluster is found at a relative energy value of -24.58 kcal/mol. The approximate activation barrier of ethylene epoxidation which has a reaction coordinate between the adsorbed O atom and the second carbon atom of ethylene molecule (C2-O) is accepted the activation barrier for ethylene oxide formation reaction on Ag₁₃(111) cluster.

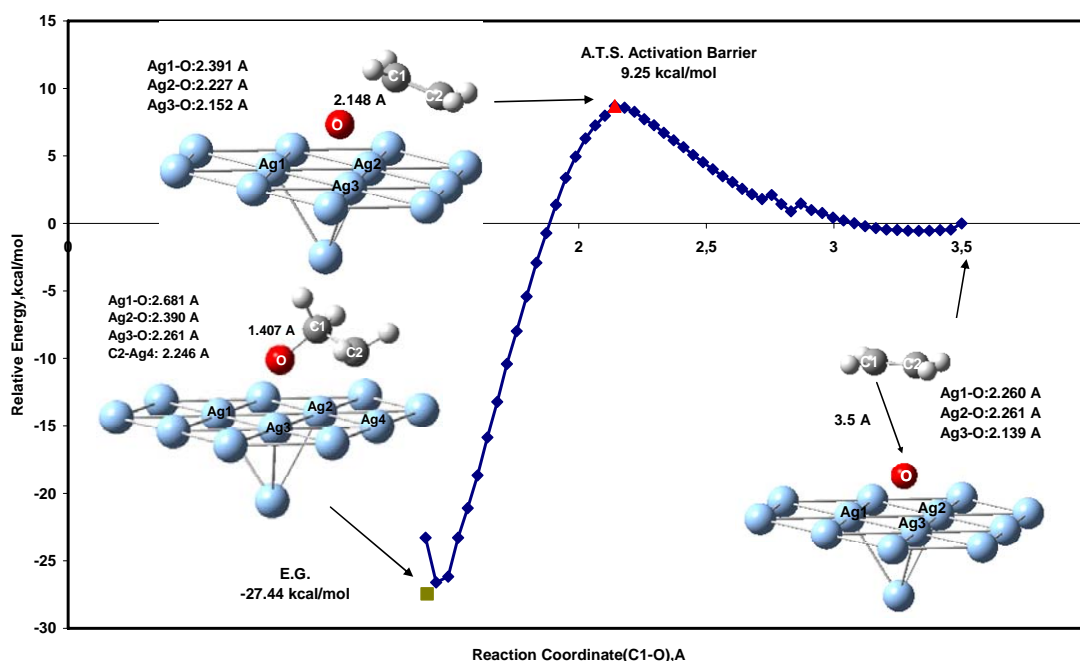


Figure 4.18 Relative energy profile along reaction coordinate (C1-O) for ethylene oxide formation on oxygen atom adsorbed on 13 atoms (111) silver surface cluster.

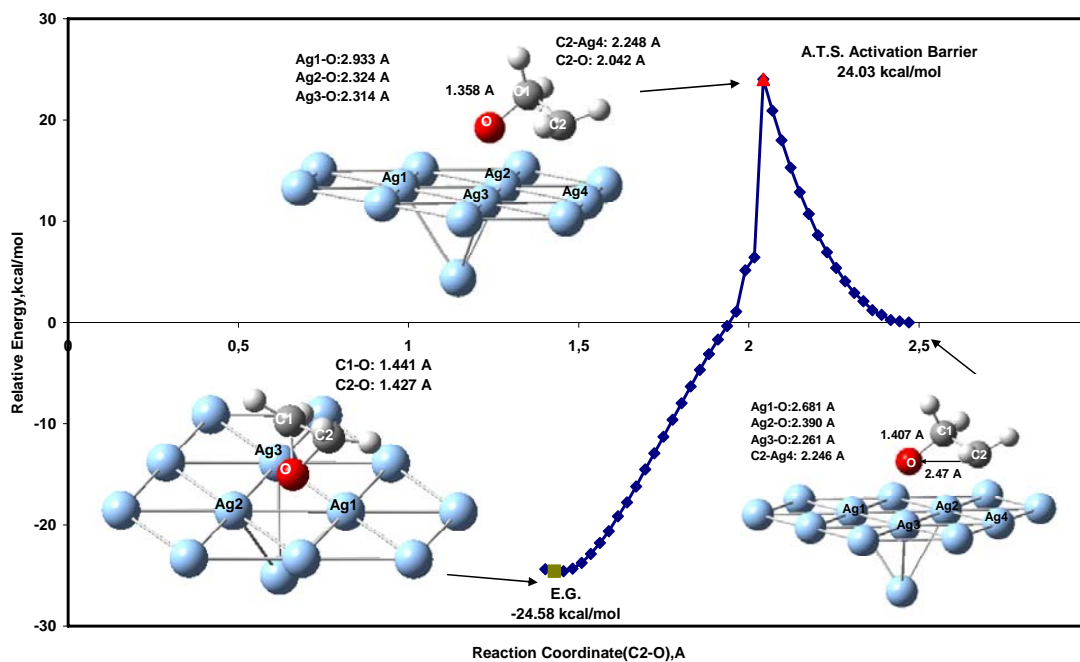


Figure 4.19 Relative energy profile along reaction coordinate (C2-O) for ethylene oxide formation on oxygen atom adsorbed on 13 atoms (111) silver surface cluster.

4.2.2.1.3. Vinyl Alcohol Formation Path

After the completion of first C activation reaction, H of the adsorbed C (first C) can go to the second C to form ethyl aldehyde or to O atom to form vinyl alcohol (Step 4, reaction 12). Figure 4.20 illustrates the relative energy profile obtained for the formation of vinyl alcohol reaction. A relative energy barrier of an approximate transition state for the second step is 33.88 kcal/mol. The final geometry of vinyl alcohol on the cluster is found at a relative energy value of -36.32 kcal/mol.

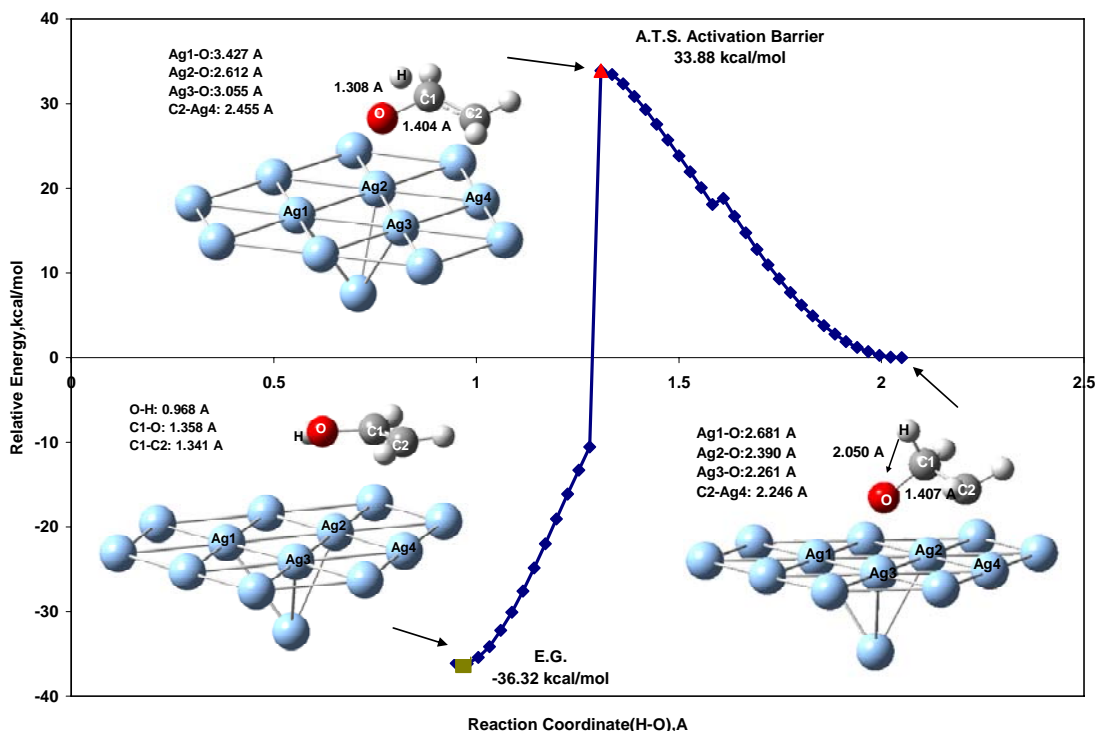


Figure 4.20 Relative energy profile along reaction coordinate (H-O) for vinyl alcohol formation on oxygen atom adsorbed on (001) silver surface cluster.

4.2.2.1.4. Vinyl Aldehyde Formation Path

Figure 4.21 represents the relative energy profile obtained for the formation of ethyl aldehyde reaction (Step 3, reaction 11) where reaction coordinate is between H atom of the first C atom and O atom. A relative energy barrier of an approximate transition state for the second step is 41.08 kcal/mol. The final geometry of ethyl aldehyde on the cluster is found at a relative energy value of -49.44 kcal/mol.

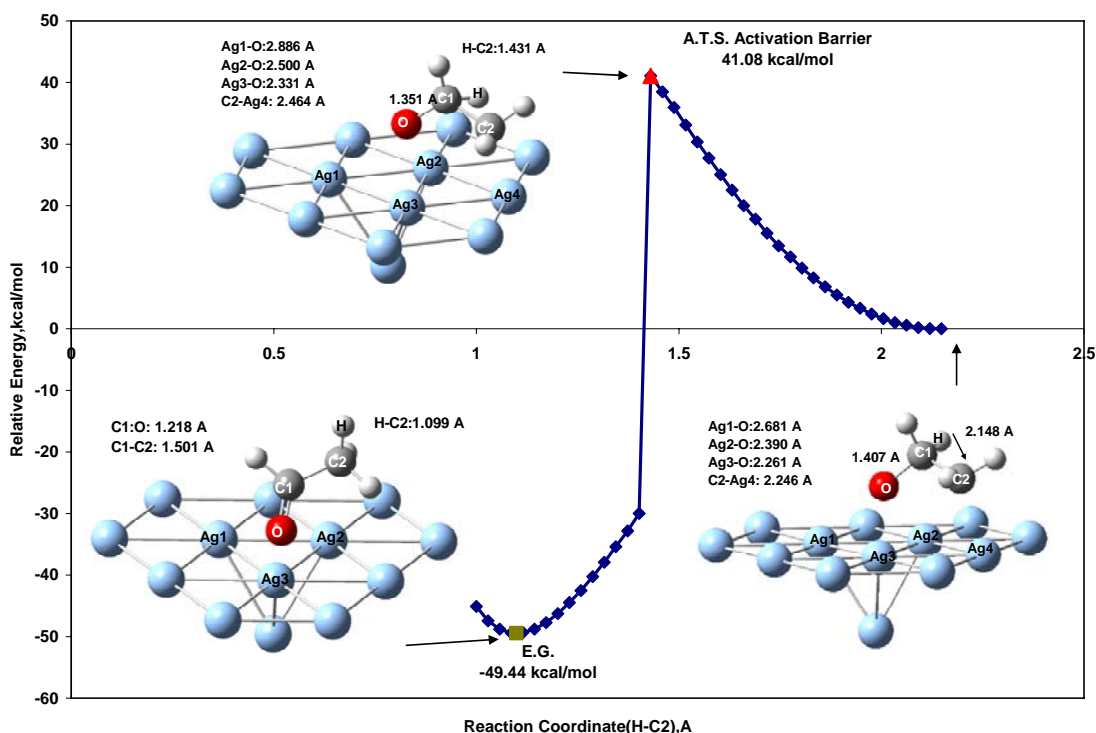


Figure 4.21 Relative energy profile along reaction coordinate (H-C2) for ethyl aldehyde formation on oxygen atom adsorbed on (001) silver surface cluster.

A comparison of activation barriers computed for the ethylene oxidation reactions (9-13) on Silver (111) cluster in this study is shown in Figure 4.22. As seen, ethyl aldehyde and vinyl alcohol can not be formed on Ag(111) surface because of those higher activation barriers while ethylene oxide can be formed on cluster. This situation is in agreement with experimental results. Table 4.2 shows a comparison of activation barriers computed for the ethylene oxide formation on Ag(111) cluster in this study with experimental and theoretical studies. As seen, activation barriers of the approximate transition states are reasonable agreement both theoretical and experimental values.

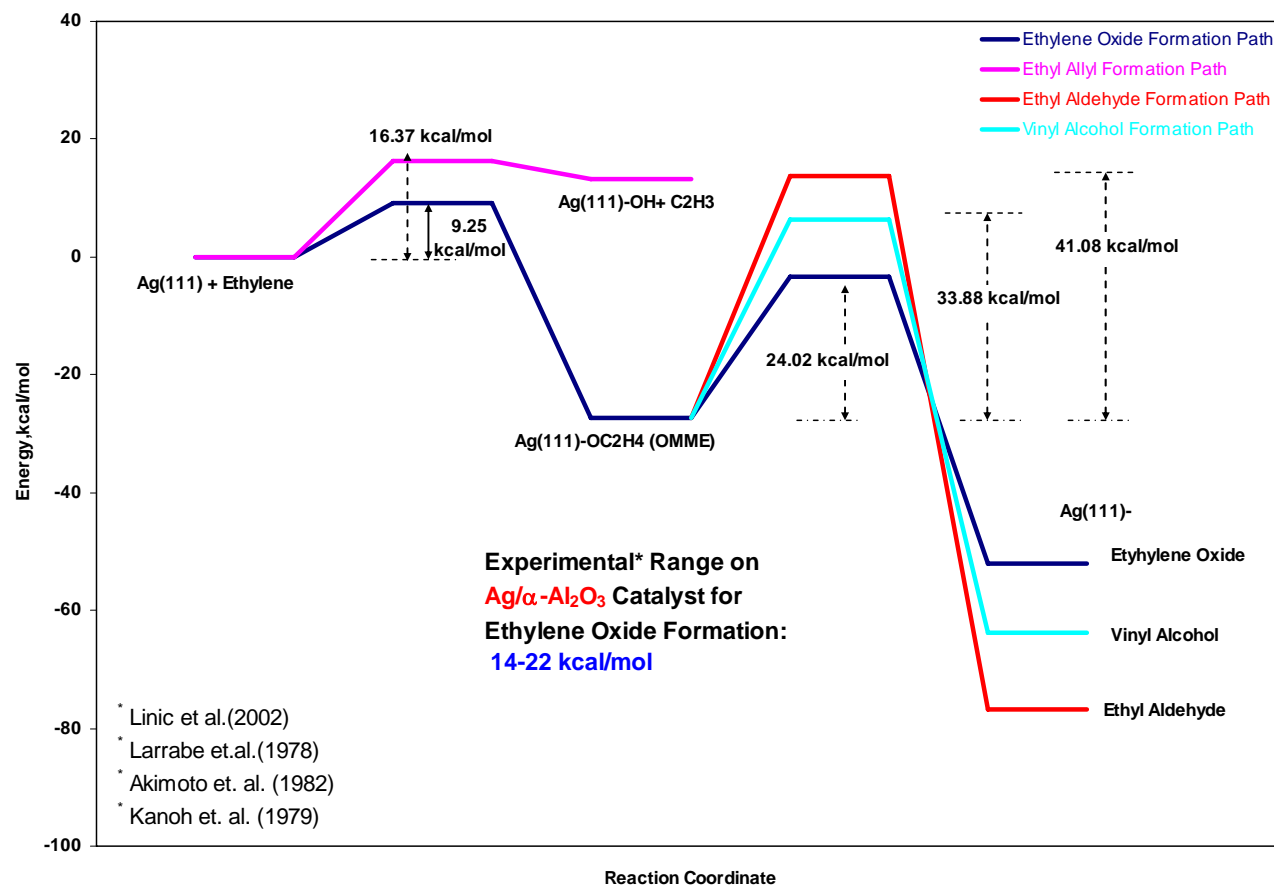


Figure 4.22 A summary energy diagram showing a comparison of the entire paths for ethylene epoxidation on (111) silver cluster.

Table 4.2 Comparison of activation barriers for ethylene oxide formation on silver (111) surface

	Method	Oxametallacycle Formation	Activation Barrier kcal/mol
This Study	Ag ₁₃ Cluster DFT/B3LYP (ATS)	YES	24.03
Other Theoretical	Ag ₁₅ Cluster DFT/Becke-Perdew (TS)	YES	13 ^a
	Periodic DFT Becke-Perdew (TS)	YES	16 ^b
	VASP/PW91/PAW p(2x2) and p(2x4) supercells (TS)	YES	18.45 ^c
Experimental (on Ag/α- Al₂O₃ catalyst)		14-22 ^{a,d,e,f}	

^a Linic et al. (2002)

^b Linic et al. (2003)

^c Torres et al. (2005)

^d Larrabe et.al. (1978)

^e Akimoto et. al. (1982)

^f Kanoh et. al. (1979)

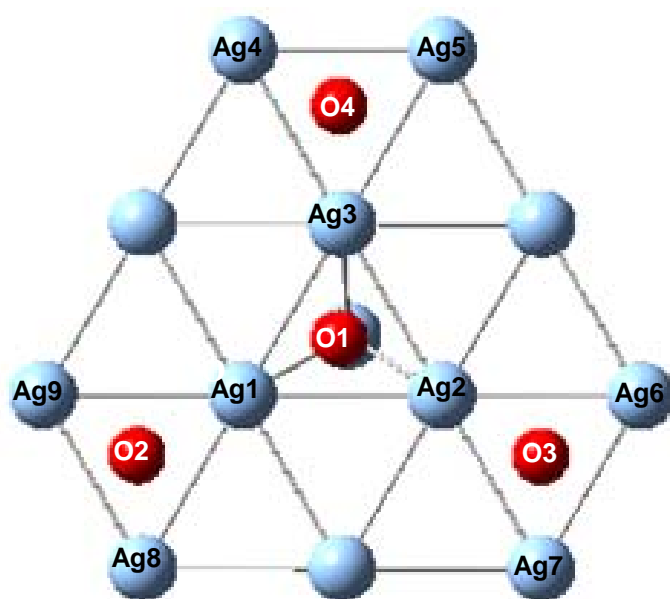
ATS: Approximate Transition State

TS: Transition state

4.2.2.2. Ethylene Epoxidation on Ag₁₃(111)(4O) Cluster (Oxygen coverage effect)

Ag₁₃(111) silver cluster including four oxygen atoms (33.33% coverage) was used to investigate the effect of oxygen coverage on ethylene oxide formation. Figure 4.23 shows the optimized equilibrium geometry of atomic oxygen atoms adsorption on the Ag cluster simulating Ag₁₃(111) surface.

(a)



(b)

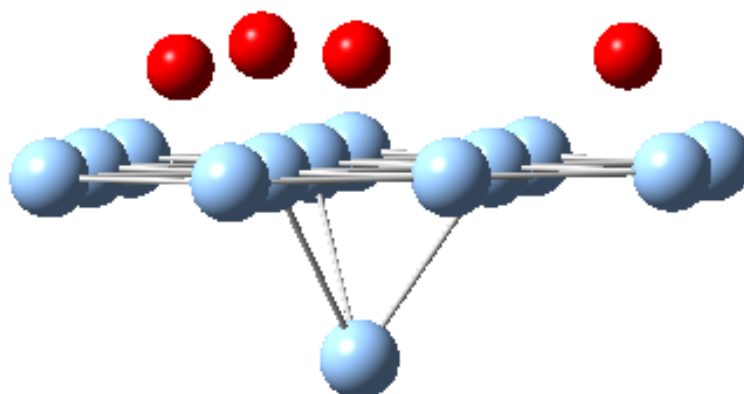
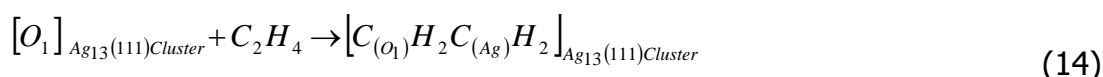


Figure 4.23 Equilibrium geometry for atomic oxygen adsorption on Ag₁₃(111) a) Top view b) Side view

Figure 4.24 depicts the relative energy profile for reaction 14 obtained when a reaction coordinate between the adsorbed O1 atom and one carbon atom of ethylene molecule (C1-O1) is chosen. The initial C1-O1 distance for the initial geometry is taken as 3.50 Å. There is an energy barrier of 7.08 kcal/mol. The final geometry which is similar to an oxametallacycle molecule is found at a relative energy value of -27.90 kcal/mole.

Ethylene adsorption



Ethylene oxide formation

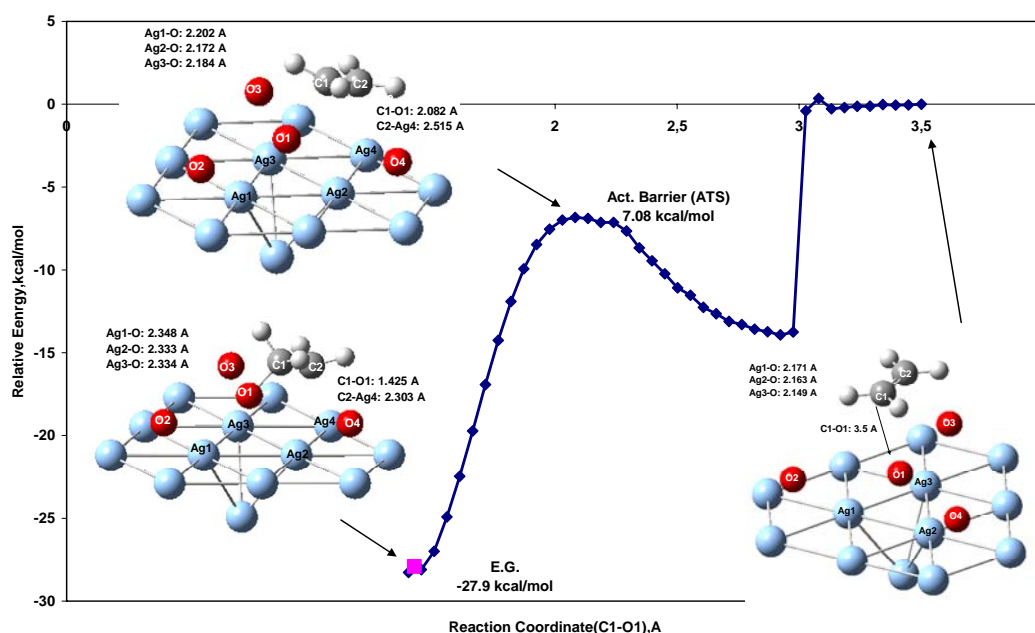
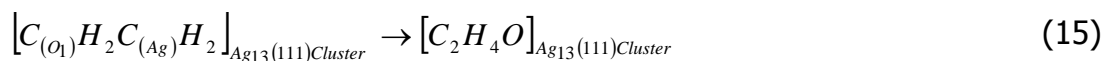


Figure 4.24 Relative energy profile along reaction coordinate (C1-O1) for ethylene oxide formation on oxygen atoms (4O) adsorbed on 13 atoms (111) silver surface cluster.

The next step (Reaction 15) is taken to be a reaction coordinate between the O atom and other carbon atom of ethylene molecule (C2-O1). The relative

energy profile obtained is represented in Figure 4.25. The initial geometry is oxametallacycle geometry where the initial C2-O distance is found as 2.52 Å. This geometry and the final geometry of the first step which has a reaction coordinate between C1 and O1 is the same. A relative energy barrier of an approximate transition state for the second step is 12.54 kcal/mol. The final geometry of ethylene oxide on the cluster is found at a relative energy value of -28.59 kcal/mol. The approximate activation barrier of ethylene epoxidation which has a reaction coordinate between the adsorbed O atom and the second carbon atom of ethylene molecule (C2-O2) is accepted the activation barrier for ethylene oxide formation reaction on Ag₁₃(111) cluster.

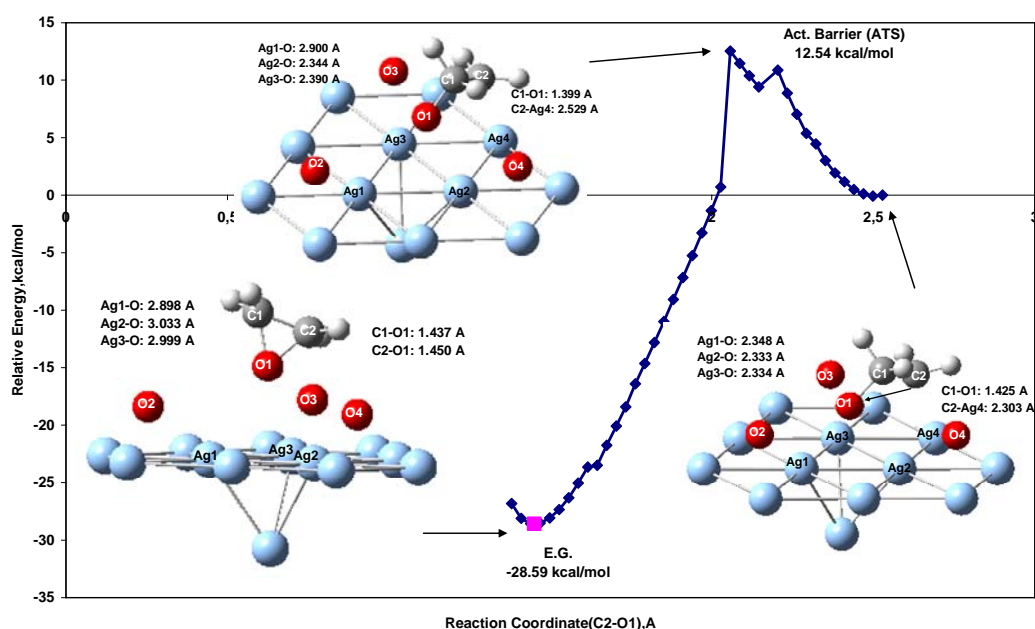


Figure 4.25 Relative energy profile along reaction coordinate (C2-O1) for ethylene oxide formation on oxygen atoms (4O) adsorbed on 13 atoms (111) silver surface cluster.

A comparison of ethylene oxide formation on silver with both 8.3% and 33.33% coverage is shown in Figure 4.26. As seen, activation barrier for ethylene oxide formation decreases with increasing oxygen coverage. Table 4.4 also gives this comparison. Table 4.4 includes different coverage values of 8.33%, 25% and 33.33%.

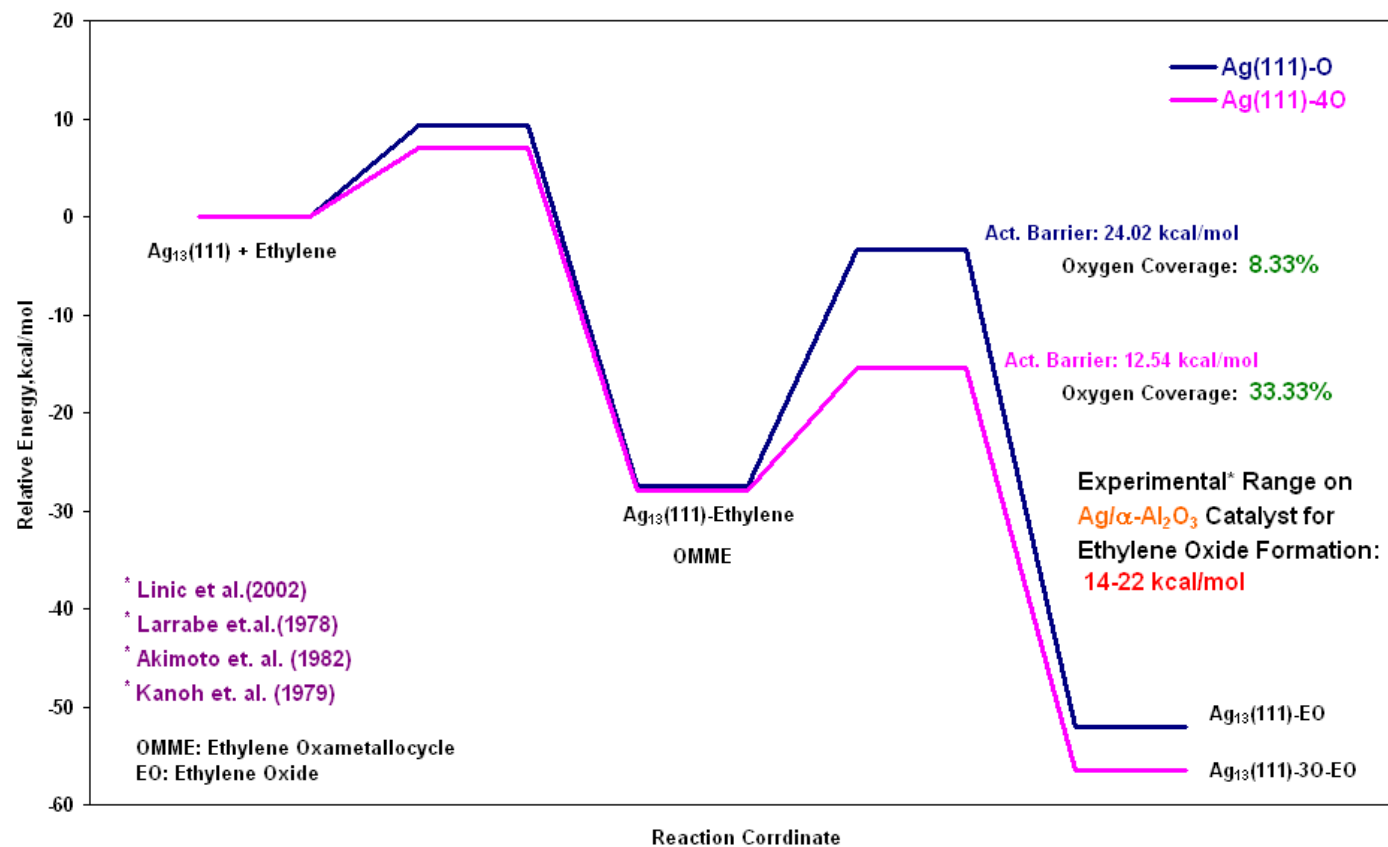


Figure 4.26 A summary energy diagram showing a comparison for ethylene oxide formation on (111) surface with different coverage values.

Table 4.3 A comparison for ethylene oxide formation with different oxygen coverage values on (111) silver surface

Reaction	Silver (111) Cluster		
	Ag ₁₃ (O)	Ag ₅ (O)	Ag ₁₃ (4O)
Ethylene Oxide Formation	Oxygen coverage (%)		
	8.33	25	33.33
	Activation Barrier (kcal/mol)		
	24.02	17.2	12.54

As seen from the Table 4.3, activation barrier for ethylene oxide formation decreases with increasing oxygen coverage. This is in consistent with experimental work that reported increasing selectivity of the silver catalyst for alkene epoxidation at increasing oxygen coverage (Lambert et al., 2005).

4.2.2.3. Ethylene Epoxidation on Slab Surface

In order to compare the geometries obtained using cluster calculations, geometries for ethylene oxidation reactions on silver surface were obtained by using VASP software which uses periodic slab method. In this method, surface used is infinite in X, Y and Z directions. Optimized geometry of O atom interaction with the slab is shown in Figure 4.27.

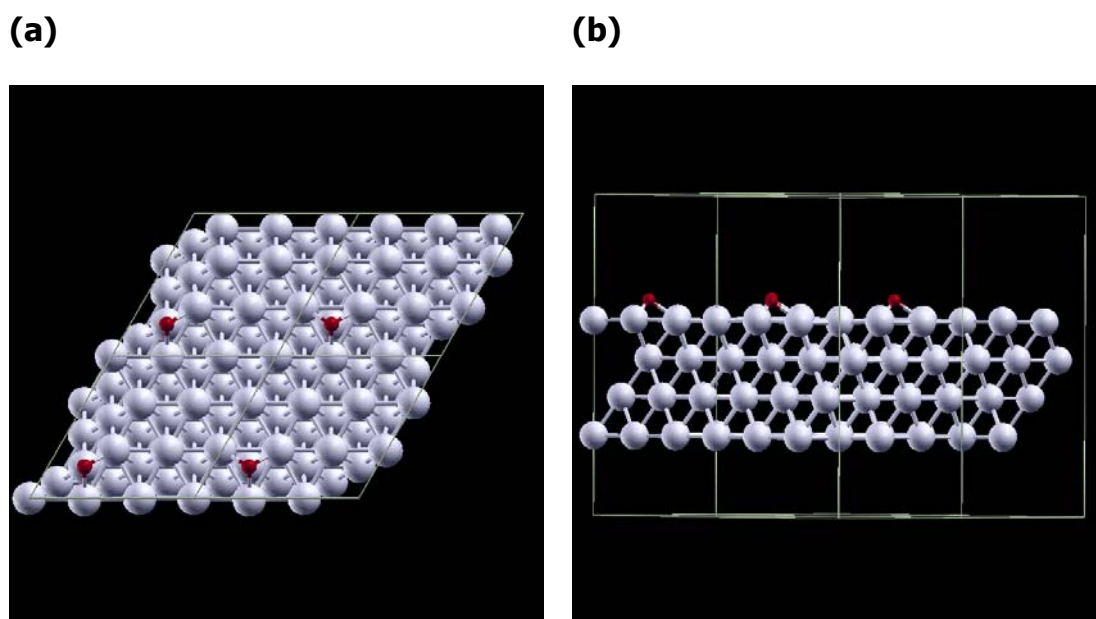
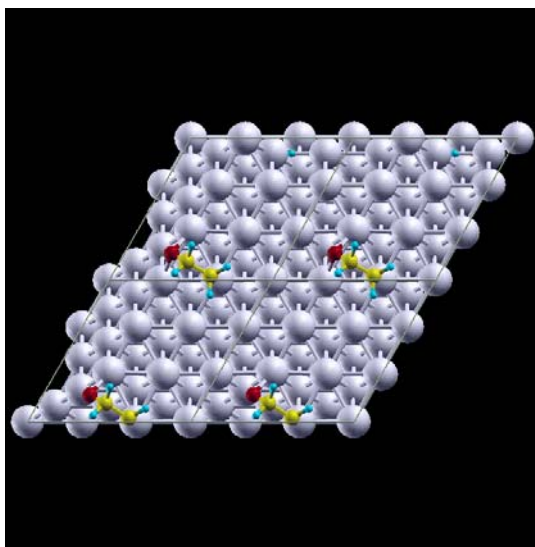


Figure 4.27 Optimized geometry of atomic O adsorption on slab a) Top view, b) Side view

Optimized geometries of OMME, ethylene oxide, ethyl aldehyde and vinyl alcohol were obtained by using VASP. These geometries are represented in Figures 4.28, 4.29, 4.30 and 4.31, respectively.

(a)



(b)

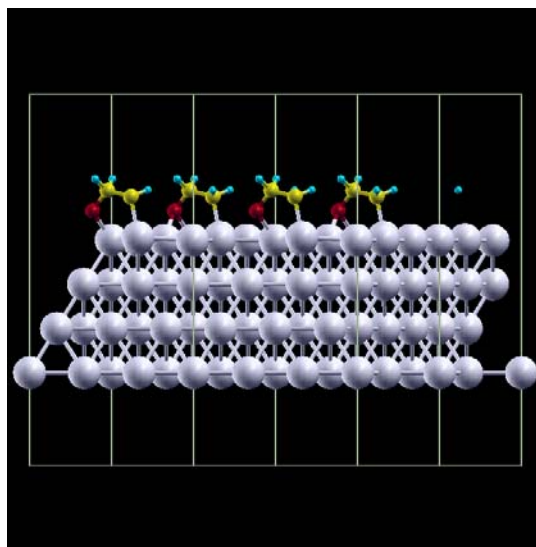
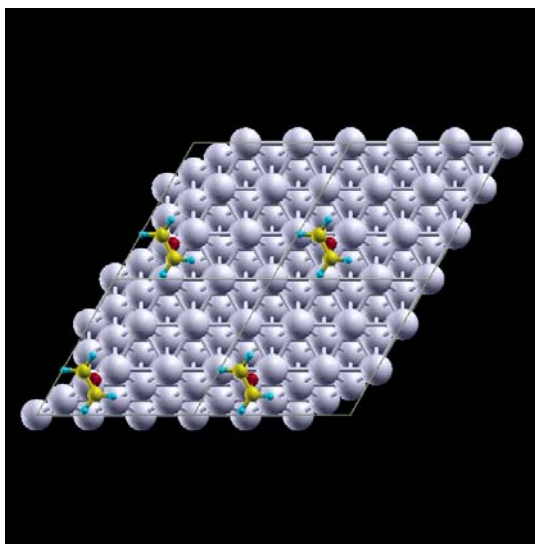


Figure 4.28 Optimized geometry of OMME on slab a) Top view, b) Side view

(a)



(b)

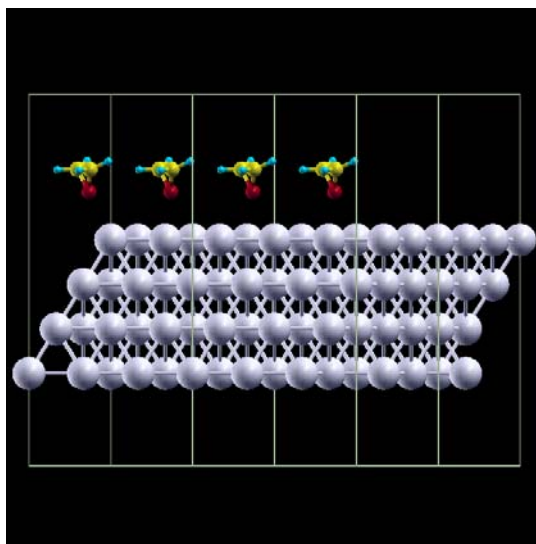
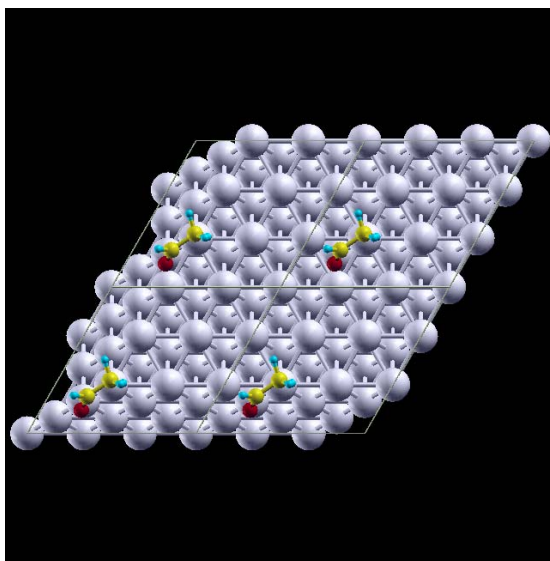


Figure 4.29 Optimized geometry of ethylene oxide ethyl aldehyde on slab a) Top view, b) Side view

(a)



(b)

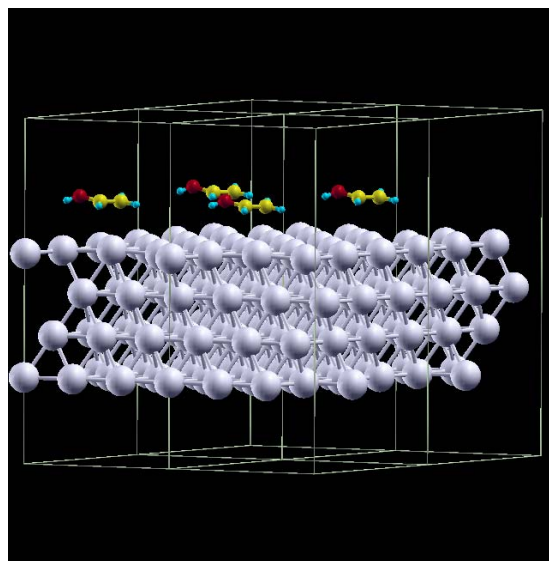
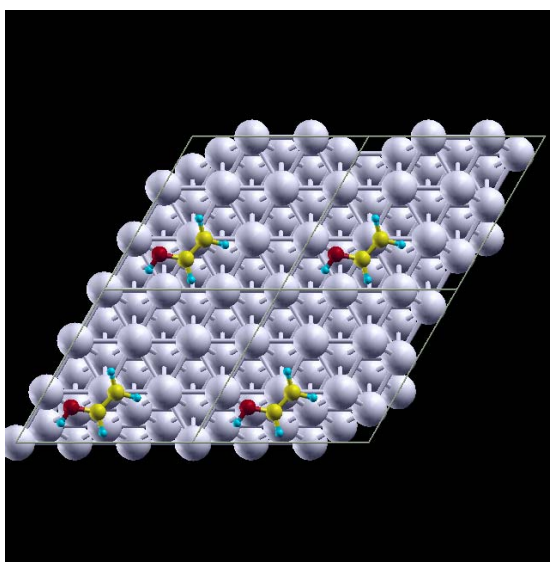


Figure 4.30 Optimized geometry of ethyl aldehyde on slab a) Top view, b) Side view

(a)



(b)

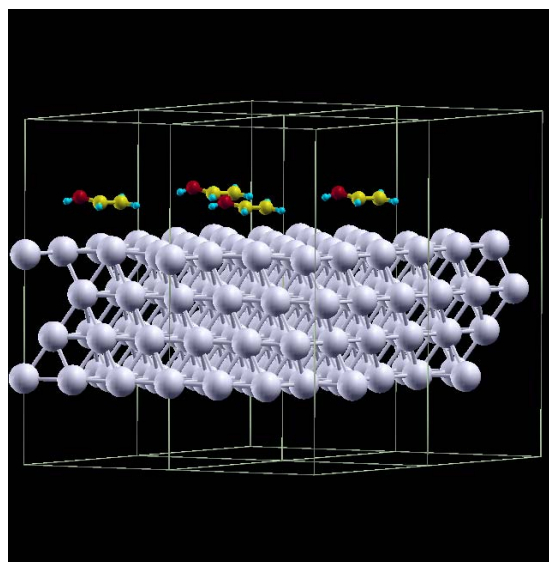


Figure 4.31 Optimized geometry of vinyl alcohol on slab a) Top view, b) Side view

Figure 4.32 shows a comparison of relative energy for ethylene epoxidation by using slab surface. For ethylene epoxidation, the qualitative trend of relative energy is the same with that of calculations obtained by using surface clusters. In other words, products order which is OMME, ethylene oxide, vinyl alcohol and ethyl aldehyde respectively is the same for cluster and slab calculations.

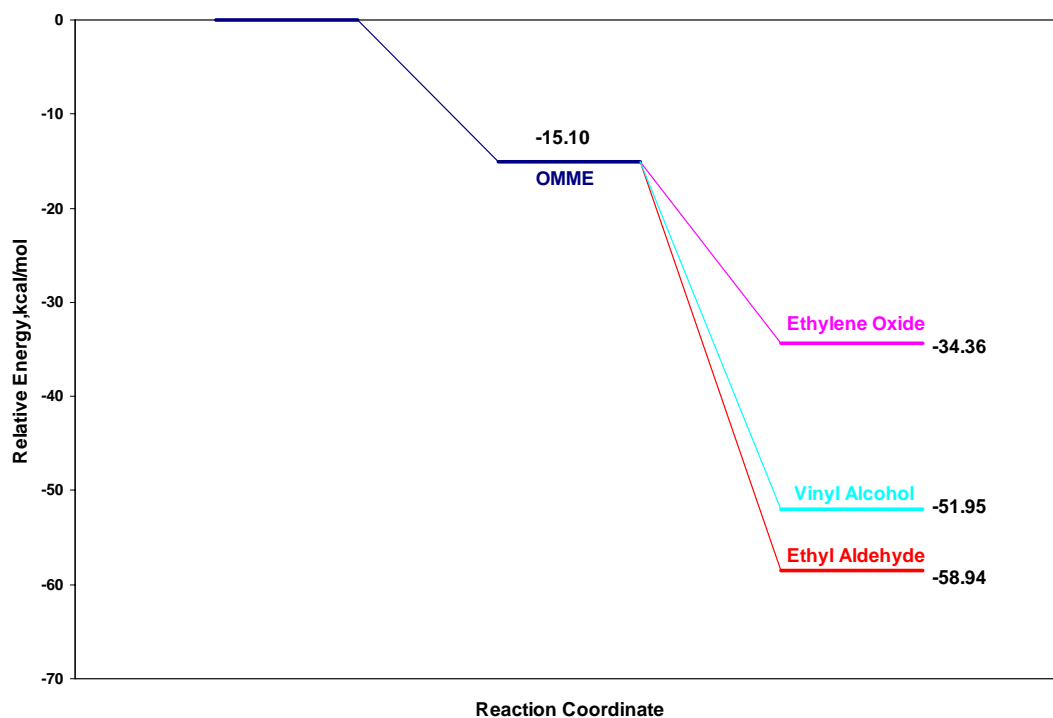
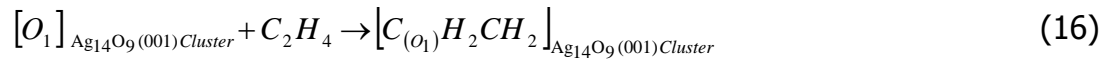


Figure 4.32 A summary energy diagram for ethylene epoxidation on 4-layer-(3x3) slab.

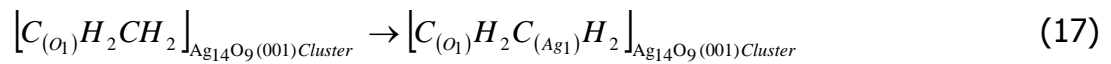
4.2.3. Ethylene Epoxidation on Silver Oxide Ag₁₄O₉(001) Surface

The proposed reaction steps for the oxidation of ethylene on the cluster are:

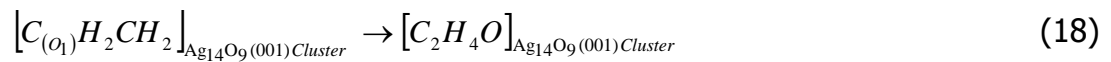
Step 1, ethylene adsorption



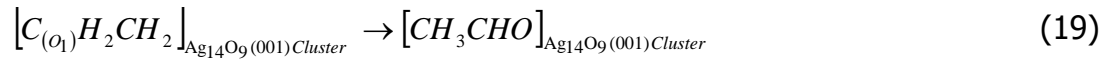
Step 2, oxametallocycle formation



Step 3, ethylene oxide formation



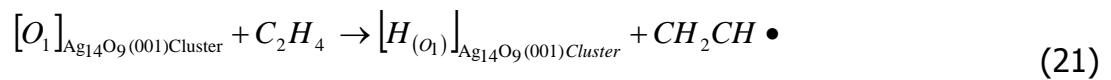
Step 4, ethyl aldehyde formation



Step 5, vinyl alcohol formation



Step 6, vinyl radical formation



4.2.3.1. Vinyl Radical Formation Path

Figure 4.33 illustrates the relative energy profile for step 6 (Reaction 21) obtained when a reaction coordinate between the adsorbed O atom and one hydrogen atom of ethylene molecule (H-O) is chosen. The initial O-H distance is taken as 3.00 Å. A relative energy barrier of an approximate transition state is 22.54 kcal/mol. The final geometry is found at an endothermic relative energy value of 16.49 kcal/mole.

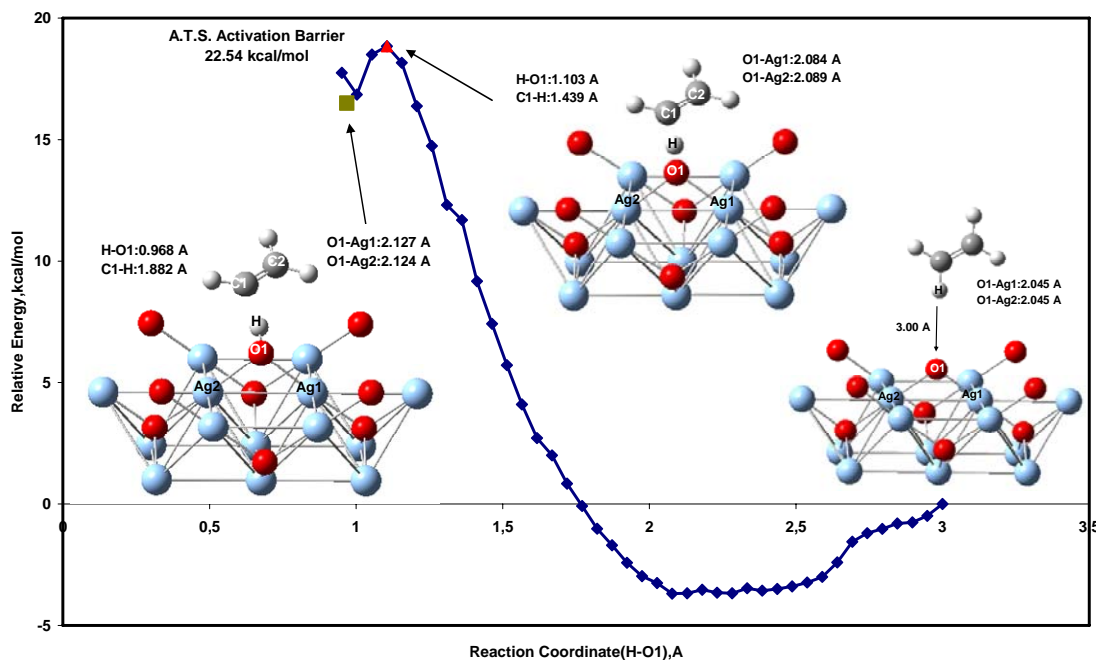


Figure 4.33 Relative energy profile along reaction coordinates (H-O) for C-H activation of ethylene on oxygen atom adsorbed on (001) silver oxide surface cluster.

4.2.3.2 Ethylene Oxide Formation Path

One step again along the reaction coordinate is the adsorption of ethylene (Step 1, reaction 16) onto the oxygen atom-adsorbed Ag_2O cluster to form ethylene oxide. Figure 4.34 depicts the relative energy profile obtained when a reaction coordinate between the adsorbed O atom and one carbon atom of ethylene molecule (C1-O) is chosen. The initial C1-O distance for the initial geometry is taken as 3.00 Å. There is an energy barrier of 8.47 kcal/mol. The final geometry which is not similar to an oxametallacycle molecule is found at a relative energy value of -8.42 kcal/mole.

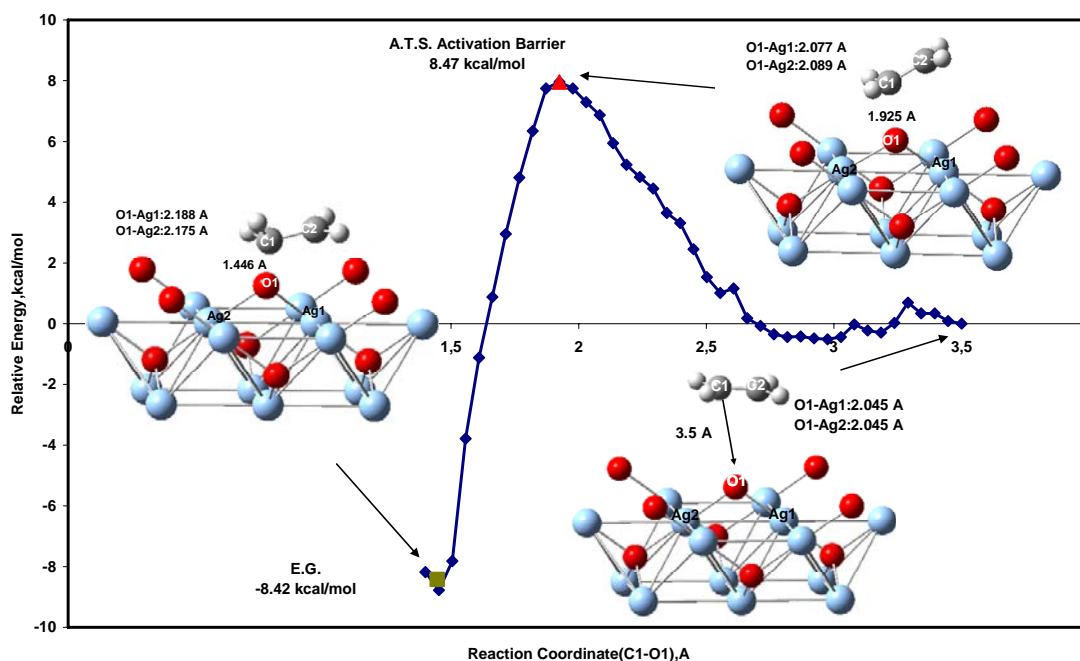


Figure 4.34 Relative energy profile along reaction coordinate (C1-O) for ethylene oxide formation on oxygen atom adsorbed on (001) silver oxide surface cluster.

Reactions coordinate between the C2 of the ethylene molecule and silver atom of the surface (C2-Ag4) is chosen to obtain oxametallacycle molecule on the surface (Step 2, reaction 17). The relative energy profile obtained is represented in Figure 4.35. Relative energy exponentially increases for this reaction.

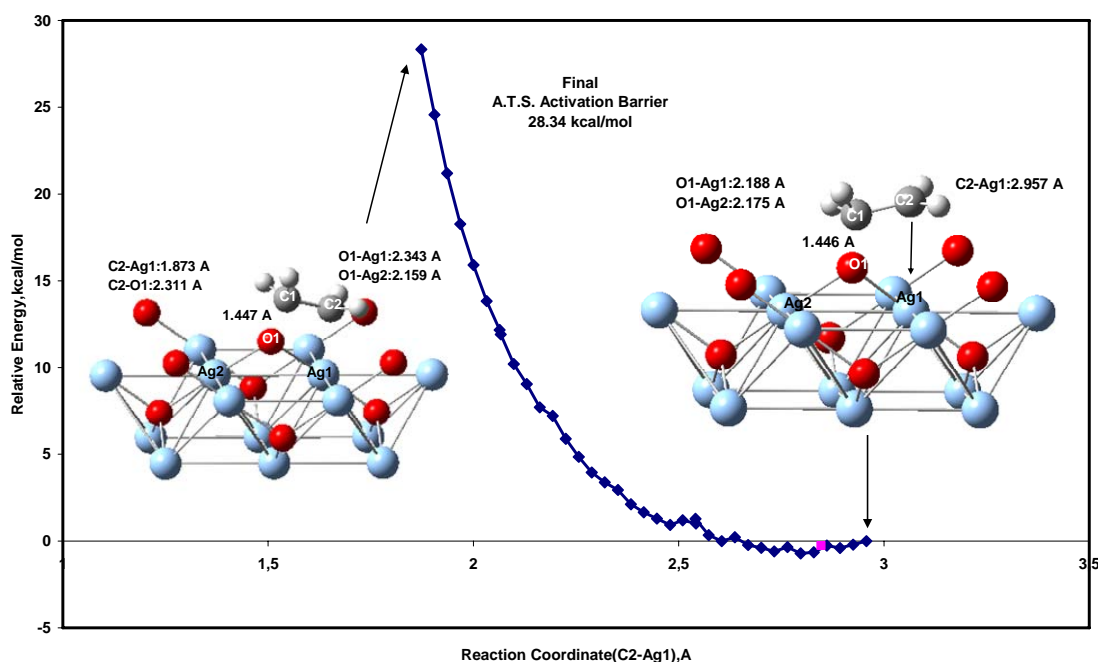


Figure 4.35 Relative energy profile along reaction coordinate (C2-Ag4) for oxametallacycle molecule formation on oxygen atom adsorbed on (001) silver oxide surface cluster.

The next step (Reaction 18, step 3) is taken to be a reaction coordinate between the O atom and other carbon atom of ethylene molecule (C2-O). Figure 4.36 shows the relative energy profile obtained. The initial geometry is oxametallacycle geometry where the initial C2-O distance is found as 2.395 Å. This geometry and the final geometry of the first step which has a reaction coordinate between C1 and O is the same. A relative energy barrier of an approximate transition state for the second step is 19.45 kcal/mol. The

final geometry of ethylene oxide on the cluster is found at a relative energy value of -7.21 kcal/mol. The approximate activation barrier of ethylene oxide formation reaction which has a reaction coordinate between the adsorbed O atom and the second carbon atom of ethylene molecule (C2-O) is accepted the activation barrier on Ag₂O(001) cluster.

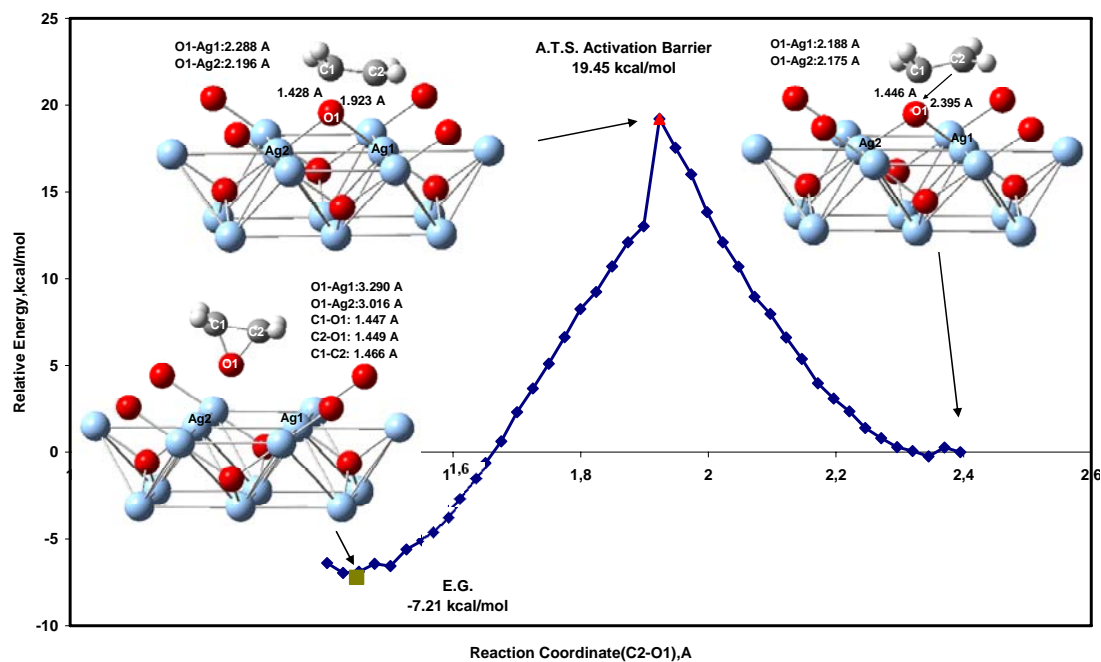


Figure 4.36 Relative energy profile along reaction coordinate (C2-O) for ethylene oxide formation on oxygen atom adsorbed on (001) silver oxide surface cluster.

4.2.3.3. Vinyl Aldehyde Formation Path

After the completion of first C activation reaction, H of the adsorbed C (first C) can go to the second C to form ethyl (vinyl) aldehyde (Step 4, reaction 19). Figure 4.37 represents the relative energy profile obtained for this reaction. A relative energy barrier of an approximate transition state for the second step is 34.76 kcal/mol. The final geometry of ethylene oxide on the

cluster is found at a relative energy value of -32.23 kcal/mol. As seen, ethyl aldehyde can not be formed on Ag_2O surface while ethylene oxide can be formed on cluster.

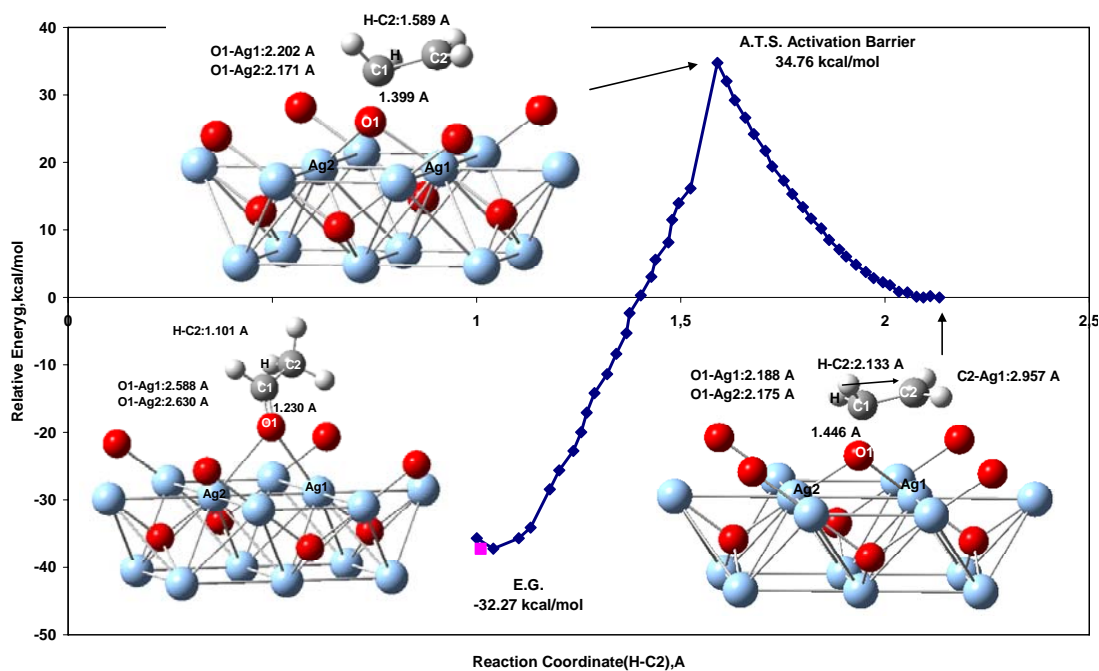


Figure 4.37 Relative energy profile along reaction coordinate (H-C2) for ethyl aldehyde formation on oxygen atom adsorbed on (001) silver oxide surface cluster.

4.2.3.4. Vinyl Alcohol Formation Path

After the completion of first C activation reaction, H of the adsorbed C (first C) can go to the second C to form ethyl aldehyde or to O1 atom to form vinyl alcohol. Figure 4.38 shows the relative energy profile obtained for the formation of vinyl alcohol reaction (Step 5, reaction 20). A relative energy barrier of an approximate transition state for the second step is 34.32 kcal/mol. The final geometry of ethylene oxide on the cluster is found at a

relative energy value of -19.71 kcal/mol. As seen, like ethyl aldehyde vinyl alcohol can not be formed on Ag_2O surface while ethylene oxide can be formed on cluster.

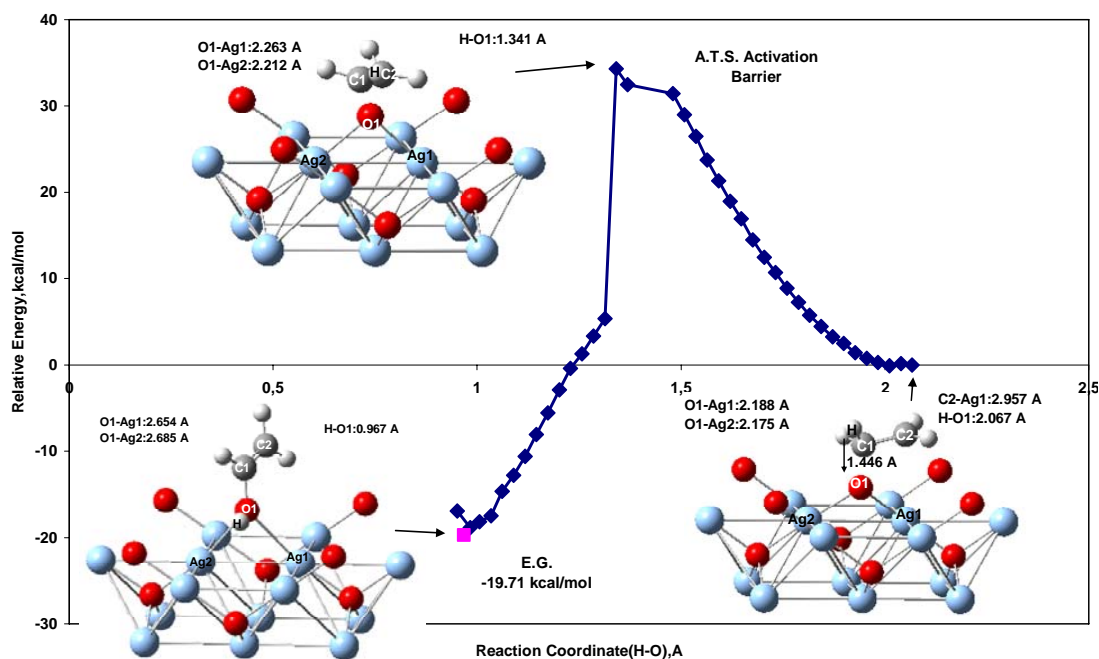


Figure 4.38 Relative energy profile along reaction coordinate (H-O1) for vinyl alcohol formation on oxygen atom adsorbed on (001) silver oxide surface cluster.

A comparison of the activation energy barriers for the oxidation reactions (16-21) of ethylene on silver oxide (001) cluster with available theoretical and experimental studies on silver and surface oxide structure on silver is given in Table 4.4. As mentioned before, there are no activation barrier data for the reactions on silver oxide in both experimental and theoretical literature. Figure 4.39 also shows a comparison of activation barriers computed for the ethylene oxide formation on $\text{Ag}_2\text{O}(001)$ clusters in this study. The most important difference between this study and other

theoretical study (Medlin and Barteau, 1999) for this reaction is the formation of ethylene oxametallocycle. This intermediate molecule is not formed on $\text{Ag}_2\text{O}(001)$ surface (relative energy for the formation of this molecule goes to infinity) while it is formed on surface oxide structure on $\text{Ag}(111)$. The reason of this may be that silver oxide structure has sub-oxygen atoms. The ATS activation barrier of the first path is calculated to be 19.45 kcal/mol which is close to theoretical value of 17.06 kcal/mol obtained on surface oxide structure on $\text{Ag}(111)$ (Bocquet et al., 2003). This value is also in good agreement with the experimental range of 14-22 kcal/mol (Akimoto et al., 1982; Kanoh et al., 1979; Larrabe and Kuczkowski 1978, Linic et al. 2002) found on $\text{Ag}/\alpha\text{-Al}_2\text{O}_3$ catalyst. As a result, silver oxide (001) like surface oxide structure on $\text{Ag}(111)$ has a similar effect on activation barrier of ethylene oxide formation. This situation is supported by the experimental study (Bukhtiyarov, 2003) which reported that the formation of a surface silver (I) oxide that is confirmed by the similarity of its spectral characteristics with those of bulk Ag_2O and experimental and theoretical STM studies (Bocquet et al., 2005; Michaelides et al., 2005; Schmid et al., 2006). The ATS activation barriers of the second and third paths (ethyl aldehyde and vinyl alcohol formation reactions, respectively) are calculated to be 34.76 kcal/mol and 34.42 kcal/mol respectively which are higher than that of ethylene oxide formation path. These barriers show that ethyl aldehyde and vinyl alcohol are not formed on silver oxide (001) surface. For the other possible reaction which gives vinyl radical, ATS barrier is 22.54 kcal/mol which seems to be somewhat higher than that of ethylene oxide formation path.

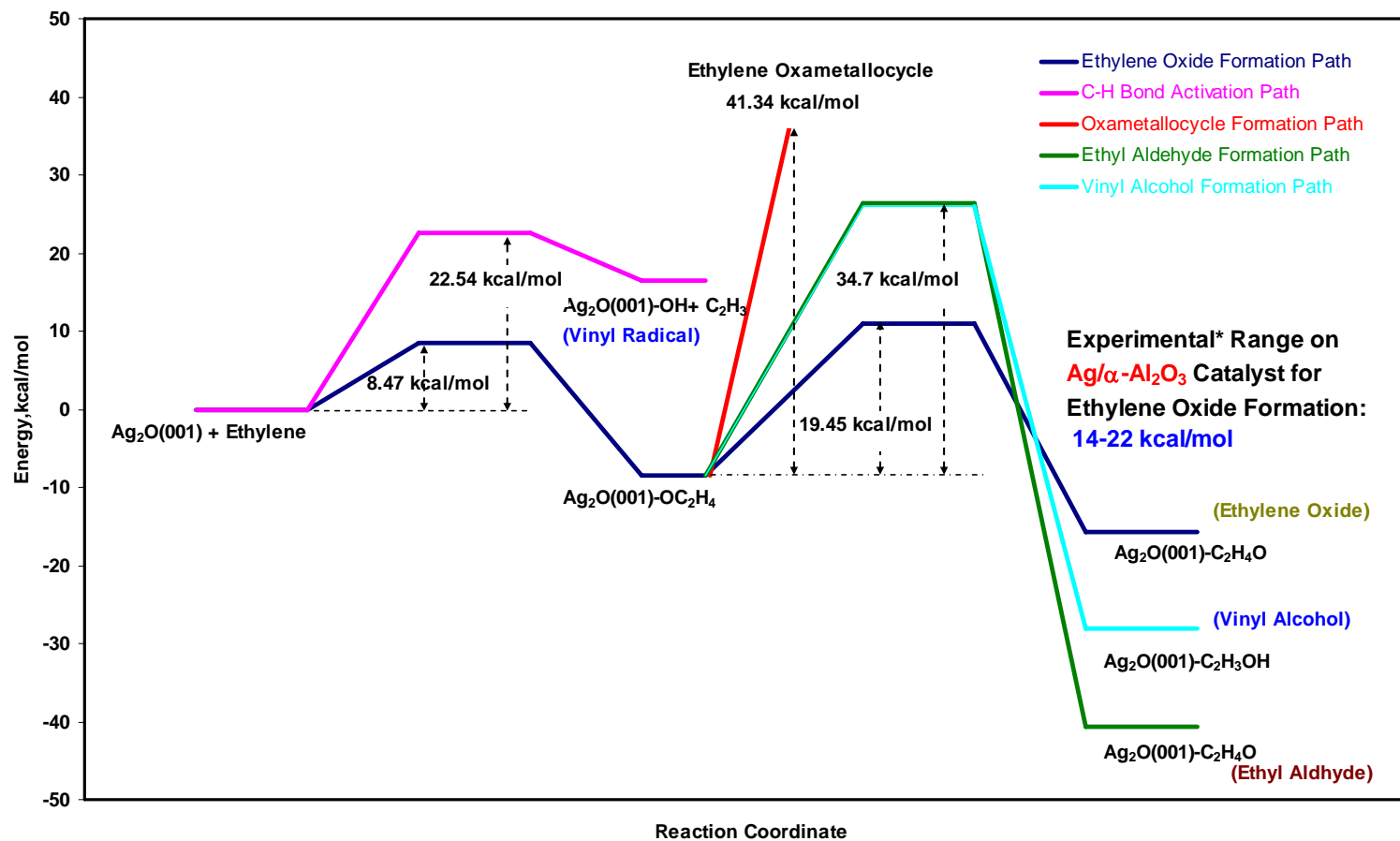


Figure 4.39 A summary energy diagram showing a comparison of the entire paths for ethylene epoxidation on (001) silver oxide cluster.

Table 4.4 The comparison of the activation energy barriers of ethylene epoxidation reactions on [Ag₁₄O₉] cluster representing (001) silver oxide.

Reactions	Activation Barrier kcal/mol	
	This Study (ATS)	Other Theoretical ^a (TS)
C1 Activation	8.47	
Oxametallocycle Formation	41.34 (increases)	17.06 ^{*,**}
C2 Activation (Ethylene Oxide Formation)	19.45	17.06 [*]
H Activation (Ethyl Aldehyde Formation)	34.76	-
H Activation (Vinyl Alcohol Formation)	34.32	-
H Activation (Vinyl Radical Formation)	22.54	-
Experimental* (Ethylene oxide formation on Ag/α-Al₂O₃)	14 - 22	

* Reaction occurs on Ag₁₁O₆/Ag(111) surface

** C1 activation and oxametallocycle formation occur simultaneously

^a Bcquet et al. 2003

* Linic et al. (2002)

* Larrabe et.al. (1978)

* Akimoto et. al. (1982)

* Kanoh et. al. (1979)

4.3. Propylene Epoxidation

4.3.1. Propylene Epoxidation on Silver Surface

Several products such as propylene oxide, acetone, propanal and Π -allyl radical can be formed during the epoxidation of propylene with atomic oxygen. These products are formed via different reactions which are parts of a mechanism of ethylene epoxidation. This reaction mechanism is shown in Figure 4.40.

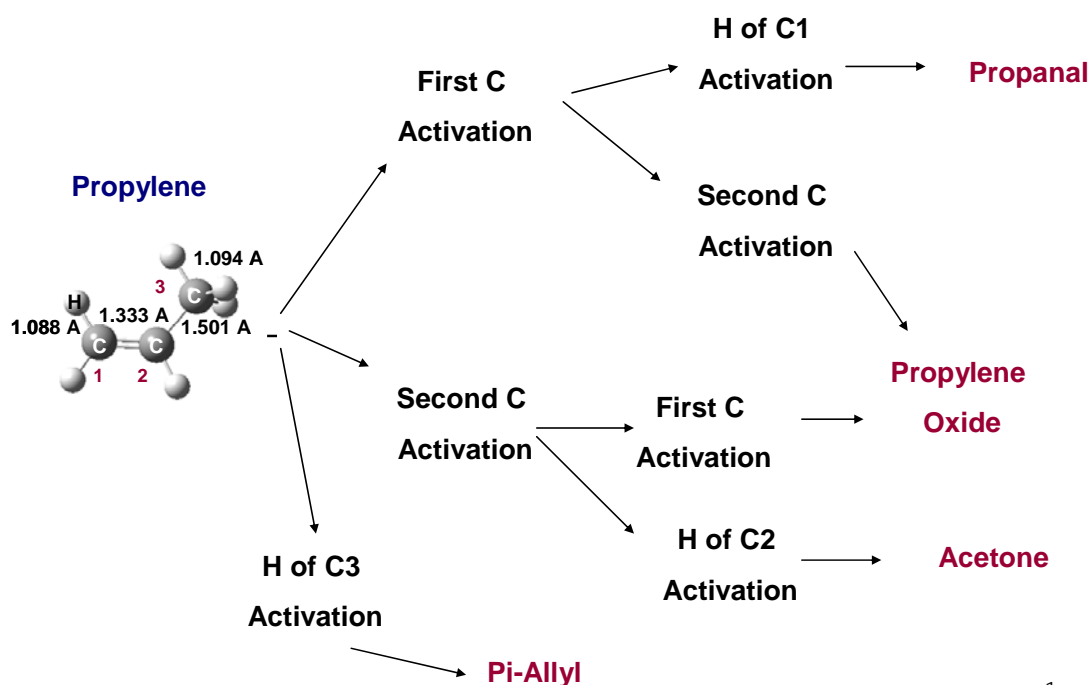
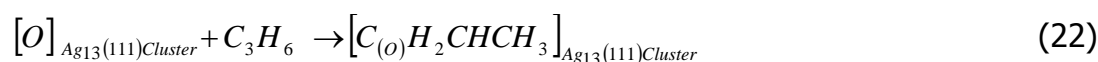


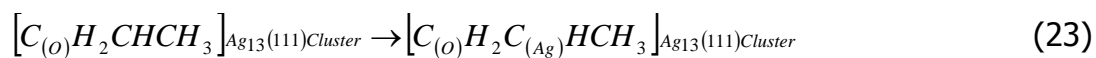
Figure 4.40 A reaction mechanism for propylene epoxidation

The proposed reaction steps for the oxidation of propylene on the cluster are:

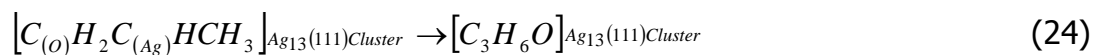
Step 1, propylene adsorption-1



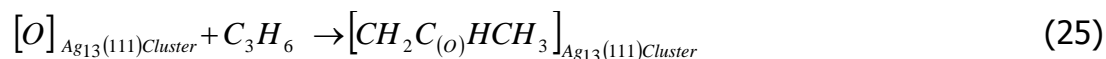
Step 2, propylene oxametallocycle (OMMP1) formation



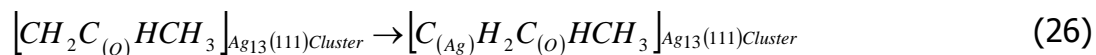
Step 3, propylene oxide formation from OMMP1



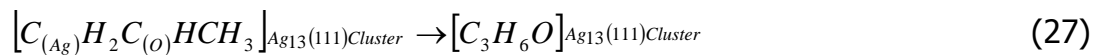
Step 4, propylene adsorption-2



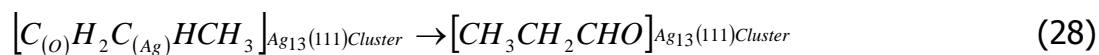
Step 5, propylene oxametallocycle (OMMP2) formation



Step 6, propylene oxide formation from OMMP2



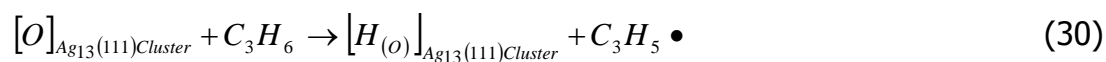
Step 7, propanal formation



Step 8, acetone formation



Step 9, Π-allyl radical formation



4.3.1.1. Propylene Epoxidation on Ag₁₃(111) Cluster

4.3.1.1.1. π -Allyl Formation Path

Figure 4.41 represents the relative energy profile for reaction 30 (Step 9) obtained when a reaction coordinate between the adsorbed O atom and one hydrogen atom of ethylene molecule (H-O) is chosen. The initial O-H distance is taken as 3.00 Å. A relative energy barrier of an approximate transition state is 6.11 kcal/mol. The final geometry is found at an exothermic relative energy value of -9.94 kcal/mole.

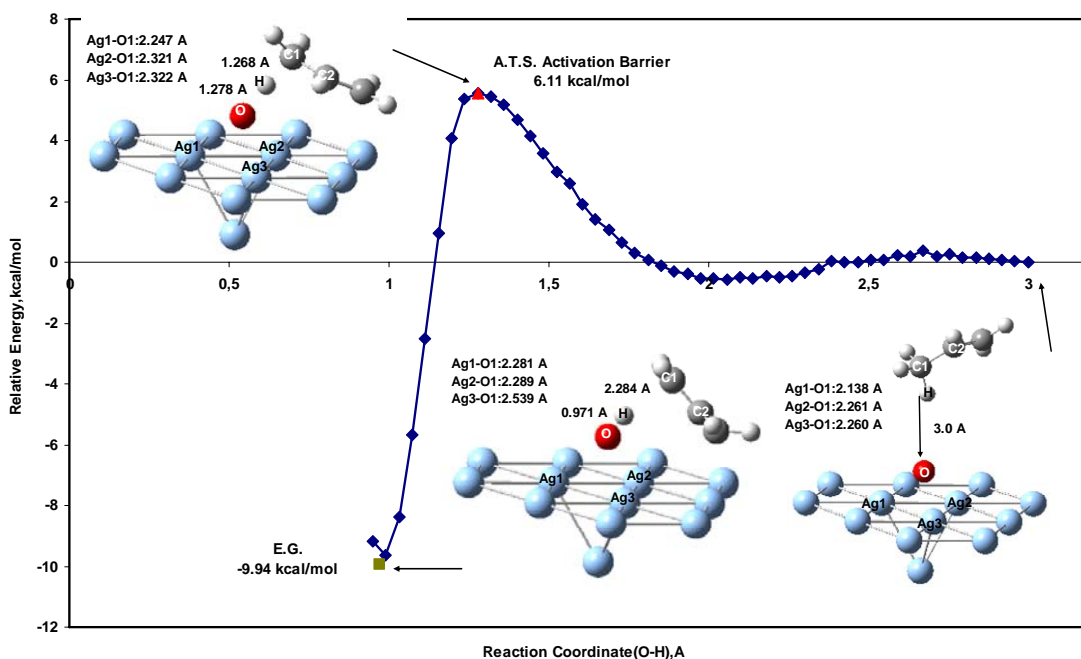


Figure 4.41 Relative energy profile along reaction coordinates (H-O) for C-H activation of propylene on oxygen atom adsorbed on 13 atoms (111) silver surface cluster.

4.3.1.1.2. Propylene Oxide Formation Path

Another possible step along the reaction coordinate is the adsorption of propylene onto the oxygen atom-adsorbed Ag cluster to form propylene oxide. Figure 4.42 depicts the relative energy profile for step 1 (Reaction 22) obtained when a reaction coordinate between the adsorbed O atom and one carbon atom of propylene molecule (C1-O) is chosen. The initial C1-O distance for the initial geometry is taken as 3.00 Å. There is an energy barrier of 13.48 kcal/mol and a relative energy value of -14.43 kcal/mole.

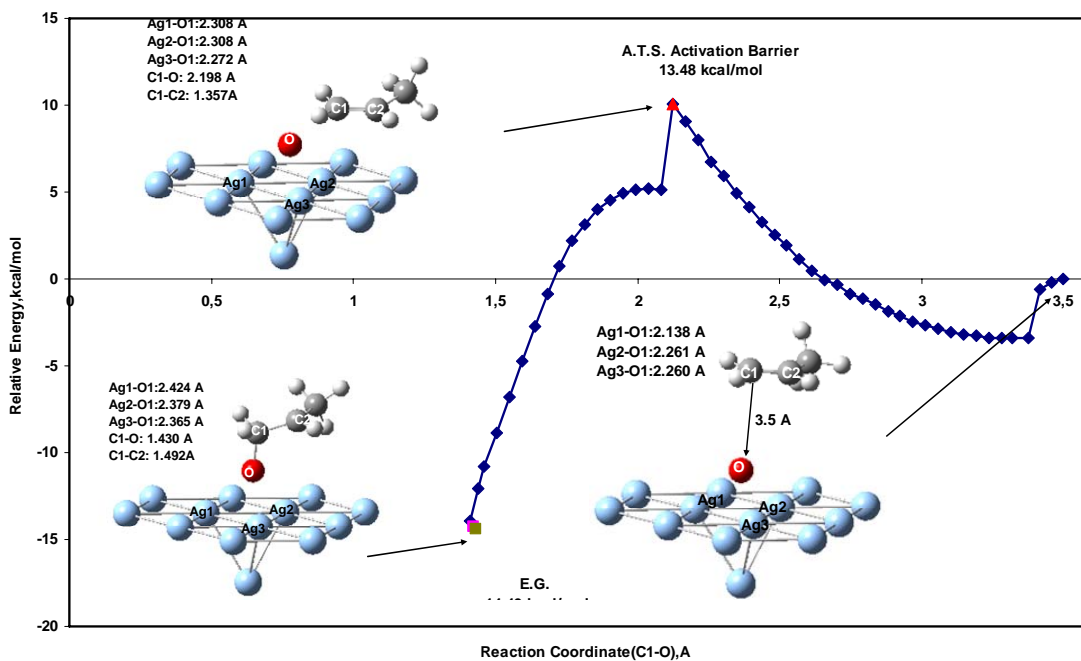


Figure 4.42 Relative energy profile along reaction coordinate (C1-O) for ethylene oxide formation on oxygen atom adsorbed on (111) silver surface cluster

Reactions coordinate between the C2 of the propylene molecule and silver atom of the surface (C2-Ag4) is chosen to obtain oxametallacycle molecule on the surface (Step 2, reaction 23). The relative energy profile obtained is depicted in Figure 4.43. The final geometry which is similar to an oxametallacycle molecule is found at a relative energy value of -8.05 kcal/mole.

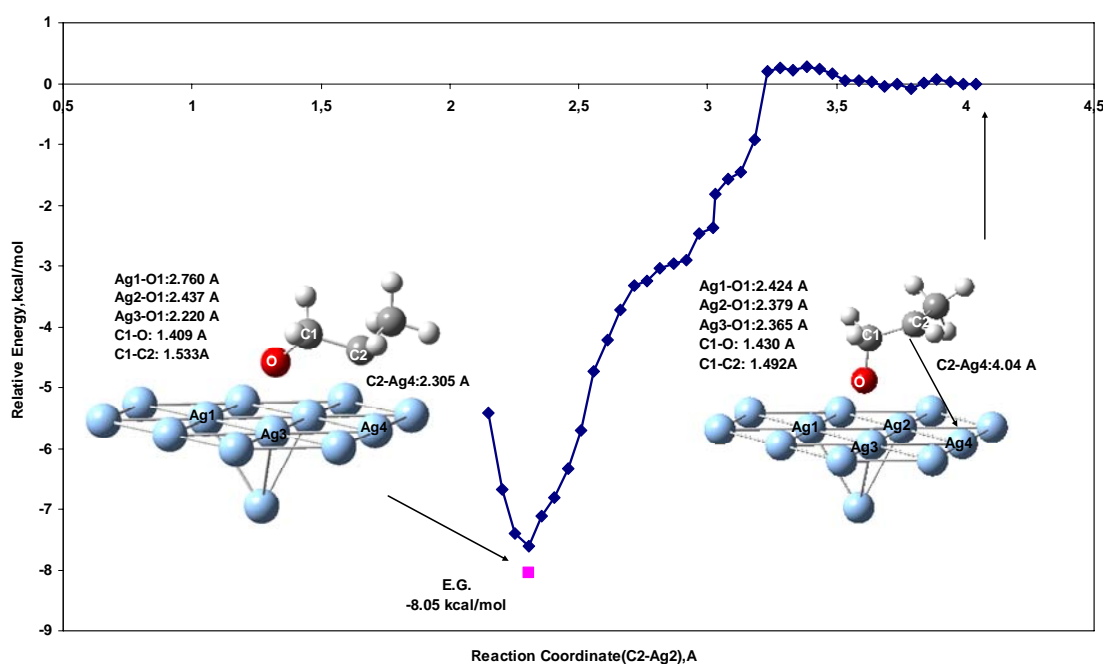


Figure 4.43 Relative energy profile along reaction coordinate (C2-Ag4) for oxametallacycle molecule formation on oxygen atom adsorbed on (111) silver surface cluster.

The next step (Reaction 24, step 3) is taken to be a reaction coordinate between the O atom and other carbon atom of propylene molecule (C2-O). Figure 4.44 shows the relative energy profile obtained. The initial geometry is oxametallacycle geometry where the initial C2-O distance is found as 2.47 Å. This geometry and the final geometry of the first step which has a

reaction coordinate between C1 and O is the same. A relative energy barrier of an approximate transition state for the second step is 15.74 kcal/mol. The final geometry of ethylene oxide on the cluster is found at a relative energy value of -33.03 kcal/mol. The approximate activation barrier of propylene epoxidation which has a reaction coordinate between the adsorbed O atom and the second carbon atom of propylene molecule (C2-O) is accepted the activation barrier for ethylene oxide formation reaction on Ag₁₃(111) cluster.

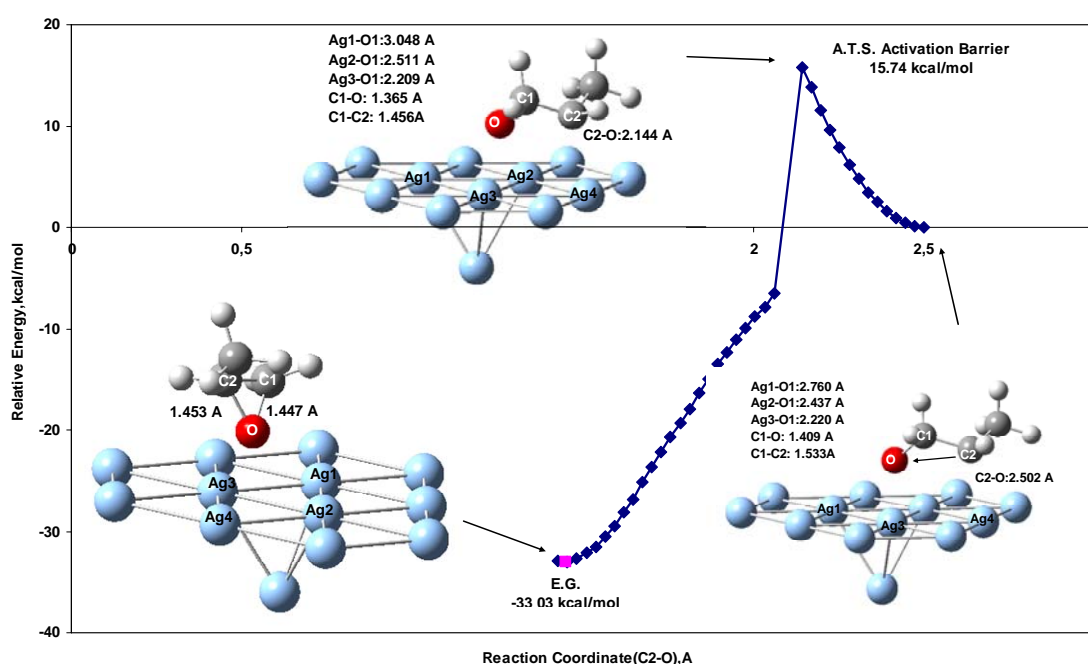


Figure 4.44 Relative energy profile along reaction coordinate (C2-O) for ethylene oxide formation on oxygen atom adsorbed on (111) silver surface cluster.

Propylene oxide can be formed by firstly activating of C2 and secondly activation of C1. Here, second carbon atom of the propylene can go to the adsorbed O atom and then first C atom form propylene oxide. First step along the reaction coordinate is the adsorption of propylene onto the oxygen atom-adsorbed on Ag cluster to form propylene oxide. Figure 4.45 illustrates

the relative energy profile for step 4 (Reaction 25) obtained when a reaction coordinate between the adsorbed O atom and one carbon atom of propylene molecule (C2-O) is chosen. The initial C1-O distance for the initial geometry is taken as 3.00 Å. There is an energy barrier of 7.01 kcal/mol and a relative energy value of -16.69 kcal/mole.

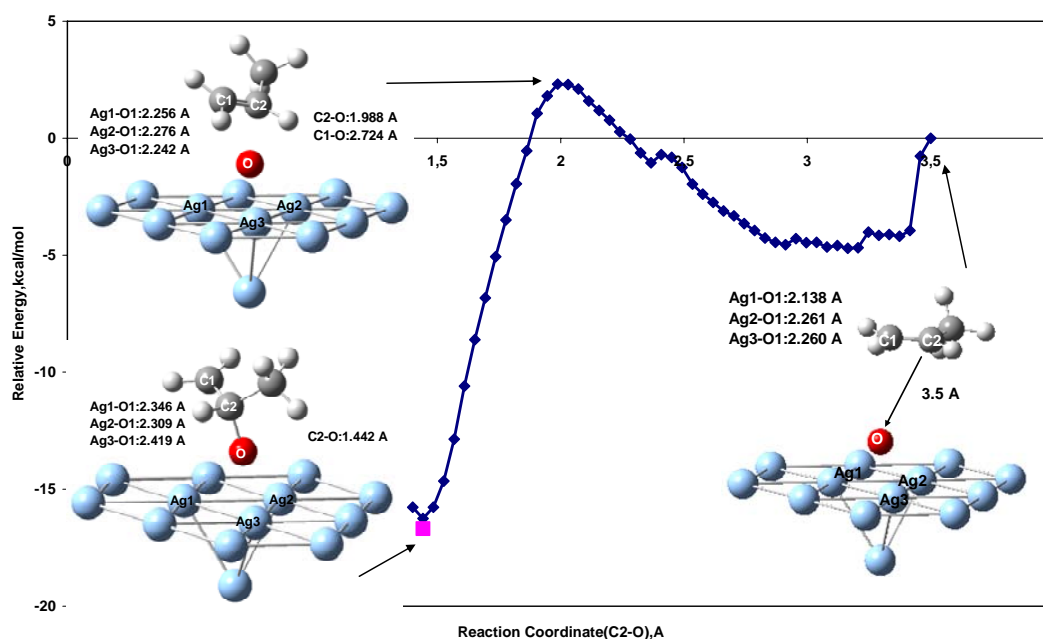


Figure 4.45 Relative energy profile along reaction coordinate (C2-O) for ethylene oxide formation on oxygen atom adsorbed on (111) silver surface cluster.

Reactions coordinate between the C1 of the propylene molecule and silver atom of the surface (C1-Ag4) is chosen to obtain oxametallacycle molecule on the surface (Step 5, reaction 26). The relative energy profile obtained is shown in Figure 4.46. The final geometry which is similar to an oxametallacycle molecule is found at a relative energy value of -18.17 kcal/mole. The next step is taken to be a reaction coordinate between the O atom and other carbon atom of propylene molecule (C1-O). Figure 4.47 shows the relative energy profile obtained for step 6 (Reaction 27). The initial geometry is oxametallacycle geometry where the initial C1-O distance

is found as 2.466 Å. This geometry and the final geometry of the first step which has a reaction coordinate between C1 and O is the same. A relative energy barrier of an approximate transition state for the second step is 21.85 kcal/mol. The final geometry of ethylene oxide on the cluster is found at a relative energy value of -26.89 kcal/mol. The approximate activation barrier of propylene epoxidation which has a reaction coordinate between the adsorbed O atom and the first carbon atom of propylene molecule (C1-O) is accepted the activation barrier for ethylene oxide formation reaction on Ag₁₃(111) cluster.

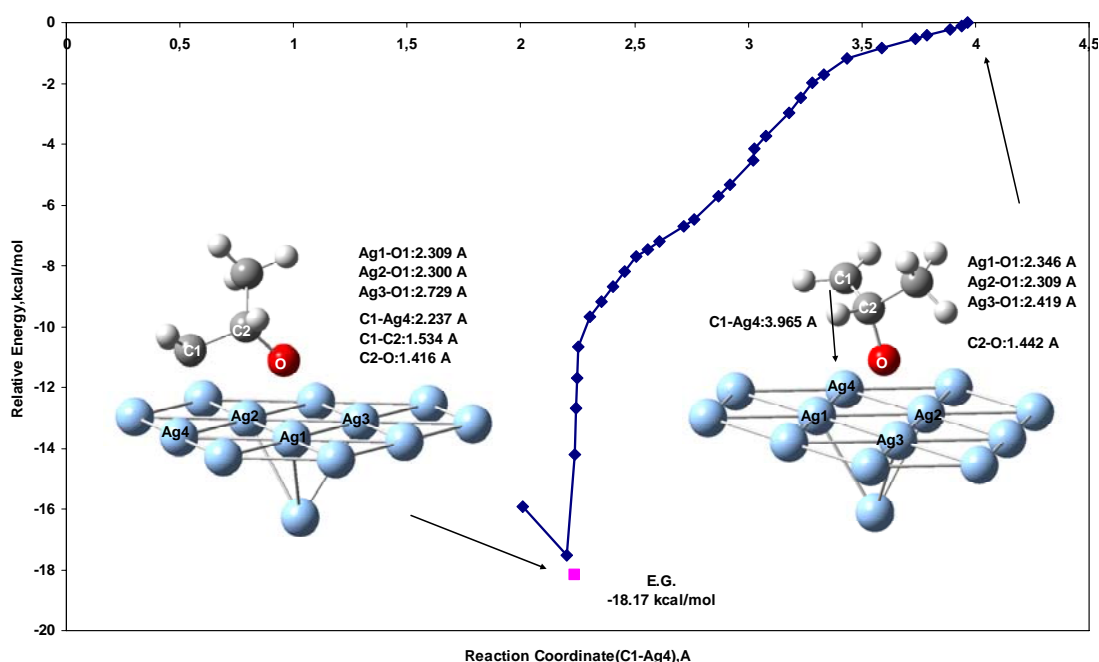


Figure 4.46 Relative energy profile along reaction coordinate (C1-Ag4) for oxametallacycle molecule formation on oxygen atom adsorbed on (111) silver surface cluster.

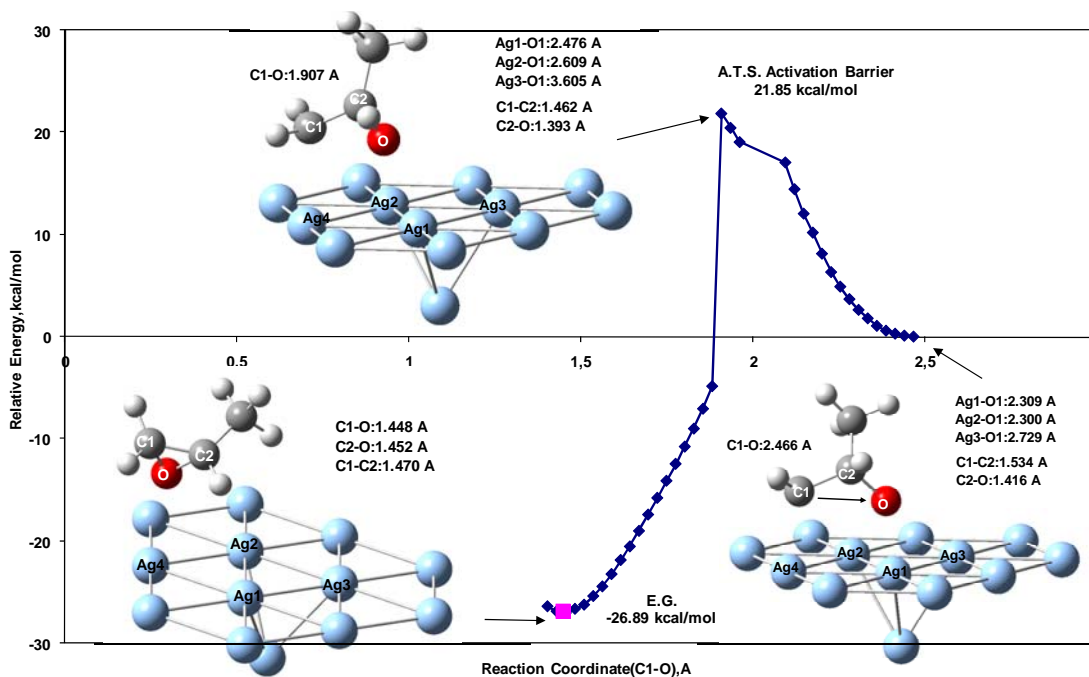


Figure 4.47 Relative energy profile along reaction coordinate (C1-O) for ethylene oxide formation on oxygen atom adsorbed on (111) silver surface cluster.

4.3.1.1.3. Propanal Formation Path

After the completing firstly first C activation reaction, H of the adsorbed C (first C) can go to the second C to form propanal (step 7, reaction 28). The relative energy profile obtained for this reaction is depicted in Figure 4.48. A relative energy barrier of an approximate transition state for the second step is 16.03 kcal/mol. The final geometry of propanal on the cluster is found at a relative energy value of -54.48 kcal/mol.

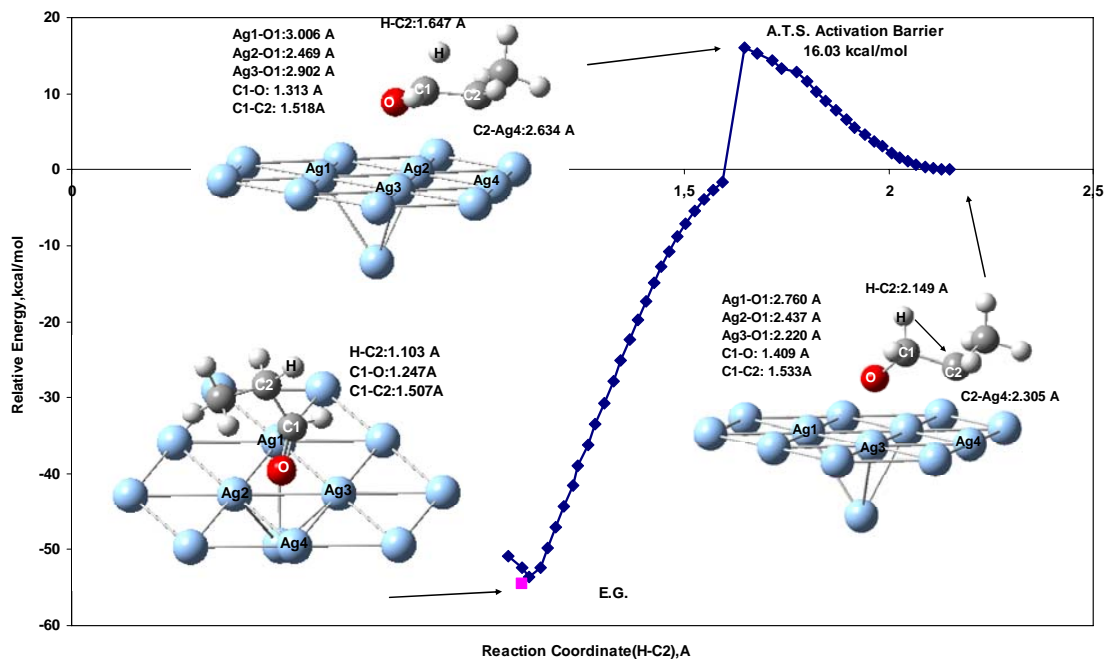


Figure 4.48 Relative energy profile along reaction coordinate (H-C2) for propanal formation on oxygen atom adsorbed on (111) silver surface cluster.

4.3.1.1.4. Acetone Formation Path

After the completing firstly second C activation reaction, H of the adsorbed C (second C) can go to the second C to form acetone (Step 8, reaction 29). Figure 4.49 illustrates the relative energy profile obtained for this reaction. A relative energy barrier of an approximate transition state for the second step is 36.03 kcal/mol. The final geometry of acetone on the cluster is found at a relative energy value of -52.66 kcal/mol.

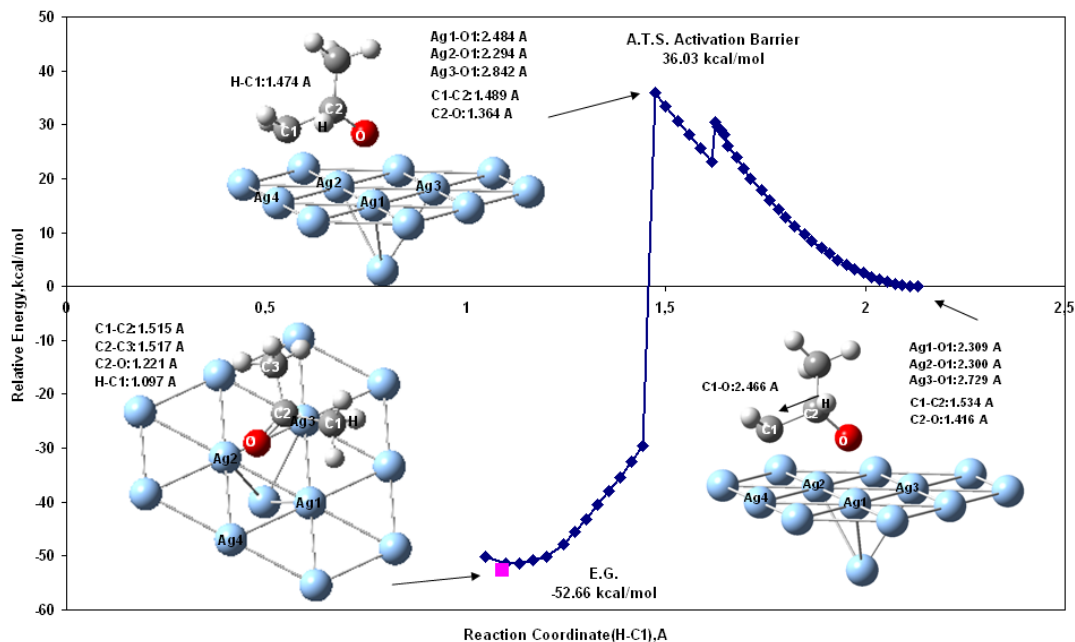


Figure 4.49 Relative energy profile along reaction coordinate (H-C1) for acetone formation on oxygen atom adsorbed on (111) silver surface cluster.

Table 4.5 gives a comparison of activation barriers computed for the propylene oxidation reactions (Steps 1-9, reactions 22-30) on $\text{Ag}_{13}(111)$ cluster in this study with the theoretical study. Figure 4.50 also shows a comparison of activation barriers computed for the propylene epoxidation reactions on $\text{Ag}(111)$ cluster in this study. As seen from the table, π -allyl formation path has the lowest activation barrier (6.11 kcal/mol). This explains why silver is not a good catalyst for the propylene oxide formation while it is a good catalyst for the ethylene oxide formation. Propylene goes to π -allyl molecule which is an intermediate molecule for combustion on silver.

Table 4.5 Comparison of activation barriers for propylene epoxidation reactions on silver (111) surface.

Reactions	This Study	Theoretical Study*
	DFT/B3LYP- ATS	TS
	Ag ₁₃ Cluster	VASP/PW91 Slab - CI-NEB
First C activation	13.48 OMMP	13.84 OMMP
Propylene Oxide formation	15.75	14.30
Second C activation	7.01 OMMP	-
Propylene Oxide formation	21.85	-
Propanal formation	16.07	12.91
Π-Allyl formation	6.11	6.92
Acetone formation	36.03	-

* Torres et al. (2007)

OMMP: Propylene oxametallacycle

TS: Transition State

ATS: Approximate Transition State

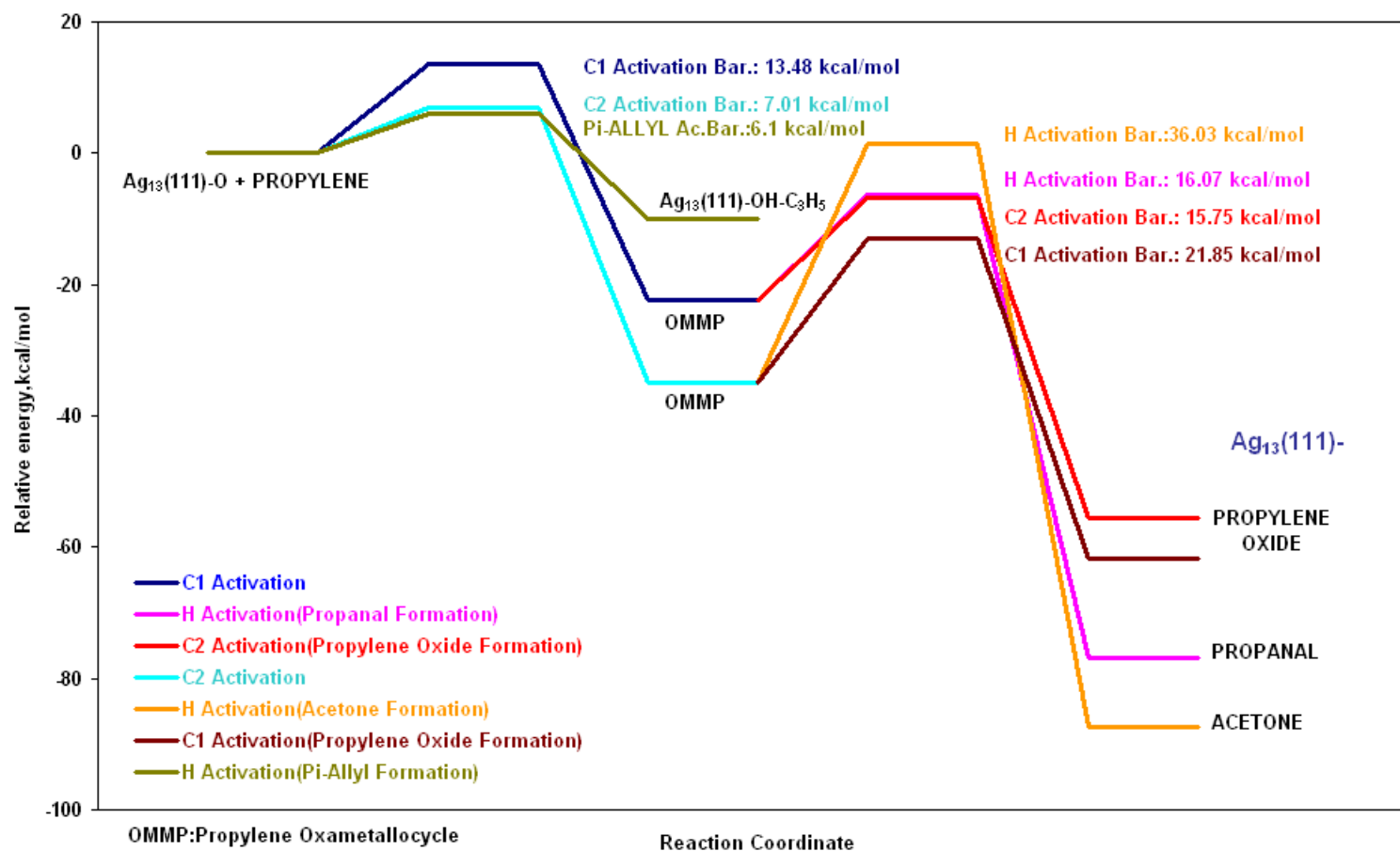


Figure 4.50 A summary energy diagram showing a comparison of the entire paths for propylene epoxidation on (111) silver cluster.

4.3.1.2. Propylene Epoxidation on Slab Surface

In order to compare the geometries obtained using cluster calculations, geometries for ethylene oxidation reactions on silver surface were obtained by using slab surface. Optimized geometries of OMMP1 and 2, propylene oxide, propanal and acetone were obtained by using VASP. These geometries are represented in Figures 4.51, 4.52, 4.53, 4.54 and 4.55, respectively.

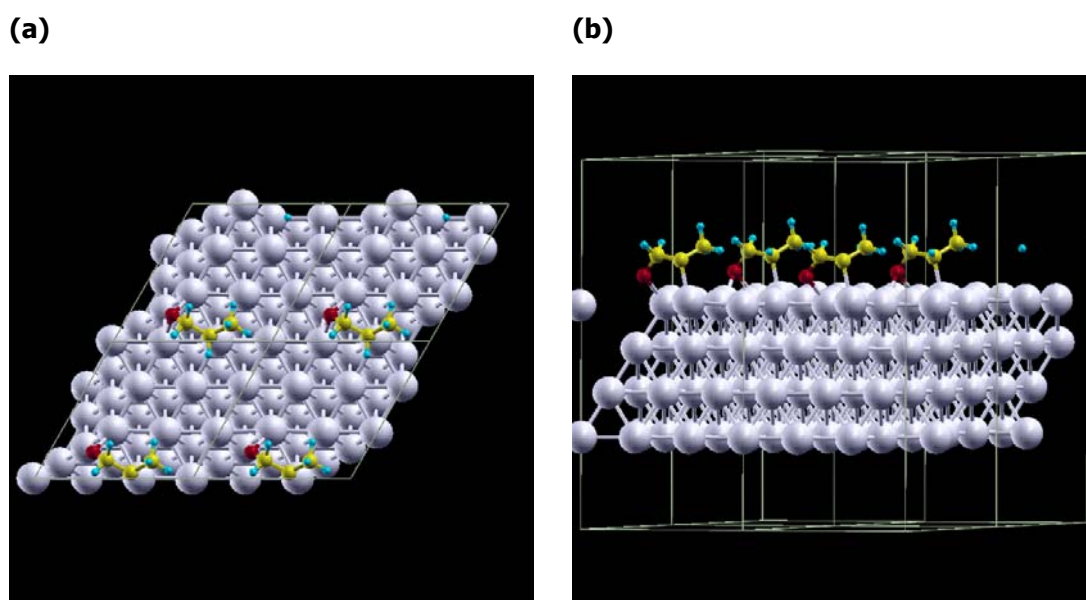
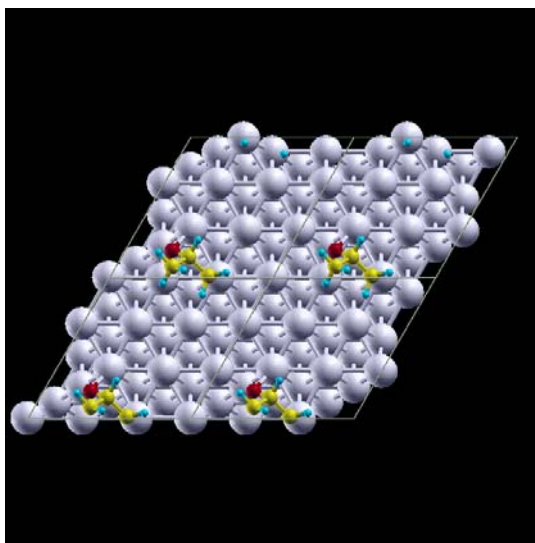


Figure 4.51 OMMP1 on slab (a) Top view, (b) Side view

(a)



(b)

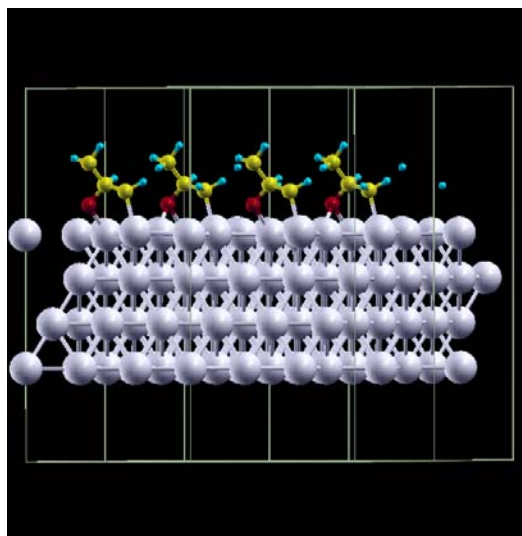


Figure 4.52 OMMP2 on slab (a) Top view, (b) Side view

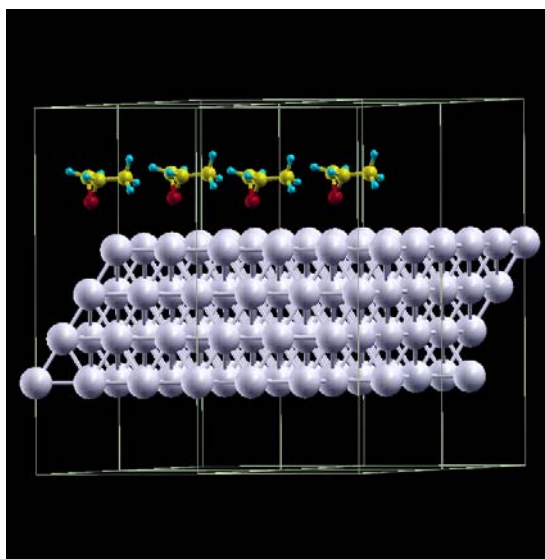
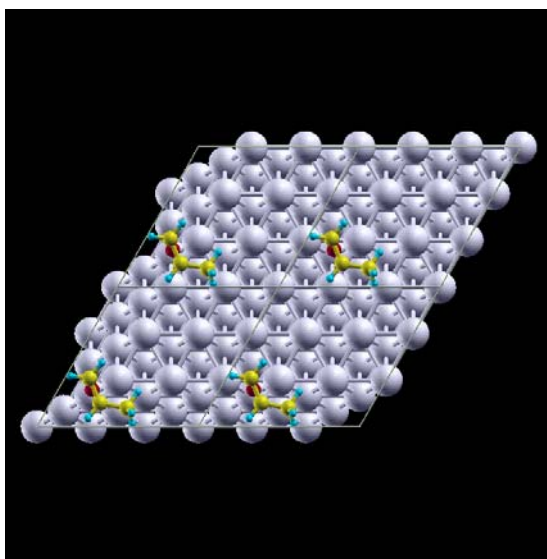
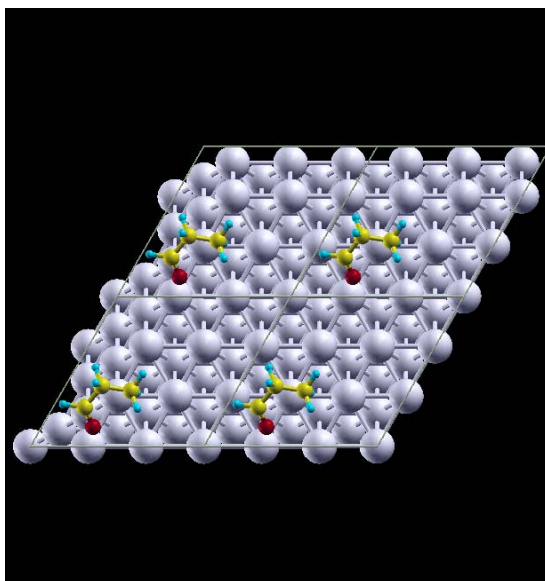


Figure 4.53 Propylene oxide on slab (a) Top view, (b) Side view

(a)



(b)

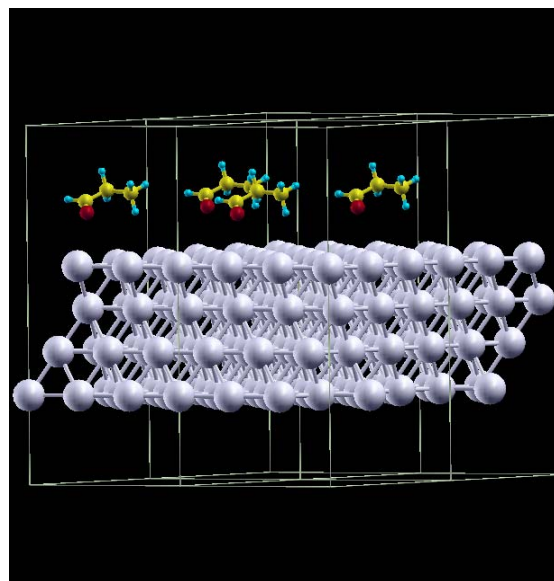
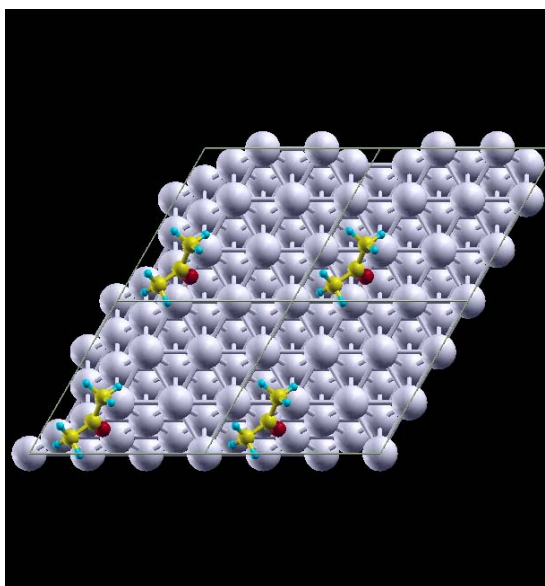


Figure 4.54 Propanal on slab (a) Top view, (b) Side view

(a)



(b)

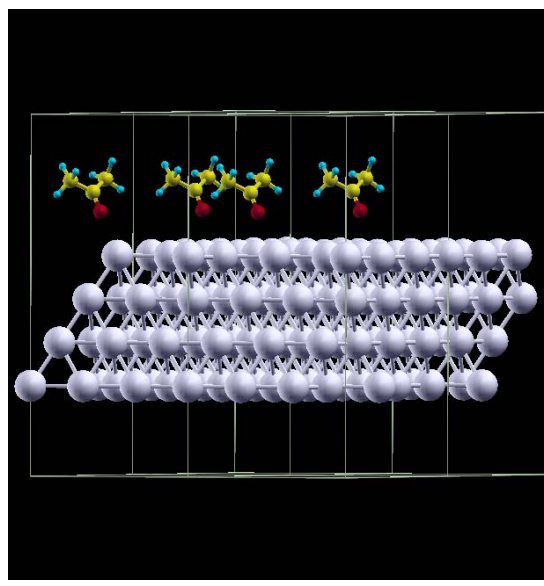


Figure 4.55 Acetone on slab (a) Top view, (b) Side view

Figure 4.56 shows a comparison of heat of reaction for propylene epoxidation by using slab surface. For ethylene epoxidation, the qualitative trend of reaction energies is the same with that of calculations obtained by using surface cluster. In other words, products order which is OMMP1, OMMP2, propylene oxide, propanal and acetone respectively is the same for cluster and slab calculations.

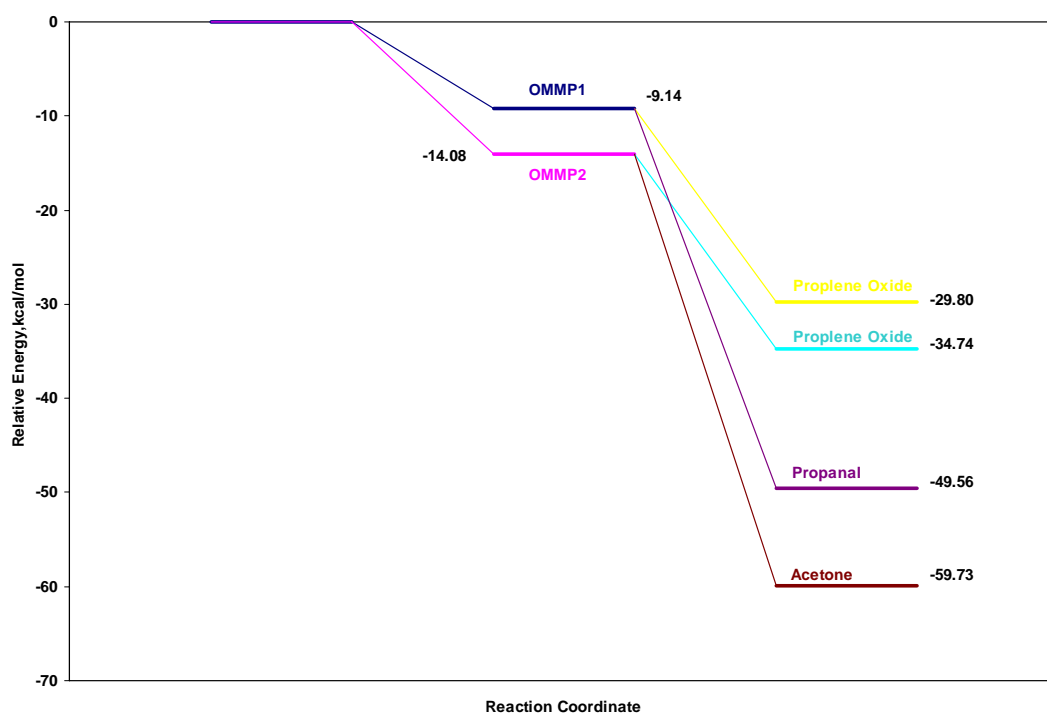
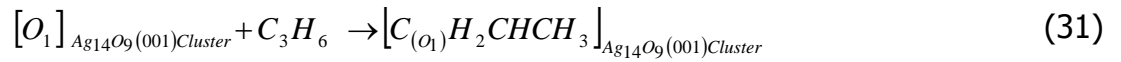


Figure 4.56 A summary energy diagram for ethylene epoxidation on 4-layer-(3x3) slab.

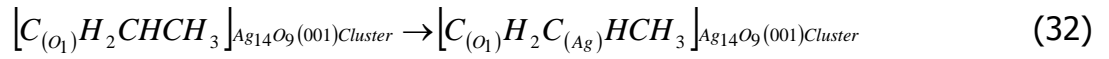
4.3.2. Propylene Epoxidation on Silver Oxide Ag₁₄O₉(001) Surface

The proposed reaction steps for the oxidation of propylene on the cluster are:

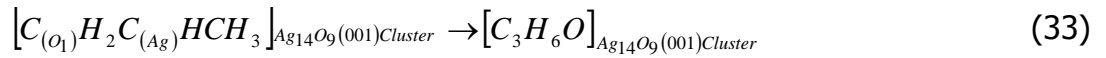
Step 1, propylene adsorption-1



Step 2, propylene oxametallocycle (OMMP1) formation



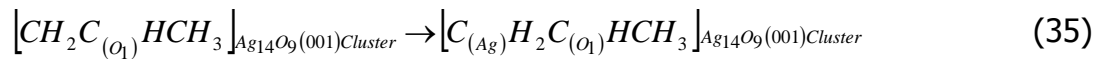
Step 3, propylene oxide formation



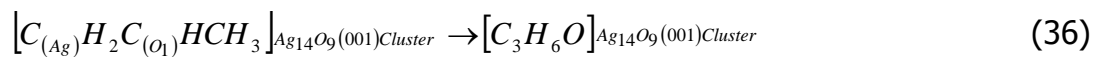
Step 4, propylene adsorption-2



Step 5, propylene oxametallocycle (OMMP2) formation



Step 6, propylene oxide formation



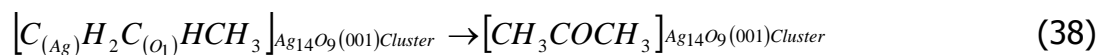
Step 7, propanal formation**Step 8, acetone formation****Step 9, Π -allyl radical formation****4.3.2.1. Π -Allyl Formation Path**

Figure 4.57 demonstrates the relative energy profile for reaction 39 (Step 9) obtained when a reaction coordinate between the O1 atom and one hydrogen atom of propylene molecule (H-O1) is chosen. The initial O1-H distance is taken as 3.00 Å. A relative energy barrier of an approximate transition state is 8.43kcal/mol. The final geometry is found at an exothermic relative energy value of -20.99 kcal/mole.

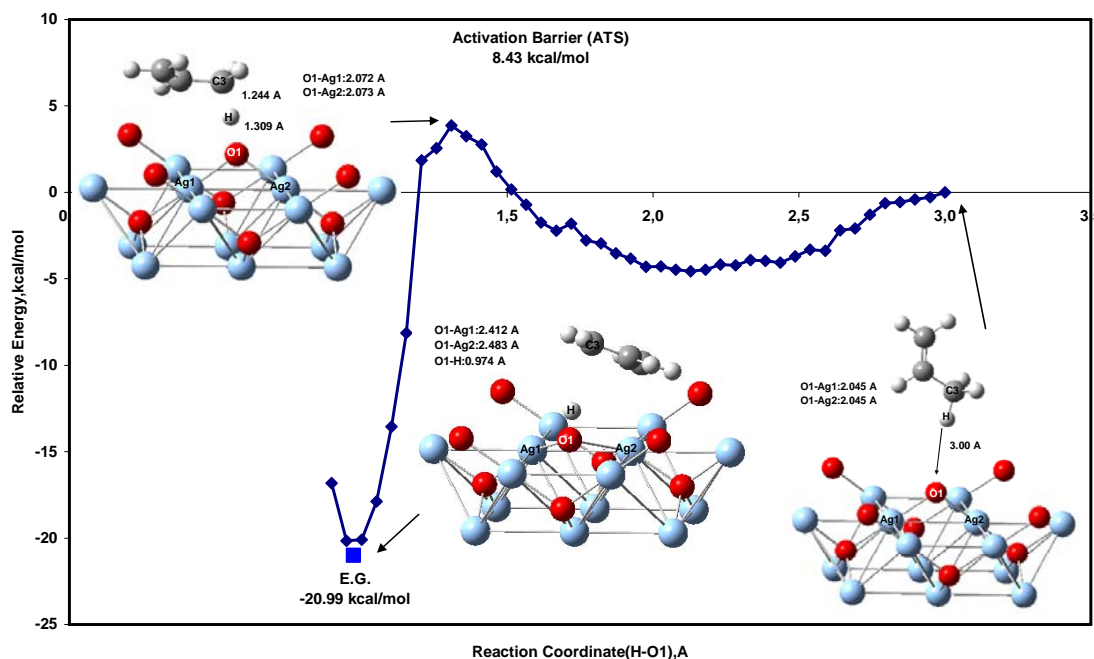


Figure 4.57 Relative energy profile along reaction coordinate (H-O1) for C-H activation of propylene on (001) silver oxide surface cluster.

4.3.2.2. Propylene Oxide Formation Path

Another possible step (Reaction 31, step 1) along the reaction coordinate is the adsorption of propylene onto the oxygen atom Ag₂O cluster to form propylene oxide. Figure 4.58 shows the relative energy profile obtained when a reaction coordinate between the O1 atom and one carbon atom of propylene molecule (C1-O1) is chosen. The initial C1-O distance for the initial geometry is taken as 3.00 Å. There is an energy barrier of 6.47 kcal/mol and a relative energy value of -17.37 kcal/mole.

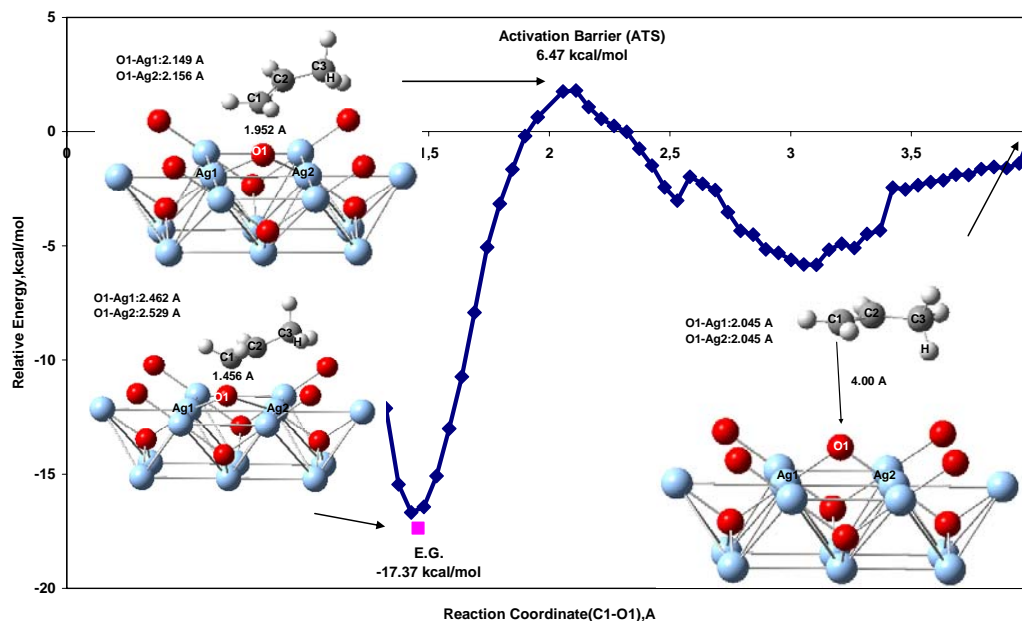


Figure 4.58 Relative energy profile along reaction coordinate (C1-O1) for propylene oxide formation on (001) silver oxide surface cluster.

A reaction coordinate between the C2 of the propylene molecule and silver atom of the surface (C2-Ag2) is chosen to obtain oxametallacycle molecule on the surface (Step 2, reaction 32). The relative energy profile obtained is represented in Figure 4.59. Relative energy of the final geometry which is similar to an oxametallacycle molecule exponentially increases (80.51 kcal/mol).

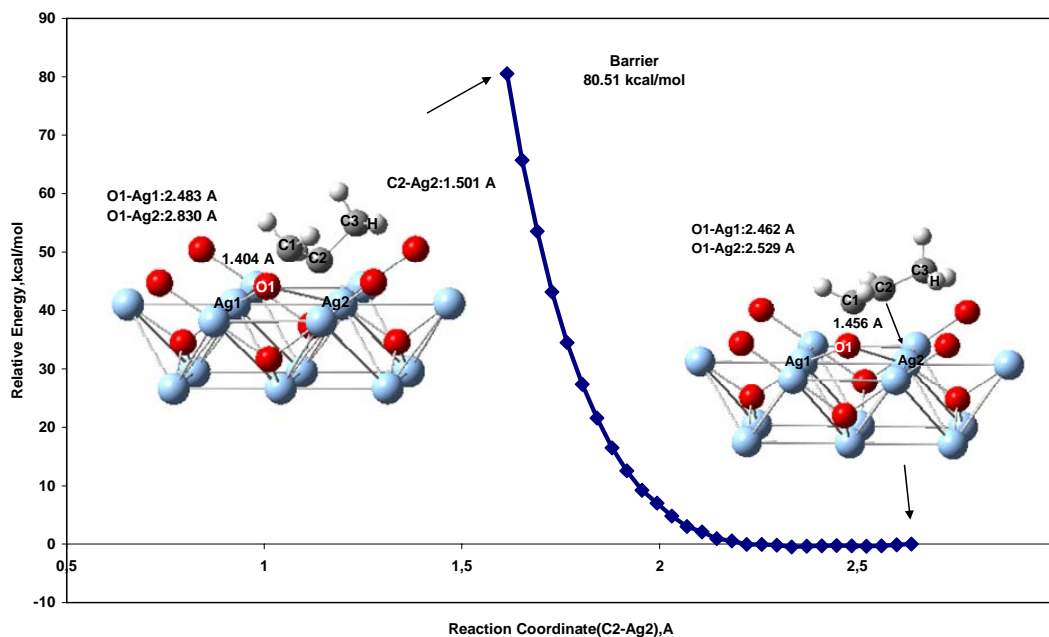


Figure 4.59 Relative energy profile along reaction coordinate (C2-Ag2) for oxametallacycle molecule formation on (001) silver oxide surface cluster.

The next step (Reaction 33, step 3) is taken to be a reaction coordinate between the O1 atom and other carbon atom of propylene molecule (C2-O1). Figure 4.60 shows the relative energy profile obtained. The initial geometry is oxametallacycle geometry where the initial C2-O distance is found as 2.437 Å. This geometry and the final geometry of the first step which has a reaction coordinate between C1 and O1 is the same. A relative energy barrier of an approximate transition state for the second step is 16.71 kcal/mol. The final geometry of ethylene oxide on the cluster is found at a relative energy value of -7.07 kcal/mol. The approximate activation barrier of propylene epoxidation which has a reaction coordinate between the adsorbed O atom and the second carbon atom of propylene molecule (C2-O) is accepted the activation barrier for ethylene oxide formation reaction on silver oxide cluster.

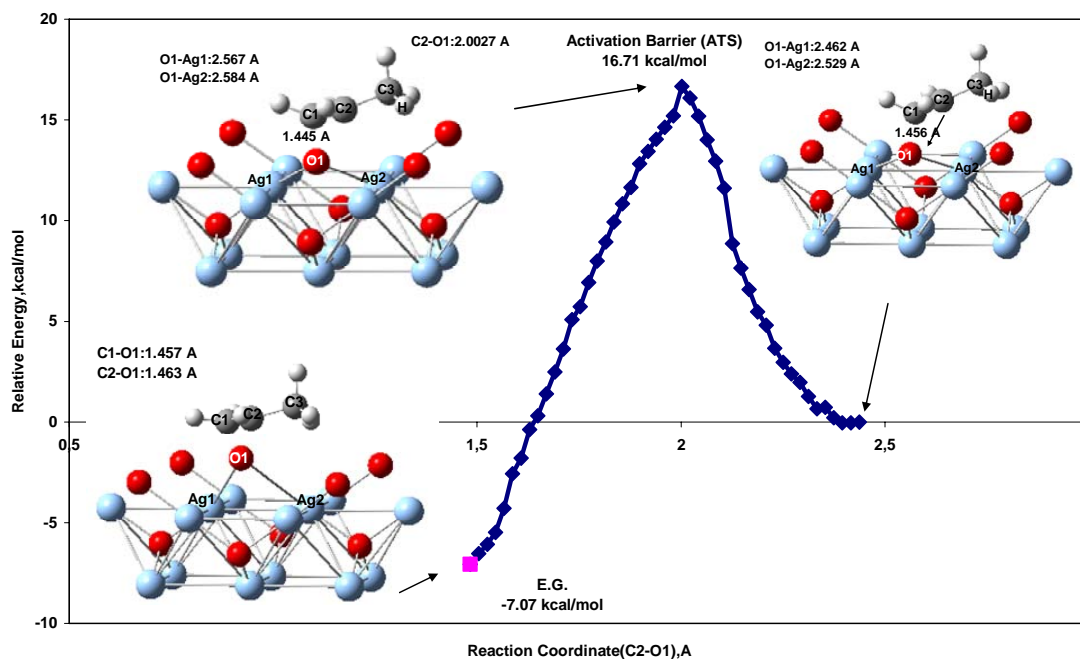


Figure 4.60 Relative energy profile along reaction coordinate (C2-O1) for propylene oxide formation on (001) silver oxide surface cluster.

Propylene oxide can also be formed by firstly activation of C2 and then secondly activation of C1. Here, second carbon atom of the propylene can go to the O atom and then first C atom form propylene oxide. One possible step along the reaction coordinate is the adsorption of propylene onto the oxygen atom Ag₂O cluster to form propylene oxide. Figure 4.61 depicts the relative energy profile for step 4 (Reaction 34) obtained when a reaction coordinate between the O1 atom and one carbon atom of propylene molecule (C2-O1) is chosen. The initial C2-O distance for the initial geometry is taken as 4.00 Å. There is an energy barrier of 9.30 kcal/mol and a relative energy value of -14.37 kcal/mole.

Reactions coordinate between the C1 of the propylene molecule and silver atom of the surface (C1-Ag2) is chosen to obtain oxametallacycle molecule on the surface (Step 5, reaction 35). The relative energy profile obtained is demonstrated in Figure 4.62. Relative energy of the final geometry which is

similar to an oxametallacycle molecule exponentially increases (48.67 kcal/mol).

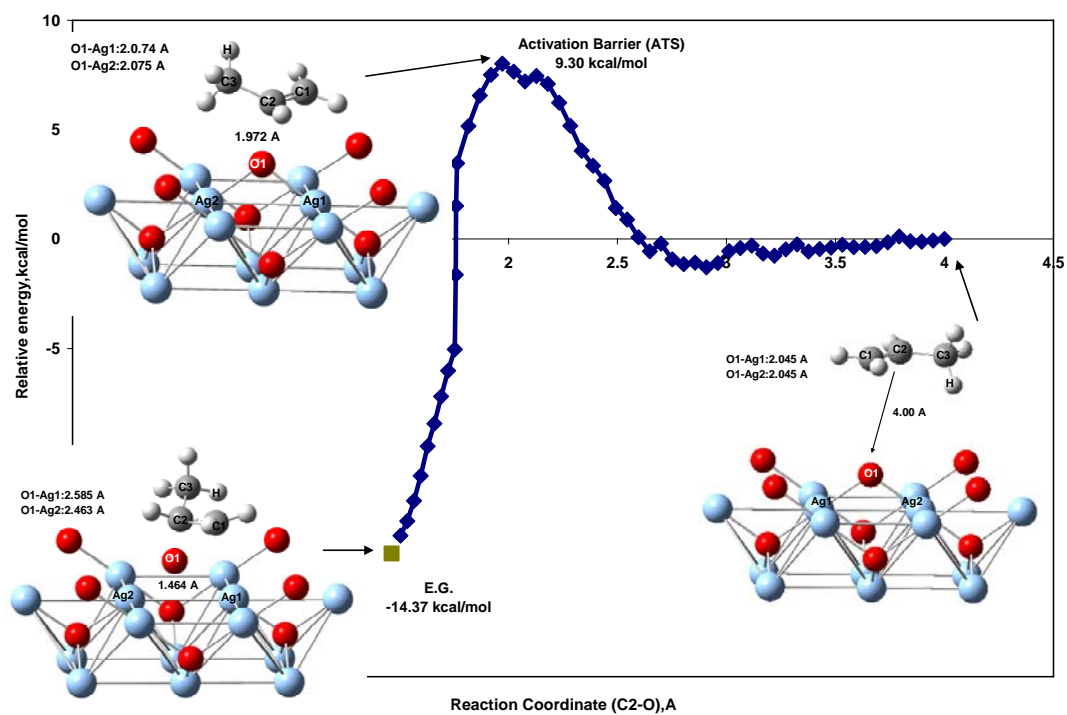


Figure 4.61 Relative energy profile along reaction coordinate (C2-O1) for propylene oxide formation on (001) silver oxide surface cluster.

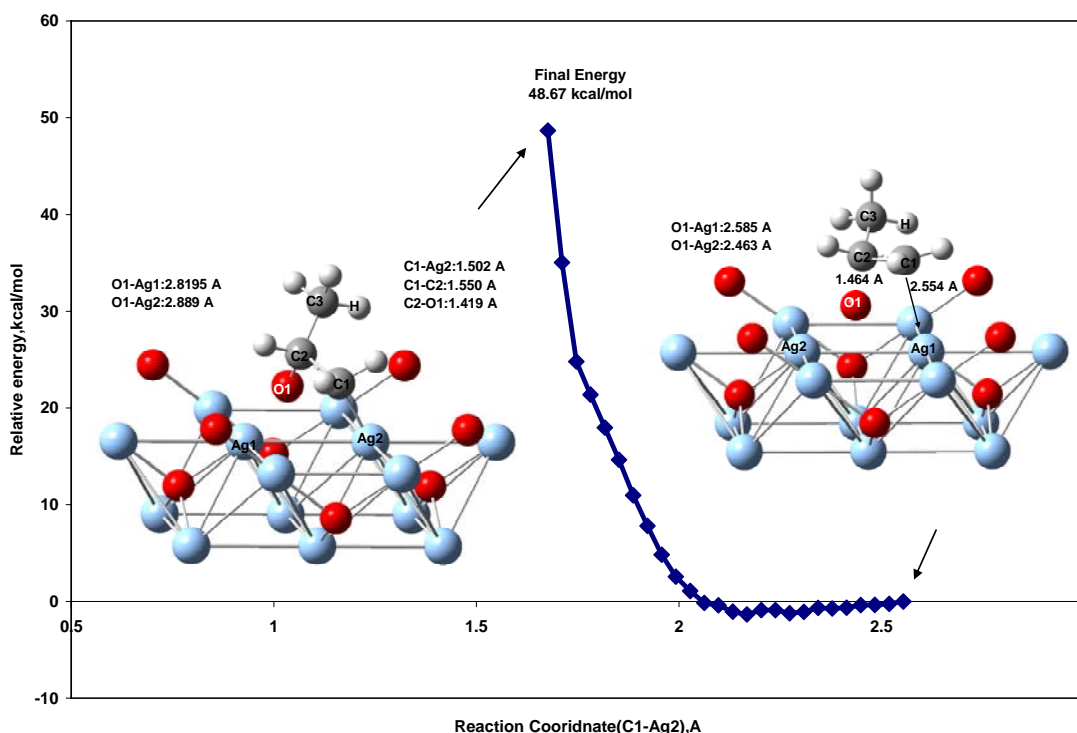


Figure 4.62 Relative energy profile along reaction coordinate (C1-Ag2) for oxametallacycle molecule formation on (001) silver oxide surface cluster.

The next step (Reaction 36, step 6) is taken to be a reaction coordinate between the O1 atom and other carbon atom of propylene molecule (C1-O1). Figure 4.63 illustrates the relative energy profile obtained. The initial geometry is oxametallacycle geometry where the initial C2-O distance is found as 2.368 Å. This geometry and the final geometry of the first step which has a reaction coordinate between C2 and O1 is the same. A relative energy barrier of an approximate transition state for the second step is 19.96 kcal/mol. The final geometry of ethylene oxide on the cluster is found at a relative energy value of -7.63 kcal/mol. The approximate activation barrier of propylene epoxidation which has a reaction coordinate between the adsorbed O atom and the second carbon atom of propylene molecule (C1-O) is accepted the activation barrier for propylene oxide formation reaction on silver oxide cluster.

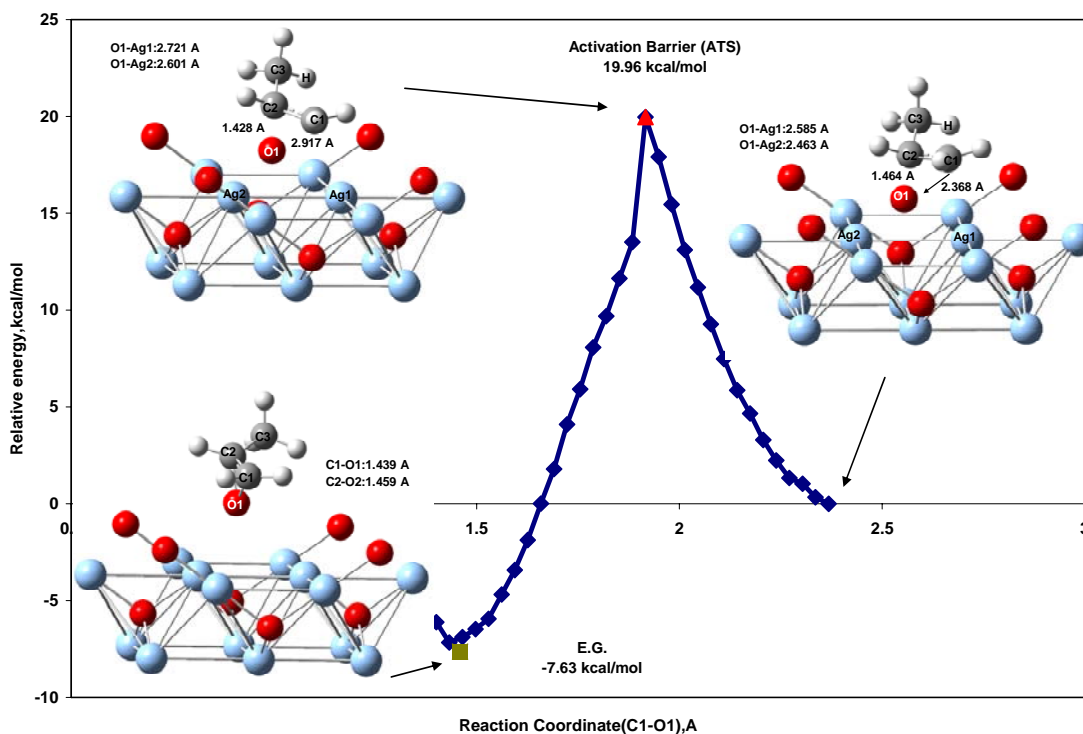


Figure 4.63 Relative energy profile along reaction coordinate (C1-O1) for propylene oxide formation on (001) silver oxide surface cluster.

4.3.2.3. Propanal Formation Path

After the completing firstly first C activation (C1) reaction, H of the adsorbed C (first C) can go to the second C (C2) to form propanal. Figure 4.64 represents the relative energy profile for step 7 (Reaction 37) obtained for the formation of propanal reaction. A relative energy barrier of an approximate transition state for the second step is 41.60 kcal/mol. The final geometry of propanal on the cluster is found at a relative energy value of -27.53 kcal/mol.

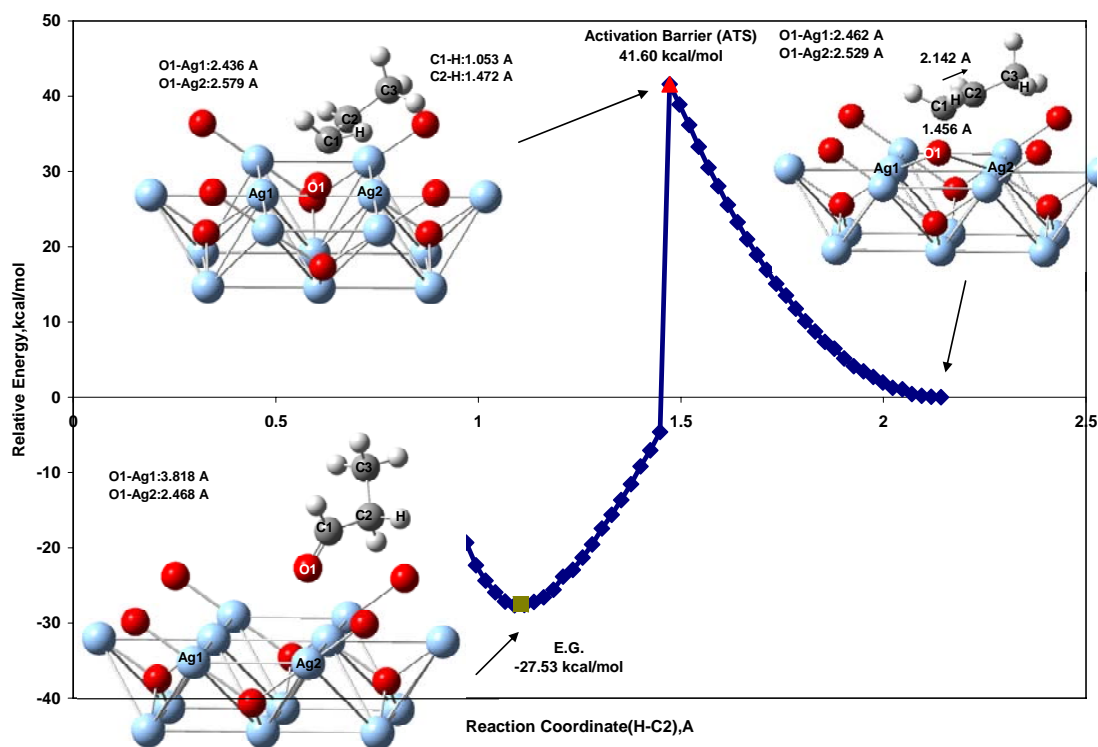


Figure 4.64 Relative energy profile along reaction coordinate (H-C2) for propanal formation on (001) silver oxide surface cluster.

4.3.2.4. Acetone Formation Path

After the completing firstly second C activation (C2) reaction, H of the adsorbed C (second C) can go to the first C (C1) to form acetone. Figure 4.65 shows the relative energy profile for step 8 (Reaction 38) obtained for the formation of acetone reaction. A relative energy barrier of an approximate transition state for the second step is 38.94 kcal/mol. The final geometry of acetone on the cluster is found at a relative energy value of -35.50 kcal/mol.

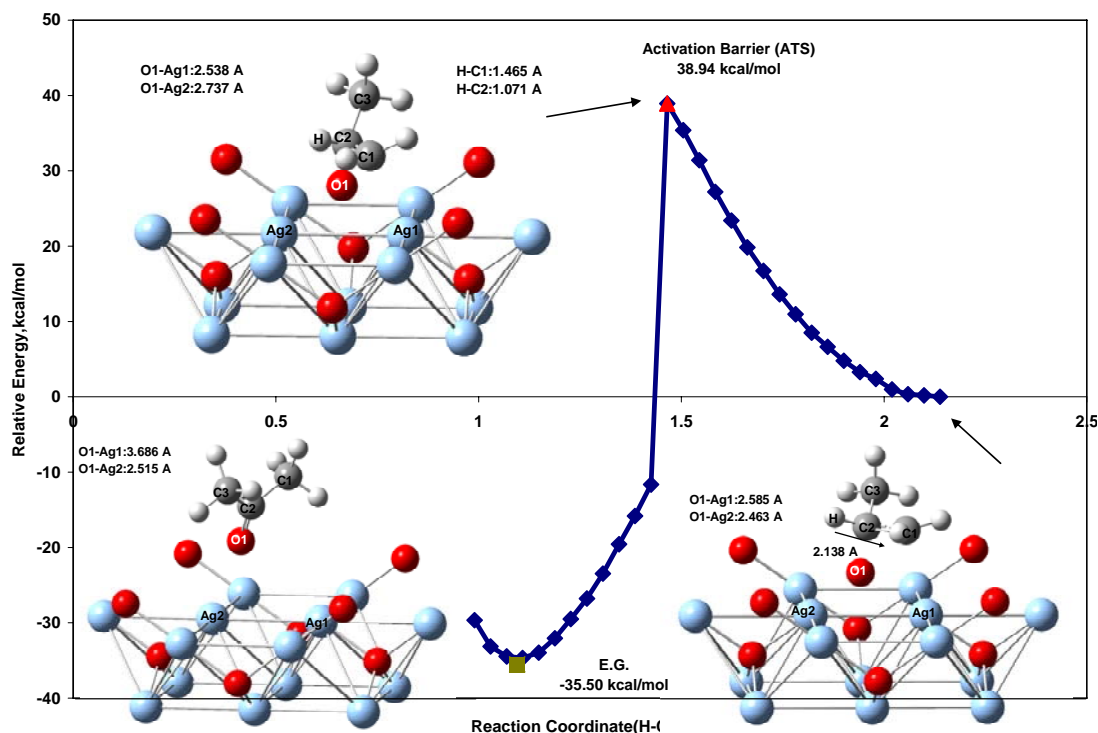


Figure 4.65 Relative energy profile along reaction coordinate (H-C1) for acetone formation on (001) silver oxide surface cluster.

Figure 4.66 shows a comparison of activation barriers computed for the propylene oxidation reactions (Steps 1-8, reactions 31-39) on Silver Oxide (001) cluster in this study. As mentioned before, there are no activation barrier data for the reactions on silver oxide in both experimental and theoretical literatures. All products except pi-allyl which is unwanted can not be formed on Ag_2O surface because of those higher activation barriers. Pi-allyl formation path has the lowest activation barrier for propylene epoxidation. This situation is the same with that for propylene epoxidation on silver surface. Propylene goes to pi-allyl molecule which is an intermediate molecule for the combustion on silver. In addition, two OMMP structures were not formed on silver oxide surface while those are formed on silver surface.

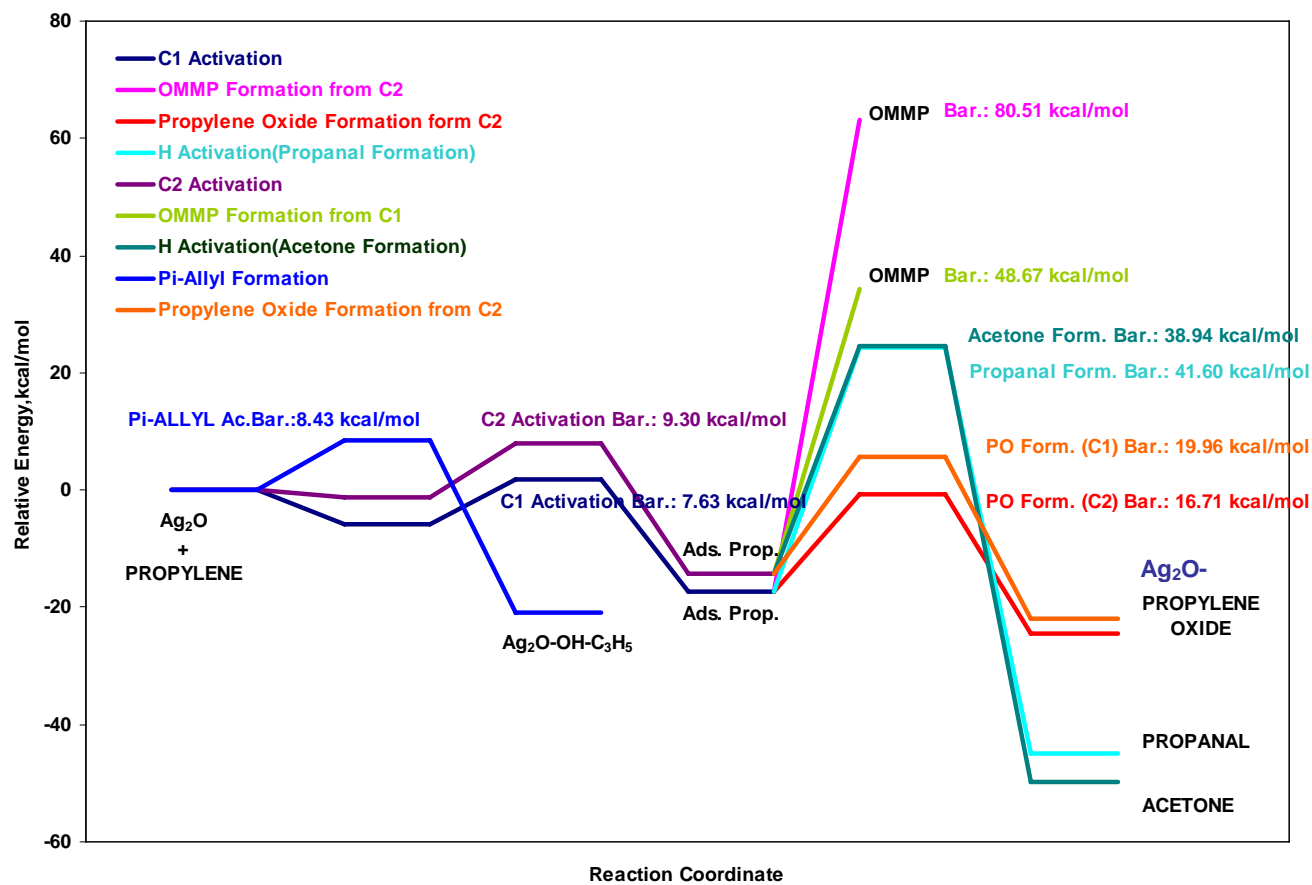
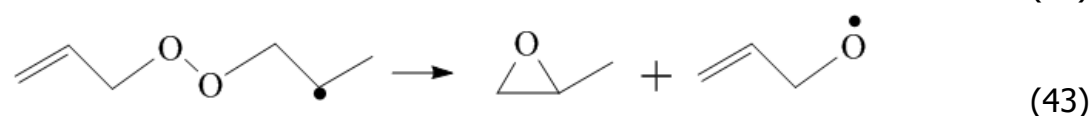
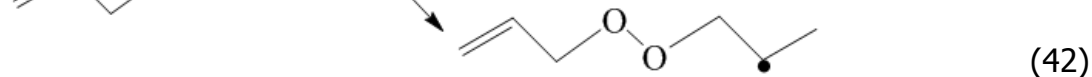
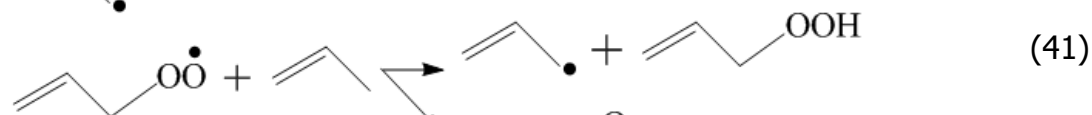
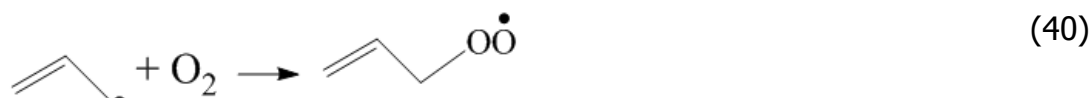


Figure 4.66 A summary energy diagram showing a comparison of the entire paths for propylene epoxidation on (111) silver oxide surface cluster.

4.3.3. Propylene Epoxidation in Gas Phase

Recently, Mimura and co-workers 2006 proposed a new catalytic system that composed of a catalytic bed and an empty post-catalytic bed volume that would selectively epoxidize propylene to propylene oxide. They reported that PO was the main oxidation product instead of the allylic oxidation product acrolein. It was also observed that the selectivity to combustion products decreased after the post-catalytic volume was introduced. Due to the significant increase in PO selectivity induced by the empty volume, they concluded that the function of the catalytic bed was to generate radicals and PO was produced mainly in the post-catalytic bed through radical chain reactions (Song et al., 2008). The likely mechanism for the gas phase propylene epoxidation at 573 K was proposed in the experimental literature as below (Mimura et al., 2006):



After optimization of the allyl radical and the oxygen molecules, a reaction coordinate calculation where a reaction coordinate is selected as the distance between the C1 atom of the allyl radical and O1 atom of the oxygen molecule is performed for Reaction 40. The reaction is found to proceed exothermically with no activation barrier and the peroxy radical formed has a relative energy value of -17.63 kcal/mol. The EG for the peroxy radical obtained is given in Figure 4.67.

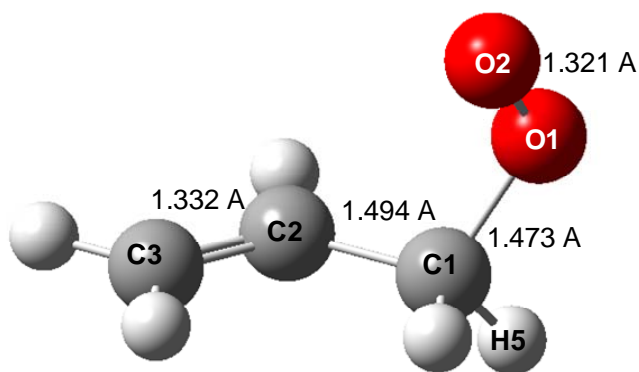


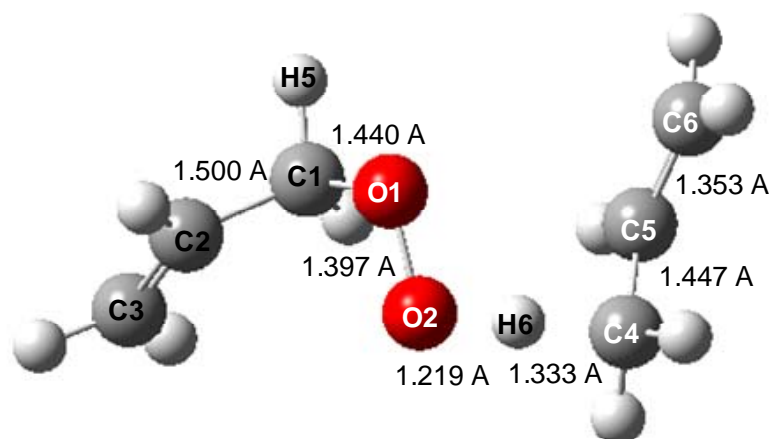
Figure 4.67 Equilibrium final geometry for Reaction-40

Following this path, the peroxy radical can undergo transition either to a peroxodimer or a hydroperoxide. The reaction coordinate is the distance between the allylic hydrogen atom (H6) of the propylene molecule and the terminal oxygen atom (O2) of the peroxy radical. The endothermic reaction that results in the formation of hydroperoxide is found to have an activation barrier of 17.63 kcal/mol and the final geometry has a relative energy value of 3.88 kcal/mol. The transition state was identified as having one imaginary vibrational frequency of 1768 cm^{-1} for the O-H stretching. The corresponding distance for the transition state is 1.219 \AA . The TS geometry and the EG of the product are represented in parts a and b of Figure 4.68, respectively.

The competing reaction (Reaction 42) of the peroxy radical, i.e. the transition to the peroxodimer yielded an activation barrier of 11.94 kcal/mol and the reaction is slightly exothermic with a relative energy value of -1.69 kcal/mol. For this reaction, the reaction coordinate is selected as the distance between the C4 atom of the propylene molecule and oxygen atom (O2) of the peroxy radical. From the comparison of the activation barrier of the two competing reactions, it can be concluded that the formation of the peroxodimer will be favored over the formation of the hydroperoxide, which is indeed a prerequisite for the chain reaction to result in the final product of PO. The

transition state was identified as having one imaginary vibrational frequency of -515 cm^{-1} for the O-O stretching. The corresponding distance for the transition state is 1.911 \AA . The TS geometry and the EG of the product are represented in parts a and b of Figures 4.69, respectively.

(a)



(b)

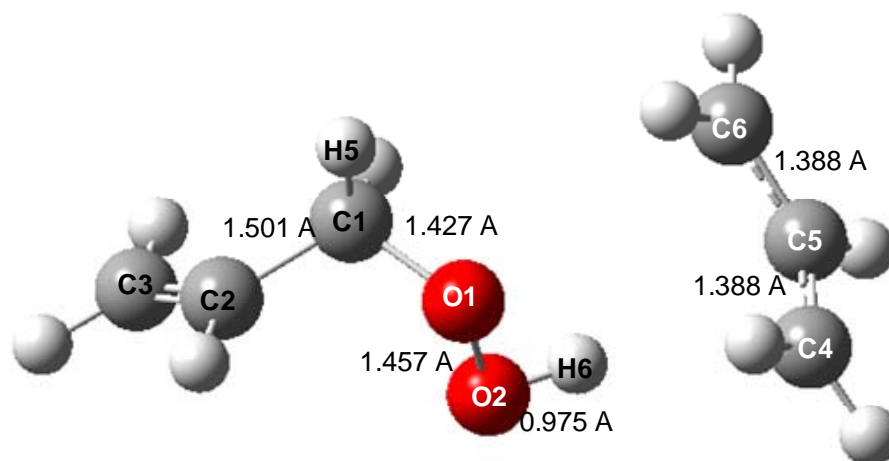
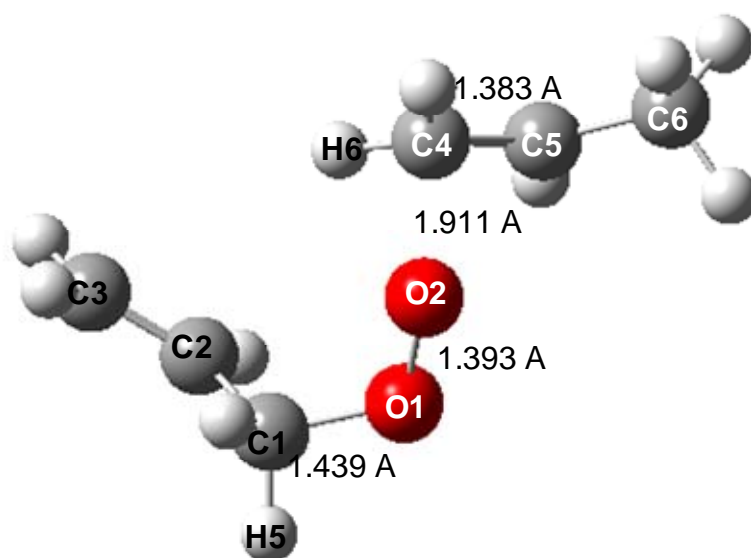


Figure 4.68 a) Transition state geometry, b) Equilibrium final geometry for Reaction-41

(a)



(b)

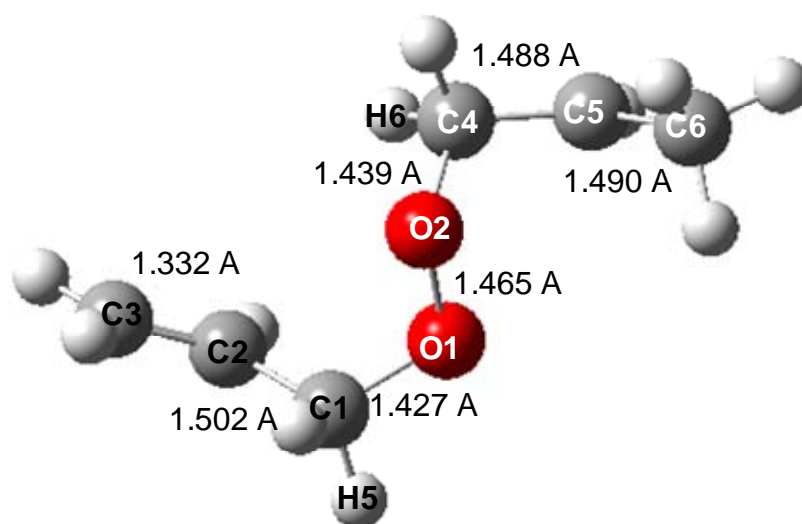
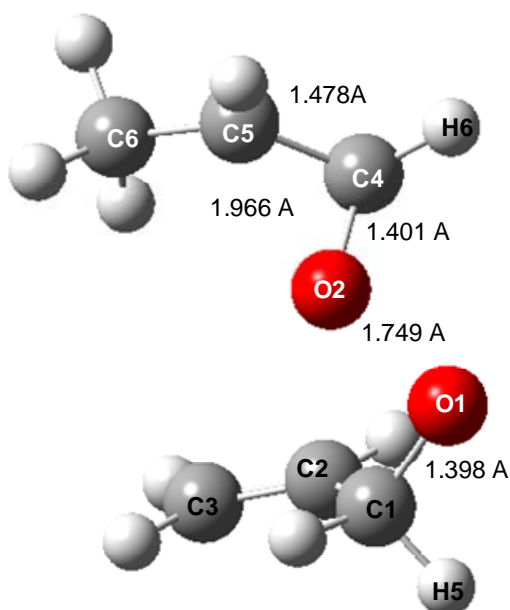


Figure 4.69 a) Transition state geometry, b) Equilibrium final geometry for Reaction-42

Reaction 43, where reactions coordinate is the distance between the O2 atom and C5 atom resulting in the formation of propylene oxide from the more probable peroxodimer pathway. Here, an activation barrier of 10.31 kcal/mol was found, and the propylene oxide molecule formed has a relative higher exothermic energy value of -25.37 kcal/mol. The transition state was

identified as having one imaginary vibrational frequency of -704 cm^{-1} for the C-O stretching. The corresponding distance for the transition state is 1.966 \AA . The TS geometry and the EG of the product are represented in parts a and b of Figures 4.70, respectively.

(a)



(b)

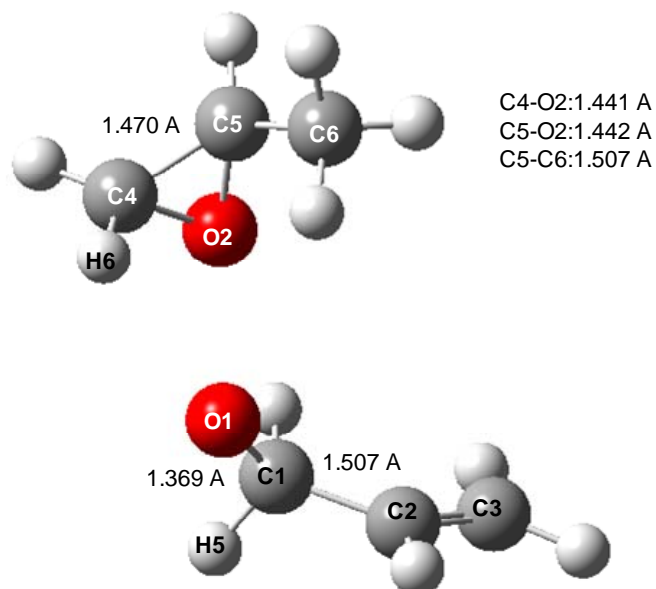


Figure 4.70 a) Transition state geometry, b) Equilibrium final geometry for Reaction-43

The calculated activation barrier value of 10.31 kcal/mol for propylene oxide formation is in a good agreement with earlier experimental value (11 kcal/mol) by Mantashyan et al. (1982, 1985). The coordinate driving calculations are also performed to investigate acrolein formation starting from the common peroxodimer intermediate. The activation energy barrier for acrolein formation was obtained as 58 kcal/mole. The relatively high difference between the activation energies of PO and acrolein formation indicates that PO formation is favored extensively over acrolein formation. Thus, the reason behind the statement in (Mimura et al., 2006) that almost no selectivity to acrolein formation contrary to high PO selectivity can be explained in the concept obtained in our results of the respective activation energies of the two competing reactions. The overall energy diagram summarizing reactions (40-43) is given in Figure 4.71.

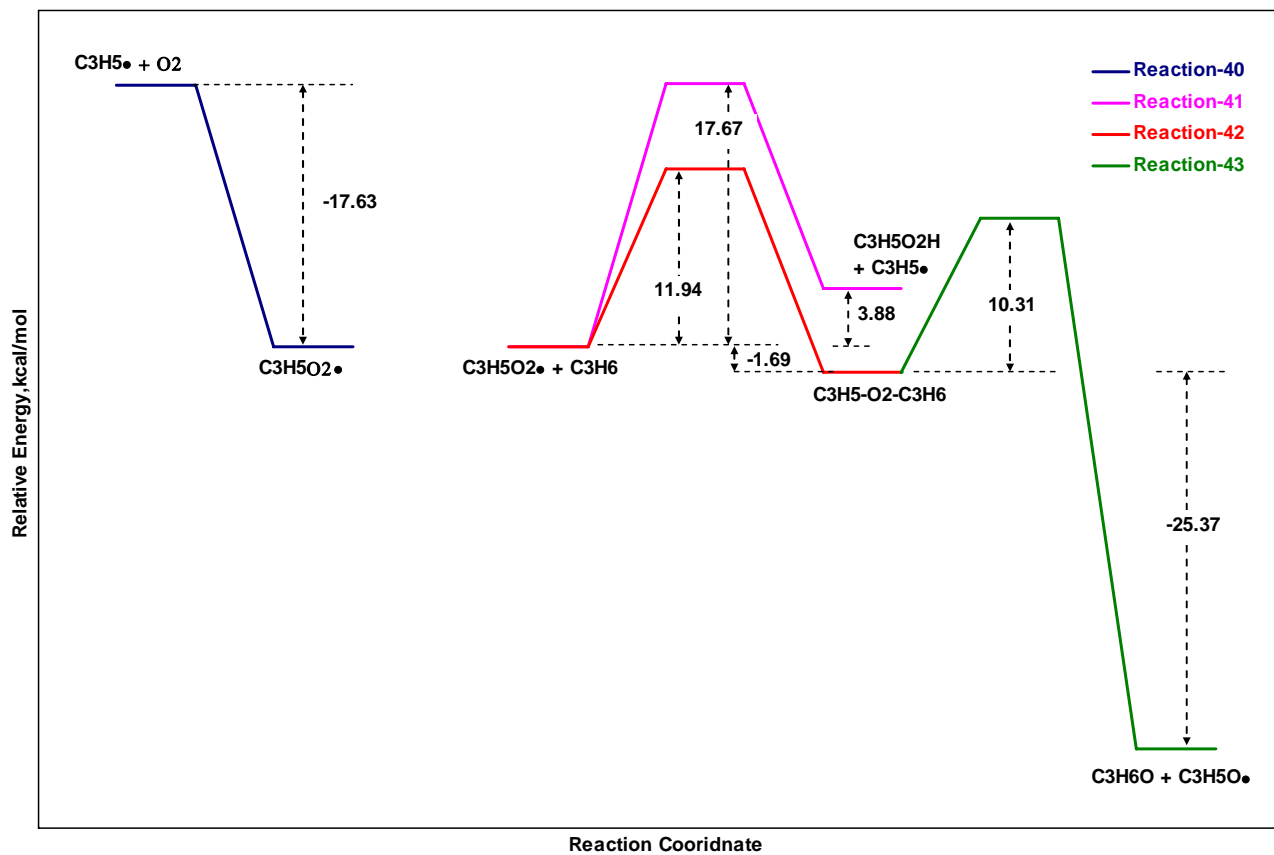


Figure 4.71 A summary energy diagram showing a comparison of steps (40-43) for gas phase propylene epoxidation reactions

CHAPTER 5

CONCLUSIONS

Ethylene and propylene partial oxidation reactions which occur on both silver and silver oxide surfaces were investigated by use of DFT calculations. $\text{Ag}_{13}(111)$ and $\text{Ag}_{14}\text{O}_9(001)$ surface cluster models were used for coordinate driving calculations which give the relative energy profile for a reaction by using Gaussian'03 software. VASP software which uses periodic slab method was also used to compare the results for the products of ethylene and propylene oxidation on silver surface obtained by using Gaussian'03 software.

Silver (110) surface is more active for ethylene oxide formation than (111) and (100) surfaces. But, activation barrier of the (111) plane is very close to experimental value, since it is a predominate surface of the real silver catalyst due to its thermodynamic stability. This is also supported with an experimental study which reports that the activity of (111) surface is a factor of 2 below the (110) surface (Campbell, 1985). Hill site of (110) surface is more active than Hollow site of (110) surface since oxygen atom weakly adsorbed on Hill site.

Ethyl aldehyde and vinyl alcohol can not be formed on Ag(111) surface because of those higher activation barriers while ethylene oxide can be formed on cluster. This situation is in agreement with experimental results.

Activation barrier for ethylene oxide formation decreases with increasing oxygen coverage. This is consistent with experimental work that reported increasing selectivity of the silver catalyst for alkene epoxidation at increasing oxygen coverage (Lambert et al. 2005).

The ethylene oxametallacycle intermediate molecule is not formed on $\text{Ag}_2\text{O}(001)$ surface while it is formed on surface oxide structure on $\text{Ag}(111)$. Silver oxide (001) like surface oxide structure on $\text{Ag}(111)$ has a similar effect on activation barrier of ethylene oxide formation. This situation is supported by the experimental study (Bukhtiyarov et al., 2003) which reported that the formation of a surface silver (I) oxide that is confirmed by the similarity of its spectral characteristics with those of bulk Ag_2O and experimental and theoretical STM studies (Bocquet et al., 2005; Michaelides et al., 2005; Schmid et al., 2006). Ethyl aldehyde and vinyl alcohol are not formed on silver oxide (001) surface.

π -allyl formation path has the lowest activation barrier on silver surface. This explains why silver is not a good catalyst for the propylene oxide formation while it is a good catalyst for the ethylene oxide formation. Propylene goes to π -allyl molecule which is an intermediate molecule for the combustion on silver.

All products except π -allyl which is undesired can not be formed on Ag_2O surface because of those higher activation barriers. π -allyl formation path has the lowest activation barrier for propylene epoxidation. This situation is the same with that for propylene epoxidation on silver surface. Propylene goes to π -allyl molecule which is an intermediate molecule for the combustion on silver. In addition, two OMMP structures were not formed on silver oxide surface while those are formed on silver surface.

The qualitative trend of relative energy obtained by slab surface is similar to those obtained by using cluster surface clusters. In other words, products order is the same for cluster and slab calculations.

REFERENCES

- Akimoto, M.K., Ichikawa, K., Echigova, E., *J. Catal.* 76, 333-344 (1982).
- Amano, F., Tanaka, T., *Catalysis Communications* 6, 269-273 (2005).
- Ananieva, E., Reitzmann, A., *Chemical Engineering Science*, 59, 5509-5517 (2004).
- Becke, A.D., *Phys. Rev. A*, 38, 3098-3100 (1988).
- Becke, A.D. and Roussel M.R., *Phys. Rev. A*, 39, 3761-3767 (1989).
- Bocquet, M.L., Michaelides, A., Loffreda, D., Sautet, P., Alavi, A., King, D.A., *J. Am. Chem. Soc.* 125, 5620-5621 (2003).
- Bocquet, M.L., Sautet, P., Cerda, J., Carlisle, C.I., Webb, M.J., King, D.A., *J. Am. Chem. Soc.* 125, 3119-3125 (2003).
- Bocquet, M.L., Loffreda, D., *J. Am. Chem. Soc.* 127, 17207-17215 (2005).
- Blaudeau, J.-P., McGrath, M. P., Curtiss, L. A., and Radom, L., *J. Chem. Phys.* 107, 5016 (1997).
- Blöchl, P. E., *Phys. Rev. B*, 50, 17953 (1994)
- Bukhtiyarov, V.I., Havecker, M., Kaichev, V.V., Gericke, A.K., Mayer, R.W., Schlögl, R., *Phys. Rev. B* 67, 235422 (2003).

Campbell, C.T., *Journal of Catalysis*, 94, 436 (1985).

Cant, N. W., Hall, W. K. J., *Journal of Catalysis* 81, 52 (1978).

Carlisle, C.I., King, D.A., Bocquet, M.L., Cerda, J., Sautet, P., *Phys. Rev. Lett.* 84, 3899-3902 (2000).

Carter, E.A., Goddard, W.A., *J. Catal.*, 112, 80-92 (1988).

Chretien, S., Gordon Mark, S., Metiu, H., *Jornal of Chemical Physics*, 121, 3756 (2004a).

Chretien, S., Gordon Mark, S., Metiu, H., *Jornal of Chemical Physics*, 121, 9931 (2004b).

Chretien, S., Gordon Mark, S., Metiu, H., *Jornal of Chemical Physics*, 121, 9925 (2004c).

Duma, V., Hönicke, D., *Journal of Catalysis*, 191, 93-104 (2000).

Frisch, M. J., G. W. Trucks, H. B. Schlegel, G. E. Scuseria, M. A. Robb, J. R. Cheeseman, J. A. Montgomery, Jr., T. Vreven, K. N. Kudin, J. C. Burant, J. M. Millam, S. S. Iyengar, J. Tomasi, V. Barone, B. Mennucci, M. Cossi, G. Scalmani, N. Rega, G. A. Petersson, H. Nakatsuji, M. Hada, M. Ehara, K. Toyota, R. Fukuda, J. Hasegawa, M. Ishida, T. Nakajima, Y. Honda, O. Kitao, H. Nakai, M. Klene, X. Li, J. E. Knox, H. P. Hratchian, J. B. Cross, V. Bakken, C. Adamo, J. Jaramillo, R. Gomperts, R. E. Stratmann, O. Yazyev, A. J. Austin, R. Cammi, C. Pomelli, J. W. Ochterski, P. Y. Ayala, K. Morokuma, G. A. Voth, P. Salvador, J. J. Dannenberg, V. G. Zakrzewski, S. Dapprich, A. D. Daniels, M. C. Strain, O. Farkas, D. K. Malick, A. D. Rabuck, K. Raghavachari, J. B. Foresman, J. V. Ortiz, Q. Cui, A. G. Baboul, S. Clifford,

J. Cioslowski, B. B. Stefanov, G. Liu, A. Liashenko, P. Piskorz, I. Komaromi, R. L. Martin, D. J. Fox, T. Keith, M. A. Al-Laham, C. Y. Peng, A. Nanayakkara, M. Challacombe, P. M. W. Gill, B. Johnson, W. Chen, M. W. Wong, C. Gonzalez, and J. A. Pople, Gaussian 03, Revision D.01, Gaussian, Inc., Wallingford CT (2004).

Gates, B.C., Katzer, J.R., Schuit, G.C.A., Chemistry of Catalytic Processes, McGraw-Hill, integrating chemical understanding of catalytic processes (1979).

Gao, W., Zhao, M., Jiang, Q., J. Phys. Chem. C 111, 4042-4046 (2007).

Geenen, P.V., Boss, H.J., Pott, G.T., J. Catal., 77, 499-510 (1982).

Grant, R.B., Lambert, R. M., Journal of Catalysis, 92, 364 (1985).

Hay, P. J. and Wadt, W. R., J. Chem. Phys. 82, 270 (1985a).

Hay, P. J. and Wadt, W. R., J. Chem. Phys. 82, 299 (1985b).

Hayashi, T., Tanaka, K., Haruta, M., J. Catalysis, 178, 566–575 (1998).

Hohenberg, P., Walte,r K., Physical Review 136 (3B), B864–B871 (1964).

Imachi, M., Egashira, M., Kuczkowski, R.L., Cant, N. W. J. Catal. 70, 177 (1981).

Jenzer, G., Mallat, T., Maciejewski, M., Eigenmann, F., Baiker A. Applied Catalysis A: General, 208,125-133 (2001).

Jiqing, Lu, Luo, M., Lei, H., Li, C., *Applied Catalysis A: General* 237, 11–19 (2002).

Jiqing, Lu, Bravo-Sua´rez, Juan J., Takahashi, A., Haruta, A., Oyama, S. Ted., *Journal of Catalysis* 232, 85–95 (2005).

Jiqing, Lu, Bravo-Sua´rez, Juan J., Haruta, M., Ted Oyama S., *Applied Catalysis A: General* 302, 283–295 (2006).

Jin, G., Lu, G., Guo, Y., Guo, Y., Wang, J., Liu, X., *Catalysis Today*, 93, 173-182 (2004).

Jin, G., Lu, G., Guo, Y., Guo, Y., Wang, J., Kong, W., Liu, X., *Journal of Molecular Catalysis A: Chemical*, 232, 165-172 (2005).

Jomoto, T., Lin, J., Nakajima, T., *J. Mol. Struc. Theochem*, 577, 143-151 (2002).

Jones, G.S., Mavrikakis, M., Barteau, M. A., Vohs J. M., *J. Am. Chem.. Soc.*, 120, 3196 (1998).

Joshi Ajay, M., Nicholas Delgass, W., and Thomson, K.T., *J. Phys. Chem. B* 110, 2572-2581 (2006).

Kanoh, H., Nishimura, T., Ayame, A., *J. Catal.*, 57. 372-379 (1979).

Karakaya, I., Thompson W.T., *J. Phase Equilibria*, 13, 137 (1992).

Kirk-Othmer Encyclopedia of Chemical Technology (E-Encyclopedia), Volume 10, 20 , (2009).

Kobayashi, H., Yoshiki, S., J. Molecular Structure: THEOCHEM 762, 57 (2006).

Kohn, W.; Sham, L. J. Phys. Rev. 140, A1133–A1138 (1965).

Kresse, G., Furthmüller, J., Comp. Mat. Sci., 6, 15 (1996)

Kresse, G., Joubert, D., Phys. Rev. B, 59, 1758 (1999)

Lambert, R.M., Federico, J.W., Rachael, L.C., Alejandra, P., Journal of Molecular Catalysis A: Chemical 228, 27–33 (2005).

Larrabe, A.D., Kuczkowski, R. L., J.Catal., 52, 72-80 (1978).

Laufer, W., Hoelderich, W. F., Applied Catalysis A: General 213, 163–171 (2001).

Lee, C., Yang, W., and Parr, R.G., Phys. Rev. B, 37, 785-789 (1988).

Linic, S., Barteau, M. A., J. Am. Chem. Soc.124 (2), 310 (2002).

Linic, S., Barteau, M. A., J. Am. Chem.. Soc. 125, 4034 (2003a).

Linic, S., Barteau, M. A., Journal of Catalysis 214, 200 (2003b).

Lopez, N., Nørskov, J.K., Surface Science 515, 175–186 (2002).

Lukaski, A.C., Barteau, M.A., Catal. Lett., 128 (2009) 9-17.

Mantashyan, A. A., Arsentiev, S. D., and Grigoryan, R. R., React. React. Kinet. Catal. L. 21, 347-350 (1982).

Mantashyan ,A. A.; Arsentiev, S. D., and Grigoryan, R. R., *Khimicheskaya fizika*, 4, 75-78 (1985).

Mavrikakis, M., Doren, D.J., Barteau, M.A., *J. Phys. Chem. B* 102, 394 (1998).

Medlin, J.W., Mavrikakis, M., Barteau, M.A., *J.Phys.Chem. B* 103, 11169-11175 (1999).

Medlin, J.W., Barteau, M.A., *J.Phys.Chem. B* 105, 10054-10061 (2001).

Michaelides, A., Bocquet, M.L., Sautet, P., Alavi, A., King, D.A., *Chem. Phys. Lett.* 367, 344-350 (2003).

Michaelides, A., Reuter, K., Scheffler, M., *J.Vac.Sci.Tech.* 23, 1487-1497 (2005).

Mills, P. L., Nicole, J. F.,*Chemical Engineering Science* 59, 5345–5354 (2004).

Mimura, N.; Tsubota, S.; Murata, K.; Bando, K. K.; Bravo-Suarez, J. J.; Haruta, M.; Oyama, S. T. *Catal. Lett.* 110, 47-51 (2006).

Miyazaki, T., Öztürk, Ş., Önal, I., Senkan, S., *Catalyst Today* 81,473-484 (2003).

Munakata, H., Y. Oumi, A. Miyamoto, *J.Phys.Chem.B* 105, 3493 (2001).

Murata, K., Liu, Y., Mimura, N., Inaba, M., *Catalysis Communications*, 4, 385–391 (2003).

Murata, K., Liu, Y., Inaba, M., Mimura, N., *Catalysis Today*, 91, 39-42 (2004).

Murata, K., Liu, Y., Mimura, N., Inaba, M, *Journal of Catalysis*, 220, 513–518 (2003).

Nijhuis, T. A., Huizinf B. J., Makkee M., Moulijn, Ind., *Eng. Chem. Res.*, 38, 884-891 (1999).

Nijhuis, T. A, Makkee, M., Moulijn, J.A., Weckhuysen, B.A., *Ind. Eng. Chem. Res.* 45, 3447-3459 (2006).

Peng, C. and Schlegel, H.B., *Israel J Chem* 33, 449 (1993).

Perdew, J.P., Chevary, J. A., Vosko, S. H., Jackson, K.A., Pederson, M.R., Singh, D.J., Fiolhais, C., *Phys. Rev. B*, 46, 6671 (1992)

Perdew J.P., Ruzsinszky, A., Tao, J., Staroverov, V.N., Scuseria, G., and Csonka, G.I. *J. Chem. Phys.* 123, 062201 (2005).

Roithova, J., Schröder, D., *J.Am.Chem.Soc.* 129, 15311-15318 (2007).

Ruipu, W., Guo, X., Wang, X., Hao, J., *Catalysis Today* 93, 217–222 (2004).

Sachtler, W. M. H., Backx, C., Van Santen, R. A., *Catal. Rev. Sci. Eng.*, 23, 127 (1981).

Satterfield, C. N., *Heterogeneous Catalysis in Industrial Practice*, (1991).

Schmid, M., A. Reicho, A. Stierle, I. Costina, J. Klikovits, P. Kostelnik, O. Dubay, G. Kresse, J. Gustafson, E. Lundgren, J. N. Andersen, H. Dosch, P. Varga, *Phys. Rev. Let.* 96 146102-1 (2006).

Schneider, W.F., Hass, K.C., Ramprasad, R., and Adams, J.B., *J. Phys. Chem B* 101, 4352 (1997).

Sinclair, P.E., Catlow, C. R. A., *J. Phys. Chem. B* 103, 1084 (1999).

Song, Z., Mimura, N., Tsubota, S., Fujitani, T., Oyama, S. T. *Catal. Lett.* 121, 33-38 (2008).

Takahashi, A., Hamakawa, N., Nakamura, I., Fujitani, T., *Applied Catalysis A: General*, 294, 34-39 (2005).

Thomas, J.M., Thomas, W.J., *Principles and Practice of Heterogeneous Catalysis*, Wiley-VCH, First Edition (1967), Second Edition (1997).

Torres, D., Lopez, N., Illas, F., Lambert, R.M., *Angew. Chem. Int. Ed.* 46, 2055–2058 (2007).

van Santen, R.A., Kuipers, H. P. C. E., *Advances In Catalysis*, 35, 265 (1987).

van Santen, R.A.; Neurock, M. *Introduction in Molecular Heterogeneous Catalysis: WILEY* (2006).

Vayssilov, G.N., van Santen, R.A., *J. Catal.* 175, 170 (1998).

Verykios, X., E., Stein, F. P., Coughlin, R. W., *Catal. Rev. Sci. Eng.* 22(2), 197 (1980).

Vignale, G.; Rasolt, M., *Physical Review Letters* 59, 2360–2363 (1987).

Wadt W. R. and Hay P. J., *J. Chem. Phys.* 82, 284 (1985).

Wells, D.H. , Delgass, W. N., Thomson, K. T., J Catal. 225, 69 (2004a).

Wells, D.H., Delgass, W. N., Thomson, K. T., J.Am.Chem.Soc. 126, 2956 (2004b).

Wells, D.H. Jr., Joshi, A. M., Delgass, W. N., Thomson, K. T., J. Phys. Chem. B, 110, 14627 (2006).

Wolfram, K., Holthausen, M. C., "A Chemist's Guide to Density Functional Theory", 2nd Ed., Wiley-VCH Verlag GmbH, New York (2001).

Wyckoff, R.W.G., "Crystal Structures", 2nd Edition, Volume 1, John Wiley & Sons, New York (1963)

Young, D.C., John Wiley & Sons, Inc. (2001)

Yu, H.G., Chem. Phys. Lett., 431, 236-240 (2006).

APPENDIX A

DENSITY FUNCTIONAL THEORY

A.1. Overview of Method

Although density functional theory has its conceptual roots in the Thomas-Fermi model, DFT was put on a firm theoretical footing by the two Hohenberg-Kohn theorems (H-K) (Hohenberg, 1964). The original H-K theorems held only for non-degenerate ground states in the absence of a magnetic field, although they have since been generalized to encompass these (Vignale et al., 1987).

The first H-K theorem demonstrates that the ground state properties of a many-electron system are uniquely determined by an electron density that depends on only 3 spatial coordinates. It lays the groundwork for reducing the many-body problem of N electrons with $3N$ spatial coordinates to 3 spatial coordinates, through the use of functionals of the electron density. This theorem can be extended to the time-dependent domain to develop time-dependent density functional theory (TDDFT), which can be used to describe excited states.

The second H-K theorem defines energy functional for the system and proves that the correct ground state electron density minimizes this energy functional.

Within the framework of Kohn-Sham DFT, the intractable many-body problem of interacting electrons in a static external potential is reduced to a tractable problem of non-interacting electrons moving in an effective potential. The effective potential includes the external potential and the effects of the Coulomb interactions between the electrons, e.g., the exchange and correlation interactions. Modeling the latter two interactions becomes the difficulty within KS DFT. The simplest approximation is the local-density approximation (LDA), which is based upon exact exchange energy for a uniform electron gas, which can be obtained from the Thomas-Fermi model, and from fits to the correlation energy for a uniform electron gas. Non-interacting systems are relatively easy to solve as the wavefunction can be represented as a Slater determinant of orbitals. Further, the kinetic energy functional of such a system is known exactly. The exchange-correlation part of the total-energy functional remains unknown and must be approximated.

Another approach, less popular than Kohn-Sham DFT (KS-DFT) but arguably more closely related to the spirit of the original H-K theorems, is orbital-free density functional theory (OFDFT), in which approximate functionals are also used for the kinetic energy of the non-interacting system (Hohenberg et al., 1964).

A.2. Derivation and Formalism

As usual in many-body electronic structure calculations, the nuclei of the treated molecules or clusters are seen as fixed (the Born-Oppenheimer approximation), generating a static external potential V in which the electrons are moving. A stationary electronic state is then described by a

wavefunction $\Psi(\vec{r}_1, \dots, \vec{r}_N)$ satisfying the many-electron Schrödinger equation

$$\hat{H}\Psi = [\hat{T} + \hat{V} + \hat{U}] \Psi = \left[\sum_i^N -\frac{\hbar^2}{2m} \nabla_i^2 + \sum_i^N V(\vec{r}_i) + \sum_{i<j}^N U(\vec{r}_i, \vec{r}_j) \right] \Psi = E\Psi \quad (\text{A1})$$

where \hat{H} is the electronic molecular Hamiltonian, N is the number of electrons, \hat{T} is the N -electron kinetic energy, \hat{V} is the N -electron potential energy from the external field, and \hat{U} is the electron-electron interaction energy for the N -electron system. The operators \hat{T} and \hat{U} are so-called universal operators as they are the same for any system, while \hat{V} is system dependent, i.e. non-universal. The difference between having separable single-particle problems and the much more complicated many-particle problem arises from the interaction term \hat{U} .

There are many sophisticated methods for solving the many-body Schrödinger equation based on the expansion of the wavefunction in Slater determinants. While the simplest one is the Hartree-Fock method, more sophisticated approaches are usually categorized as post-Hartree-Fock methods. However, the problem with these methods is the huge computational effort, which makes it virtually impossible to apply them efficiently to larger, more complex systems.

Here DFT provides an appealing alternative, being much more versatile as it provides a way to systematically map the many-body problem, with \hat{U} , onto a single-body problem without \hat{U} . In DFT the key variable is the particle density $n(\vec{r})$, which for a normalized Ψ is given by

$$n(\vec{r}) = N \int d^3r_2 \int d^3r_3 \cdots \int d^3r_N \Psi^*(\vec{r}, \vec{r}_2, \dots, \vec{r}_N) \Psi(\vec{r}, \vec{r}_2, \dots, \vec{r}_N) \quad (\text{A2})$$

This relation can be reversed, i.e. for a given ground-state density $n_0(\vec{r})$ it is possible, in principle, to calculate the corresponding ground-state wavefunction $\Psi_0(\vec{r}_1, \dots, \vec{r}_N)$. In other words, Ψ_0 is a unique functional of n_0 , (Hohenberg, 1964)

$$\Psi_0 = \Psi[n_0] \quad (\text{A3})$$

and consequently the ground-state expectation value of an observable \hat{O} is also a functional of n_0

$$O[n_0] = \langle \Psi[n_0] | \hat{O} | \Psi[n_0] \rangle \quad (\text{A4})$$

In particular, the ground-state energy is a functional of n_0

$$E_0 = E[n_0] = \langle \Psi[n_0] | \hat{T} + \hat{V} + \hat{U} | \Psi[n_0] \rangle \quad (\text{A5})$$

where the contribution of the external potential $\langle \Psi[n_0] | \hat{V} | \Psi[n_0] \rangle$ can be written explicitly in terms of the ground-state density n_0

$$V[n_0] = \int V(\vec{r}) n_0(\vec{r}) d^3r \quad (\text{A6})$$

More generally, the contribution of the external potential $\langle \Psi | \hat{V} | \Psi \rangle$ can be written explicitly in terms of the density n ,

$$V[n] = \int V(\vec{r}) n(\vec{r}) d^3r \quad (\text{A7})$$

The functionals $T[n]$ and $U[n]$ are called universal functionals, while $V[n]$ is called a non-universal functional, as it depends on the system under study. Having specified a system, i.e., having specified \hat{V} , one then has to minimize the functional

$$E[n] = T[n] + U[n] + \int V(\vec{r})n(\vec{r})d^3r \quad (\text{A8})$$

with respect to $n(\vec{r})$, assuming one has got reliable expressions for $T[n]$ and $U[n]$. A successful minimization of the energy functional will yield the ground-state density n_0 and thus all other ground-state observables.

The variational problems of minimizing the energy functional $E[n]$ can be solved by applying the Lagrangian method of undetermined multipliers (Sham, 1964). First, one considers an energy functional that doesn't explicitly have an electron-electron interaction energy term,

$$E_s[n] = \langle \Psi_s[n] | \hat{T}_s + \hat{V}_s | \Psi_s[n] \rangle \quad (\text{A9})$$

where \hat{T}_s denotes the non-interacting kinetic energy and \hat{V}_s is an external effective potential in which the particles are moving. Obviously, $n_s(\vec{r}) \stackrel{\text{def}}{=} n(\vec{r})$ if \hat{V}_s is chosen to be

$$\hat{V}_s = \hat{V} + \hat{U} + (\hat{T} - \hat{T}_s) \quad (\text{A10})$$

Thus, one can solve the so-called Kohn-Sham equations of this auxiliary non-interacting system,

$$\left[-\frac{\hbar^2}{2m} \nabla^2 + V_s(\vec{r}) \right] \phi_i(\vec{r}) = \epsilon_i \phi_i(\vec{r}) \quad (\text{A11})$$

which yields the orbitals ϕ_i that reproduce the density $n(\vec{r})$ of the original many-body system

$$n(\vec{r}) \stackrel{\text{def}}{=} n_s(\vec{r}) = \sum_i^N |\phi_i(\vec{r})|^2 \quad (\text{A12})$$

The effective single-particle potential can be written in more detail as

$$V_s(\vec{r}) = V(\vec{r}) + \int \frac{e^2 n_s(\vec{r}')}{|\vec{r} - \vec{r}'|} d^3 r' + V_{\text{XC}}[n_s(\vec{r})] \quad (\text{A13})$$

where the second term denotes the so-called Hartree term describing the electron-electron Coulomb repulsion, while the last term V_{XC} is called the exchange-correlation potential. Here, V_{XC} includes all the many-particle interactions. Since the Hartree term and V_{XC} depend on $n(\vec{r})$, which depends on the ϕ_i , which in turn depend on V_s , the problem of solving the Kohn-Sham equation has to be done in a self-consistent (i.e., iterative) way. Usually one starts with an initial guess for $n(\vec{r})$, then calculates the corresponding V_s and solves the Kohn-Sham equations for the ϕ_i . From these one calculates a new density and starts again. This procedure is then repeated until convergence is reached.

A.3. Approximations (Exchange-correlation functionals)

The major problem with DFT is that the exact functionals for exchange and correlation are not known except for the free electron gas. However, approximations exist which permit the calculation of certain physical quantities quite accurately. In physics the most widely used approximation is the local-density approximation (LDA), where the functional depends only on the density at the coordinate where the functional is evaluated:

$$E_{\text{XC}}[n] = \int \epsilon_{\text{XC}}(n) n(\vec{r}) d^3 r. \quad (\text{A14})$$

The local spin-density approximation (LSDA) is a straightforward generalization of the LDA to include electron spin:

$$E_{XC}[n_{\uparrow}, n_{\downarrow}] = \int \epsilon_{XC}(n_{\uparrow}, n_{\downarrow}) n(\vec{r}) d^3r. \quad (\text{A15})$$

Highly accurate formulae for the exchange-correlation energy density $\epsilon_{XC}(n_{\uparrow}, n_{\downarrow})$ have been constructed from quantum Monte Carlo simulations of a free electron model (Perdew et al., 2005)

Generalized gradient approximations (GGA) are still local but also take into account the gradient of the density at the same coordinate:

$$E_{XC}[n_{\uparrow}, n_{\downarrow}] = \int \epsilon_{XC}(n_{\uparrow}, n_{\downarrow}, \vec{\nabla} n_{\uparrow}, \vec{\nabla} n_{\downarrow}) n(\vec{r}) d^3r. \quad (\text{A16})$$

Using the latter (GGA) very good results for molecular geometries and ground-state energies have been achieved.

Potentially more accurate than the GGA functionals are meta-GGA functions. These functionals include a further term in the expansion, depending on the density, the gradient of the density and the Laplacian (second derivative) of the density.

Difficulties in expressing the exchange part of the energy can be relieved by including a component of the exact exchange energy calculated from Hartree-Fock theory. Functionals of this type are known as hybrid functionals

A.4. Applications

In practice, Kohn-Sham theory can be applied in several distinct ways depending on what is being investigated. In solid state calculations, the local density approximations are still commonly used along with plane wave basis sets, as an electron gas approach is more appropriate for electrons delocalised through an infinite solid. In molecular calculations, however,

more sophisticated functionals are needed, and a huge variety of exchange-correlation functionals have been developed for chemical applications. Some of these are inconsistent with the uniform electron gas approximation, however, they must reduce to LDA in the electron gas limit. Among physicists, probably the most widely used functional is the revised Perdew-Burke-Ernzerhof exchange model (a direct generalized-gradient parametrization of the free electron gas with no free parameters); however, this is not sufficiently calorimetrically accurate for gas-phase molecular calculations. In the chemistry community, one popular functional is known as BLYP (from the name Becke for the exchange part and Lee, Yang and Parr for the correlation part). Even more widely used is B3LYP which is a hybrid functional in which the exchange energy, in this case from Becke's exchange functional, is combined with the exact energy from Hartree-Fock theory. Along with the component exchange and correlation functionals, three parameters define the hybrid functional, specifying how much of the exact exchange is mixed in. The adjustable parameters in hybrid functionals are generally fitted to a 'training set' of molecules. Unfortunately, although the results obtained with these functionals are usually sufficiently accurate for most applications, there is no systematic way of improving them (in contrast to some of the traditional wavefunction-based methods like configuration interaction or coupled cluster theory). Hence in the current DFT approach it is not possible to estimate the error of the calculations without comparing them to other methods or experiments.

For molecular applications, in particular for hybrid functionals, Kohn-Sham DFT methods are usually implemented just like Hartree-Fock itself.

APPENDIX B

BASIS SETS

A basis set is a set of functions used to describe the shape of the orbitals in an atom. Molecular orbitals and entire wave functions are created by taking linear combinations of basis functions and angular functions. Most semiempirical methods use a predefined basis set. When ab-initio or density functional theory calculations are done, a basis set must be specified. The type of calculation performed and basis set chosen are the two biggest factors in determining the accuracy of results (Young, 2001).

The orbitals almost always have the functional form given in Eq. (B.1):

$$\varphi = Y_{lm} \sum_i C_i \sum_j C_{ij} e^{-\xi_{ij} r^2}$$

(B1)

The Y_{lm} function gives the orbital the correct symmetry (s, p, d, etc.). $\exp(-r^2)$ is called a Gaussian primitive function. The contraction coefficients C_{ij} and exponents ξ_{ij} are read from a database of standard functions and do not change over the course of the calculation. This predefined set of coefficients and exponents is called a basis set. An enormous amount of work is involved in optimizing a basis set to obtain a good description of an individual atom. By using such a predefined basis set, the program must only optimize the

molecular orbital coefficients C_i . As seen above, each C_i may weigh a sum of typically one to nine primitive Gaussian functions, called a contraction. Basis sets of contracted functions are called segmented basis sets.

The orbitals in Eq. (B.1) are referred to as Gaussian type orbitals, or GTO, since they incorporate Gaussian functions, $\exp(-\xi r^2)$. The exact solution to the Schrödinger equation for the hydrogen atom is a Slater type orbital, or STO, of the form $\exp(-\xi r)$. GTO basis sets require more primitives to describe the wave function than are needed for STO calculations. However, the integrals over GTO primitives can be computed analytically, which is so much faster than the numeric integrals over STO functions that any given accuracy can be obtained most quickly using GTO functions. As such, STO basis sets are sometimes used for high-accuracy work, but most calculations are now done with GTO basis sets.

Choosing a standard GTO basis set means that the wave function is being described by a finite number of functions. This introduces an approximation into the calculation since an infinite number of GTO functions would be needed to describe the wave function exactly. Differences in results due to the quality of one basis set versus another are referred to as basis set effects. In order to avoid the problem of basis set effects, some high-accuracy work is done with numeric basis sets. These basis sets describe the electron distribution without using functions with a predefined shape. A typical example of such a basis set might be a cubic spline set in which a large number of third-order polynomials are used.

B.1. Notation

Most calculations today are done by choosing an existing segmented GTO basis set. These basis sets are identified by one of a number of notation

schemes. These abbreviations are often used as the designator for the basis set in the input to ab-initio computational chemistry programs. The following is a look at the notation for identifying some commonly available contracted GTO basis sets. The smallest basis sets are called minimal basis sets. The most popular minimal basis set is the **STO-3G** set. This notation indicates that the basis set approximates the shape of a STO orbital by using a single contraction of three GTO orbitals. One such contraction would then be used for each orbital, which is the definition of a minimal basis. Minimal basis sets are used for very large molecules, qualitative results, and in certain cases quantitative results. There are **STO-nG** basis sets for $n = 2 - 6$.

Another popular minimal basis set is the MINI set described below. Another family of basis sets, commonly referred to as the Pople basis sets, are indicated by the notation **6-31G**. This notation means that each core orbital is described by a single contraction of six GTO primitives and each valence shell orbital is described by two contractions, one with three primitives and the other with one primitive. These basis sets are very popular, particularly for organic molecules. Other Pople basis sets in this set are **3-21G**, **4-31G**, **4-22G**, **6-21G**, **6-311G**, and **7-41G**. The Pople basis set notation can be modified by adding one or two asterisks, such as **6-31G*** or **6-31G****. A single asterisk means that a set of d primitives has been added to atoms other than hydrogen. Two asterisks mean that a set of p primitives has been added to hydrogen as well. These are called polarization functions because they give the wave function more flexibility to change shape. Adding polarization functions usually decreases the variational total energy by about the same amount as adding another contraction. However, this energy change is almost completely systematic, so it changes the relative energies very little. Polarization functions are used because they often result in more accurate computed geometries and vibrational frequencies. The **3-21G*** basis is an exception to the notation above. In this particular case, the d functions are added only to 2nd row atoms, Al through Ar. In order to indicate

this difference, this basis is sometimes given the notation **3-21G(*)**. One or two plus signs can also be added, such as **6-31+G*** or **6-31++G***. A single plus sign indicates that diffuse functions have been added to atoms other than hydrogen. The second plus sign indicates that diffuse functions are being used for all atoms. These diffuse functions are primitives with small exponents, thus describing the shape of the wave function far from the nucleus.

Diffuse functions are used for anions, which have larger electron density distributions. They are also used for describing interactions at long distances, such as van der Waals interactions. The effect of adding diffuse functions is usually to change the relative energies of the various geometries associated with these systems. Basis sets with diffuse functions are also called augmented basis sets. Very diffuse orbitals are called Rydberg orbitals since they are used to describe Rydberg states of molecules.

As the Pople basis sets have further expanded to include several sets of polarization functions, f functions and so on, there has been a need for a new notation. In recent years, the types of functions being added have been indicated in parentheses. An example of this notation is **6-31G(dp,p)** which means that extra sets of p and d functions have been added to nonhydrogens and an extra set of p functions have been added to hydrogens. Thus, this example is synonymous with **6-31+G****.

Many basis sets are just identified by the author's surname and the number of primitive functions. Some examples of this are the Huzinaga, Dunning, and Duijneveldt basis sets. For example, **D95** and **D95V** are basis sets created by Dunning with nine s primitives and five p primitives. The V implies one particular contraction scheme for the valence orbitals. Another example would be a basis set listed as "Duijneveldt 13s8p".

In order to describe the number of primitives and contractions more directly, the notation $(6s,5p)\rightarrow(1s,3p)$ or $(6s,5p)/(1s,3p)$ is sometimes used. This example indicates that six s primitives and five p primitives are contracted into one s contraction and three p contractions. Thus, this might be a description of the **6-311G** basis set. However, this notation is not precise enough to tell whether the three p contractions consist of three, one, and one primitives or two, two, and one primitives. The notation **(6,311)** or **(6,221)** is used to distinguish these cases. Some authors use round parentheses () to denote the number of primitives and square brackets [] to denote the number of contractions.

An older, but still used, notation specifies how many contractions are present. For example, the acronym **TZV** stands for triple-zeta valence, meaning that there are three valence contractions, such as in a 6-311G basis. The acronyms **SZ** and **DZ** stand for single zeta and double zeta, respectively. A P in this notation indicates the use of polarization functions. Since this notation has been used for describing a number of basis sets, the name of the set creator is usually included in the basis set name (i.e., Ahlrichs VDZ). If the author's name is not included, either the Dunning-Hay set is implied or the set that came with the software package being used is implied (Young, 2001).

B.2. Treating Core Electrons

Unlike semiempirical methods that are formulated to completely neglect the core electrons, ab-initio methods must represent all the electrons in some manner. However, for heavy atoms it is desirable to reduce the amount of computation necessary. This is done by replacing the core electrons and their basis functions in the wave function by a potential term in the Hamiltonian. These are called core potentials, **effective core potentials (ECP)**, or

relativistic effective core potentials (RECP). Core potentials must be used along with a valence basis set that was created to accompany them. As well as reducing the computation time, core potentials can include the effects of the relativistic mass defect and spin coupling terms that are significant near the nuclei of heavy atoms. This is often the method of choice for heavy atoms, Rb and up. The energy obtained from a calculation using ECP basis sets is termed valence energy. Also, the virial theorem no longer applies to the calculation. Some molecular properties may no longer be computed accurately if they are dependent on the electron density near the nucleus. There are several issues to consider when using ECP basis sets. The core potential may represent all but the outermost electrons. In other ECP sets, the outermost electrons and the last called shell will be in the valence orbital space. Having more electrons in the core will speed the calculation, but results are more accurate if the $n-1$ shell is outside of the core potential. Some ECP sets are designated as shape-consistent sets, which mean that the shape of the atomic orbitals in the valence region matches that for all electron basis sets. ECP sets are usually named with an acronym that stands for the authors' names or the location where it was developed. Some common core potential basis sets are listed below. The numbers of primitives given are those describing the valence region (Young, 2001).

- **CREN** Available for Sc(4s) through Hs(0s6p6d), this is a shape consistent basis set developed by Emler and coworkers that has a large core region and small valence. This is also called the CEP-4G basis set. The CEP-31G and CEP-121G sets are related split valence sets.
- **SBKJC VDZ** Available for Li(4s4p) through Hg(7s7p5d), this is a relativistic basis set created by Stevens and coworkers to replace all but the outermost electrons. The double-zeta valence contraction is designed to have accuracy comparable to that of the 3-21G all-electron basis set.

- **Hay-Wadt MB** Available for K(5s5p) through Au(5s6p5d), this basis set contains the valence region with the outermost electrons and the previous shell of electrons. Elements beyond Kr are relativistic core potentials. This basis set uses a minimal valence contraction scheme. These sets are also given names starting with "LA" for Los Alamos, where they were developed.
- **LANL2DZ** Available for H(4s) through Pu(7s6p2d2f), this is a collection of double-zeta basis sets, which are all-electron sets prior to Na.
- **CRENBL** Available for H(4s) through Hs(0s3p6d5f), this is a collection of shape-consistent sets, which use a large valence region and small core region.

B.3. Common Basis Sets

Below is a listing of commonly used basis sets (Young, 2001);

- **STO-nG (n = 2 – 6)** n primitives per shell per occupied angular momentum (s; p; d). STO-3G is heavily used for large systems and qualitative results. The STO-3G functions have been made for H with three primitives (3s) through Xe(15s12p6d). STO-2G is seldom used due to the poor quality of its results. The larger STO-nG sets are seldom used because they have too little flexibility.
- **3-21G** Same number of primitives as STO-3G, but more flexibility in the valence orbitals. Available for H through Cs. Popular for qualitative and sometimes quantitative results for organic molecules.
- **6-31G** Available for H(4s) through Ar(16s10p). Very popular for quantitative results for organic molecules.
- **6-311G** Available for H(5s) through Kr(14s12p5d). Very popular for quantitative results for organic molecules.

- **D95 and D95V** Available for H(4s) and B through F(9s5p). Used for quantitative results.
- **Dunning-Hay DZ** Available for H(4s) through Cl(11s7p). **DZP** adds one polarization function. If this notation is used without an author's name, this is the set that is usually implied.
- **Ahlrichs VDZ, pVDZ, VTZ** Available for Li(4s) to (11s) through Kr(14s10p5d) to (17s13p6d). These have been used for many high accuracy calculations.
- **cc-pVnZ (n = D,T,Q,5,6)** Correlation-consistent basis sets that always include polarization functions. Atoms H through Ar are available. The 6Z set goes up to Ne only. The various sets describe H with from (2s1p) to (5s4p3d2f 1g) primitives. The Ar atoms is described by from (4s3p1d) to (7s6p4d3f 2g1h) primitives. One to four diffuse functions are denoted by prepending the notation with "aug-" or "n-aug-", where n = d, t, q.
- **DZVP, DZVP2, TZVP DFT-optimized functions.** Available for H(5s) through Xe(18s14p9d) plus polarization functions.

Some of the basis sets discussed here is used more often than others. The STO-3G set is the most widely used minimal basis set. The Pople sets, particularly, 3-21G, 6-31G, and 6-311G, with the extra functions described previously are widely used for quantitative results, particularly for organic molecules. The correlation consistent sets have been most widely used in recent years for high-accuracy calculations. The CBS and G2 methods are becoming popular for very-high-accuracy results. The Wachters and Hay sets are popular for transition metals. The core potential sets, particularly LANL2DZ, Dolg, and SBKJC, are used for heavy elements, Rb and heavier.

APPENDIX C

OPTIMIZED GEOMETRIES AND PARAMETERS OF REACTANTS AND PRODUCTS

DFT/B3LYP method and 6-31G** basis set was used for geometry optimization in Gaussian'03 software where tight keyword was used. PAW-GGA method was used for optimization in VASP software where high precision was used.

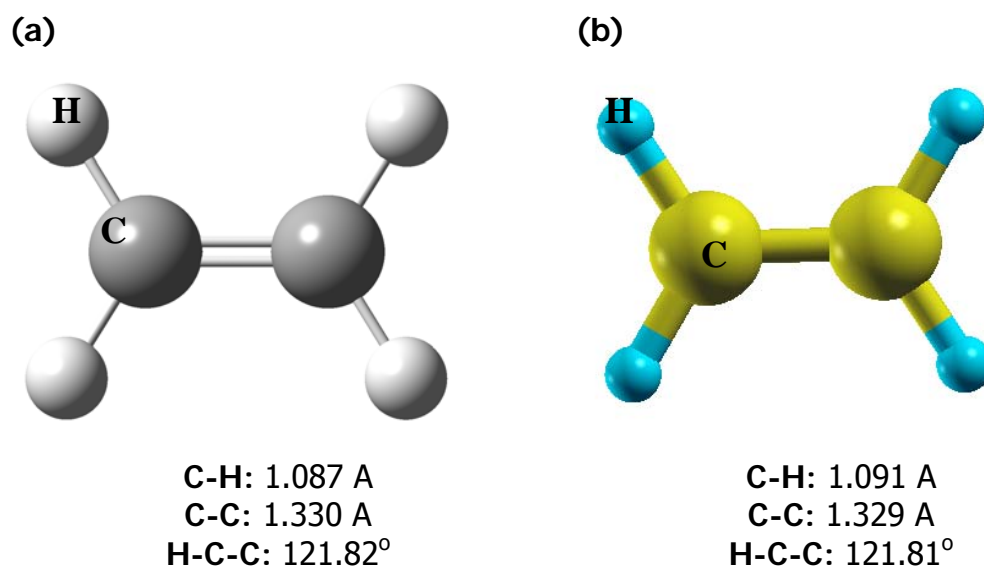


Figure C.1 Optimized geometry of Ethylene a) in Gaussian 03 software b) in VASP software

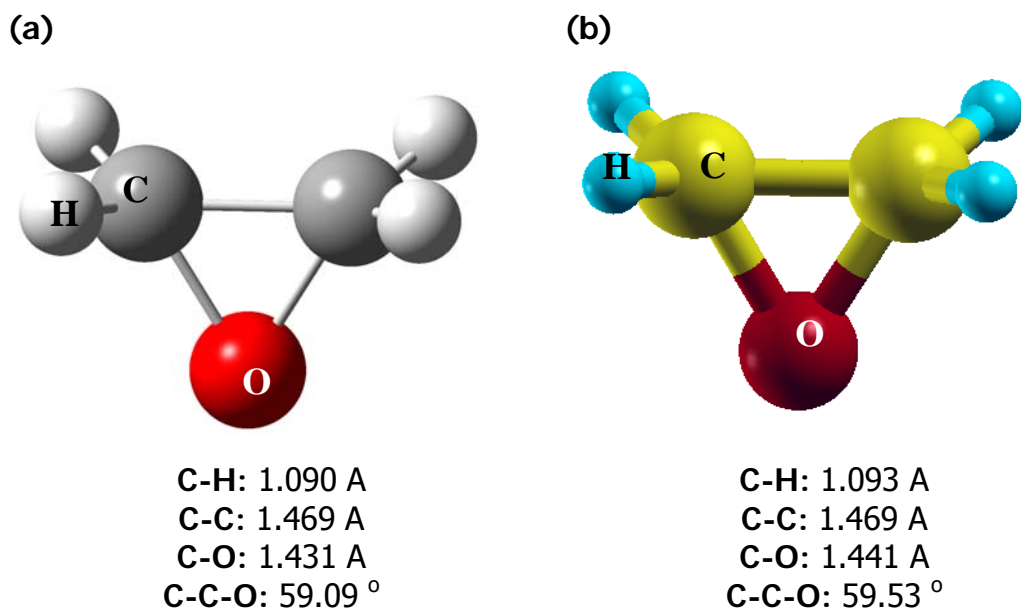


Figure C.2 Optimized geometry of Ethylene Oxide a) in Gaussian 03 software b) in VASP software

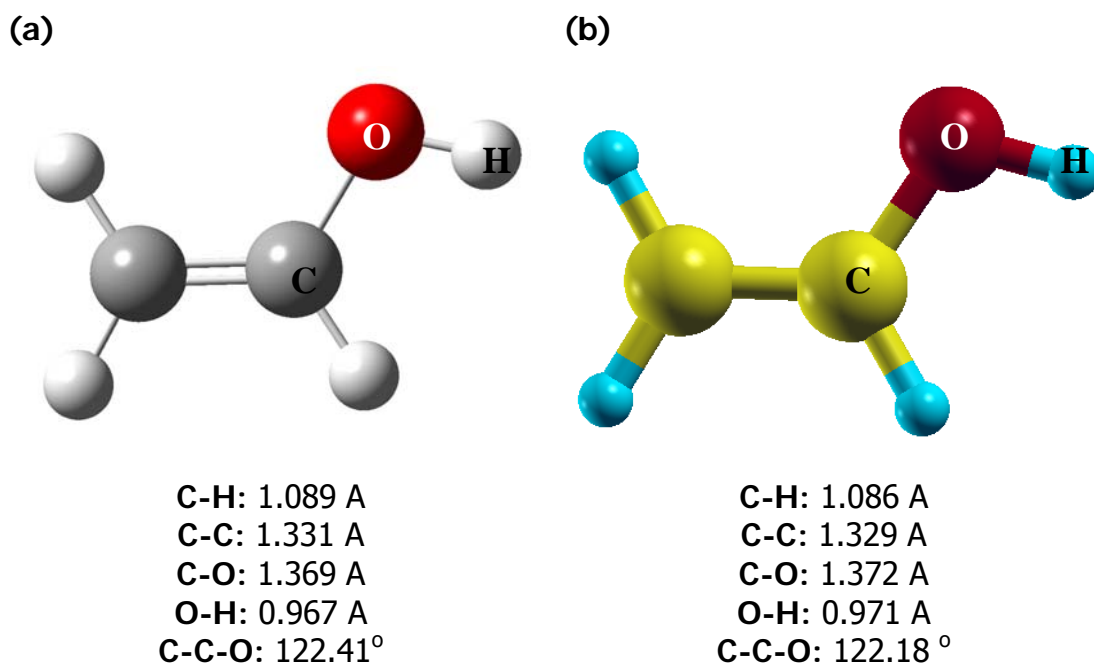


Figure C.3 Optimized geometry of Vinylalcohol a) in Gaussian 03 software b) in VASP software

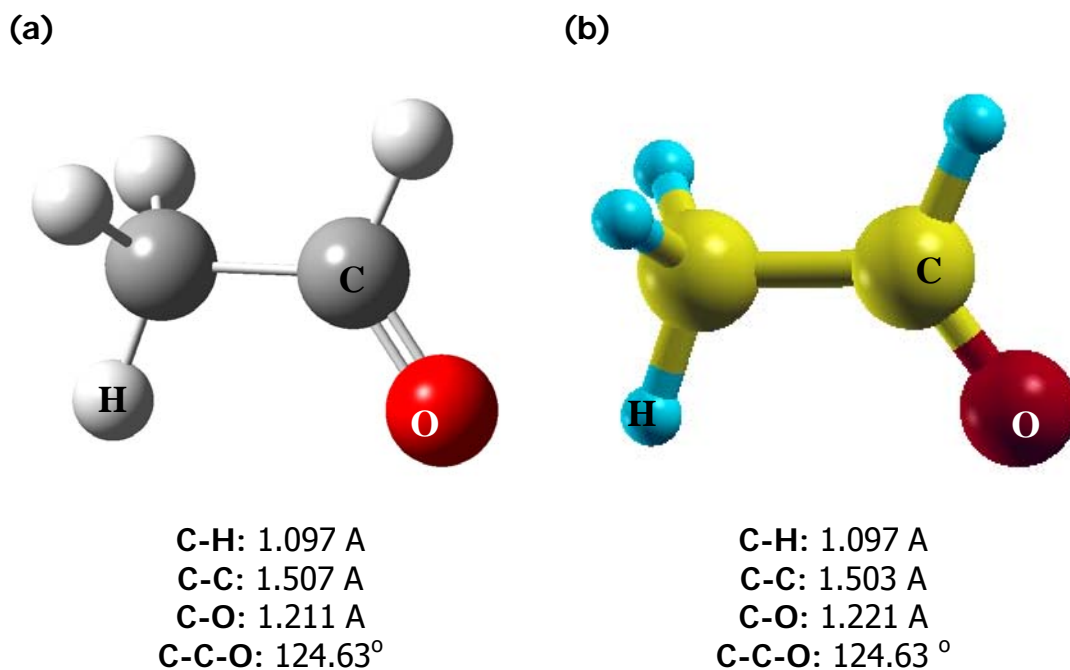


Figure C.4 Optimized geometry of Vinylaldehyde a) in Gaussian 03 software b) in VASP software

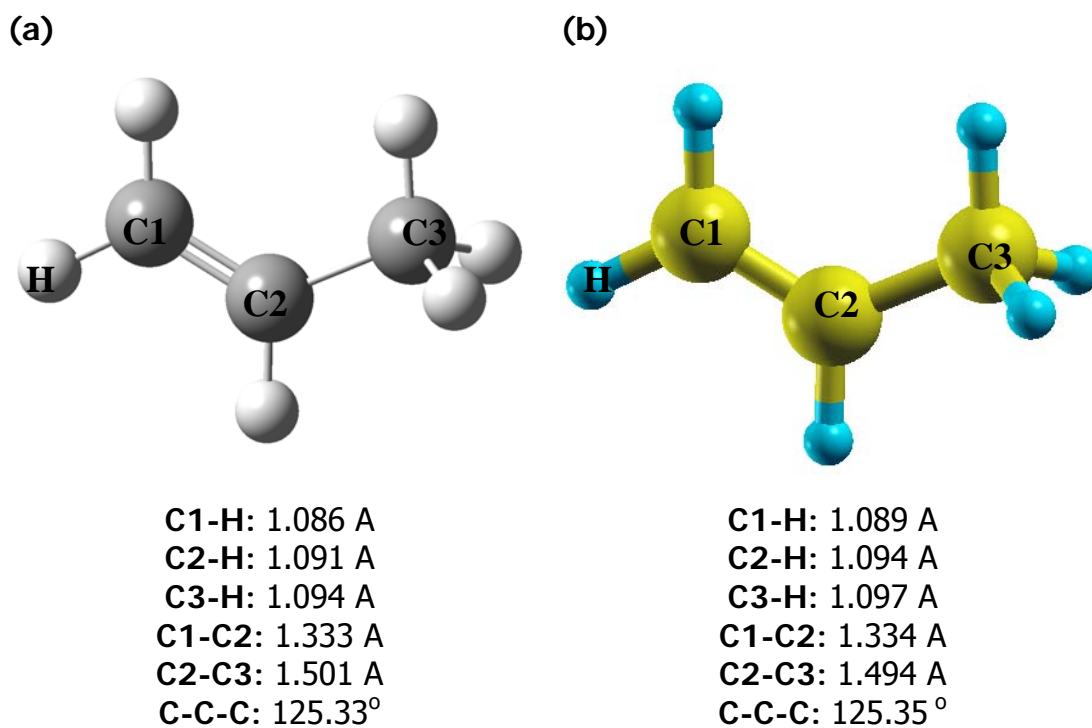


Figure C.5 Optimized geometry of Propylene a) in Gaussian 03 software b) in VASP software

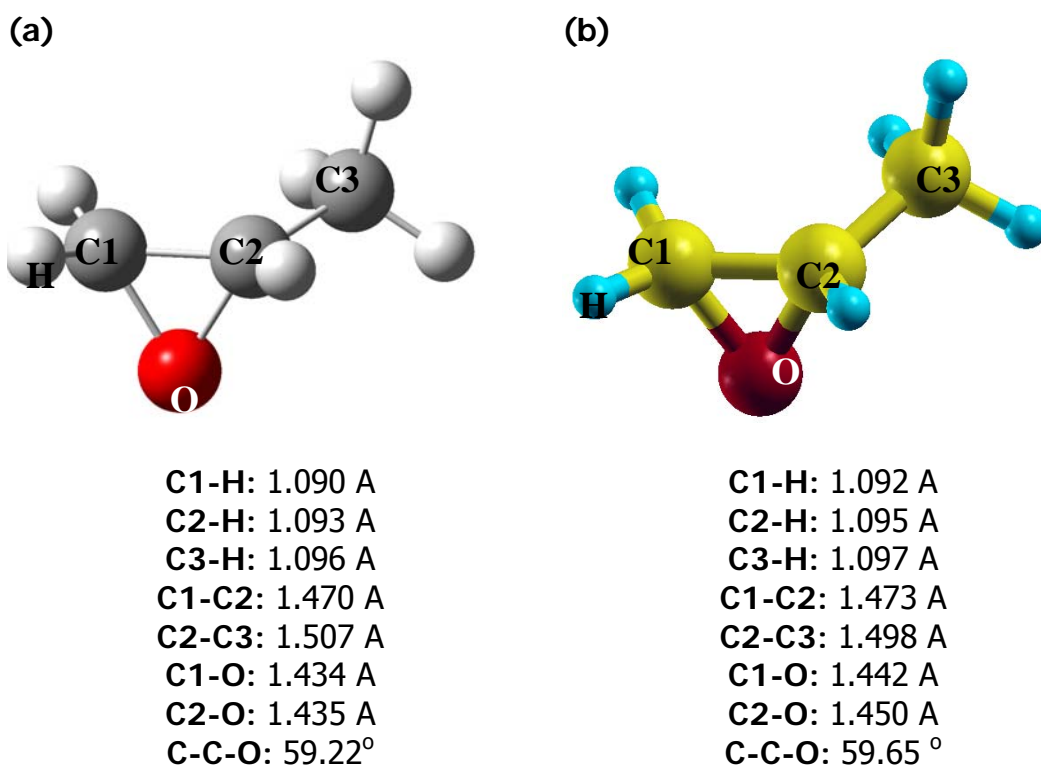


Figure C.6 Optimized geometry of Propyleneoxide a) in Gaussian 03 software b) in VASP software

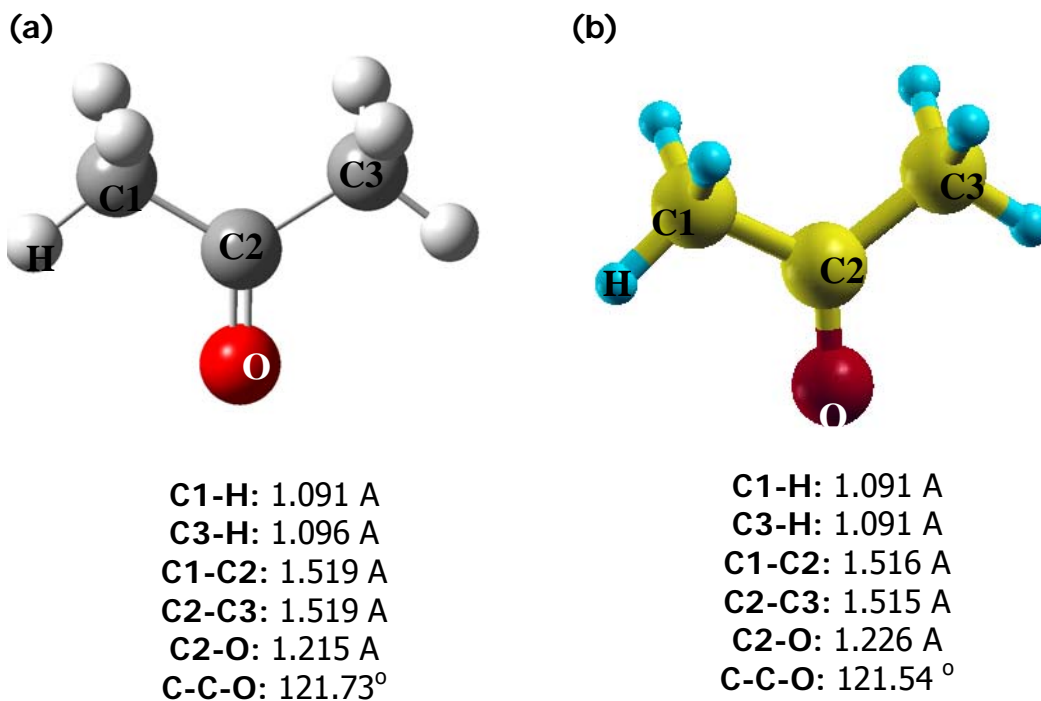


Figure C.7 Optimized geometry of Acetone a) in Gaussian 03 software b) in VASP software

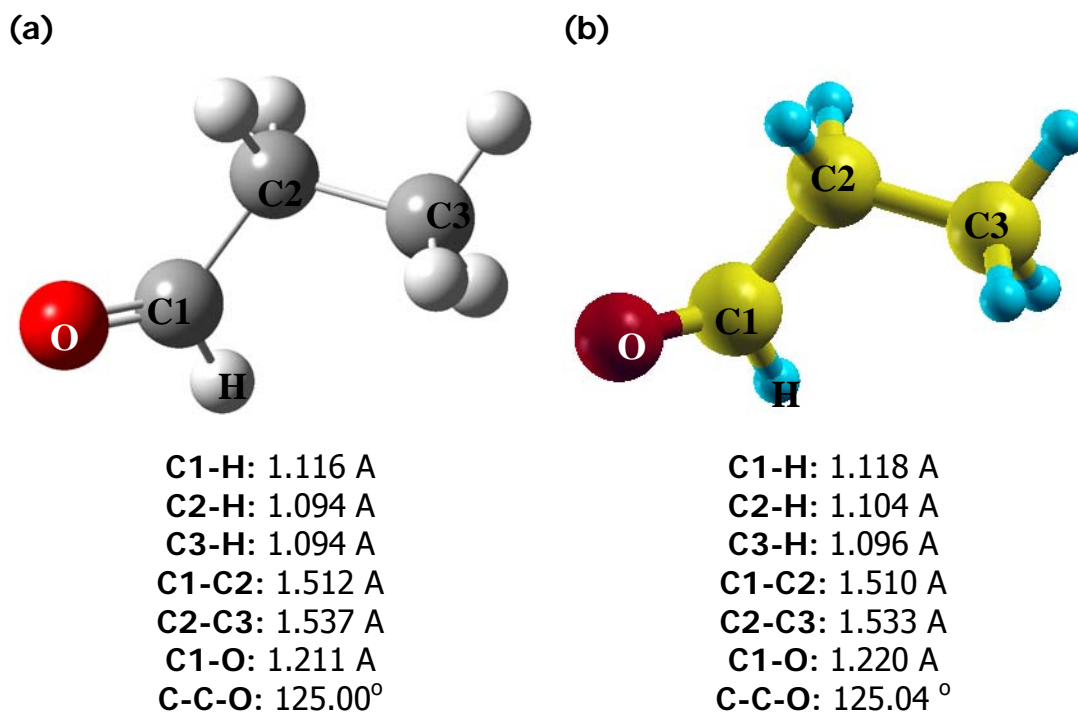


Figure C.8 Optimized geometry of Propanal a) in Gaussian 03 software b) in VASP software

APPENDIX D

SAMPLE INPUT AND OUTPUT FILES

Table D.1 Input file of the calculation for optimization of ethylene molecule in Gaussian 03 software

```
%chk=ethylene.chk  
%mem=450MW  
%nprocshared=2  
# opt=(maxcycle=1000,tight) b3lyp/6-31g(d,p) nosymm geom=connectivity  
  
ethylene  
0 1  
H      -6.43117700  -1.44240300  -5.56775000  
C      -5.44124400  -1.09924300  -5.86808500  
C      -4.84384600   0.06710500  -5.20398100  
H      -5.15822100  -1.34001900  -6.89270000  
H      -5.39523300   0.58006100  -4.41610500  
H      -4.12224800   0.68251600  -5.74108000  
  
1 2 1.0  
2 3 1.0 4 1.0  
3 5 1.0 6 1.0  
4  
5  
6
```

Annotations in the image:

- Keywords section**: points to the first three lines of the input file.
- Calculation Name**: points to the line "ethylene".
- Charge and Spin Multiplicity**: points to the line "0 1".
- Atomic Coordinates**: points to the list of atomic coordinates.
- Atoms connectivity's**: points to the connectivity lines.

Table D.2 Output file of the calculation for optimization of ethylene molecule in Gaussian 03 software

```
Entering Gaussian System, Link 0=/home/dft/bin/g03/g03
Input=Ethylene.gjf
Output=Ethylene.log
Initial command:
/home/dft/bin/g03/l1.exe /tmp/Gau-15336.inp -scrdir=/tmp/
Entering Link 1 = /home/dft/bin/g03/l1.exe PID= 15338.
```

Copyright (c) 1988,1990,1992,1993,1995,1998,2003,2004, Gaussian, Inc.
All Rights Reserved.

This is the Gaussian(R) 03 program. It is based on the the Gaussian(R) 98 system (copyright 1998, Gaussian, Inc.), the Gaussian(R) 94 system (copyright 1995, Gaussian, Inc.), the Gaussian 92(TM) system (copyright 1992, Gaussian, Inc.), the Gaussian 90(TM) system (copyright 1990, Gaussian, Inc.), the Gaussian 88(TM) system (copyright 1988, Gaussian, Inc.), the Gaussian 86(TM) system (copyright 1986, Carnegie Mellon University), and the Gaussian 82(TM) system (copyright 1983, Carnegie Mellon University). Gaussian is a federally registered trademark of Gaussian, Inc.

This software contains proprietary and confidential information, including trade secrets, belonging to Gaussian, Inc.

This software is provided under written license and may be used, copied, transmitted, or stored only in accord with that written license.

The following legend is applicable only to US Government contracts under FAR:

RESTRICTED RIGHTS LEGEND

Use, reproduction and disclosure by the US Government is subject to restrictions as set forth in subparagraphs (a) and (c) of the Commercial Computer Software - Restricted Rights clause in FAR 52.227-19.

Gaussian, Inc.
340 Quinnipiac St., Bldg. 40, Wallingford CT 06492

Table D.2 Continued

Warning -- This program may not be used in any manner that competes with the business of Gaussian, Inc. or will provide assistance to any competitor of Gaussian, Inc. The licensee of this program is prohibited from giving any competitor of Gaussian, Inc. access to this program. By using this program, the user acknowledges that Gaussian, Inc. is engaged in the business of creating and licensing software in the field of computational chemistry and represents and warrants to the licensee that it is not a competitor of Gaussian, Inc. and that it will not use this program in any manner prohibited above.

Cite this work as:

Gaussian 03, Revision D.01,
M. J. Frisch, G. W. Trucks, H. B. Schlegel, G. E. Scuseria,
M. A. Robb, J. R. Cheeseman, J. A. Montgomery, Jr., T. Vreven,
K. N. Kudin, J. C. Burant, J. M. Millam, S. S. Iyengar, J. Tomasi,
V. Barone, B. Mennucci, M. Cossi, G. Scalmani, N. Rega,
G. A. Petersson, H. Nakatsuji, M. Hada, M. Ehara, K. Toyota,
R. Fukuda, J. Hasegawa, M. Ishida, T. Nakajima, Y. Honda, O. Kitao,
H. Nakai, M. Klene, X. Li, J. E. Knox, H. P. Hratchian, J. B. Cross,
V. Bakken, C. Adamo, J. Jaramillo, R. Gomperts, R. E. Stratmann,
O. Yazyev, A. J. Austin, R. Cammi, C. Pomelli, J. W. Ochterski,
P. Y. Ayala, K. Morokuma, G. A. Voth, P. Salvador, J. J. Dannenberg,
V. G. Zakrzewski, S. Dapprich, A. D. Daniels, M. C. Strain,
O. Farkas, D. K. Malick, A. D. Rabuck, K. Raghavachari,
J. B. Foresman, J. V. Ortiz, Q. Cui, A. G. Baboul, S. Clifford,
J. Cioslowski, B. B. Stefanov, G. Liu, A. Liashenko, P. Piskorz,
I. Komaromi, R. L. Martin, D. J. Fox, T. Keith, M. A. Al-Laham,
C. Y. Peng, A. Nanayakkara, M. Challacombe, P. M. W. Gill,
B. Johnson, W. Chen, M. W. Wong, C. Gonzalez, and J. A. Pople,
Gaussian, Inc., Wallingford CT, 2004.

Gaussian 03: AM64L-G03RevD.01 13-Oct-2005
2-Jul-2009

%chk=ethylene.chk
%mem=450MW
%nprocshared=2
Will use up to 2 processors via shared memory.

Table D.2 Continued

opt=(maxcycle=1000,tight) b3lyp/6-31g(d,p) nosymm geom=connectivity

1/6=1000,7=10,14=-1,18=20,26=3,38=1,57=2/1,3;
2/9=110,15=1,17=6,18=5,40=1/2;
3/5=1,6=6,7=101,11=2,16=1,25=1,30=1,74=-5/1,2,3;
4//1;
5/5=2,38=5/2;
6/7=2,8=2,9=2,10=2,28=1/1;
7/30=1/1,2,3,16;
1/6=1000,14=-1,18=20/3(3);
2/9=110,15=1/2;
6/7=2,8=2,9=2,10=2,19=2,28=1/1;
99//99;
2/9=110,15=1/2;
3/5=1,6=6,7=101,11=2,16=1,25=1,30=1,74=-5/1,2,3;
4/5=5,16=3/1;
5/5=2,38=5/2;
7/30=1/1,2,3,16;
1/6=1000,14=-1,18=20/3(-5);
2/9=110,15=1/2;
6/7=2,8=2,9=2,10=2,19=2,28=1/1;
99/9=1/99;

ethylene

Symbolic Z-matrix:

Charge = 0 Multiplicity = 1

H	-6.43118	-1.4424	-5.56775
C	-5.44124	-1.09924	-5.86809
C	-4.84385	0.06711	-5.20398
H	-5.15822	-1.34002	-6.8927
H	-5.39523	0.58006	-4.4161
H	-4.12225	0.68252	-5.74108

Grad

Berny optimization.

Initialization pass.

! Initial Parameters !
! (Angstroms and Degrees) !

Table D.2 Continued

! Name	Definition	Value	Derivative Info.	!
! R1	R(1,2)	1.0899	estimate D2E/DX2	!
! R2	R(2,3)	1.4691	estimate D2E/DX2	!
! R3	R(2,4)	1.0899	estimate D2E/DX2	!
! R4	R(3,5)	1.0899	estimate D2E/DX2	!
! R5	R(3,6)	1.0899	estimate D2E/DX2	!
! A1	A(1,2,3)	119.6522	estimate D2E/DX2	!
! A2	A(1,2,4)	115.1726	estimate D2E/DX2	!
! A3	A(3,2,4)	119.6535	estimate D2E/DX2	!
! A4	A(2,3,5)	119.6503	estimate D2E/DX2	!
! A5	A(2,3,6)	119.6524	estimate D2E/DX2	!
! A6	A(5,3,6)	115.1778	estimate D2E/DX2	!
! D1	D(1,2,3,5)	0.0045	estimate D2E/DX2	!
! D2	D(1,2,3,6)	-152.5386	estimate D2E/DX2	!
! D3	D(4,2,3,5)	152.5409	estimate D2E/DX2	!
! D4	D(4,2,3,6)	-0.0021	estimate D2E/DX2	!

Trust Radius=3.00D-01 FncErr=1.00D-07 GrdErr=1.00D-06
 Number of steps in this run= 100 maximum allowed number of steps= 100.

GradGradGradGradGradGradGradGradGradGradGradGradGradGradGradGrad
 GradGrad

Input orientation:

Center Number	Atomic Number	Atomic Type	Coordinates (Angstroms)		
			X	Y	Z
1	1	0	-6.431177	-1.442403	-5.567750
2	6	0	-5.441244	-1.099243	-5.868085
3	6	0	-4.843846	0.067105	-5.203981
4	1	0	-5.158221	-1.340019	-6.892700
5	1	0	-5.395233	0.580061	-4.416105
6	1	0	-4.122248	0.682516	-5.741080

Distance matrix (angstroms):

		1	2	3	4	5
1	H	0.000000				
2	C	1.089921	0.000000			
3	C	2.220487	1.469111	0.000000		
4	H	1.840215	1.089913	2.220496	0.000000	

Table D.2 Continued

5 H 2.547514 2.220456 1.089908 3.142675 0.000000
6 H 3.142686 2.220483 1.089913 2.547571 1.840257
6
6 H 0.000000
Symmetry turned off by external request.
Stoichiometry C2H4
Framework group C1[X(C2H4)]
Deg. of freedom 12
Full point group C1
Rotational constants (GHZ): 140.8756169 25.6995237 22.0656362
Standard basis: 6-31G(d,p) (6D, 7F)
Integral buffers will be 131072 words long.
Raffenetti 2 integral format.
Two-electron integral symmetry is turned off.
50 basis functions, 84 primitive gaussians, 50 cartesian basis
functions
8 alpha electrons 8 beta electrons
nuclear repulsion energy 31.6667420827 Hartrees.
NAtoms= 6 NActive= 6 NUniq= 6 SFac= 7.50D-01 NATFMM= 80
NAOKFM=F Big=F
One-electron integrals computed using PRISM.
NBasis= 50 RedAO= T NBF= 50
NBsUse= 50 1.00D-06 NBFU= 50
Harris functional with IExCor= 402 diagonalized for initial guess.
ExpMin= 1.61D-01 ExpMax= 3.05D+03 ExpMxC= 4.57D+02 IAcc=1
IRadAn= 1 AccDes= 1.00D-06
HarFok: IExCor= 402 AccDes= 1.00D-06 IRadAn= 1 IDoV=1
ScaDFX= 1.000000 1.000000 1.000000 1.000000
Requested convergence on RMS density matrix=1.00D-08 within 128 cycles.
Requested convergence on MAX density matrix=1.00D-06.
Requested convergence on energy=1.00D-06.
No special actions if energy rises.
Keep R1 integrals in memory in canonical form, NReq= 2576859.
Integral accuracy reduced to 1.0D-05 until final iterations.
Initial convergence to 1.0D-05 achieved. Increase integral accuracy.
SCF Done: E(RB+HF-LYP) = -78.5664278032 A.U. after 11 cycles
Convg = 0.1177D-08 -V/T = 2.0144
S**2 = 0.0000

Table D.2 Continued

Population analysis using the SCF density.

```
*****
*****

Alpha occ. eigenvalues -- -10.20373 -10.20338 -0.72943 -0.58646 -
0.45120
Alpha occ. eigenvalues -- -0.39805 -0.36381 -0.24878
Alpha virt. eigenvalues -- -0.02437 0.11958 0.14399 0.15249
0.23472
Alpha virt. eigenvalues -- 0.28391 0.50987 0.53748 0.56128 0.61505
Alpha virt. eigenvalues -- 0.64181 0.66791 0.81793 0.84948 0.90039
Alpha virt. eigenvalues -- 0.91565 0.99780 1.06359 1.36131 1.39503
Alpha virt. eigenvalues -- 1.58759 1.81888 1.86164 1.89947 1.90759
Alpha virt. eigenvalues -- 2.05161 2.17795 2.18456 2.34384 2.38563
Alpha virt. eigenvalues -- 2.45818 2.49159 2.60814 2.70355 2.73396
Alpha virt. eigenvalues -- 2.95039 3.18496 3.31748 3.38280 3.60736
Alpha virt. eigenvalues -- 4.13544 4.44599
Condensed to atoms (all electrons):
      1      2      3      4      5      6
1 H  0.582047 0.384582 -0.032330 -0.044943 -0.006032 0.004028
2 C  0.384582 4.916920 0.603886 0.384580 -0.032333 -0.032331
3 C -0.032330 0.603886 4.916905 -0.032331 0.384583 0.384583
4 H -0.044943 0.384580 -0.032331 0.582049 0.004028 -0.006031
5 H -0.006032 -0.032333 0.384583 0.004028 0.582042 -0.044938
6 H 0.004028 -0.032331 0.384583 -0.006031 -0.044938 0.582037
Mulliken atomic charges:
      1
1 H  0.112649
2 C -0.225305
3 C -0.225296
4 H  0.112649
5 H  0.112651
6 H  0.112653
Sum of Mulliken charges= 0.00000
Atomic charges with hydrogens summed into heavy atoms:
      1
1 H  0.000000
2 C -0.000007
3 C  0.000007
4 H  0.000000
5 H  0.000000
```

Table D.2 Continued

6 H 0.000000
 Sum of Mulliken charges= 0.00000
 Electronic spatial extent (au): $\langle R^{**2} \rangle = 3397.3223$
 Charge= 0.0000 electrons
 Dipole moment (field-independent basis, Debye):
 X= -0.3494 Y= 0.3545 Z= -0.3083 Tot= 0.5855
 Quadrupole moment (field-independent basis, Debye-Ang):
 XX= -9.6642 YY= -13.5583 ZZ= -9.6161
 XY= -0.5666 XZ= 2.6781 YZ= -0.8389
 Traceless Quadrupole moment (field-independent basis, Debye-Ang):
 XX= 1.2820 YY= -2.6121 ZZ= 1.3301
 XY= -0.5666 XZ= 2.6781 YZ= -0.8389
 Octapole moment (field-independent basis, Debye-Ang**2):
 XXX= 176.8491 YYY= 21.2121 ZZZ= 187.9519 XXY= 68.9097
 XXY= 2.7352 XXZ= 54.1256 XZZ= 48.1224 YZZ= 4.7067
 YYZ= 74.3833 XYZ= -2.7777
 Hexadecapole moment (field-independent basis, Debye-Ang**3):
 XXXX= -1944.8219 YYYY= -76.7668 ZZZZ= -2217.2692 XXXY= -53.7695
 XXXZ= -1008.8871 YYYYX= -117.9634 YYYZ= -127.5105 ZZZX= -988.9455
 ZZZY= -69.9196 XYYX= -366.3110 XXZZ= -659.6981 YYZZ= -424.9100
 XXYZ= 11.9643 YYXZ= -379.2220 ZZXY= 11.9695
 N-N= 3.166674208265D+01 E-N=-2.444291183439D+02 KE=
 7.744768386701D+01

Center Number	Atomic Number	Forces (Hartrees/Bohr)		
		X	Y	Z
1	1	0.007697778	-0.006181017	0.008007953
2	6	0.028779339	0.100629892	0.035433820
3	6	-0.058744697	-0.070240328	-0.061864577
4	1	0.008786303	-0.006094189	0.006874011
5	1	0.006195528	-0.009097401	0.006337300
6	1	0.007285749	-0.009016956	0.005211493

Cartesian Forces: Max 0.100629892 RMS 0.037318512

GradGradGradGradGradGradGradGradGradGradGradGradGradGradGradGrad
 GradGrad
 Berny optimization.
 Internal Forces: Max 0.111296927 RMS 0.029807065
 Search for a local minimum.
 Step number 1 out of a maximum of 100

Table D.2 Continued

All quantities printed in internal units (Hartrees-Bohrs-Radians)

Second derivative matrix not updated -- first step.

The second derivative matrix:

	R1	R2	R3	R4	R5
R1	0.34822				
R2	0.00000	0.35847			
R3	0.00000	0.00000	0.34823		
R4	0.00000	0.00000	0.00000	0.34823	
R5	0.00000	0.00000	0.00000	0.00000	0.34823
A1	0.00000	0.00000	0.00000	0.00000	0.00000
A2	0.00000	0.00000	0.00000	0.00000	0.00000
A3	0.00000	0.00000	0.00000	0.00000	0.00000
A4	0.00000	0.00000	0.00000	0.00000	0.00000
A5	0.00000	0.00000	0.00000	0.00000	0.00000
A6	0.00000	0.00000	0.00000	0.00000	0.00000
D1	0.00000	0.00000	0.00000	0.00000	0.00000
D2	0.00000	0.00000	0.00000	0.00000	0.00000
D3	0.00000	0.00000	0.00000	0.00000	0.00000
D4	0.00000	0.00000	0.00000	0.00000	0.00000
	A1	A2	A3	A4	A5
A1	0.16000				
A2	0.00000	0.16000			
A3	0.00000	0.00000	0.16000		
A4	0.00000	0.00000	0.00000	0.16000	
A5	0.00000	0.00000	0.00000	0.00000	0.16000
A6	0.00000	0.00000	0.00000	0.00000	0.00000
D1	0.00000	0.00000	0.00000	0.00000	0.00000
D2	0.00000	0.00000	0.00000	0.00000	0.00000
D3	0.00000	0.00000	0.00000	0.00000	0.00000
D4	0.00000	0.00000	0.00000	0.00000	0.00000
	A6	D1	D2	D3	D4
A6	0.16000				
D1	0.00000	0.01175			
D2	0.00000	0.00000	0.01175		
D3	0.00000	0.00000	0.00000	0.01175	
D4	0.00000	0.00000	0.00000	0.00000	0.01175

Eigenvalues --- 0.01175 0.01971 0.01971 0.16000 0.16000

Eigenvalues --- 0.16000 0.16000 0.34822 0.34823 0.34823

Eigenvalues --- 0.34823 0.358471000.000001000.000001000.00000

RFO step: Lambda=-4.48399816D-02.

Linear search not attempted -- first point.

Maximum step size (0.300) exceeded in Quadratic search.

-- Step size scaled by 0.553

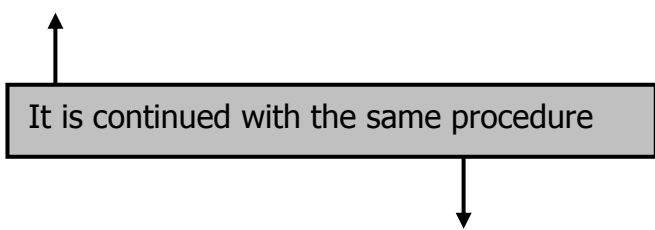
Table D.2 Continued

Iteration 1 RMS(Cart)= 0.05892311 RMS(Int)= 0.00513967
 Iteration 2 RMS(Cart)= 0.00467313 RMS(Int)= 0.00298639
 Iteration 3 RMS(Cart)= 0.00001092 RMS(Int)= 0.00298638
 Iteration 4 RMS(Cart)= 0.00000002 RMS(Int)= 0.00298638

Variable	Old X	-DE/DX (Linear)	Delta X (Quad)	Delta X (Total)	Delta X	New X
R1	2.05965	-0.00284	0.00000	-0.00400	-0.00400	2.05565
R2	2.77622	-0.11130	0.00000	-0.15272	-0.15272	2.62349
R3	2.05964	-0.00283	0.00000	-0.00399	-0.00399	2.05565
R4	2.05963	-0.00284	0.00000	-0.00399	-0.00399	2.05564
R5	2.05964	-0.00284	0.00000	-0.00399	-0.00399	2.05564
A1	2.08832	0.00234	0.00000	0.02241	0.01781	2.10613
A2	2.01014	0.00377	0.00000	0.02813	0.02333	2.03347
A3	2.08835	0.00234	0.00000	0.02240	0.01780	2.10615
A4	2.08829	0.00234	0.00000	0.02242	0.01781	2.10610
A5	2.08833	0.00234	0.00000	0.02241	0.01780	2.10613
A6	2.01023	0.00377	0.00000	0.02811	0.02331	2.03354
D1	0.00008	0.00000	0.00000	0.00000	0.00000	0.00007
D2	-2.66230	-0.02071	0.00000	-0.17753	-0.17871	-2.84101
D3	2.66234	0.02070	0.00000	0.17749	0.17867	2.84101
D4	-0.00004	0.00000	0.00000	-0.00003	-0.00003	-0.00007

Item	Value	Threshold	Converged?
Maximum Force	0.111297	0.000015	NO
RMS Force	0.029807	0.000010	NO
Maximum Displacement	0.125246	0.000060	NO
RMS Displacement	0.060505	0.000040	NO

Predicted change in Energy=-2.002984D-02



Input orientation:

Center Number	Atomic Number	Atomic Type	Coordinates (Angstroms)		
			X	Y	Z
1	1	0	-6.374134	-1.459604	-5.509833
2	6	0	-5.502444	-0.953324	-5.915628
3	6	0	-4.961556	0.102674	-5.314282
4	1	0	-5.096743	-1.356873	-6.839420

Table D.2 Continued

```

5      1      0    -5.367229  0.506196 -4.390465
6      1      0    -4.089861  0.608948 -5.720073

```

Distance matrix (angstroms):

```

      1      2      3      4      5
1 H  0.000000
2 C  1.086661  0.000000
3 C  2.115261  1.330153  0.000000
4 H  1.846641  1.086664  2.115325  0.000000
5 H  2.476129  2.115325  1.086664  3.088943  0.000000
6 H  3.088853  2.115260  1.086661  2.476127  1.846641
      6
6 H  0.000000

```

Symmetry turned off by external request.

Stoichiometry C2H4

Framework group C1[X(C2H4)]

Deg. of freedom 12

Full point group C1

Rotational constants (GHZ): 147.0507205 30.0909943 24.9794488

Standard basis: 6-31G(d,p) (6D, 7F)

Integral buffers will be 131072 words long.

Raffenetti 2 integral format.

Two-electron integral symmetry is turned off.

50 basis functions, 84 primitive gaussians, 50 cartesian basis functions

8 alpha electrons 8 beta electrons

nuclear repulsion energy 33.3565379087 Hartrees.

NAtoms= 6 NActive= 6 NUniq= 6 SFac= 7.50D-01 NATFMM= 80

NAOKFM=F Big=F

One-electron integrals computed using PRISM.

NBasis= 50 RedAO= T NBF= 50

NBsUse= 50 1.00D-06 NBFU= 50

Initial guess read from the read-write file:

Requested convergence on RMS density matrix=1.00D-08 within 128 cycles.

Requested convergence on MAX density matrix=1.00D-06.

Requested convergence on energy=1.00D-06.

No special actions if energy rises.

Keep R1 integrals in memory in canonical form, NReq= 2576275.

SCF Done: E(RB+HF-LYP) = -78.5938094301 A.U. after 6 cycles

Conv g = 0.6033D-08 -V/T = 2.0105

S**2 = 0.0000

Center Atomic Forces (Hartrees/Bohr)

Table D.2 Continued

Number	Number	X	Y	Z
1	1	0.000000322	0.000002292	0.000004006
2	6	-0.000002900	-0.000008619	-0.000002587
3	6	0.000004924	0.000006754	0.000004273
4	1	-0.000000545	0.000002748	-0.000000292
5	1	-0.000001408	-0.000000917	-0.000001371
6	1	-0.000000392	-0.000002258	-0.000004029

Cartesian Forces: Max 0.000008619 RMS 0.000003598

Grad

Berny optimization.

Internal Forces: Max 0.000004229 RMS 0.000002195

Search for a local minimum.

Step number 8 out of a maximum of 100

All quantities printed in internal units (Hartrees-Bohrs-Radians)

Update second derivatives using D2CorX and points 2 3 4 5 6

7 8

Trust test= 1.02D+00 RLast= 3.12D-03 DXMaxT set to 2.12D-01

The second derivative matrix:

	R1	R2	R3	R4	R5
R1	0.34780				
R2	0.00655	0.64603			
R3	-0.00044	0.00652	0.34777		
R4	-0.00044	0.00654	-0.00045	0.34778	
R5	-0.00043	0.00656	-0.00045	-0.00045	0.34778
A1	-0.00113	0.01090	-0.00119	-0.00118	-0.00117
A2	0.00268	-0.02018	0.00277	0.00276	0.00275
A3	-0.00108	0.01092	-0.00113	-0.00112	-0.00111
A4	-0.00114	0.01100	-0.00120	-0.00119	-0.00118
A5	-0.00109	0.01087	-0.00115	-0.00114	-0.00113
A6	0.00271	-0.02023	0.00280	0.00279	0.00278
D1	0.00000	-0.00029	0.00000	0.00001	0.00001
D2	0.00004	0.00089	0.00003	0.00004	0.00004
D3	-0.00004	-0.00089	-0.00003	-0.00003	-0.00004
D4	-0.00001	0.00028	-0.00001	0.00000	-0.00001
	A1	A2	A3	A4	A5
A1	0.15339				
A2	0.00526	0.14384			
A3	-0.00649	0.00497	0.15362		

Table D.2 Continued

A4	-0.00666	0.00534	-0.00654	0.15330		
A5	-0.00652	0.00505	-0.00641	-0.00657	0.15357	
A6	0.00533	-0.01633	0.00504	0.00542	0.00512	
D1	0.00004	0.00005	0.00002	0.00004	0.00003	
D2	-0.00017	-0.00038	-0.00016	-0.00017	-0.00015	
D3	0.00019	0.00052	0.00017	0.00020	0.00017	
D4	-0.00001	0.00010	-0.00002	-0.00001	-0.00001	
	A6	D1	D2	D3	D4	
A6	0.14350					
D1	0.00003	0.01902				
D2	-0.00038	0.00620	0.03453			
D3	0.00050	0.00621	-0.01219	0.03451		
D4	0.00009	0.00513	0.00440	0.00436	0.01537	
Eigenvalues ---	0.01175	0.03323	0.04670	0.11283	0.16000	
Eigenvalues ---	0.16000	0.16000	0.34636	0.34822	0.34823	
Eigenvalues ---	0.34823	0.648971000	0.000010000	0.000010000	0.000010000	0.00000

RFO step: Lambda= 0.00000000D+00.
 Quartic linear search produced a step of 0.01952.
 Iteration 1 RMS(Cart)= 0.00002249 RMS(Int)= 0.00000000
 Iteration 2 RMS(Cart)= 0.00000000 RMS(Int)= 0.00000000

Variable	Old X	-DE/DX (Linear)	Delta X (Quad)	Delta X (Total)	Delta X	New X
R1	2.05349	0.00000	0.00000	0.00000	0.00000	2.05349
R2	2.51362	0.00000	0.00000	0.00001	0.00001	2.51363
R3	2.05350	0.00000	0.00000	0.00000	0.00000	2.05349
R4	2.05350	0.00000	0.00000	0.00000	0.00000	2.05349
R5	2.05349	0.00000	0.00000	0.00000	0.00000	2.05349
A1	2.12615	0.00000	0.00000	-0.00002	-0.00002	2.12613
A2	2.03077	0.00000	0.00000	0.00004	0.00004	2.03081
A3	2.12626	0.00000	0.00000	-0.00002	-0.00002	2.12624
A4	2.12626	0.00000	0.00000	-0.00002	-0.00002	2.12624
A5	2.12615	0.00000	0.00000	-0.00002	-0.00002	2.12613
A6	2.03077	0.00000	0.00000	0.00004	0.00004	2.03081
D1	-0.00003	0.00000	-0.00004	0.00003	0.00000	-0.00003
D2	3.14158	0.00000	-0.00003	0.00004	0.00001	3.14159
D3	-3.14154	0.00000	-0.00003	-0.00002	-0.00005	3.14159
D4	0.00007	0.00000	-0.00002	-0.00002	-0.00004	0.00003

Item	Value	Threshold	Converged?
Maximum Force	0.000004	0.000015	YES
RMS Force	0.000002	0.000010	YES
Maximum Displacement	0.000042	0.000060	YES
RMS Displacement	0.000022	0.000040	YES

Predicted change in Energy=-3.348763D-10

Table D.2 Continued

Optimization completed.

-- Stationary point found.

```

-----
! Optimized Parameters !
! (Angstroms and Degrees) !
-----
! Name Definition      Value      Derivative Info.      !
-----
! R1  R(1,2)           1.0867    -DE/DX = 0.0          !
! R2  R(2,3)           1.3302    -DE/DX = 0.0          !
! R3  R(2,4)           1.0867    -DE/DX = 0.0          !
! R4  R(3,5)           1.0867    -DE/DX = 0.0          !
! R5  R(3,6)           1.0867    -DE/DX = 0.0          !
! A1  A(1,2,3)         121.8196   -DE/DX = 0.0          !
! A2  A(1,2,4)         116.3548   -DE/DX = 0.0          !
! A3  A(3,2,4)         121.8256   -DE/DX = 0.0          !
! A4  A(2,3,5)         121.8257   -DE/DX = 0.0          !
! A5  A(2,3,6)         121.8195   -DE/DX = 0.0          !
! A6  A(5,3,6)         116.3548   -DE/DX = 0.0          !
! D1  D(1,2,3,5)        -0.0019    -DE/DX = 0.0          !
! D2  D(1,2,3,6)        179.9995   -DE/DX = 0.0          !
! D3  D(4,2,3,5)        180.0029   -DE/DX = 0.0          !
! D4  D(4,2,3,6)         0.0042    -DE/DX = 0.0          !
-----

```

Grad

Input orientation:

```

-----
Center  Atomic  Atomic  Coordinates (Angstroms)
Number  Number  Type    X         Y         Z
-----
  1      1      0    -6.374134 -1.459604 -5.509833
  2      6      0    -5.502444 -0.953324 -5.915628
  3      6      0    -4.961556  0.102674 -5.314282
  4      1      0    -5.096743 -1.356873 -6.839420
  5      1      0    -5.367229  0.506196 -4.390465
  6      1      0    -4.089861  0.608948 -5.720073
-----

```

Distance matrix (angstroms):

```

      1      2      3      4      5
1 H  0.000000
-----

```

Table D.2 Continued

```

2 C  1.086661  0.000000
  3 C  2.115261  1.330153  0.000000
  4 H  1.846641  1.086664  2.115325  0.000000
  5 H  2.476129  2.115325  1.086664  3.088943  0.000000
  6 H  3.088853  2.115260  1.086661  2.476127  1.846641
      6
  6 H  0.000000
Symmetry turned off by external request.
Stoichiometry  C2H4
Framework group  C1[X(C2H4)]
Deg. of freedom  12
Full point group          C1
Rotational constants (GHZ):  147.0507205   30.0909943   24.9794488

```


Population analysis using the SCF density.


```

Alpha occ. eigenvalues -- -10.18441 -10.18351 -0.75517 -0.57654 -
0.46397
Alpha occ. eigenvalues -- -0.41580 -0.35182 -0.26745
Alpha virt. eigenvalues --  0.01740  0.12237  0.14054  0.15812  0.24447
Alpha virt. eigenvalues --  0.33135  0.47289  0.54826  0.56350  0.63742
Alpha virt. eigenvalues --  0.65374  0.69914  0.83100  0.84453  0.91319
Alpha virt. eigenvalues --  0.92172  1.10259  1.18855  1.38518  1.39104
Alpha virt. eigenvalues --  1.52937  1.83797  1.88816  1.95878  2.03737
Alpha virt. eigenvalues --  2.04268  2.12953  2.21371  2.36510  2.44607
Alpha virt. eigenvalues --  2.50922  2.62274  2.67898  2.67994  2.75765
Alpha virt. eigenvalues --  3.02309  3.16842  3.33758  3.46990  3.76884
Alpha virt. eigenvalues --  4.17889  4.49561
      Condensed to atoms (all electrons):
          1      2      3      4      5      6
  1 H  0.595962  0.388074 -0.035260 -0.045585 -0.009819  0.005417
  2 C  0.388074  4.817392  0.679405  0.388072 -0.035257 -0.035260
  3 C -0.035260  0.679405  4.817392 -0.035257  0.388072  0.388074
  4 H -0.045585  0.388072 -0.035257  0.595957  0.005416 -0.009819
  5 H -0.009819 -0.035257  0.388072  0.005416  0.595957 -0.045585

```

Table D.2 Continued

6 H 0.005417 -0.035260 0.388074 -0.009819 -0.045585 0.595962
Mulliken atomic charges:
1
1 H 0.101211
2 C -0.202427
3 C -0.202427
4 H 0.101216
5 H 0.101216
6 H 0.101211
Sum of Mulliken charges= 0.00000
Atomic charges with hydrogens summed into heavy atoms:
1
1 H 0.000000
2 C 0.000000
3 C 0.000000
4 H 0.000000
5 H 0.000000
6 H 0.000000
Sum of Mulliken charges= 0.00000
Electronic spatial extent (au): $\langle R^{*2} \rangle = 3457.9280$
Charge= 0.0000 electrons
Dipole moment (field-independent basis, Debye):
X= 0.0000 Y= 0.0000 Z= 0.0000 Tot= 0.0000
Quadrupole moment (field-independent basis, Debye-Ang):
XX= -13.1339 YY= -13.1107 ZZ= -12.9050
XY= 1.0635 XZ= -0.8726 YZ= 0.9470
Traceless Quadrupole moment (field-independent basis, Debye-Ang):
XX= -0.0840 YY= -0.0608 ZZ= 0.1449
XY= 1.0635 XZ= -0.8726 YZ= 0.9470
Octapole moment (field-independent basis, Debye-Ang**2):
XXX= 206.1476 YYY= 16.7289 ZZZ= 217.3812 XYY= 67.6906
XXY= -5.5421 XXZ= 82.8749 XZZ= 77.3160 YZZ= -5.1450
YYZ= 72.8105 XYZ= -10.5545
Hexadecapole moment (field-independent basis, Debye-Ang**3):
XXXX= -2186.1773 YYYY= -63.3137 ZZZZ= -2472.1959 XXXY= -7.6347
XXXZ= -1231.3683 YYYYX= -95.0263 YYYZ= -102.3782 ZZZX= -1222.2373
ZZZY= -10.4829 XXYY= -363.7773 XXZZ= -880.5235 YYZZ= -419.2555
XXYZ= 49.5792 YYXZ= -377.1098 ZZZY= 52.8245
N-N= 3.335653790871D+01 E-N=-2.481220045037D+02 KE=
7.778074169159D+01
1\1\GINC-DFT7\FOpt\RB3LYP\6-31G(d,p)\C2H4\DFT\02-Jul-2009\0\#\n
opt=(ma
xcycle=1000,tight) b3lyp/6-31g(d,p) nosymm geom=connectivity\\ethylene

Table D.2 Continued

\\0,1\H,-6.3741342037,-1.459604358,-5.5098330137\C,-5.5024444394,-0.95
33237646,-5.9156275458\C,-4.9615564944,0.1026736302,-
5.3142821846\H,-5
.0967434499,-1.3568730538,-6.8394202781\H,-
5.3672289536,0.5061960963,-
4.3904652094\H,-4.089861459,0.60894845,-
5.7200727683\\Version=AM64L-G0
3RevD.01\HF=-78.5938094\RMSD=6.033e-09\RMSF=3.598e-
06\Thermal=0.\Dipol
e=0.0000082,-0.0000082,0.0000072\PG=C01 [X(C2H4)]\ \@

PATIENCE IS THE ABILITY TO IDLE YOUR MOTOR WHEN
YOU FEEL LIKE STRIPPING YOUR GEARS.

Job cpu time: 0 days 0 hours 5 minutes 54.6 seconds.

File lengths (MBytes): RWF= 13 Int= 0 D2E= 0 Chk= 6 Scr=
1

Normal termination of Gaussian 03 at Thu Jul 2 10:41:54 2009.

Table D.3 Input file of the calculation for optimization of Ag₁₃O cluster in Gaussian 03 software

```
%chk=Ag13-OEG2.chk
%mem=450MW
%nprocshared=4
# opt=(modredundant,maxcycle=1000) b3lyp/genecp nosymm
geom=connectivity scf=(conver=4,maxcycle=1000)
```

Ag13 + O optimization

```
0 2
Ag      -3.73800000  -0.34000000  -3.65600000
Ag      -1.69800000   1.70000000  -3.65600000
Ag       0.34200000   3.74000000  -3.65600000
Ag      -5.77800000  -0.34000000  -1.61600000
Ag      -5.77800000   1.70000000   0.42400000
Ag      -3.73800000   1.70000000  -1.61600000
Ag      -1.69800000   1.70000000   0.42400000
Ag      -1.69800000   3.74000000  -1.61600000
Ag      -3.73800000   3.74000000   0.42400000
Ag      -1.69800000   5.78000000   0.42400000
Ag       0.34200000   5.78000000  -1.61600000
Ag      -5.77800000   3.74000000   2.46400000
Ag      -3.73800000   5.78000000   2.46400000
H       -4.94100000  -1.54200000  -3.65600000
H       -5.77800000  -1.54200000  -2.81800000
H       -3.73800000  -1.54200000  -4.85800000
H       -2.53600000  -1.54200000  -3.65600000
H       -2.53600000  -0.34000000  -4.85800000
H       -1.69800000   0.49800000  -4.85800000
H       -6.98100000  -1.54200000  -1.61600000
H       -5.77800000  -1.54200000  -0.41400000
H       -6.98100000  -0.34000000  -0.41400000
H       -6.98100000   0.49800000   0.42400000
H       -5.77800000   0.49800000   1.62600000
H       -6.98100000   1.70000000   1.62600000
H       -6.98100000   2.53800000   2.46400000
H       -5.77800000   2.53800000   3.66600000
H       -6.98100000   3.74000000   3.66600000
H       -5.77800000   4.94200000   3.66600000
H       -4.94100000   5.78000000   3.66600000
H       -2.53600000   5.78000000   3.66600000
H       -1.69800000   6.98200000   1.62600000
```

Table D.3 Continued

H	-2.53600000	6.98200000	2.46400000
H	-3.73800000	6.98200000	3.66600000
H	-0.49600000	6.98200000	0.42400000
H	0.34200000	6.98200000	-0.41400000
H	1.54400000	4.94200000	-3.65600000
H	1.54400000	5.78000000	-2.81800000
H	1.54400000	3.74000000	-4.85800000
H	-0.49600000	1.70000000	-4.85800000
H	0.34200000	2.53800000	-4.85800000
H	-0.49600000	0.49800000	0.42400000
H	-1.69800000	0.49800000	1.62600000
H	-0.49600000	1.70000000	1.62600000
H	1.54400000	6.98200000	-1.61600000
H	-0.49600000	5.78000000	1.62600000
H	1.54400000	5.78000000	-0.41400000
H	1.54400000	2.53800000	-3.65600000
H	-0.49600000	0.49800000	-3.65600000
H	-3.73800000	-1.54200000	-2.45400000
H	-4.57600000	-1.54200000	-1.61600000
H	-4.57600000	-0.34000000	-0.41400000
H	-4.57600000	0.49800000	0.42400000
H	-3.73800000	0.49800000	-0.41400000
H	-2.90100000	0.49800000	0.42400000
H	-4.57600000	1.70000000	1.62600000
H	-2.90100000	1.70000000	1.62600000
H	-3.73800000	2.53800000	1.62600000
H	-4.57600000	2.53800000	2.46400000
H	-4.57600000	3.74000000	3.66600000
H	-3.73800000	4.57800000	3.66600000
H	-1.69800000	2.90200000	1.62600000
H	-2.53600000	3.74000000	1.62600000
H	-1.69800000	4.57800000	1.62600000
H	-2.53600000	4.57800000	2.46400000
H	-0.49600000	2.90200000	0.42400000
H	-0.49600000	3.74000000	-0.41400000
H	-0.49600000	4.57800000	0.42400000
H	0.34200000	4.57800000	-0.41400000
H	1.54400000	3.74000000	-2.45400000
H	1.54400000	4.57800000	-1.61600000
H	-0.49600000	1.70000000	-2.45400000
H	0.34200000	2.53800000	-2.45400000
H	-0.49600000	1.70000000	-0.77800000
H	-0.49600000	2.53800000	-1.61600000

Table D.3 Continued

H	-2.53600000	-0.34000000	-2.45400000
H	-1.69800000	0.49800000	-2.45400000
H	-2.53600000	0.49800000	-1.61600000
H	-1.69800000	0.49800000	-0.77800000
O	-3.94725400	3.86389900	-1.82440200

1 2 1.0 4 1.0 6 1.0 14 1.0 16 1.0 17 1.0 18 1.0 50 1.0 76 1.0
2 3 1.0 6 1.0 8 1.0 19 1.0 40 1.0 49 1.0 72 1.0 77 1.0
3 8 1.0 11 1.0 37 1.0 39 1.0 41 1.0 48 1.0 70 1.0 73 1.0
4 5 1.0 6 1.0 15 1.0 20 1.0 21 1.0 22 1.0 51 1.0 52 1.0
5 6 1.0 9 1.0 12 1.0 23 1.0 24 1.0 25 1.0 53 1.0 56 1.0
6 7 1.0 8 1.0 9 1.0 54 1.0 78 1.0
7 8 1.0 9 1.0 42 1.0 43 1.0 44 1.0 55 1.0 57 1.0 62 1.0 66 1.0 74 1.0 79 1.0
8 9 1.0 10 1.0 11 1.0 67 1.0 75 1.0
9 10 1.0 12 1.0 13 1.0 58 1.0 63 1.0
10 11 1.0 13 1.0 32 1.0 35 1.0 46 1.0 64 1.0 68 1.0
11 36 1.0 38 1.0 45 1.0 47 1.0 69 1.0 71 1.0
12 13 1.0 26 1.0 27 1.0 28 1.0 29 1.0 59 1.0 60 1.0
13 30 1.0 31 1.0 33 1.0 34 1.0 61 1.0 65 1.0
14
15
16
17
18
19
20
21
22
23
24
25
26
27
28
29
30
31
32
33
34
35
36
37

Table D.3 Continued

38
39
40
41
42
43
44
45
46
47
48
49
50
51
52
53
54
55
56
57
58
59
60
61
62
63
64
65
66
67
68
69
70
71
72
73
74
75
76
77
78
79
80

Table D.3 Continued

X 1 F
X 2 F
X 3 F
X 4 F
X 5 F
X 6 F
X 7 F
X 8 F
X 9 F
X 10 F
X 11 F
X 12 F
X 13 F
X 14 F
X 15 F
X 16 F
X 17 F
X 18 F
X 19 F
X 20 F
X 21 F
X 22 F
X 23 F
X 24 F
X 25 F
X 26 F
X 27 F
X 28 F
X 29 F
X 30 F
X 31 F
X 32 F
X 33 F
X 34 F
X 35 F
X 36 F
X 37 F
X 38 F
X 39 F
X 40 F
X 41 F
X 42 F
X 43 F

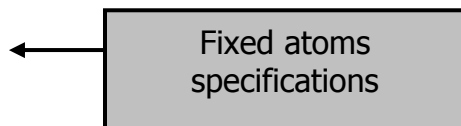


Table D.3 Continued

X 44 F
X 45 F
X 46 F
X 47 F
X 48 F
X 49 F
X 50 F
X 51 F
X 52 F
X 53 F
X 54 F
X 55 F
X 56 F
X 57 F
X 58 F
X 59 F
X 60 F
X 61 F
X 62 F
X 63 F
X 64 F
X 65 F
X 66 F
X 67 F
X 68 F
X 69 F
X 70 F
X 71 F
X 72 F
X 73 F
X 74 F
X 75 F
X 76 F
X 77 F
X 78 F
X 79 F

6 7 8 9 0

lanl2dz

1 2 3 4 5 10 11 12 13 0

lanl2mb

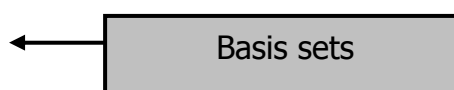


Table D.3 Continued

O H 0

6-31g**

6 7 8 9 0

lanl2dz

1 2 3 4 5 10 11 12 13 0

lanl2mb

Table D.4 Input files of the calculation for optimization of ethylene molecule in VASP software

INCAR (Keywords file)

```
SYSTEM = Ag (111)O 3x3
PREC = HIGH
IBRION = 2
NSW = 150
LREAL = Auto
ISMEAR = 0; SIGMA = 0.1;
```

POSCAR (Atoms coordinates file)

```
System: C H Surface Nx= 3 Ny= 3 N
1.000000000000000000
 8.8144886609000004 0.0000000000000000 0.0000000000000000
 4.4072443302000002 7.6335714766000002 0.0000000000000000
 0.0000000000000000 0.0000000000000000 10.0000000000000000
2 4
Selective dynamics
Cartesian
7.25156717 4.01412757 5.07638510
5.99681391 3.57607176 5.02095764
8.09612864 3.33101072 5.10634107
7.48794456 5.07461643 5.09422162
5.76043671 2.51558218 5.00312045
5.15225243 4.25918860 4.99100166
```

X,y,z vectors



F F F
T T T
T T T
T T T
T T T
T T T

Fixed or relaxed atoms



Atoms coordinate



K-POINTS

```
K-Points
0
Monkhorst Pack
1 1 1
0 0 0
```

Table D.5 Output file of the calculation for optimization of ethylene molecule in VASP software

OUTCAR

vasp.4.6.31 08Feb07 complex
executed on LinuxIFC date 2009.05.06 16:25:40
running on 2 nodes
distr: one band on 1 nodes, 2 groups

INCAR:

POTCAR: PAW_GGA C 05Jan2001

POTCAR: PAW_GGA H 07Jul1998

POTCAR: PAW_GGA C 05Jan2001

VRHFIN =C: s2p2

LEXCH = 91

EATOM = 147.4688 eV, 10.8386 Ry

TITEL = PAW_GGA C 05Jan2001

LULTRA = F use ultrasoft PP ?

IUNSCR = 0 unscreen: 0-lin 1-nonlin 2-no

RPACOR = .000 partial core radius

POMASS = 12.011; ZVAL = 4.000 mass and valenz

RCORE = 1.500 outmost cutoff radius

RWIGS = 1.630; RWIGS = .863 wigner-seitz radius (au A)

ENMAX = 400.000; ENMIN = 300.000 eV

ICORE = 2 local potential

LCOR = T correct aug charges

LPAW = T paw PP

EAUG = 644.873

DEXC = .000

RMAX = 2.266 core radius for proj-oper

RAUG = 1.300 factor for augmentation sphere

RDEP = 1.501 radius for radial grids

RDEPT = 1.300 core radius for aug-charge

QCUT = -5.516; QGAM = 11.033 optimization parameters

Description

I	E	TYP	RCUT	TYP	RCUT
0	.000	23	1.200		
0	.000	23	1.200		

Table D.5 Continued

```

1 .000 23 1.500
  1 2.500 23 1.500
  2 .000 7 1.500
local pseudopotential read in
atomic valenz-charges read in
non local Contribution for L= 0 read in
real space projection operators read in
non local Contribution for L= 0 read in
real space projection operators read in
non local Contribution for L= 1 read in
real space projection operators read in
non local Contribution for L= 1 read in
real space projection operators read in
PAW grid and wavefunctions read in

number of l-projection operators is LMAX = 4
number of lm-projection operators is LMMAX = 8

```

```

POTCAR: PAW_GGA H 07Jul1998
VRHFIN =H: ultrasoft test
LEXCH = 91
EATOM = 12.5313 eV, .9210 Ry

```

```

TITEL = PAW_GGA H 07Jul1998
LULTRA = F use ultrasoft PP ?
IUNSCR = 0 unscreen: 0-lin 1-nonlin 2-no
RPACOR = .000 partial core radius
POMASS = 1.000; ZVAL = 1.000 mass and valenz
RCORE = 1.100 outmost cutoff radius
RWIGS = .700; RWIGS = .370 wigner-seitz radius (au A)
ENMAX = 250.000; ENMIN = 200.000 eV
RCLOC = .701 cutoff for local pot
LCOR = T correct aug charges
LPAW = T paw PP
EAUG = 400.000
RMAX = 2.174 core radius for proj-oper
RAUG = 1.200 factor for augmentation sphere
RDEP = 1.112 core radius for depl-charge
QCUT = -5.749; QGAM = 11.498 optimization parameters

```

Description

```

I E TYP RCUT TYP RCUT
0 .000 23 1.100

```

Table D.5 Continued

```

0 .500 23 1.100
1 -.300 23 1.100
local pseudopotential read in
atomic valenz-charges read in
non local Contribution for L= 0 read in
real space projection operators read in
non local Contribution for L= 0 read in
real space projection operators read in
non local Contribution for L= 1 read in
real space projection operators read in
PAW grid and wavefunctions read in

number of l-projection operators is LMAX = 3
number of lm-projection operators is LMMAX = 5

```

```

-----
|
| ADVICE TO THIS USER RUNNING 'VASP/VAMP' (HEAR YOUR MASTER'S
VOICE ...): |
|
| You have a (more or less) 'small supercell' and for smaller cells |
| it is recommended to use the reciprocal-space projection scheme! |
| The real space optimization is not efficient for small cells and it |
| is also less accurate ... |
| Therefore set LREAL=.FALSE. in the INCAR file |
|
|
-----

```

Optimization of the real space projectors (new method)

maximal supplied QI-value = 25.13
 optimisation between [QCUT,QGAM] = [11.31, 28.40] = [35.82,225.87] Ry
 Optimized for a Real-space Cutoff 0.93 Angstroem

l	n(q)	QCUT	max X(q)	W(low)/X(q)	W(high)/X(q)	e(spline)
0	8	11.310	5.568	0.35E-04	0.13E-04	0.14E-07
0	8	11.310	69.244	0.28E-03	0.21E-03	0.12E-06
1	7	11.310	2.779	0.38E-04	0.51E-04	0.23E-07
1	7	11.310	4.506	0.27E-03	0.37E-03	0.86E-07

Optimization of the real space projectors (new method)

maximal supplied QI-value = 34.20
 optimisation between [QCUT,QGAM] = [11.29, 28.39] = [35.68,225.69] Ry

Table D.5 Continued

Optimized for a Real-space Cutoff 0.83 Angstroem

l	n(q)	QCUT	max X(q)	W(low)/X(q)	W(high)/X(q)	e(spline)
0	7	11.287	4.435	0.56E-04	0.25E-04	0.12E-07
0	7	11.287	16.011	0.35E-03	0.26E-04	0.83E-07
1	6	11.287	4.617	0.14E-03	0.32E-03	0.23E-07

PAW_GGA C 05Jan2001 :
energy of atom 1 EATOM= -147.4688
kinetic energy error for atom= 0.0076 (will be added to EATOM!!)
PAW_GGA H 07Jul1998 :
energy of atom 2 EATOM= -12.5313
kinetic energy error for atom= 0.0020 (will be added to EATOM!!)

EXHCAR: internal setup
exchange correlation table for LEXCH = 7
RHO(1)= 0.500 N(1) = 2000
RHO(2)= 100.500 N(2) = 4000

POSCAR: System: C H 001 Surface Nx= 3 Ny= 3 N
positions in cartesian coordinates
velocities in cartesian coordinates
No initial velocities read in

ion position nearest neighbor table
1 0.560 0.526 0.508- 4 1.09 3 1.09 2 1.33
2 0.446 0.468 0.502- 6 1.09 5 1.09 1 1.33
3 0.700 0.436 0.511- 1 1.09
4 0.517 0.665 0.509- 1 1.09
5 0.489 0.330 0.500- 2 1.09
6 0.306 0.558 0.499- 2 1.09

LATTYP: Found a hexagonal cell.
ALAT = 8.8144889857
C/A-ratio = 1.1344957168

Lattice vectors:

A1 = (4.4072443307, -7.6335714766, 0.0000000000)
A2 = (-8.8144886609, 0.0000000000, 0.0000000000)
A3 = (0.0000000000, 0.0000000000, -10.0000000000)

Table D.5 Continued

Subroutine PRICEL returns:
Original cell was already a primitive cell.

Analysis of symmetry for initial positions (statically):

Routine SETGRP: Setting up the symmetry group for a hexagonal supercell.

Subroutine GETGRP returns: Found 2 space group operations (whereof 1 operations were pure point group operations) out of a pool of 24 trial point group operations.

The static configuration has the point symmetry C_{2v} .
The point group associated with its full space group is S_6 .

Analysis of symmetry for dynamics (positions and initial velocities):

Subroutine DYNSYM returns: Found 2 space group operations (whereof 1 operations were pure point group operations) out of a pool of 2 trial space group operations (whereof 1 operations were pure point group operations) and found also 1 'primitive' translations

The dynamic configuration has the point symmetry C_{2v} .
The point group associated with its full space group is S_6 .

Analysis of constrained symmetry for selective dynamics:

Subroutine DYNSYM returns: Found 1 space group operations (whereof 1 operations were pure point group operations) out of a pool of 2 trial space group operations (whereof 1 operations were pure point group operations) and found also 1 'primitive' translations

The constrained configuration has the point symmetry C_{2v} .

KPOINTS: K-Points

Table D.5 Continued

Automatic generation of k-mesh.

Subroutine IBZKPT returns following result:

=====

Found 1 irreducible k-points:

Following reciprocal coordinates:

Coordinates	Weight
0.000000 0.000000 0.000000	1.000000

Following cartesian coordinates:

Coordinates	Weight
0.000000 0.000000 0.000000	1.000000

Dimension of arrays:

k-Points NKPTS = 1 number of bands NBANDS= 10
number of dos NEDOS = 301 number of ions NIONS = 6
non local maximal LDIM = 4 non local SUM 2l+1 LMDIM = 8
total plane-waves NPLWV = 327680
max r-space proj IRMAX = 1696 max aug-charges IRDMAX= 2557
dimension x,y,z NGX = 64 NGY = 64 NGZ = 80
dimension x,y,z NGXF= 98 NGYF= 98 NGZF= 112
support grid NGXF= 98 NGYF= 98 NGZF= 112
ions per type = 2 4
NGX,Y,Z is equivalent to a cutoff of 12.07, 12.07, 13.30 a.u.
NGXF,Y,Z is equivalent to a cutoff of 18.48, 18.48, 18.62 a.u.

I would recommend the setting:

dimension x,y,z NGX = 64 NGY = 64 NGZ = 73
SYSTEM = Ag (111) 1x1
POSCAR = System: C H 001 Surface Nx= 3 Ny= 3 N

Startparameter for this run:

NWRITE = 2 write-flag & timer
PREC = high medium, high low
ISTART = 1 job : 0-new 1-cont 2-samecut
ICHARG = 0 charge: 1-file 2-atom 10-const
ISPIN = 1 spin polarized calculation?

Table D.5 Continued

LNONCOLLINEAR = F non collinear calculations
LSORBIT = F spin-orbit coupling
INIWAV = 1 electr: 0-lowe 1-rand 2-diag
LASPH = F aspherical Exc in radial PAW
METAGGA= F non-selfconsistent MetaGGA calc.

Electronic Relaxation 1

ENCUT = 500.0 eV 36.75 Ry 6.06 a.u. 16.07 16.07 18.23*2*pi/ulx,y,z
ENINI = 500.0 initial cutoff
ENAUG = 644.9 eV augmentation charge cutoff
NELM = 60; NELMIN= 2; NELMDL= 0 # of ELM steps
EDIFF = 0.1E-03 stopping-criterion for ELM
LREAL = T real-space projection
LCOMPAT= F compatible to vasp.4.4
LREAL_COMPAT= F compatible to vasp.4.5.1-3
GGA_COMPAT = T GGA compatible to vasp.4.4-vasp.4.6
LMAXPAW = -100 max onsite density
LMAXMIX = 2 max onsite mixed and CHGCAR
VOSKOWN= 0 Vosko Wilk Nusair interpolation
ROPT = -0.00040 -0.00040

Ionic relaxation

EDIFFG = 0.1E-02 stopping-criterion for IOM
NSW = 150 number of steps for IOM
NBLOCK = 1; KBLOCK = 150 inner block; outer block
IBRION = 2 ionic relax: 0-MD 1-quasi-New 2-CG
NFREE = 1 steps in history (QN), initial steepest desc. (CG)
ISIF = 2 stress and relaxation
IWAVPR = 11 prediction: 0-non 1-charg 2-wave 3-comb
ISYM = 2 0-nonsym 1-usesym 2-fastsym
LCORR = T Harris-Foulkes like correction to forces

POTIM = 0.50 time-step for ionic-motion
TEIN = 0.0 initial temperature
TEBEG = 0.0; TEEND = 0.0 temperature during run
SMASS = -3.00 Nose mass-parameter (am)
estimated Nose-frequency (Ω) = 0.10E-29 period in steps =*****
mass= -0.178E-26a.u.
NPACO = 256; APACO = 16.0 distance and # of slots for P.C.
PSTRESS= 0.0 pullay stress

Mass of Ions in am

POMASS = 12.01 1.00

Ionic Valenz

Table D.5 Continued

ZVAL = 4.00 1.00

Atomic Wigner-Seitz radii

RWIGS = -1.00 -1.00

NELECT = 12.0000 total number of electrons

NUPDOWN= -1.0000 fix difference up-down

DOS related values:

EMIN = 10.00; EMAX = -10.00 energy-range for DOS

ISMEAR = 0; SIGMA = 0.10 broadening in eV -4-tet -1-fermi 0-gaus

Electronic relaxation 2 (details)

IALGO = 38 algorithm

LDIAG = T sub-space diagonalisation

IMIX = 4 mixing-type and parameters

AMIX = 0.40; BMIX = 1.00

AMIX_MAG = 1.60; BMIX_MAG = 1.00

AMIN = 0.10

WC = 100.; INIMIX= 1; MIXPRE= 1

Intra band minimization:

WEIMIN = 0.0010 energy-eigenvalue tresh-hold

EBREAK = 0.25E-05 absolut break condition

DEPER = 0.30 relativ break condition

TIME = 0.10 timestep for ELM

volume/ion in A,a.u. = 112.14 756.78

Fermi-wavevector in a.u.,eV,Ry = 0.427721 2.489118 0.182945

Second variation

LSECVAR= F do a second variation

Write flags

LWAVE = T write WAVECAR

LCHARG = T write CHGCAR

LVTOT = F write LOCPOT, local potential

LELF = F write electronic localiz. function (ELF)

LORBIT = 0 0 simple, 1 ext, 2 COOP (PROOUT)

Dipole corrections

IDIPOL = 0 1-x, 2-y, 3-z

LDIPOL = F correct potential

Table D.5 Continued

conjugate gradient relaxation of ions
using selective dynamics as specified on POSCAR
WARNING: If single coordinates had been selected the selection of
coordinates
is made according to the corresponding `direct` coordinates!
Don't support selection of single cartesian coordinates -- sorry ...
!
charge density will be updated during run
non-spin polarized calculation
Variant of blocked Davidson
Davidson routine will perform the subspace rotation
performe sub-space diagonalisation
after iterative eigenvector-optimisation
modified Broyden-mixing scheme, `WC = 100.0`
initial mixing is a Kerker type mixing with `AMIX = 0.4000` and `BMIX = 1.0000`
Hartree-type preconditioning will be used
using additional bands `4`
real space projection scheme for non local part
calculate Harris-corrections to forces
(improved forces if not selfconsistent)
use gradient corrections
use of overlap-Matrix (Vanderbilt PP)
Gauss-broadening in eV `SIGMA = 0.10`

energy-cutoff : 500.00
volume of cell : 672.86
direct lattice vectors reciprocal lattice vectors
8.814488661 0.000000000 0.000000000 0.113449576 -0.065500140
0.000000000
4.407244330 7.633571477 0.000000000 0.000000000 0.131000280
0.000000000
0.000000000 0.000000000 10.000000000 0.000000000 0.000000000
0.100000000

length of vectors
8.814488661 8.814488985 10.000000000 0.131000285 0.131000280
0.100000000

Table D.5 Continued

old parameters found on file WAVECAR:
energy-cutoff : 500.00
volume of cell : 672.86
direct lattice vectors reciprocal lattice vectors
8.814488661 0.000000000 0.000000000 0.113449576 -0.065500140
0.000000000
4.407244330 7.633571477 0.000000000 0.000000000 0.131000280
0.000000000
0.000000000 0.000000000 10.000000000 0.000000000 0.000000000
0.100000000

length of vectors

k-points in units of $2\pi/\text{SCALE}$ and weight: K-Points
0.00000000 0.00000000 0.00000000 1.000

k-points in reciprocal lattice and weights: K-Points
0.00000000 0.00000000 0.00000000 1.000

position of ions in fractional coordinates (direct lattice)
0.55976130 0.52585184 0.50763851
0.44610279 0.46846640 0.50209576
0.70032069 0.43636334 0.51063411
0.51711605 0.66477617 0.50942216
0.48874812 0.32954197 0.50031205
0.30554340 0.55795490 0.49910017

position of ions in cartesian coordinates (Angst):
7.25156717 4.01412757 5.07638510
5.99681391 3.57607176 5.02095764
8.09612864 3.33101072 5.10634107
7.48794456 5.07461643 5.09422162
5.76043671 2.51558218 5.00312045
5.15225243 4.25918860 4.99100166

k-point 1 : 0.00000.00000.00000 plane waves: 17059

maximum and minimum number of plane-waves per node : 17059 17059

Table D.5 Continued

maximum number of plane-waves: 17059

maximal index in each direction:

IXMAX= 16 IYMAX= 16 IZMAX= 18

IXMIN=-16 IYMIN=-16 IZMIN=-18

WARNING: wrap around error must be expected set NGX to 66

WARNING: wrap around error must be expected set NGY to 66

NGZ is ok and might be reduce to 74

real space projection operators:

total allocation : 375.65 KBytes

max/ min on nodes : 375.65 375.65

parallel 3dFFT wavefunction:

minimum data exchange during FFTs selected (reduces bandwidth)

parallel 3dFFT charge:

minimum data exchange during FFTs selected (reduces bandwidth)

For storing wavefunctions 2.73 MBYTES are necessary

For predicting wavefunctions 10.95 MBYTES are necessary

Broyden mixing: mesh for mixing (old mesh)

NGX = 33 NGY = 33 NGZ = 37

(NGX = 98 NGY = 98 NGZ =112)

gives a total of 40293 points

charge density for first step will be calculated from the start-wavefunctions

Maximum index for non-local projection operator 1599

Maximum index for augmentation-charges 1154 (set IRDMAX)

initial charge from wavefunction

First call to EWALD: gamma= 0.202

Maximum number of real-space cells 3x 3x 2

Maximum number of reciprocal cells 3x 3x 3

FEWALD: VPU time 0.00: CPU time 0.00

Table D.5 Continued

----- Iteration 1(1) -----

POTLOK: VPU time 1.27: CPU time 1.29
SETDIJ: VPU time 0.01: CPU time 0.01
EDDAV : VPU time 1.10: CPU time 1.15
DOS : VPU time 0.00: CPU time 0.00
CHARGE: VPU time 0.17: CPU time 0.17
MIXING: VPU time 0.02: CPU time 0.02

LOOP: VPU time 2.57: CPU time 2.64

eigenvalue-minimisations : 20
total energy-change (2. order) :-0.3208505E+02 (-0.2838548E-02)
number of electron 11.9999992 magnetization
augmentation part 0.2796894 magnetization

Broyden mixing:

rms(total) = 0.14906E-01 rms(broyden)= 0.14905E-01
rms(prec) = 0.20383E-01
weight for this iteration 100.00

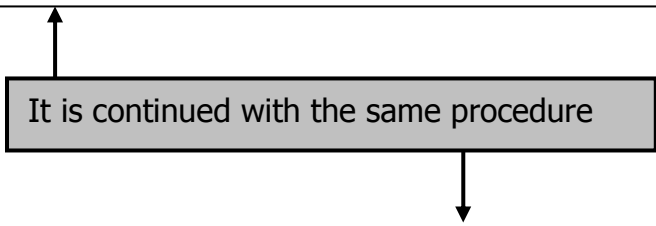
Free energy of the ion-electron system (eV)

alpha Z PSCENC = 0.89206134
Ewald energy TEWEN = 206.00835436
-1/2 Hartree DENC = -482.35423207
-V(xc)+E(xc) XCENC = 39.17532418
PAW double counting = 157.61356597 -160.40518852
entropy T*S EENTRO = 0.00000000
eigenvalues EBANDS = -138.05468169
atomic energy EATOM = 345.03974294

free energy TOTEN = -32.08505349 eV

energy without entropy = -32.08505349 energy(sigma->0) = -
32.08505349

Table D.5 Continued



----- Iteration 2(1) -----

POTLOK: VPU time 1.26: CPU time 1.29
 SETDIJ: VPU time 0.01: CPU time 0.01
 EDDAV : VPU time 1.11: CPU time 1.16
 DOS : VPU time 0.00: CPU time 0.00
 CHARGE: VPU time 0.17: CPU time 0.17
 MIXING: VPU time 0.02: CPU time 0.02

 LOOP: VPU time 2.57: CPU time 2.65

eigenvalue-minimisations : 20
 total energy-change (2. order) :-0.3208497E+02 (-0.6054092E-02)
 number of electron 11.9999992 magnetization
 augmentation part 0.2773201 magnetization

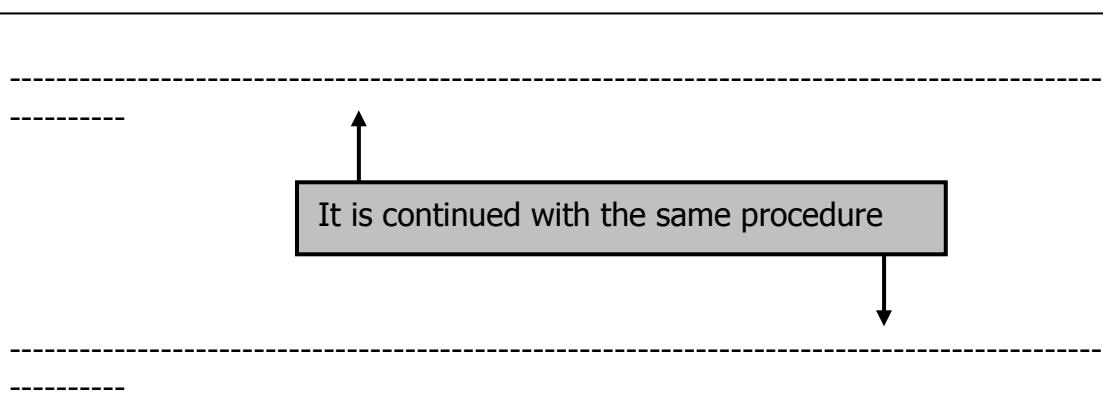
Broyden mixing:
 rms(total) = 0.11984E-01 rms(broyden)= 0.11980E-01
 rms(prec) = 0.14976E-01
 weight for this iteration 100.00

Free energy of the ion-electron system (eV)

 alpha Z PSCENC = 0.89206134
 Ewald energy TEWEN = 204.64132009
 -1/2 Hartree DENC = -482.16094423
 -V(xc)+E(xc) XCENC = 39.16896714
 PAW double counting = 158.18377389 -160.97733294
 entropy T*S EENTRO = 0.00000000
 eigenvalues EBANDS = -136.87255425
 atomic energy EATOM = 345.03974294

 free energy TOTEN = -32.08496602 eV
 energy without entropy = -32.08496602 energy(sigma->0) = -
 32.08496602

Table D.5 Continued



reached required accuracy - stopping structural energy minimisation
writing wavefunctions

LOOP+: VPU time 6.95: CPU time 7.10

General timing and accounting informations for this job:

=====
=====

Total CPU time used (sec):	34.062
User time (sec):	31.850
System time (sec):	2.212
Elapsed time (sec):	35.025
Maximum memory used (kb):	0.
Average memory used (kb):	0.
Minor page faults:	46315
Major page faults:	0
Voluntary context switches:	5752

Table D.6 Input file of the calculation for optimization of Ag(3x3) slab in VASP software

INCAR

SYSTEM = Ag (111) 3x3
 PREC = HIGH
 IBRION = 2
 NSW = 150
 LREAL = Auto
 ISMEAR = 1; SIGMA = 0.1;
 LMAXMIX = 6
 EDIFFG = -0.01

POSCAR

System: Ag111O Surface Nx= 3 Ny= 3 N

1.000000000000000000
 8.8144886609000004 0.0000000000000000 0.0000000000000000
 4.4072443302000002 7.6335714766000002 0.0000000000000000
 0.0000000000000000 0.0000000000000000 20.0000000000000000

36

Selective dynamics

Cartesian

0.000000	0.000000	5.000000	F F F
2.938163	0.000000	5.000000	F F F
5.876326	0.000000	5.000000	F F F
1.469081	2.544524	5.000000	F F F
4.407244	2.544524	5.000000	F F F
7.345407	2.544524	5.000000	F F F
2.938163	5.089048	5.000000	F F F
5.876326	5.089048	5.000000	F F F
8.814488	5.089048	5.000000	F F F
10.283569	5.937222	7.408216	T T T
7.345407	5.937222	7.408216	T T T
4.407244	5.937222	7.408216	T T T
5.876326	3.392699	7.408216	T T T
2.938163	3.392699	7.408216	T T T
7.345407	0.848175	7.408216	T T T
4.407245	0.848175	7.408216	T T T
1.469082	0.848175	7.408216	T T T
8.814488	3.392699	7.408216	T T T
2.938163	1.696349	9.802826	T T T
5.876327	1.696349	9.802826	T T T

Table D.6 Continued

8.814489	1.696349	9.802826	T T T
4.407245	4.240874	9.802826	T T T
7.345408	4.240874	9.802826	T T T
10.283571	4.240874	9.802826	T T T
5.876326	6.785398	9.802826	T T T
8.814489	6.785398	9.802826	T T T
11.752652	6.785398	9.802826	T T T
0.000000	0.000000	12.206554	T T T
2.938163	0.000000	12.206554	T T T
5.876326	0.000000	12.206554	T T T
1.469081	2.544524	12.206554	T T T
4.407244	2.544524	12.206554	T T T
7.345407	2.544524	12.206554	T T T
2.938163	5.089048	12.206554	T T T
5.876326	5.089048	12.206554	T T T
8.814488	5.089048	12.206554	T T T

K-POINTS

K-Points

0

Monkhorst Pack

6 6 1

0 0 0

CURRICULUM VITAE

PERSONAL INFORMATION

Surname, Name: FELLAH, Mehmet Ferdi

Nationality: Turkish (TC)

Date and Place of Birth: November 19, 1978 - Gaziantep

Marital Status: Married, a Daughter

e-mail: mfellah@metu.edu.tr, mffellah@gmail.com

EDUCATION

<u>Degree</u>	<u>Institution</u>	<u>Year of Graduation</u>
BS	Osmangazi University, Eskişehir Chemical Engineering Department (<i>First-ranking student</i>)	2000
High School	19 Mayıs High School, Gaziantep	1996

WORK EXPERIENCE

<u>Year</u>	<u>Place</u>	<u>Enrollment</u>
2003 - Present	METU, Chemical Engineering Dept.	Research Assistant

SHORT TERM CONFERENCE VISITS AND WORKSHOP PARTICIPATIONS

Visit for some meetings to discuss research collaborations with an invitation of Prof. Dr. Rutger A. van SANTEN in laboratory of inorganic chemistry and catalysis of Eindhoven Technology University, Eindhoven, The Netherlands (April, 12-19 2009).

Second National Catalysis Conference (NCC-2), June 18-22, 2008, Palandöken, Erzurum, TURKEY.

IDECAT Summerschool on Computational Methods for Catalysis and Materials Science 15-22 September 2007, Porquerolles, FRANCE.

First National Catalysis Conference (NCC-1), January 17-21, 2007, Middle East Technical University Northern Cyprus Campus, Guzelyurt NORTHERN CYPRUS.

First Anatolian School on Catalysis, Workshops: Master Class Catalysis and Computational Catalysis, by Schuit Catalysis Institute of the Eindhoven University of Technology and Middle East Technical University, September 25-October 6, 2006, Ankara, TURKEY.

19th North American Catalysis Society (NACS) Meeting, May 22-27, 2005 in Philadelphia, PA USA.

PUBLICATIONS

Kizilkaya, A.C., Fella, M.F., Onal, I., "Direct Gas-Phase Epoxidation of Propylene to Propylene Oxide through Radical Reactions: A DFT Study", Submitted to *Chemical Physics Letters*.

Fella M.F., Onal I., "Methane Activation on M- and OM-ZSM-5 (M= Ag, Au, Cu, Rh and Ru) Clusters: A Density Functional Theory Study", Submitted to **NGCS**.

Fella M.F., Onal I., "Methane Oxidation to Methanol by N₂O on Fe- and Co-ZSM-5: A Density Functional Study", Submitted to *Journal of Physical Chemistry C*.

Fella M.F., van Santen R.A., Onal I., "Oxidation of Benzene to Phenol by N₂O on Fe⁺²-ZSM-5 Cluster: A Density Functional Theory Study", *Journal of Physical Chemistry C*, 2009, 113, 15307–15313.

Erdogan R., Fella M.F., Onal I., "An ONIOM and DFT Study of Water Adsorption on Rutile TiO₂ (110) Cluster", Accepted, *International Journal of Quantum Chemistry*, 2009, doi:10.1002/qua.22400.

Fella M.F., Onal I., "Benzene Oxidation to Phenol by N₂O on Fe- and Co-ZSM-5: A Density Functional Study", *Turkish Journal of Chemistry*, 2009, 33, 333-345.

Fellah M.F., Onal I., "A Density Functional Study of 1, 1, 5-Tris (4-dimethylaminophenyl)-3-methyl-divinylene", Accepted, *International Journal of Quantum Chemistry*, 2009, doi:10.1002/qua.22087.

Fellah M.F., Onal I., "N₂O Decomposition on Fe- and Co-ZSM-5: A Density Functional Study", *Catalysis Today*. 2008, 137(2-4), 410-417.

Fellah M.F., Onal I., "Activation of Light Alkanes on Pure and Fe and Al Doped Silica Clusters: A Density Functional and ONIOM Study", *Turkish Journal of Chemistry*, 31(5), 2007, Pages 415-426.

Fellah M.F., Onal I., "C-H bond activation of methane by pure and Fe and Al doped silica: A density functional study", *International Journal of Pure and Applied Chemistry*, 2(1), 2007, 127.

Ozbek M.O., Kizilkaya A.C., Fellah M.F., Onal I., "A DFT study on Cu doped Ag surfaces for propylene epoxidation", *21st North American Catalysis Society (NACS) Meeting*, June 7-12, 2009 in San Francisco, California, USA.

Fellah M.F., Onal I., "Propylene epoxidation on silver: A density functional study", *International Congress on Catalysis (14th ICC)*, July 13-18 2008, COEX, Seoul, KOREA.

Fellah M.F., Onal I., "Benzene Oxidation to Phenol by N₂O on Fe- and Co-ZSM-5: A Density Functional Study", *Second National Catalysis Conference (NCC-2)*, 18-22 June 2008, Palandöken, Erzurum, TURKEY.

Fellah M.F., Onal I., "Methane Oxidation to Methanol by N₂O on Fe- and Co-ZSM-5: A Density Functional Study", *Second National Catalysis Conference (NCC-2)*, 18-22 June 2008, Palandöken, Erzurum, TURKEY.

Fellah M.F., Onal I., "Light Alkene Epoxidation: A Density Functional Study", *Second National Catalysis Conference (NCC-2)*, 18-22 June 2008, Palandöken, Erzurum, TURKEY.

Fellah M.F., Ugurlu C., Senkan S., Onal I., "Density Functional Theory Study of N₂O Decomposition on Clusters Representing Fe- and Co-ZSM-5", *AWPA 2007 International Symposium On Air And Water Pollution Abatement*, 21-23 June 2007, Zakopane, POLAND.

Fellah M.F., Turkmenoglu E., Onal I., "Propylene Epoxidation on Ag (111) surface: A Density Functional and ONIOM Study", **First National Catalysis Conference (NCC-1)**, 17-20 January 2007 , Middle East Technical University Northern Cyprus Campus, Guzelyurt, Northern CYPRUS.

Fellah M.F., Turkmenoglu E., Onal I., "Application of Quantum Chemical Methods in Heterogeneous Catalysis Involving Transition Metals", **First National Catalysis Conference (NCC-1)**, 17-20 January 2007 , Middle East Technical University Northern Cyprus Campus, Guzelyurt, Northern CYPRUS.

Fellah M.F., Onal I., "Catalyst Screening of C-H Bond Activation of Methane: A Density Functional Study", **ECOSS 24, European Conference on Surface Science**, September 4-8 2006 Paris, FRANCE.

Fellah M.F., Senkan S., Onal I., "Activation of C-H Bond of Ethane by Pure and Fe and Al Doped Silica: A Density Functional Study", **Operando - II, Second International Congress on Operando Spectroscopy**, 2006 , Toledo, SPAIN.

Fellah M.F., Senkan S., Onal I., "Effect of Fe Doping on the Catalytic Activity of Silica in the Partial Oxidation of Methane to Formaldehyde – A Quantum Chemical Study." , **19th North American Catalysis Society (NACS) Meeting**, May 22-27, 2005 in Philadelphia, PA USA.